universität innsbruck

Fakultät für Technische Wissenschaften

Analysis of the Building Energy Simulation Process

From input parametrization to results evaluation comparing different BES tools and modelling approaches

Dipl.-Ing Mara Magni

Innsbruck, September 2022

Dissertation

eingereicht an der Leopold-Franzens-Universität Innsbruck, Fakultät für Technische Wissenschaften zur Erlangung des akademischen Grades

Doktorin der Technischen Wissenschaften

Erste/r Beurteiler/in:	Univ.-Prof. Dipl.-Ing. Dr. Wolfgang Streicher Universität Innsbruck, Institut für Konstruktion und Materialwissenschaften, Arbeitsbereich für Energieeffizientes Bauen
Zweite/r Beurteiler/in:	Prof. Dipl.-Ing. Thomas Auer Technische Universität München, Fakultät für Architektur, Gebäudetechnologie und klimagerechtes Bauen

Hauptbetreuer/in: Univ.-Prof. Dipl.-Ing. Dr. Wolfgang Streicher
Universität Innsbruck, Institut für Konstruktion und Materialwissenschaften, Arbeitsbereich für Energieeffizientes Bauen

dedicato a mio padre

Acknowledgment

Many thanks to all the people that supported this work directly or indirectly.

I'd like to express my deepest gratitude to my supervisor Wolfgang Streicher for the opportunity to pursue this PhD programme and for supporting this work during these years.

I am deeply grateful to Fabian Ochs for trusting me and for the chance to participate in many interesting projects. Thank you also for sharing your knowledge with me and for the countless and very stimulating exchanges. You have been a great mentor and supervisor, always ready to offer an advice and always able to keep the mood high even in challenging times.

Special thanks to Prof. Auer for your availability to be a reviewer of this thesis despite the short notice and limited time available.

The participation in the IEA SHC Task 56 strongly supported this research work. I would like to thank all my co-authors for their efforts and for the fruitful collaboration. I owe my gratitude to Samuel de Vries for his endeavour in calibrating the EnergyPlus model and support during our collaboration. A special thanks also to all the Task 56 team, it was a pleasure to be part of this Task.

My sincere gratitude goes to all the colleagues and friends of the unit of Energy Efficient Building. Thank you for the scientific, but also personal exchange and support, it was a privilege to work in such a pleasant working environment. Thanks to Abdulrahman Dahash, Elisa Venturi, Georgios Dermentzis, Alice Tosatto, William Monteleone, Sascha Hammes and Apeksha Shandilya for sharing the rocky road towards a PhD.

Finally, but most importantly, I would like to thank my Family. Thank you for your support and love throughout my academic years. Without you, this would not have been possible.
My gratitude also to my partner Niccolò for your love, unconditional support and understanding.

Kurzfassung

Um die für 2050 gesetzten Klimaziele zu erreichen, müssen nicht nur alle neuen Gebäude nach den höchsten Qualitätsstandards geplant werden, sondern es ist auch wichtig die Renovierungsraten zu erhöhen. In diesem Szenario können energetische Gebäudesimulationen eine wichtige Rolle spielen, da sie den Planungsprozess beschleunigen und unter geringem Kosteneinsatz die Gebäudeleistung optimieren können. Aufgrund unzureichender Glaubwürdigkeit der Ergebnisse, die mit solchen Tools erzielt werden, und der daraus abgeleiteten Entscheidungen, wird die Verbreitung dynamischer Simulationstools in der Praxis gebremst.
Diese Arbeit bietet Einblicke in alle wichtigen Schritte des Simulationszyklus mit dem Ziel zukünftige Nutzer und Nutzerinnen von Gebäudesimulationstools in den Phasen der Modellierung, Parametrisierung, Verifizierung und Validierung zu unterstützen.

Ein Modell der Referenz-Bürozelle, welche im Rahmen der IEA SHC Task 56 definiert wurde, wurde mit verschiedenen Simulationswerkzeugen implementiert (d.h. EnergyPlus v.9.3, TRNSYS 18, Simulink/CarnotUIBK, Simulink/ALMABuild, IDA ICE v.4.8, Modelica Buildings library v.5.0.1 zusammen mit Dymola v. 2020x, DALEC und PHPP). Während dieses Prozesses wurde die Komplexität einer Übersetzung der realen Welt oder ihrer Beschreibung in ein Modell hervorgehoben. Viele Iterationen waren notwendig, um eine gute Übereinstimmung zwischen den Ergebnissen der verschiedenen Tools zu erreichen. In der Anfangsphase wurden hohe Abweichungen in Bezug auf den Energiebedarf festgestellt. Es war notwendig Benutzerfehler zu identifizieren und die Eingaben der Werkzeuge mit einem höheren oder niedrigeren Abstraktionsgrad im Vergleich zur Gebäudebeschreibung zu parametrisieren, um die Übereinstimmung zwischen den Ergebnissen der verschiedenen Tools zu verbessern. Um die Ergebnisse der verschiedenen Tools miteinander zu vergleichen, wurden Schwierigkeiten, wie die Definition der Referenzergebnisse, die Anwendung der statistischen Indizes, ihre Normalisierung und Festlegung von Grenzwerten, behandelt.

Die verschiedenen Modellierungsmethoden, die von den verschiedenen Tools angeboten werden, wurden in Simulink implementiert, um ihren Einfluss auf die Genauigkeit der Ergebnisse, die Rechenzeit und die erforderliche Modellparametrisierung zu bewerten. Auf diese Weise wurde ein Überblick gegeben, der das empfindliche Gleichgewicht zwischen Rechenzeit, Modellparametrisierung und Genauigkeit der Ergebnisse darstellt und somit zukünftigen Nutzern und Nutzerinnen bei der Wahl des besten Tools, Modells oder sub-Teil des Modells für den jeweiligen Zweck helfen kann. Dabei wurde die Aufmerksamkeit auch auf Aspekte gelenkt, die oft übersehen werden, aber für die Genauigkeit der Ergebnisse eine Rolle spielen (z.B. Modell der adiabatischen Struktur, Kapazität des Luftknotens, Konvektions- und Strahlungsaustauschkoeffizienten, Himmelsmodell und Verteilung der solaren und internen Gewinne über die Hüllflächen).

Es wurde ein neuer Modellierungsansatz entwickelt und mit TRNSYS 18 verglichen, um die Simulation des Strahlungstemperaturfelds mit einer günstigen Rechenzeit (im Vergleich zur CFD-Simulation) zu ermöglichen. Dieser Modellierungsansatz wurde mit anderen Ansätzen zur Modellierung der thermischen Zone verglichen, um die Abweichungen in Bezug auf den Energiebedarf und die vorhergesagte Temperatur an verschiedenen Punkten des Raums aufzuzeigen.

Schließlich wurde das Simulink-Modell für eine technisch-wirtschaftliche Analyse verwendet, um die Energie- und Kosteneinsparungen zu bewerten, die mit verschiedenen Technologiekombinationen (wie z.B. Wärmepumpentypen, PV, LED, Batterien) ermöglicht werden können.

Abstract

To achieve the climate targets set for 2050, it is not only necessary to design all new buildings to the highest quality standards, but it is also essential to boost the renovation rate. In this scenario, building energy simulation tools can play a key role as they can speed up the design process and optimise building performance at a low cost. Unfortunately, the lack of credibility of the results obtained with such tools and the decisions derived from them holds back the spread of the use of dynamic simulation tools in practice.
This work provides insights into all the main steps of the simulation cycle with the aim to support future users of building simulation tools in the modelling, parametrization, verification, and validation phases.

A model of the reference office cell, defined within the IEA SHC Task 56, has been implemented using different simulation tools (i.e., EnergyPlus v.9.3, TRNSYS 18, Simulink/CarnotUIBK, Simulink/ALMABuild, IDA ICE v.4.8, Modelica Buildings library v.5.0.1 together with Dymola v. 2020x, DALEC and PHPP). During this process, the complexities related to the translation of the real world or a description of it into a model were highlighted. Many iterations were necessary to reach a good agreement between the results of the different tools. In the initial phase, high deviations were detected in terms of energy demand. To enhance the agreement between the results of the different tools it was necessary to identify user errors and to parametrize the inputs of the tools with a higher or lower level of abstraction compared to the building description.
To cross-compare the results of the different tools difficulties were addressed such as the definition of the reference results, the application of the statistical indices, their normalization, and thresholds.

The different modelling approaches proposed by the different tools were implemented in Simulink to assess their influence on the results accuracy, computational time and required model parametrization. In this way, a picture representing the delicate balance between computational time, model parametrization and results accuracy was depicted that can guide future users in the choice of the best tool, model, or sub-part of the model for the specific purpose. This was done by focusing also the attention on aspects that are generally overlooked, but that play a role in the accuracy of the results (e.g., model of the adiabatic structure, capacity of the air node, convective and radiative exchange coefficients, sky model and distribution of the solar and internal gains over the surfaces of the enclosure).

A new modelling approach was developed and cross-compared against TRNSYS 18 to enable the simulation of the radiative temperature field with an affordable computational time (compared to CFD simulation). This modelling approach was compared against other

approaches for modelling the thermal zone highlighting the deviations in terms of energy demand and predicted temperature at different points of the room.

Finally, the cross-compared Simulink model was used to perform a techno-economic analysis assessing the energy and cost savings that can be achieved with different technology combinations (i.e., different heat pumps typologies, PV, LED, batteries).

Contents

1 Introduction

1.1 Status of Energy in Buildings

Building construction and operation, as reported in the Global Status Report 2021 [1], accounted for 36 % of the global final energy use and 37 % of the energy-related carbon dioxide emissions in 2020. The residential building contributed with the largest share.

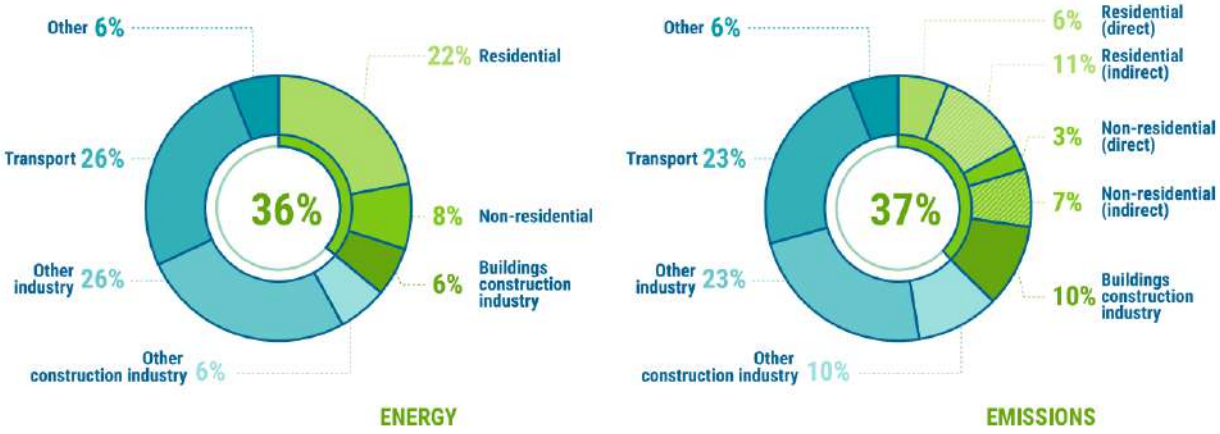

Figure 1: Global share of buildings and construction final energy and emissions, 2021 [1]

To reach the net-zero energy scenario by 2050, it is necessary to reduce the actual CO_2 emission to zero and offset the expected increase in energy demand and CO_2 emission related to the growth of the world population. To realize this, it is anticipated that electrification and increased energy efficiency in buildings will account for about 70% of the reduction of CO_2 emissions. According to [1], more than 85% of the building stock must be zero carbon ready by 2050[1], where half of the building's energy needs will be covered by heat pumps, 10% by district heating and the rest with other renewable sources. In this scenario, the increasing use of heat pumps will influence the electricity and district heating networks, and building energy demand leading to a strong mutual interaction between these different elements [2].

Building energy codes and subsidies are the main engines of this transition process. In [1] a positive trend is highlighted, where from 2015 to 2020 the number of countries with building energy codes increased by 30.6 % and investment by 39.5 %. Yet, this progress is not worldwide uniformly distributed since the application in sub-Saharan Africa, south and central

[1] According to [44] Zero carbon-ready buildings are defined as follows: *"A zero carbon-ready building is highly energy efficient and either uses renewable energy directly or an energy supply that can be fully decarbonised, such as electricity or district heat.*

America remain low and the countries where the highest population growth is expected are also those that have the lowest coverage with energy policies.
In Europe, all new buildings must be nearly zero-energy buildings starting in 2021 anyway it has been proven that the minimum requirements set by EU member states are not ambitious enough and that a cost-optimal solution would require a lower energy demand [3]. In addition, each member state has set its own policies with different boundaries and requirements therefore the ambition levels within Europe are difficult to be compared [4].

Today about 75% of the European building stock is energy inefficient [5] therefore to reduce the energy demand of the building stock it is necessary to increase the renovation rate (European renovation rate is around 1.1%, far below the expected rate of 3% necessary to achieve the climate neutrality goals by 2050 [6]). As highlighted by [7], the decision process of a housing renovation is complex and dependent on many factors (e.g. technical, economic, psychological, social, etc…). Between these factors, according to [6], disruption of inhabitants, high initial costs, and long payback periods are among the main causes hindering refurbishment. To overcome these problems, new design tools are needed to help planners in finding the optimal approach, also considering innovative technological solutions [8] (e.g. decentral compact heat pump possibly integrated into the façade or prefabricated façade elements allowing a minimal disruptive renovation and minimizing the construction time).

1.2 Building Simulation Lifecycle

1.2.1 Overview

In this framework (see Section 1.1), the field of Building Simulation is playing an important role in the optimization and design of low-energy buildings and in supporting the development of policies that drive the energy goals in this field [9]. Building simulations can give a great contribution to this endeavour since they allow to speed up the design process and optimize the building performance at a low cost [10].

The advancement in building simulation techniques progresses alongside the evolution of computer technology. Before the 1960s, hand calculation methods (e.g. bin and degree days) were the only option, while since the mid-1960s the first simulation methods appeared [11]. During the 70s, building simulation received high attention from the energy research community due to the oil crisis [12]. Since the 90s global awareness and attention to climate protection issues have raised again the attention towards Building Energy Simulation (BES). This trend led to the development of a wide range of BES tools with different focuses and levels of detail (a comprehensive list is provided in [13] and [14]).

From the list of BESs tools in [14] it is immediately clear how wide the range of applications is. Without aiming at having a complete list, Table 1, reports an overview of the applications covered by the available tools published in [14].

Table 1: different application fields of the tools listed in [14].

Material properties	Calculation of thermal bridges
	Calculation of vapour diffusion in the building construction
	Calculation of the heat transfer coefficient
	Calculation of the window properties
	Transient heat transfer analysis
HVAC / Renewables	Piping designer
	Planning of natural and mechanical ventilation
	Psychrometric analysis for air conditioning
	Setpoint calculation based on adaptive thermal comfort
	HVAC sizing
	Performance of the refrigerant cycle
	Design of the heat pump geothermal field
	Design of photovoltaic and solar thermal systems
	Generation of the occupancy and domestic hot water profiles
	Design of the power distribution systems
Building Simulation	Whole building energy simulation
	Calculation of the heating and cooling load and demand
	Window optimization
	Lighting modelling
	Acoustic modelling
	Multizone airflow simulation
Methods/ utilities	Plugin for building optimization or parametric modelling (e.g., GenOpt)
	Hardware in the loop application
	File format protocols (e.g., gbXML)
	User interfaces
	Support decisions in energy audit – energy management
	Management of remote monitoring
	Comfort and weather analysis
	Atlas of weather data
City/ Districts	Urban energy simulation
	Solar irradiation in urban areas
	Wind effects on urban areas
	District heating energy balance
Results analysis	Data analysis (collection, validation, analysis and visualization);
	Lifecycle analysis
	Energy dataset
	Lighting and daylighting visualization

It is noteworthy to mention that the tools in this list implement a different degree of detail and find a place in the whole building simulation process (see Figure 2) in different positions. Some tools (i.e., for the calculation of the window properties, heat transfer coefficient, occupancy profile, domestic hot water profile, shading calculation, thermal bridges calculation, etc..) can be used to parametrize the input needed for the building simulation tool. Other tools operate as

an interface between the simulation engine and the user, others can be used for the analysis of monitored data and output of the simulation and others could be coupled to the simulation engine to perform parametric simulations.

Figure 2 depicts all the elements and steps of the simulation lifecycle [15]: definition of the requirements, the construction of the model (including its parametrization), the simulation and the verification, validation and testing process. At the top of Figure 2, it can be noticed that BES can be applied at different stages of the project (i.e. planning, design development, optimization, monitoring and management, fault detection), in addition, the person commissioning the simulation study (i.e. stakeholder) typically differ from the modeller (e.g. engineers, architects, building physicists, planners and researchers) making the communications even more complex (see Figure 2). In general, the process of creating the model and parametrizing it is error-prone since it is easy to make unrepresentative assumptions or just commit user errors in preparing building input files. In this context, the application of Building Information Modelling to Building Energy Modelling (BIM to BEM) is receiving increasing attention as it aims to ease the data handling and the creation of the BES model by automatizing the exchange of information, thus reducing the possibility of committing user mistakes and speeding up the whole process reducing also the cost [16]. Nevertheless, BIM to BEM approach is still facing many challenges that hinder its diffusion. As highlighted in [16], in order to apply BIM to BEM in practice, further development in terms of availability and agreement in information transfer is required.

The different building phases (i.e., planning, design development, optimization, monitoring and management, fault detection) might be focused on the optimization of various aspects and are characterized by the availability of different degrees of detail of the available information. Consequently, it would be highly desirable to be able to reuse the model or sub-models initially developed (or even developed in other projects) by evolving it at various stages of the project [17]. To achieve this goal the construction of a conceptual model [15], [18], providing a high-level description of the system thus helping the modellers to understand the model, is fundamental (see also Section 1.2.2).
Every model, independently of its level of detail and complexity, is an approximation of the real world, therefore, it is characterized by uncertainties and quantifying and assessing them is very important for the credibility of the model (see also Section 1.3). Typically for every step of the project, the used model is improved iteratively until the model is able to assess the problem requirements. The developing status of the model can be described through the model maturity that provides guidance for the model evaluation and reuse and for the management of the workflow possibly reducing the modelling time and enhancing the reusability of the model [15], [18], [19].

In practice, the workflow described above is not likely to be applied as the different steps lack of commonly agreed definition [15] and because of time constraints, some steps might be skipped (e.g. verification, uncertainty analysis or model description) [20]. Therefore, the entire process relies on the modeller's knowledge and experience. This is particularly critical during the design stage, as it can drastically affect the performance of the building and the design questions might evolve faster than the simulation process making it useless, for these reasons BES tools are rarely applied [21], [20] in this phase. To tackle this problem, many user-friendly tools that can be used by non-specialists have been developed [21]. However, this trend was slowed down if not reversed by the growing awareness that without the appropriate knowledge it is not possible to ensure obtaining reliable results [22].

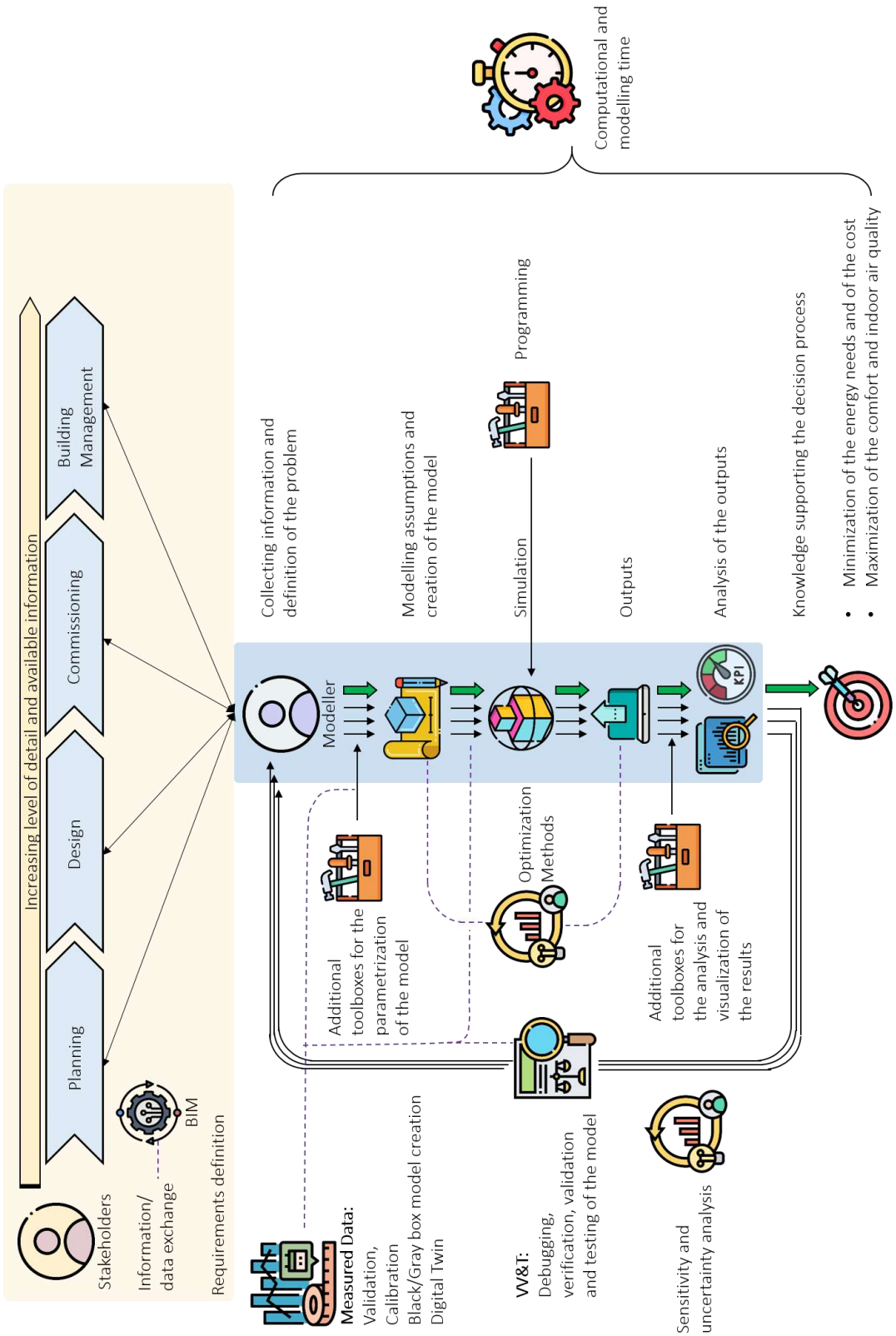

Figure 2: Building energy simulation lifecycle[2].

[2] This Figure has been designed using resources from Flaticon.com

1.2.2 Challenges of the Modelling Process

The design of the model has a strong impact on the data requirements, the computational and modelling time, validity and confidence of the results [23], moreover, a good understanding of the model and its construction process could support the development of automated code generation [24]. The process of abstraction of the real world into a simulation model can be related to the field of conceptual modelling. This process relies on the expertise (i.e. technical knowledge about a specific physical process) and experience (i.e. background in the field of building simulation) of the modeller and it is the most difficult part of the simulation cycle since it should ensure that the model is built at the right level of detail in relation to the objectives or requirements of the given problem [24]. Stewart R. [24] provides a literature review of this field, highlighting that the number of publications remains low and several challenges are still open. One of the first challenges is already the lack of agreement over the definition of conceptual modelling itself, this field encompasses several different areas of research and requires not only scientific but also artistic skills to replicate the reality into the machine. The lack of a definition has made it difficult to define a framework for this topic, and in all likelihood, there will be the need to define different frameworks for the various domains of simulation.

It is often thought that the building simulation process, especially with the new always more powerful whole building simulation tools, is an automatic process where one can get the answer with a few clicks. On the contrary, the simulation study is rarely a one-step process, in most of the cases, once the output step is reached, by analysing the results an experienced user can realise that a mistake has been made or that something needs to be improved in the previous steps and therefore the user needs to go back and repeat the process until the model reproduces the input-output behaviour with sufficient accuracy for the given experimental frame [23]. From this point onwards, the model starts to be useful and can be applied to obtain the knowledge needed to assess the objectives of the analysed problem (see Figure 2).

According to Robinson [23], the conceptual model is built over four main components, namely requirements (i.e., of the model and of the project), inputs, outputs and model content. The project requirements (e.g., time frame, ease of use, etc..) and the modelling requirements (i.e., purposes of the project) influence the model construction. Through the input, the quality of the model can be improved and through the output, it can be assessed if the simulation model is able to support the modelling objective. The model can be described by two main elements: the boundary and the level of detail of each component. During the creation of the model, the modeller is called to make assumptions (necessary due to uncertainties of the real world) and simplifications (necessary to reduce the simulation and modelling time).

From this context, it is clear that if the modeller had a large variety of simulation models available it was possible to follow the process described so far literally. However, in the field of BES, already known tools are typically used, since learning a new one is time expansive. These tools may offer varying levels of detail of the various sub-parts of the model (e.g., thermal zone, windows, walls, etc… or even different approaches for the convective and radiative heat

exchange), but not an infinite number. Moreover, it could be necessary to program a new part of the software to respond to specific requirements that cannot be assessed with the existing tools. Here it is necessary to point out that some BES tools allow the user to modify or add the software parts easily, while others do not (e.g. software like Modelica and EnergyPlus allow the user to visualize and modify the equations of the model while DALEC is an online tool that does not allow the user to modify the code).
Before starting the simulation process, the user should understand if at all, a dynamic simulation is the right tool for answering the project requirements. This analysis could also lead to a negative conclusion for example when: the available models are not able to address the project requirements or it would be too expansive, the problem can be solved with simpler tools, within the project there is not enough time to implement a useful model, the model cannot be verified, etc… [25].
Once it has been established that the simulation is the right tool, the model has to be built as simple as possible to meet the objectives of the simulation study [23]. A simple model requires less modelling and generally less computational time, less data and it is easier to understand leading to higher chances of avoiding user mistakes. It is noteworthy to mention that the potential overall inaccuracy in performance predictions is a function of both the degree of approximation of the physical phenomena as well as the degree of estimation of uncertain input parameters [Publication A]. Therefore, increasing the model complexity without the availability of detailed input data would lead to low accuracy and high cost and at the same time reducing the model complexity too far could require a high effort to well parametrize the model (assumption, simplification and input) in order to reach an acceptable accuracy.

Last but not least it has to be highlighted that the BES does not create solutions or answers to the problems, instead, it helps to increase the understanding of a certain phenomenon and out of this the user (or the decision maker that could be a different person from the user increasing the complexity of the process) has to derive conclusion for his specific case study [9].
Based on the goals the user has to select the most important Key Performance Indicator (KPI) or Quantity of Interest (QOI) to be analysed from the simulation results. Depending on the specific case study the selected KPI can be different (different variants, time scales etc..). Typically, the final goals are to minimize the cost and the energy consumption. Anyway, indoor environmental quality is receiving increasing attention and it is expected that this trend will continue in the future. Therefore it is often necessary to define cost functions where more than one object is addressed [25].

Each step of a building project (i.e., Planning, Design, Commissioning and Management/Monitoring) requires the redefinition of performance requirements and targets. Therefore, the building simulation process reported in Figure 2 has to be retraced and over each step, the model initially defined in the design stage will be modified and enriched in order to

enable the assessment of the specific questions posed by each construction stage. In this framework, the reusability of the input data and of the model or subparts of the model could guarantee significant time savings. BIM aims at creating a common language for the data exchange and management between different tools and different building phases, but unfortunately, it is not yet an integrant part of many BES tools [16].
Reference Models [17] aim at enhancing the standardization and therefore reusability of the models or subcomponents. Nevertheless, as highlighted in [17] this conceptual framework lacks a commonly agreed definition and it is not yet applied in the field of building simulation even though it could lead to high savings in terms of modelling time.

1.2.3 Additional Tools and Methods

In parallel, many methods (e.g., optimization, sensitivity analysis, calibration, etc…) have been developed and can be applied to the building simulation process depending on the specific case study (see Figure 2). For example, optimization methods allow to explore a large design space guiding it towards optimal solutions. Often more than one contrasting optimization target is set. In this case, a multi-objective optimization process should be performed where a Pareto front will be defined as a set of optimal solutions.
Uncertainty and sensitivity analyses can be also included in the simulation process to be able to assess the robustness of the results. Faster models can be generated (e.g., black box model) when a large data set is available (i.e., from measurements or from results of a white-box model). This is achieved by applying techniques such as artificial neural networks. The generated model has the advantage to be faster and therefore can be easier applied in optimization, sensitivity, uncertainty analyses or real-time simulation nevertheless they are generally only applicable within the boundary of the available data with which they have been built [20].
Gray box model represents another option to perform building simulation using a simplified or reduced-order model that is computationally more efficient compared to a white box model and at the same time more interpretable than a black box model [26]. Nevertheless, gray box models require an extensive parametrization that can be carried out by applying a forward (i.e. direct calculation) or an inverse approach (i.e. data-driven algorithm) [26].
The application of digital twin is also receiving increasing attention in the last years and its main application is to track and predict the health status (i.e. fault detection) of the simulated object [15]. The definition of digital twin is not univocally defined within the scientific community, nevertheless, it differs from a standard simulation process due to the fact that in a digital twin a data exchange between the model and the physical object is carried out to keep the model consistent with the physical object [15].

1.3 Building Energy Simulation and Credibility

One of the main challenges that also prevent BES to be further spread is the quality assurance of the results and of the decision derived from the results.

First of all, it is important to pinpoint that:

- All simulation models are a simplification of the reality [27];
- In general, the aim should be: to keep the model as simple as possible to meet the objectives of the simulation study [23];
- No model can be completely validated, instead, it is only possible to increase the level of confidence [28].

While for every instrument and measurement the uncertainty has to be defined and clearly stated, the same cannot yet be said for the field of building simulation. Especially nowadays that the buildings are becoming increasingly efficient, a high building simulation uncertainty could make the simulation completely useless. This problem has been highlighted in many papers [28], [29], [23].
A model can be defined as valid if it is sufficiently accurate for the specific case study [23], anyway this definition is difficult to be applied in practice as it lacks quantitative criteria.

1.3.1 Performance Gap Hampering Building Simulation Credibility

As highlighted in [28] and [25] the field of uncertainty analysis, verification and validation for BES is receiving increasing attention but at the moment there is a lack of standards defining clear guidelines, a common vocabulary and reference quantities. As highlighted in [30] different papers refer to the same statistical index using different equations.
The increasing awareness in the field of uncertainty analysis and risk assessment of building simulation is driven by the so-called performance gap, namely the difference between measured and prediction of the building performance that has been often detected [31], [32]. The causes of the performance gap can be related to the design (e.g., unpredictable future use and performance deterioration of the building, correct implementation of the model depending on the case study etc..), construction (e.g., actual quality of the building not in accordance with the specifications) and operational stages (e.g., occupant behaviour) [32]. In the construction process of a real building, BES tools are not often applied, instead, certification tools (e.g., energy classification) and standard calculation (e.g., heating and cooling demand and load) are used, where standard and simplified assumptions for the occupancy are applied, unavoidably leading to a performance gap.

When measurements are available (e.g., when the analysed building reaches the operational stage) it is possible to assess the uncertainty of the model against measured data. In this case, the uncertainty of the measurements has to be included in the analysis. [32] highlights the need of improving the building monitoring to depict also construction errors and occupants' behaviour, developing a solid approach for model calibration and transferring this knowledge to the actual building engineering practice. The calibration of the model can close the performance gap, anyway, does not improve the quality of the mathematical model, and there might be different combinations of model parameters that equally well contribute to a better fit of the model results with the measured data [28]. In addition after the calibration, the model should be subjected to a validation process using a different data set compared to the calibration [28].

At the design stage, when measurements are not available, benchmark data or shared dataset could be used for a plausibility check. Anyway, there is the need to assess and reduce the sensitivity of the building's performance to uncertain environments [33]. The robustness of the building energy performances against uncertainties (e.g., occupant behaviour, climate etc…) can be analysed using probabilistic and non-probabilistic approaches. Sensitivity analysis techniques can also be used to reach a robust design [34] and uncertainty analysis can be applied together with sensitivity analysis techniques to assess the risk of a certain design concept [35]. Uncertainty analysis considers uncertainties in the input parameter assigning a probability distribution while sensitivity analysis aims at modifying model input to assess the impact on the outputs [35]. Although these techniques can be a very useful means to assess a design risk and improve the credibility of BES, they are very computationally expensive due to the high number of required simulations [34] and therefore not very used in practice [32].

1.3.2 Verification, Validation and Testing Techniques

To enhance the credibility in building simulation it is necessary to test the model and its inputs in order to verify (i.e., for the identification of errors or inaccuracy in the model) and validate the model (i.e., to guarantee that the model is accurate for the objectives of the specific case study) [28], [25]. The testing techniques can be validation-oriented or verification-oriented [25].

Judkoff [36] classified the sources of errors of a simulation program as internal sources of errors:

- Simplification of the equations describing the actual physical process;
- Inaccuracy or errors in the numerical solution of the equations;
- Coding errors.

And external sources of errors:

- Differences between the actual weather and the weather data used in the simulation;
- Differences between the actual effect of occupant behaviour and the one assumed in the simulation;

- User errors in deriving the building input files;
- Differences between the actual thermal performances and the building properties assumed in the simulation.

In addition, Judkoff [36] described a verification and validation methodology including three steps:

- Analytical verification;
- Empirical Validation;
- Code-to-Code comparison.

All three approaches (i.e., analytical, empirical and code to code) have pros and cons. As an example, an analytical solution is only available for simple configurations (e.g., wall model). Empirical validations have to deal with measurement uncertainties and are usually limited to a specific amount of data for a limited period of time. Cross-validation enables to analyse many different configurations and to minimize the input uncertainties, nevertheless, the definition of the set of reference results is a challenging task. In both empirical and code-to-code validations, it is always important to have in mind that all possible error sources can act together offsetting each other and preventing the user to conclude on the accuracy of the results.

1.3.2.1 Tool Verification

Firstly, when a new tool is developed it has to be tested in order to correct and exclude any programming errors. This approach was then adopted by the well-known BESTTEST methodology [37], [38], where a series of test cases are described and reference results against which a tool can be tested are provided. This can be classified as a verification method against which the modelling errors can be identified and corrected. Nevertheless, the reference results are in turn generated with a simulation tool subject to error, the sources of error are not differentiated (i.e. input, model, numeric), the purpose is not defined and the acceptability span can be in some cases quite high (i.e. up to 47% [39]).

1.3.2.2 Conceptual model verification and validation

Once the tool has been tested and it is ready to be used, having a testing procedure for the conceptual modelling phase would be of great support for the modeller. Balci [40] with the proposed verification validation and testing techniques (VV&T) aims to assess the correctness of the whole modelling process. In fact, the accuracy of the model is important but also the accuracy of the formulation of the problem plays a key role in the final accuracy of the results (see also Section 1.2). This technique (VV&T) aims to avoid three main types of errors:

- I overcomplicating the model because it is believed that the model is not credible;
- II oversimplifying the model because it is believed that the model is credible;
- III creating a model that is suitable only for different problems.

The first type of error makes the simulation study costly the second and third types of error lead to useless results. Nevertheless, Balci himself [40] concludes that the integration of the VV&T techniques throughout the simulation lifecycle would be time-consuming and costly.

1.3.2.3 Validation against measured data

When a set of reference results for the specific case study is available, it is possible to compare the predicted performances against the reference dataset. In this framework, the Uniform Methods Project [41] and ASHRAE Guideline 14-2014 [42] are widely recognized guidelines aiming at establishing a method for measuring the accuracy of building models as well as the Federal Energy Management Program (FEMP) [43] and the International Performance Measurement and Verification Protocol (IPMVP) [44], which refer to ASHRAE Guideline 14-2014 [42]. These documents suggest thresholds, which are different for monthly or hourly results, for the Normalized Mean Bias Error (NMBE) and Normalized Root Mean Square Error (NRMSE). In addition, it has been suggested to analyse a time frame of at least one year and to compare the simulation results with the utility bills and/or spot measurements. However, as highlighted in [45], calibration approaches do not address the indoor condition and temperatures.

1.4 Research Objectives

From Section 1.1 it is clear that to reach the climate goal all new buildings and buildings under renovation have to reach a high-quality standard and integrate renewable sources, transforming the buildings from consumer to prosumer. In this framework, BES can contribute to speeding up the design process and guiding to optimized building performance at the lowest cost. Nevertheless, as described in Sections 1.2 and 1.3 BES diffusion suffers from a lack of credibility. Nowadays many whole simulation tools are available which also offer different approaches for each part of the model. In general, there is a tendency to use overly complicated tools as if this would increase their credibility. Actually to improve the simulation accuracy and minimize computational and modelling time, as pointed out in section 1.2, the user should decide which model has to be used according to the available data and the purpose of the simulation.

This research aims at:

A. Supporting the users in choosing a fit-for-purpose simulation tool by providing a broad overview of the modelling approaches available in white-box models widely used in the academia (i.e. EnergyPlus, TRNSYS, Simulink libraries CarnotUIBK and ALMABuild, IDA ICE, Modelica/Dymola buildings library and DALEC) as well as PHPP (a widely used quasi-steady-state planning tool), comparing also the computational time and the parametrization effort for a given case study;
B. Showing the impact of the parametrization process on the results for the given case study considering the tools used in point A. The parametrization process required by

tools implementing a higher or lower level of detail with respect to the available data is thoroughly described and the impact on the results is reported;

C. Supporting the user in choosing a fit-for-purpose modelling approach.
   To achieve this, the modelling approaches of the different tools used in the comparison (point A) are analysed, together with a new dynamic model for the evaluation of the mean radiant temperature field (developed and cross-validated within this work), by means of the cross-validated Simulink model in order to assess the influence of each modelling approach on the results and computational time;
D. Shedding some light on the strengths, weaknesses, and applicability of the mainly used statistical indices and normalization means for the evaluation of the deviations;
E. Showing an example of techno-economic analysis for the minimization of equivalent annual cost and final energy demand. This is carried out, using the cross-validated Simulink model (point A), considering different heating systems, lighting technologies and control strategies in combination with photovoltaic panels and batteries.

2 Methodology

2.1 Comparison of Building Energy Simulation Tools

A reference office cell is described within the framework of the IEA SHC Task 56 [41], [42] and the report is distributed to different research groups with the aim to implement the model of the same office cell using different BES tools.
The following white-box models, widely used in the academia, are included in this comparison:

- EnergyPlus;
- TRNSYS;
- Matlab/Simulink using the CarnotUIBK and ALMABUILD Simulink libraries;
- IDA ICE;
- Modelica/Dymola buildings library.

In addition, DALEC, a simplified simulation tool focused on daylight analysis and PHPP, a design excel tool are included in the comparison.
Most of the white box tools offer a range of modelling approaches with different degrees of detail while the simplified tools (e.g., Passive House Planning Package-PHPP and DALEC a design tool focused on daylight applications[3]) offer only simplified calculations of the thermal balance. Tools with different focuses also have various levels of detail in different sections of the model (e.g., DALEC is focused on daylight simulation while the calculation of the thermal balance of the zone is simplified). In [Publication A] an overview of all the different modelling approaches of the different tools is given. In addition, the computational time for each tool for the given case study is also reported in [Publication A].

2.1.1 Parametrization of the different models

Despite the fact that the description of the input is comprehensive, in order to reach an acceptable agreement between the results of the different BES tools, many iterations have been necessary.
To achieve a good agreement, it is essential to identify user mistakes and the influence of the adopted assumptions and simplifications on the results. All the components of the energy balance on a monthly and hourly basis are analysed, as the various sources of error can act simultaneously leading to a cancellation effect (e.g., higher losses can balance higher gains leading to the same energy demand).

[3] The calculation of the energy balance for both DALEC and PHPP is based on the standard EN ISO 13790. DALEC performs dynamic hourly calculations while PHPP is based on quasi steady state monthly balances.

The early stage of this comparison is published in [Publication F] and the final work in [Publication A], where the influence of the parameterization process of the models that require higher or lower input details compared to the building description is reported, as well as the applied modelling approaches of the different tools and the user mistakes that have been made in this specific case study.

2.1.2 Analysis and Quantification of the Deviations

One additional important aspect, analysed in [Publication A], is the analysis of the deviation between the results of the different tools. The commonly used statistical indices and normalization means are critically analysed to help shed some light on their application. The hourly results and equations used for the analysis of the deviations are published in [Publication C] to make this dataset available for future cross-comparisons.

2.2 Modelling Approaches and Level of Detail

The different modelling approaches available in the white box models used in the comparison of [Publication A] are implemented into the cross-validated Simulink model and compared in terms of computational time and influence on the results. This comparison is carried out using only one platform (i.e., Matlab/Simulink) to be able to exclude other sources of deviations.
The analysed approaches cover different levels of detail for the different sub-models:

- Thermal zone;
- Air capacity;
- Distribution of the internal radiative and solar gain;
- Convective and radiative heat transfer;
- Window;
- Adiabatic structure;
- Sky;
- Preruntime;
- Solver.

All the components of the thermal balance are analysed for each variation to better understand the effect of each approach on the results but a weighted average between the Goodness of Fit (GOF) calculated on the heating and cooling demands is used as the main indicator together with the computational time. In the calculation of the GOF the NRMSE and NMBE are used since the combination of these two indices allows depicting deviations related to final energy demand (i.e., NMBE) and deviations in terms of dynamic behaviour (i.e., NRMSE).

Typically building simulations are applied to minimize the energy demand while maximizing comfort. In this regards the accuracy of the predicted room temperature plays an important role.

The different models of the thermal zone typically used in BES allow the prediction of the thermal zone temperatures with different degrees of accuracy.
In particular within this work (see [Publication D]) a model for the calculation of the radiant temperature field is developed in Simulink and cross-compared against TRNSYS 18 model implementing a similar approach and then used in the comparison reported in [Publication B]. The operative temperature predicted by the simplified approaches is compared against the operative temperature predicted by the developed model (RM) in different points of the office cell to show the differences.

It has been necessary to implement a new model able to bridge the gap between an excessive computational time (e.g., CFD or co-simulation) and level of detail (i.e., allowing at the same time to simulate the radiative temperature field). This is done in [Publication D] where such a model has been implemented in Simulink. The calculation of the view factors is necessary to enable the calculation of the surface-to-surface radiative exchange and of the radiative temperature field. This task is accomplished using the Matlab Contour Double Integral Formula (CDIF) routine, which results are compared against the calculation carried out with two commercial software (i.e., TRISCO and Comsol Multiphysics). Using the developed model, the behaviour of six different heat emitters (i.e., classic floor heating, ceiling, lightweight suspended ceiling, hot water radiator, wall heating and convective heating) are compared using the model of one room of a residential building considering also different insulation levels of the envelope. This comparison is carried out by analysing the differences in terms of vertical and horizontal distribution of the operative temperature in the different cases, considering the different dynamic behaviour of the different heat emitters and also calculating the Predicted Mean Vote (PMV) distribution within the room.

2.3 Specific Case Study – Techno-Economic Analysis

The model of the office cell implemented in Matlab/Simulink and cross-compared in [Publication A] is used in [Publication E] to analyse the impact of different control strategies and Heating Ventilation and Air Conditioning (HVAC) configurations including also renewables on the primary energy and cost calculated as equivalent annual cost using the annuity method. The input parameters used for the cost analysis are varied to assess their influence on the results of the cost analysis. The primary energy is calculated considering monthly conversion factors as explained in [43]. The implementation of technologies for the reduction of primary energy typically implies also additional costs leading to a problem in which contrasting goals have to be minimized. This results in the definition of a Pareto front from which the “best” solutions can be highlighted.

3 Main Results and Discussion

3.1 Comparison of Different Tools and Parametrization Process

A description of the modelling approaches of the tools included in the (i.e., EnergyPlus v.9.3, TRNSYS 18, Simulink/CarnotUIBK, Simulink/ALMABuild, IDA ICE v.4.8, Modelica Buildings library v.5.0.1 together with Dymola v. 2020x, DALEC and PHPP) is provided in [Publication A]. In addition, the difficulties encountered during the setting up and parametrization process are described for the specific case (i.e., an office cell located in Rome, Stuttgart, and Stockholm with different building envelope properties).

To reach a good agreement between the different tools many loops were necessary ([Publication A] and [Publication F]). Table 2 (from [Publication A]) reports the annual heating demand (HD) and cooling demand (CD) of the different tools, considering the climate of Rome (ROM) and Stockholm (STO), for different iteration loops. In addition, the maximum and minimum NMBE are reported considering as reference the median value. On the right side, the box plot gives an impression of the span reduction between the results of the different tools throughout the different iterations.

Table 2: Annual Heating and Cooling demand for each tool in the climates of Rome and Stockholm through the different iteration rounds (V1, V2 and V3) required to reach a good agreement (taken from [Publication A]).

		V1 (04/2018)		V2 (04/2019)		V3 (04/2021)	
		HD	CD	HD	CD	HD	CD
		[kWh/m^2]					
ROM	EP	1.0	-51.2	3.6	-36.4	3.9	-32.3
	TRN	3.4	-32.4	3.5	-33.3	3.5	-31.4
	SIM_IBK	7.9	-29.9	5.8	-38.2	3.2	-30.5
	SIM_BO	-	-	3.1	-33.4	3.5	-31.3
	IDA	-	-	-	-	3.4	-33.5
	MOD	-	-	7.1	-34.0	4.0	-31.3
	DAL	6.1	-31.0	5.9	-35.9	3.8	-31.0
	PHPP	-	-	5.7	-37.9	3.0	-30.8
	MEDIAN	**4.7**	**-31.7**	**5.7**	**-35.9**	**3.5**	**-31.3**
	Max NMBE	67%	61%	25%	6%	12%	7%
	Min NMBE	-79%	-6%	-46%	-7%	-16%	-2%
STO	EP	13.5	-34.6	17.0	-32.2	16.7	-24.4
	TRN	20.4	-23.3	21.3	-23.8	18.2	-23.8
	SIM_IBK	15.0	-23.8	14.5	-31.0	16.9	-23.4
	SIM_BO	-	-	17.4	-23.6	17.1	-24.0
	IDA	-	-	-	-	18.1	-24.0
	MOD	-	-	14.5	-30.0	16.9	-24.1
	DAL	14.2	-21.8	16.9	-28.2	18.0	-24.9
	PHPP	-	-	14.6	-31.0	17.1	-24.3
	MEDIAN	**14.6**	**-23.5**	**16.9**	**-30.0**	**17.1**	**-24.1**
	Max NMBE	40%	47%	26%	7%	6%	3%
	Min NMBE	-7%	-7%	-14%	-21%	-2%	-3%

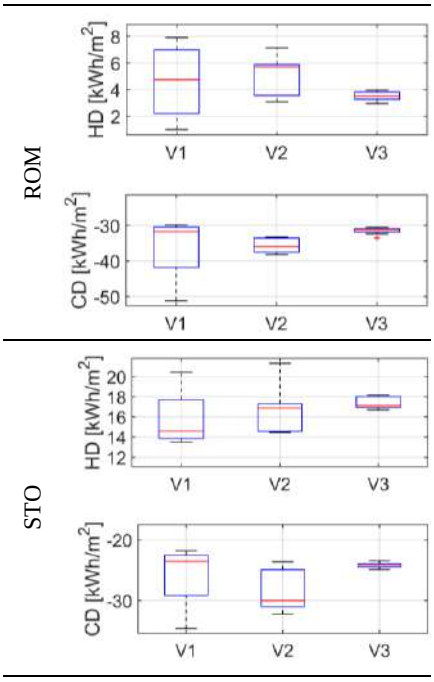

Throughout the different iterations, the user mistakes were detected and corrected:

- Flipped order of the layers of the constructions;
- Calculation of the heat transfer coefficient;
- Weather file;
- Starting day of the internal load profiles;
- Thermal capacity of the walls;
- etc...

Besides the user mistakes, the different researchers interpreted differently the building description (e.g., control logic of the ventilation, shading etc..). In addition, missing information was replaced by predefined data that assumed different values in the different tools (e.g., air density, emission and absorption coefficient, convective exchange coefficients etc…).

Tools that are either more simplified (e.g., PHPP and DALEC) or more complex (e.g., Modelica and EnergyPlus), with respect to the building description written using TRNSYS as a reference, required a tedious parametrization process. The window model and its input parameters highly influence the results in this specific case study. The properties at the glazing level of the glazing system were given as input, while EnergyPlus and Modelica require data at the level of the individual windowpane. To retrieve this information starting from a lower level of detail was time-consuming and error-prone.

In addition, not all tools allow the user to model the complex control logics required for this case study (i.e., control of the ventilation and shading systems). In particular, PHPP, being based on monthly balances, does not allow for implementing a dynamic control strategy, therefore a parametrization process was necessary to define the constant ventilation rate and shading coefficients to be used in PHPP using the results of the other more detailed dynamic simulation tools. In DALEC was as well necessary to parametrize the control of the shading, and of the ventilation system. In addition in both tools, the constant U value of the windows was parametrized based on the results of the dynamic simulation tools (see [Publication A]).

Table 3 (from [Publication A]) reports the annual heating and cooling demands and their relative deviation to the reference result for the stage pre and post-parametrization of PHPP and DALEC.

Table 3: Annual Heating and Cooling demand (HD, CD) calculated with DALEC and PHPP pre and post-parametrization compared against the reference heating and cooling demand (median of all the tools), for the climate of Stockholm [Publication A].

	HD [kWh/(m^2)]	ΔRef [%]	CD [kWh/(m^2)]	ΔRef [%]
DAL_online	17.8	1%	-17.0	-30%
DAL_par	18.0	2%	-24.9	3%
PHPP_nonpar	6.3	-64%	-21.5	-11%
PHPP_par	17.2	-2%	-24.3	1%
Reference	**17.5**	**-**	**-24.1**	**-**

It is recommended to define input parameters starting at the most detailed scale and the lowest level of abstraction to reduce the number of assumptions and simplification that the modeller has to apply or to select the tool/model accordingly to the available data. Typically, during the design stage of a building project, detailed input might not be available and the problems to address change rapidly, therefore it is favourable to dispose of simplified calculation or simulation approaches that allow fast evaluation based on limited input availability.
At the same time, it was demonstrated that simplified tools if well parametrized could reach a good agreement with the other more sophisticated tools at least in terms of annual energy balance.

3.2 Quantification of Deviations

During the comparison of the results of the different tools [Publication A], it was important to consider all the components of the thermal balance and the predicted temperatures since higher gains could be compensated by higher losses (or vice versa) leading to the same energy demand. Moreover, to assess the cause of deviations, it was important to perform additional simulations to isolate particular phenomena. In contrast to what could be expected, some components of the energy balance are defined differently within the various tools (e.g. solar gains can be defined as the directly transmitted part or the directly transmitted plus the part that is absorbed and reemitted internally consequently also the definition of the window transmission losses will change and transmission losses of the opaque structure can be defined as the total flux in different points of the structure). Therefore, each modeller needed to review the definition applied in the used model to understand how the outputs are defined and finally be able to consistently compare the results against the reference. In a real simulation study, where typically there are no means of comparison, many of these mistakes could remain undetected.
To enable the comparison of the results it was necessary to define a set of reference results, decide the reference time frames, select the outputs to be compared, and decide which indices and thresholds have to be used. Each of these points represented a challenge as there is a lack of guidelines in this field.
It was decided to use the median of the results of all the tools for each time step as a reference dataset to reduce the dependency on the outliers. In addition, the results were compared on an hourly, monthly, and annual basis.
The quantification of the deviations and the assessment of whether deviations can be considered acceptable represented quite a challenge. The thresholds suggested by ASHRAE Guideline 14–2014 were used as a basis for this evaluation. The widely used statistical indices and normalization means were analysed to derive general guidelines:

- The MBE/NMBE is needed to show the sign of the deviation, but another index has to be used since the MBE suffers from the cancellation effect;
- The R^2 is not a good index when the analysed variable is mainly constant;
- The normalization of the RMSE is a complex step and has to be performed carefully, especially when the average of the dataset lies close to zero. This is often the case in the

field of BES when for example hourly heating or cooling powers are considered (e.g., summer for heating and winter for cooling or typical day/night behaviour) leading to an infinite NRMSE. In these cases, an alternative normalization means has to be selected (e.g., average value excluding the values equal to 0);

- Having a larger dataset (hourly data for the entire year) makes the evaluation of the deviations more robust. Therefore, when hourly data are considered, the indices should be calculated over the whole year;
- The absolute thresholds suggested by ASHRAE Guideline 14– 2014 can lead to misleading conclusions regarding the validity of cases with low energy demand (i.e., high-quality buildings or warm climates).

The hourly results of the cross-validated tools (i.e. EnergyPlus v.9.3, TRNSYS 18, Simulink/CarnotUIBK, Simulink/ALMABuild, IDA ICE v.4.8, Modelica Buildings library v.5.0.1 together with Dymola v. 2020x, DALEC) were published in [Publication C]. This publication provides a wide dataset that can be used for the validation of other models for the simulation of office buildings. The published dataset reports hourly results of each component of the energy balance and of the convective and radiative temperature. In addition, the excel sheets ease the calculation of the main used statistical indices and can be used for a detailed evaluation of deviations also for other typologies of buildings rather than only an office cell. When measured data are available, these can replace the median value, used as a reference, extending the usability of the proposed excel sheet to different case studies. Of course, also the measurement has uncertainties and errors that should be evaluated separately.

3.3 Evaluation of the Different Modelling Approaches

The different modelling aspects of the tools included in the comparison [Publication A] were implemented one at a time in the cross-validated Simulink tool and compared against the reference model [Publication B]. For each variation, all the components of the energy balance and the temperatures of the thermal zone were analysed, and the computational time was measured. The Goodness of fit (GOF) calculated as a weighted average between the GOF of the heating and cooling demand was used as an indicator of the deviation of the results from the reference case (for more details see [Publication B]). NRMSE and NMBE were used for the calculation of the GOF since the combinations of these two indices allow to depict deviations related to final energy demand (i.e., NMBE) and deviations in terms of dynamic behaviour (i.e., NRMSE). Depending on the aim of the study, more importance can be attributed to the dynamic behaviour of the model (i.e., NRMSE) or to the overall energy balance (i.e., NMBE). In this case study, the same weight is assigned to both indices.

In this work [Publication B], the numerical model developed in Simulink (RM) [Publication D] for the calculation of the surface-to-surface radiative exchange and the radiative temperature

field was cross-compared against a similar approach developed in TRNSYS 18. The Simulink model was then included in the comparison of different modelling approaches [Publication B] to assess the influence of the thermal zone model on the predicted room temperature and thermal balance. The modelling approaches included in this comparison are:

- the two-star model (REF);
- detailed radiative model (RM);
- one-star model with one capacity for the whole building (TS1s UA);
- one-star model coupled with finite difference –RC– model of the walls (TS1s).

Figure 3 (from [Publication B]) reports the hourly operative temperature of the RM considering different positions within the room against the hourly operative temperature of the REF, TS1s and TS1s UA models (the windows are placed in the plane at y=0).

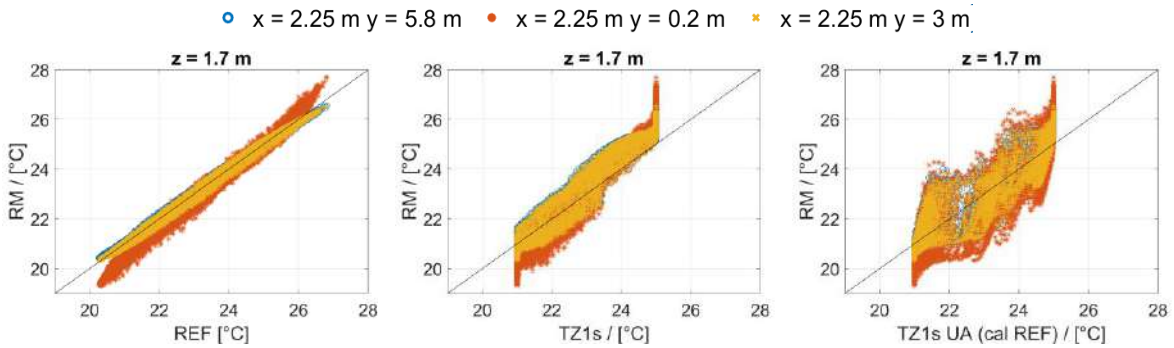

Figure 3: operative temperature of the two-star model (REF) vs the detailed longwave radiation model (RM) for the climate of Stockholm at 1.7 m from the floor considering different sensor positions within the room (i.e. blue circle [x: 2.25 m, y: 5.8 m], facing the window: red asterisk [x: 2.25 m, y: 0.2 m] and in the centre of the room: yellow plus [x: 2.25 m, y: 3 m]) (from [Publication B]).

The two-star model (REF) presents a good agreement with the detailed longwave radiative exchange approach (RM) in terms of energy demand and operative temperature in the centre of the room, but deviations are present when the operative temperature of the two-star model is compared with the operative temperature near the window of the RM (see Figure 3). The RM can deliver more detailed information about the temperature distribution within the room but at the same time, it requires higher computational time and detailed geometry inputs.

The one-star models allow the simulation of only one temperature of the thermal zone, which can be correlated to the operative temperature. This leads, as highlighted in Figure 3, to deviations due to a simplified model of the capacity of the thermal zone and to a different control of the HVAC system (since it will be controlled on the operative temperature instead of the convective as required in this case study).

Nevertheless, when the building capacity of the simplified model is calibrated using the results of the reference model, it can reproduce the energy demand of the building with an accuracy that can be acceptable for some applications and significantly reduced computational time (i.e. this might be beneficial when a high number of simulations have to be run such as in multi-objective optimization).

Within this work [Publication B], it was assessed that simplifying the model does not always lead to a lower computational time (e.g. increasing the capacity of the convective node considering the furniture allows to speed up the simulation and improves the quality of the results[4]). In this case study, the window model played an important role in the energy balance, in particular, the simplified window model based on a constant heat transfer coefficient can lead to high deviations in terms of transmission losses, especially when the given heat transfer coefficient is measured under boundary conditions that are different from the average boundary conditions applying during the simulated period. At the same time, a detailed window model requires the knowledge of a high number of inputs (i.e., optical properties at each side of each glass pane) that are not always available.

In publications [Publication D] the developed numerical model for the calculation of the radiative temperature distribution was applied to analyse the influence of different heat emitters (i.e. floor, ceiling, wall surface heating systems, radiator and convective heating system) on the energy demand, and comfort conditions considering also different envelope qualities (the radiator size was increased with the poorer envelope quality while the size of the other heat emitters was kept constant). It was highlighted that the radiant floor heating system can guarantee good performance both in well thermally insulated as well as poorly-thermally insulated rooms. Nevertheless, with a well thermally insulated envelope the maximum surface temperature of the heat emitters is reduced leading to a more uniform temperature field within the room and therefore higher comfort. Also, the maximum floor surface temperature is restricted due to comfort and health reasons.

3.4 Techno-Economic Analysis

In [Publication E] the cross-validated model of the office cell (see [Publication A]) was used to analyse the impact of different technologies and control strategies on the primary energy and cost savings considering different climates (i.e., Stockholm, Stuttgart, and Rome). The minimization of both cost and primary energy leads to the definition of a Pareto front composed of the best solutions (see Figure 4 [Publication E]). The solutions allowing high-energy savings with low additional cost are represented, in Stockholm and Stuttgart, by heat pump in combination or not with LED and PV. Since Rome is characterized by a low heating demand the installation of a heat pump only for heating purposes cannot lead to high energy savings[5].

[4] Increasing the capacity (in this case of the convective node) leads to a slower variation of the convective temperature, which in turn allows the calculation to be made with an increased time step.

[5] In this study a pre-existing split unit for cooling purpose was considered and the installation of a heat pump for heating was calculated with the full cost of an additional machine. If the cooling heat pump could be used for heating purpose without additional costs, this would be of course beneficial in comparison to a direct electric heating system.

In all the analysed climates the application of a battery system in combination with air-to-air heat pump, PV, and LED leads to limited energy savings with high additional costs.

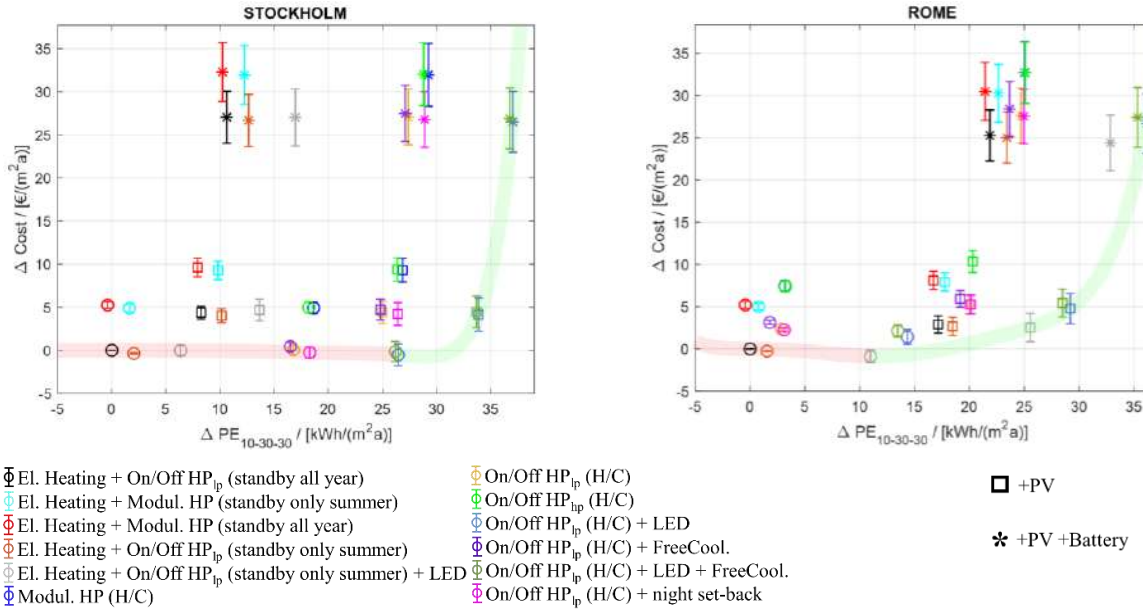

Figure 4: Primary energy savings according to 10-30-30 scenario conversion factors vs additional cost of the analysed technologies for the climates of Stockholm and Rome (from [Publication E]).

In addition, it was highlighted that the choice of the primary energy conversion factors (e.g., monthly factors vs an annual constant factor) could influence the ranking of the technologies.

4 Conclusions and Outlooks

This thesis provides insights into the different steps of the simulation cycle aiming at supporting a future user of building simulation tools to increase the simulation accuracy while minimizing the computational and modelling time.

In this work, an overview of the modelling approaches offered by widely used white box building simulation tools (i.e. EnergyPlus v.9.3, TRNSYS 18, Simulink/CarnotUIBK, Simulink/ALMABuild, IDA ICE v.4.8, Modelica Buildings library v.5.0.1 together with Dymola v. 2020x, DALEC and PHPP) is provided and the model of a reference office cell has been implemented by different researchers using the different tools. This work highlighted that without any quality control, the results of the different tools had deviations up to 61% for the annual cooling demand and 40% for the heating demand. The deviations were then reduced to a maximum of 7% for the annual cooling demand and 6% for the heating demand by finding user mistakes, correcting misinterpretation of the building description, and performing a parametrization process for the tools with different levels of detail compared to the given description of the building. The parametrization process was time expansive but fundamental to define equivalent input for tools implementing different modelling approaches, therefore, leading to results in good agreement. With predesign tools such as PHPP it is not straightforward to model aspects such as dynamic shading and ventilation control, which are required by this case study. Using the results of the other dynamic simulation tools, it was possible to parametrize the seasonally constant parameters defining the ventilation rate and shading coefficients for the summer and winter period reducing the deviations from - 64% to - 2% for the heating demand and from -11% to 1% for the cooling demand. Nevertheless, also tools such as EnergyPlus and Modelica required a parametrization of the window properties as the building description provided information at the glazing level while data at the level of the individual windowpane were required.

To speed up this step it is advisable to define the input parameters starting at the most detailed scale or when this is not possible (e.g., during the planning phase detailed information might not be available) to use a tool that requires input with a level of detail compatible with the available data.

Comparing the results of the various tools presented several challenges, in particular, it was necessary to define a reference, select statistical indicators to quantify deviations and define thresholds for these indicators to delineate when a set of results can be perceived as acceptable. Normalized Mean Bias Error (NMBE) and Normalized Root Mean Square Error (NRMSE) were used to assess the degree of agreement of the results with the median value used as a reference. The RMSE is usually normalized using the average of the reference results,

nevertheless, this could be problematic when the average value approaches zero (e.g., heating power might be zero during the interim season and in summer). Therefore, the average of the absolute values higher than zero was chosen as normalization means for the RMSE.
The thresholds for NMBE and NRMSE suggested by ASHRAE Guideline 14-2014 were used as a basis even though it was highlighted that they can lead to unjust conclusions regarding the validity of cases with low energy demand (i.e., high-quality buildings or warm climates).
In addition to the comparison of the results and the overview of the modelling approaches, also the computational time was reported to provide a complete overview of the performances of the different tools included in the comparison.
From these results, it can be concluded that, excluding the user errors, the potential overall inaccuracy in performance predictions is a function of both the degree of approximation of the physical phenomena as well as the degree of estimation of uncertain input parameters. In addition, the evaluation of the inaccuracy should be always put in relation to the goal of the simulation study.
To better address these aspects, the different modelling approaches were implemented in the cross-validated Simulink model to analyse the influence of each modelling approach on the results' accuracy and computational time. The results were evaluated using the Goodness-of-Fit for the energy demand and the Mean Absolute Error for the temperature. In this comparison, special attention was paid to the thermal zone model and the predicted temperature.
A Matlab/Simulink model able to simulate the 3D distribution of the mean radiative temperature was developed, cross-compared against TRNSYS 18 and used as a reference to show the deviation of the predicted room temperature of simplified thermal zone modelling approaches (i.e., two-star and one-star models). The deviations were particularly high near the window, therefore, when comfort has to be analysed or when the heating and cooling control logic is influenced by the radiative temperature field, it can be important to use a model, which allows the calculation of the temperature distribution.
It was also found that many aspects, which are often overlooked (e.g., adiabatic structure model, capacity of the air node, convective and radiative exchange coefficients, sky model and distribution of the solar and internal gains over the surfaces of the enclosure) affect the energy balance of the building and do not always lead to a reduction of the computational time. As an example, increasing the capacity of the convective node including the thermal mass of the furniture reduces the computational time, while increasing the accuracy of the results[4]. In addition, for this case study it was found that the results are strongly affected by the accuracy of the window model. The simplified window model based on a constant heat transfer coefficient led to high deviations, especially when the heat transfer coefficient given as input to the window model is measured with boundary conditions that are different from the average conditions of the simulation study. Nevertheless, the detailed window model requires the knowledge of a high number of inputs that are not always available

Finally, the cross-validated Simulink model was used to perform a techno-economic analysis considering different technologies applicable for the renovation of an office building (i.e., heat pumps for heating and cooling purposes in combination with photovoltaic panels - PV, battery, and efficient LED lighting). To assess the environmental impact, the primary energy was calculated by applying constant and monthly conversion factors representing different scenarios with different shares of renewables in the electricity mix. High-energy savings with low additional cost are achievable with heat pump in combination or not with LED and PV, in Stockholm and Stuttgart, and with LED and PV in combination with electric heating in Rome[5]. Battery brings additional energy savings with high additional costs.

In future work, the same methodology could be applied to multi-zone simulations showing how the different tools allow modelling the heat transfer and air exchange between the different thermal zones and providing insights about how to select a specific zoning strategy for a given building.

5 Relevant Publications

This chapter includes the relevant publications of this thesis. Every publication is in the original format and is included here with the permission of the corresponding editor.

5.1 Publication A

Title

Detailed cross comparison of building energy simulation tools results using a reference office building as a case study

Authors

Mara Magni, Fabian Ochs, Samuel de Vries, Alessandro Maccarini, Ferdinand Sigg

Published in

Energy & Buildings 250 (2021) 111260
https://doi.org/10.1016/j.enbuild.2021.111260

Own contribution

Coordination of the data exchange and analysis of all the data as well as the development of the methodology and the writing of the paper. The first Author modelled the reference office cell using the following tools/libraries: ALMABuild, CarnotUIBK, Dalec, PHPP and TRNSYS.

Energy & Buildings 250 (2021) 111260

Contents lists available at ScienceDirect

Energy & Buildings

journal homepage: www.elsevier.com/locate/enb

Detailed cross comparison of building energy simulation tools results using a reference office building as a case study

Mara Magni [a,*], Fabian Ochs [a], Samuel de Vries [b], Alessandro Maccarini [c], Ferdinand Sigg [d]

[a] University of Innsbruck, Unit for Energy Efficient Buildings, Innsbruck, Austria
[b] Eindhoven University of Technology, Eindhoven, the Netherlands
[c] Aalborg University Copenhagen, Denmark
[d] Rosenheim Technical University of Applied Sciences, Germany

ARTICLE INFO

Article history:
Received 18 February 2021
Revised 28 May 2021
Accepted 4 July 2021
Available online 7 July 2021

Keywords:
Statistical indices
Computational cost
Modelling approaches
Cross comparison
Building Simulation

ABSTRACT

Building Energy Simulation (BES) tools play a key role in the optimization of the building system during the different phases, from pre-design through commissioning to operation. BES tools are increasingly used in research as well as in companies. New BES tools and updated versions are continuously being released. Each tool follows an independent validation process but rarely all the tools are compared against each other using a common case study. In this work, the modelling approaches of widespread dynamic simulation tools (i.e. EnergyPlus, TRNSYS, Simulink libraries CarnotUIBK and ALMABuild, IDA ICE, Modelica/Dymola and DALEC), as well as PHPP (a well-known quasi-steady-state tool), are described and the results of all the tools modelling the same characteristic office cell, defined within the IEA SHC Task 56, are compared on a monthly and hourly basis for the climates of Stockholm, Stuttgart and Rome. Unfortunately, different tools require different levels of input detail, which are often not matching with available data, hence the parametrization process highly influences the quality of the simulation results. In the current study to evaluate the deviation between the tools, frequently used statistical indices and normalization methods are analysed and the problems related to their application, in a cross-comparison of different tools, are investigated. In this regard, the deviation thresholds indicated by ASHRAE Guideline 14-2014 are used as a basis to identify results that suggest an acceptable level of disagreement between the predictions of a particular model and the outcomes of all models. The process of reaching a good agreement between all tools required several iterations and great effort on behalf of the modellers. To aid the definition of building component descriptions and future references for inter-model comparison a short history of the executed steps is presented in this work. Together with the comparison of the results of the tools, their computational cost is evaluated and an overview of the modelling approaches supported by the different tools for this case study is provided aiming to support the users in choosing a fit-for-purpose simulation tool.

1. Introduction

A large number of Building Energy Simulation (BES) tools, with different focus and level of detail, have been developed in the last six decades [1,2]. A comprehensive list of BES is provided in [3] and [4]. BES tools are used in research and increasingly in building design, construction, commissioning and operation for accelerating and improving the design and planning process, optimizing building performance, developing building controls, testing new products and evaluating the market potential of novel concepts. Moreover, ever-stricter building codes and energy standards have stimulated the usage of BES [5].

1.1. Model complexity: approximation versus estimation

The two main aspects under which the different tools can be classified are first, the complexity of the mathematical models depending on the purpose and focus of the tool, and second, the possibility to access the BES source code (which is particularly relevant in the research field). When the source code is accessible and can be easily modified, the user can tailor the equations to

* Corresponding author at: Technikerstraße 13, 5. Stock, A-6020, Innsbruck, Austria.
E-mail address: Mara.Magni@uibk.ac.at (M. Magni).

https://doi.org/10.1016/j.enbuild.2021.111260
0378-7788/

Nomenclature

Acronyms and abbreviations:

av	Average
av > 0	Average including only values higher than zero
BC	Boundary Conditions
BES	Building Energy Simulation
CD	Cooling Demand
DAL	DALEC
EP	EnergyPlus
h	Hourly
HD	Heating Demand
HTC	Heat Transfer Coefficient
Inf	Infiltration losses
iqr	Interquartile range
m	Monthly
MAE	Mean Absolute Error
MBE	Mean Bias Error
ME	Mean Error
MOD	Modelica
nm	Normalization means
NMAE	Normalized Mean Absolute Error
NMBE	Normalized Mean Bias Error
NRMSE	Normalized Root Mean Square Error
PHPP	Passive House Planning Package
RMSE	Root Mean Square Error
ROM	Rome
SHGC	Solar Heat Gain Coefficient
SIM_BO	Simulink library developed by the University of Bologna (ALMABuild)
SIM_IBK	Simulink library developed by the University of Innsbruck (CarnotUIBK)
SOL	Solar gains
std	Standard deviation
STO	Stockholm
STU	Stuttgart
TMY	Typical Meteorological Year
TR	Transmission losses
TRN	TRNSYS
TZ	Thermal Zone
Vent	Ventilation losses

Variables and Parameters:

F	View Factor [-]
H	Radiosity [W/m^2]
I	Solar irradiation [W/m^2]
K	Constant heat exchange coefficient [W/(m^{2}K)]
N	Number of considered data points [-]
$\dot{Q}$	Heat flux [W/m^2]
r	Reference results
R	Thermal resistance [W/(m^2 K)]
R^2	Coefficient of Determination [%]
s	Simulated results
T	Temperature [K]
v	Wind Velocity [m/s]
α	Absorption factor [%]
β	Constant [-]
ε	Emissivity [%]
ϑ	Temperature [°C]
σ	Stefan–Boltzmann constant 5.670 373 (21) $\times$ 10–8 [W/(m^2 K^4)]
τ	Solar transmittance [%]

Subscripts:

amb	Ambient
av	Average
av > 0	Average considering only numbers higher than zero
C	Convective
CD	Cooling Demand
ce	Convective external
ci	Convective internal
ext	External
g	Global
gnd	Ground
h	Hourly
HD	Heating Demand
hor	Horizontal
i	ith time step
inf	Infiltration
int	Internal
m	Monthly
p1	Point one
p2	Point two
R	Radiative
re	Radiative external
ri	Radiative internal
se	Surface external
si	Surface internal
sky	Sky
sol	Solar
south	South
tr	Transmission
vent	Ventilation
win	Windows

perfectly suit the specific case study increasing the degree of detail[1]. Unfortunately, this will also lead to an increase in the total simulation time, modelling effort and skill that is required. Dynamic simulation tools such as TRNSYS, Modelica/Dymola, IDA ICE, EnergyPlus, and Simulink, focus on the transient behaviour of systems and allow detailed analysis. However, their application requires a high level of user expertise and expert knowledge of many input parameters. Moreover, the modelling and simulation process can be time-consuming in terms of computational cost [5] and modeller effort. In addition, the suitability of a particular level of model complexity, or a particular modelling tool, can only be assessed in relation to the objectives and constraints of the simulation study. In the present study, in order to develop a meaningful conclusion to a specific problem, both the degree of detail of the model as well as the accuracy of the available input data are the defining aspects. As a result, the potential overall error in performance predictions is a function of both the degree of approximation of the physical phenomena involved as well as the degree of estimation of uncertain input parameters. Therefore, the process of minimization of the overall

[1] This is possible only in the case of white and grey box models and not in black-box models [81]. White box models require detailed knowledge of the physical process while black box models do not require full knowledge of the system and are developed using a data-driven approach. Grey box model preserve the physical description of the system, but their parameters are estimated using system identification methods [81].

error involves balancing the complexity of the model with the information, time and other resources available to the simulation study [6].

In general, the process of model parametrisation is error-prone since it is easy to make unrepresentative assumptions or just commit user errors in preparing building input files. Fortunately, the number of inputs to be parametrized can be reduced by using a tool with the degree of detail required by the modelling phase. Typing errors might be avoided by increasing the usage of automated procedures. In this regard, Building Information Modelling (BIM) might have the capability to lead to a more automated process and thus reduce user mistakes. Nevertheless, further development in terms of availability and agreement in information transfer is required to apply BIM to BES in practice (see [7;8]).

In order to assess the extent to which different simulation tools fit the need of a particular simulation study, modellers require an overview of the complexity or degree of abstraction of the component models that are applied in the different tools as well as the input parameters, skill effort and time that are required to use them. In this context, Crawley et al. [3] comprehensively and extensively reported the modelling features for a large number of available tools, which helps the BES user to select the right tool according to the purpose. However, this kind of BES tools comparison needs to be updated since new component models are constantly being developed. In addition, new versions and tools are available such as Matlab/Simulink toolboxes (e.g. CARNOT toolbox [9], CarnotUIBK [10] and ALMABuild [11]), Modelica libraries [12], DALEC [13], PHPP [14]. Unfortunately, using a tool with a high degree of detail might not only be time-consuming to create the simulation model, but also for the computation itself. Certainly, some particular aspects can be analysed only if the model describes them. For example, a detailed comfort analysis can only be done if the models calculate the temperature distribution in the room [15]. The aspect of the computational cost has been qualitatively mentioned in [16–19]. Quantitative comparisons in terms of the computational time of different tools have been proposed in [20] including DALEC, Radiance, Relux and EnergyPlus, in [21] comparing eQUEST against EnergyPlus, in [22] including EnergyPlus and DOE2 and in [23] where TRNSYS and Modelica have been compared. Yet, this is an important topic especially in the expanding field of simulation-based optimization [24] and studies presenting updated comparison of the computational cost including a wide range of BES tools are needed.

The results of such a comprehensive analysis that also show the impact on the computational time, would be a helpful instrument for supporting the user in the decision of which tool to be used for a certain study.

1.2. Validation and trust in BES

According to Feist [25], the five major reasons for the deviations between different simulation models are: (1) different algorithms, (2) numerical errors (errors in the calculation), (3) programming errors (errors in implementation), (4) non-identical inputs, and (5) different processing of the weather data that is used by the BES. Additionally, the results are influenced by different physical approaches with different levels of detail and different numerical schemes. As an example, the thermal zone can be modelled with a 2-star or star-node approach and the wall model with the finite difference method or transfer function. To gain trust in the building simulation, it is important to validate the models. Therefore, many validation studies have been published over the years and the level of attention on this subject has increased significantly in the recent years. According to Judkoff et al. [26] and [27], the results of BES tools can be validated against measurements (empirical validation), analytical solution (analytical validation), or against other codes (cross-validation). In this context, an analytical solution is only available for simple configurations (e.g. wall model and verification of system simulations [7,8]). Empirical validations involving different tools are presented in [16,28], and [29]; this kind of validation has to deal with the measurement uncertainties and is usually limited to a specific amount of data for a limited period of time. Whereas cross-validation allows to minimize the input uncertainties and allows analysis of many different configurations with a high level of detail [5,30,31,32]. Nevertheless, the main drawback of the cross-validation approach is that it is difficult to precisely define the set of reference results.

The BESTEST methodology, established by the ANSI/ASHRAE Standard 140–2017 [33] and later updated by [34], EN 15255 [35] and EN 15265 [36] and German guidelines such as VDI 6020 [37], VDI 2078 [38] and VDI 6007 [39], describe different test cases against which the implemented algorithms or models have to be tested to correct code errors, modelling limitations or input errors eventually present in the tool [40]. Comparative values are given for the evaluation of the calculated results. However, only specific parameters are analysed within each BESTEST case. The spread between the minimum and maximum thresholds, suggested by BESTEST for the tool validation, can be as large as 47% [34] in some test cases.

Moreover, in both empirical and cross-validations, when only heating and cooling demands are considered and all the other contributions are discarded of the thermal balance (i.e., thermal losses, solar gains, internal gains, ventilation and infiltration losses and temperatures of the surfaces and air), it is difficult to interpret the results since all possible error sources are acting simultaneously [40]. Thus, conclusions about the model accuracy have to be derived, preventing as much as possible the offsetting errors by considering as many as possible outputs and different time scales. This is difficult to achieve with empirical validation since the available measurements refer to a limited time frame and do not cover the majority of the outputs of a simulation tool. For these reasons in the current work a detailed cross-comparison, focused on a solar-driven, reference office test cell that includes shading and ventilation control logic, is carried out that considers all the components of the energy balance on a monthly and hourly basis for one year of simulation.

1.3. Statistical indices for the quantification of the deviations among the results of the different tools

The definition of accuracy indices is required to quantify the deviations between time series and therefore to assess the goodness of the results of a model against other simulations or measured data. As highlighted in [27], there is the need to find appropriate system performance indices. In this field, Uniform Methods Project [41] and ASHRAE Guideline 14-2014 [42] are widely recognized guidelines aiming at establishing a method for measuring the accuracy of building models as well as the Federal Energy Management Program (FEMP) [43] and the International Performance Measurement and Verification Protocol (IPMVP) [44], which refer to ASHRAE Guideline 14-2014 [42]. These documents suggest thresholds, which are different for monthly or hourly calibration, for the Normalized Mean Bias Error (NMBE) and Normalized Root Mean Square Error (NRMSE). In addition, it has been suggested to analyze a time frame of at least one year and to compare the simulation results with the utility bills and/or spot measurements. However, as highlighted in [45] the indoor condition and temperatures are not addressed in the suggested calibration approaches. Numerous papers using calibration methods are available in the literature, as reported in [45] nevertheless, varying approaches have been applied by different researchers in the previous works due to lack of a standard procedure. These

approaches use different indicators, applied to different variables with varying resolution and time frames to quantify the model accuracy. As an example [16] and [29] calculate the statistical indices (i.e. Coefficient of determination (R^2), Root Mean Square Error (RMSE) and NRMSE are used in [16]; Mean Error (ME), RMSE, standard deviation and maximum error are used in [29]) based on temperatures, while [46] bases its analysis on the energy consumption of the building calculating the Mean Bias Error (MBE) and the NRMSE for each month and the whole year using hourly data. In general, it is not uncommon to find literature referring to the same index with different names or definitions as highlighted in [47]. In the current work, the main statistical indices and normalization means that are used are critically analysed to help shed some light on the difficulties that are encountered so a new normalization method can be proposed.

As reported in [4] a long list of BES tools exist, which includes tools from different countries. However, in the current work, EnergyPlus [48], TRNSYS [49], Matlab/Simulink (ALMABuild [11] and CarnotUIBK [10]), the Modelica/Dymola buildings library [50], and IDA ICE [51] are analyzed along with DALEC [20] and PHPP [14], which can be classified as predesign tools. Almost all these tools have already undergone a validation process following the BESTEST method (i.e. EnergyPlus in [52], ALMABuild [11], Modelica [53], IDA [54], TRNSYS [34]), and all the tools except the Simulink libraries ALMABuild and CarnotUIBK have been compared against measured data in [16,28,29,20] and [55]. However, they have not been compared against each other using a solar-driven building as a common test case. Finally, only a few recent studies have presented a quantitative and comprehensive comparison in terms of computational time including a wide variety of dynamic building simulation tools.

With each tool, the reference office cell was modelled starting from the same description (specially tailored on the TRNSYS input). Even though almost all the tools are successfully validated using the BESTEST methodology (i.e. EnergyPlus in [52], ALMABuild [11], Modelica [53], IDA [54], TRNSYS [34]), high deviations between the results of the analysed tools were experienced during the first itarations of the cross-comparison process. Indeed, to reach a good agreement between the tools, several iterations were necessary due mainly to a lack of equivalent inputs in the building description, user mistakes and different modelling approaches of the tools under analysis.

2. Methodology

In this section, the building model used for this case study is described, and the modelling features of the different tools are introduced and the parametrization process is explained. Moreover, the statistical indices are described and the boundary conditions, applied for the evaluation of the computational cost, are reported.

2.1. Boundary conditions

Three different locations Rome (ROM), Stuttgart (STU) and Stockholm (STO), characterized by different European climates (Mediterranean, oceanic climate and humid continental climate respectively, according to the Köppen climate classification [56]) were considered in this study. Table 2.1 shows the annual average ambient temperature ($\bar{\vartheta}_{amb,av}$), annual global irradiation on a horizontal surface ($I_{g,hor}$) and annual irradiation on a south-oriented vertical surface (I_{south}) for each location.

All the tools use the same Typical Meteorological Year (TMY2) for each location. Therefore, the ambient temperature and global irradiation on the horizontal were the same (see [57] for more details). Nevertheless, it is important to highlight that DALEC calculates the I_{south} using a diffuse isotropic sky model[2] described in [58] whereas all the other tools implement the Perez model (i.e. EnergyPlus, Simulink, IDA ICE and Modelica used the Perez 1990 model [59] while TRNSYS used the Perez 1999 model (see [60] page 7–99). Therefore, Simulink, EnergyPlus, TRNSYS, Modelica and IDA ICE present negligible deviations in terms of I_{south}, while DALEC underestimates I_{south} in all the climates (see Figure 2.5). To perform a fair comparison, the solar gains of DALEC have been aligned with the solar gains of the other tools by calibrating the shading control thresholds (see Section 2.4).

Table 2.1
Main boundary conditions: yearly average ambient temperature ($\bar{\vartheta}_{amb,av}$), yearly global irradiation on a horizontal surface ($I_{g,hor}$) and yearly irradiation on a south-oriented vertical surface (I_{south}).

Location	$\bar{\vartheta}_{amb,av}$ [°C]	$I_{g,hor}$ [kWh/m^2]	I_{south} [kWh/m^2]
Rome	15.8	1632	1253
Stuttgart	9.9	1101	889
Stockholm	7.8	952	884

2.2. Building description

The reference building was chosen to be representative of a typical European office cell located on the middle floor of a high-rise building. Figure 2.1 shows the office cell, which has a heated area of 27 m^2 and a volume of 81 m^3. All the surfaces are considered adiabatic, except for the façade oriented towards the South (with a window-to-wall ratio of 60%) where ambient boundary conditions are applied and solar active technologies such as daylighting systems can be installed[3]. Shadings from adjacent obstacles were not considered, whereas external movable shading, able to block 70% of the incoming radiation, was activated when direct solar radiation impinging the south façade was higher than 120 W/m^2.

Table 2.2 reports the heat transfer coefficient (HTC) of the opaque wall element and the characteristics of the windows such as HTC, Solar Heat Gain Coefficient (SHGC) and the solar transmittance (τ_{sol}) for the three climates. The HTC of the window can be calculated as the area-weighted HTC of the frame and the glass. The internal walls were typical plasterboard walls, while the exterior wall consists of a three-layer structure with different insulation thicknesses depending on the climate.

User behaviour (e.g., occupancy, appliances and lighting) was taken into account by employing hourly resolution profiles that show different user behaviour for weekday and weekends [61] (see Figure 2.2).

The natural infiltration rate was assumed to be constant and the air change per hour was set to 0.15 ACH. A fresh air supply of 40 m^3/h per person was provided by a mechanical ventilation system with a sensible heat recovery of 70% efficiency. A bypass of the heat recovery was activated when the temperature of the zone was higher than 23 °C and the ambient temperature was lower than the indoor temperature (see Figure 2.3).

A simplified ideal all-air heating and cooling system was used by all the models. The set-point for the indoor convective temperature applied for the heating and cooling control was

[2] A 'uniform sky' defines a sky distribution which has a constant luminance over the hemisphere. This isotropic distribution is therefore independent on the height and azimuth of the sun and is only scaled with respect to the intensity. In this model the diffuse solar irradiation on a vertical surface is equal to the diffuse solar irradiation on the horizontal divided by 2.

[3] Not applied in the present comparison. A preliminary study including the comparison of SIM_BO, EP and TRN modelling the office cell equipped with photovoltaic panels and air to air heat pump is presented in [82] Section 2.1.5.

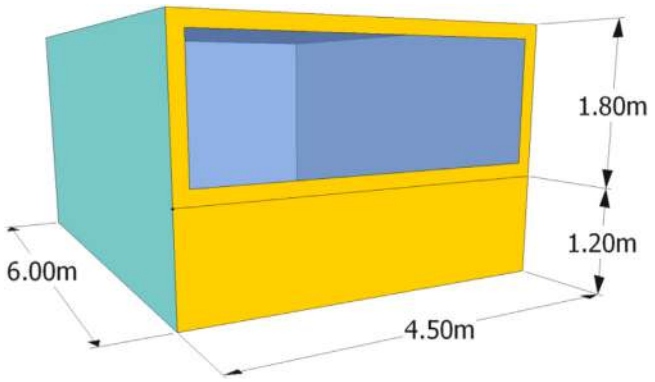

Figure 2.1. Representation of the reference office zone.

21 °C and 25 °C, respectively. When the convective temperature was between 21 °C and 25 °C neither the cooling system nor the heating system is activated.

A summary of the building data and boundary conditions is reported in the appendix in Table C1 and further information is reported in [57].

2.3. Modelling features of the tools

The tools analysed in this work had different modelling features as follows:

- EnergyPlus™ v.9.3 (EP) is a building energy simulation program that is used to model energy consumption, lighting, plug and process loads and water use in buildings [62]. The development of the program was funded by the United States Department of Energy's (DOE) Building Technologies Office and managed by the National Renewable Energy Laboratory (NREL). The software is open-source and is collaboratively developed by NREL, various other DOE national laboratories, academic institutions and private firms;
- TRNSYS 18 (TRN) is a commercial transient system simulation program, developed at the University of Wisconsin, based on a component approach with a modular structure. The TRNSYS library includes a detailed multi-zone building model and components for HVAC systems, renewable energy systems, etc. [49];
- CarnotUIBK (SIM_IBK) and ALMAbuild (SIM_BO) are two open-source Matlab/Simulink libraries, compatible with CARNOT Toolbox [9], developed by the University of Innsbruck (AT) [10] and the University of Bologna (IT) [11] respectively;
- IDA ICE v.4.8 (IDA) is a commercial software, developed by EQUA Simulation AB. It is focused on detailed and dynamic multi-zone simulation applications for the study of thermal indoor climate as well as the energy consumption of the entire building involving envelope, HVAC systems, plant and control strategies [63]. The model inputs are described using the equation-based Neutral Model Format language [64];
- DALEC (DAL) is a free web tool developed by Bartenbach (AT), University of Innsbruck (AT) and Zumtobel (AT). The main focus of DALEC is on combined thermal and lighting building simulations in early design phases [13];
- MODELICA (MOD) is a non-proprietary, object-oriented, equation-based language for modelling complex physical systems developed by Modelica Association. Currently, several Modelica libraries exist for building components and HVAC systems, and these are continuously being upgraded. In this work, the Buildings library v.5.0.1 was used together with the Modelica standard library [50]. The Dymola modeling and simulation environment (v. 2020x) was also used;
- PHPP v.9.1 Passive House Planning Package is a commercial quasi-steady-state calculation tool, developed as a spreadsheet by the Passive House Institute, for use by architects, engineers and planning experts [14].

Table 2.2
Main properties of the south-oriented façade.

Properties	Rome (Italy)	Stuttgart (Germany)	Stockholm (Sweden)
$HTC_{ext,wall}$ [W/(m²K)]	0.80	0.40	0.30
HTC_{win} [W/(m²K)]	1.26	1.35	0.90
SHGC [%]	0.33	0.59	0.63
τ_{sol} [%]	0.26	0.43	0.46

The different tools implement different models with different levels of detail to approach the numerical solution of the building system using different equations. An extensive description of the equations implemented in TRN, IDA and EP is provided in [16], a description of the mathematical model used in DAL is provided in [20,58] and of MOD in [12]. SIM_BO and SIM_IBK do not provide user manuals, while CARNOT toolbox provides only an introduction to the library in [65].

Table 2.3 provides a summary of the approaches applied in this work (in black) and available (in grey) in each tool for different aspects of the building model. The model of the thermal zone is used to calculate the convective and radiative temperature. The most detailed approach would be a CFD simulation considering a distribution of the convective as well as the radiative temperature within the room. Such a model requires a high computational cost and therefore, it is not usually applied in annual energy simulation [66]; however MOD and IDA offer the possibility of using a simplified CFD approach[4] (see [67;68], respectively). EP, TRN, SIM_BO, IDA and MOD, for convex and closed volume, can model the air in the room as one unique node while calculating the radiative exchange between the surfaces using view factors. EP, TRN, SIM_BO and IDA ICE can additionally calculate the view factors between the internal surfaces and a matrix of points in the room, whose location is defined by the user, allowing the calculation of the mean radiative temperature field in the room. The two-star node approaches [69] (implemented in SIM_IBK, SIM_BO) include a convective node and a radiative node (the long-wave radiative exchange between the surfaces is modelled using the star network). In the simplified calculation mode, TRN implements a star network (see [70] Figure 5.4.1–7) where an artificial temperature node is used to consider the parallel energy flow from the inside wall surface to the zone air by convection and the long-wave radiation exchange between the surfaces. DAL is based on the Standard ISO 13790:2008 [71] where the room thermal balance is solved considering three nodes and both the air and mean radiant temperatures are calculated [20]. In DAL the nodes are connected through a specific coupling conductance defined in the Standard ISO 13790:2008 [71]. The total thermal capacity of the walls and air volume is connected to the node representing the mean radiant temperature. PHPP is a quasi-steady-state tool based on Standard ISO 13790:2008 [71] that calculates losses and gains on monthly basis considering a fixed set point temperature (different for winter and summer energy balances).

The convective heat transfer coefficient (see Table 2.3 and Table 2.4) is considered as a constant (Table 2.4: C1/C2) in PHPP and DAL. Contrariwise EP, TRN, IDA and MOD offer both constant

[4] Not included in the current study.

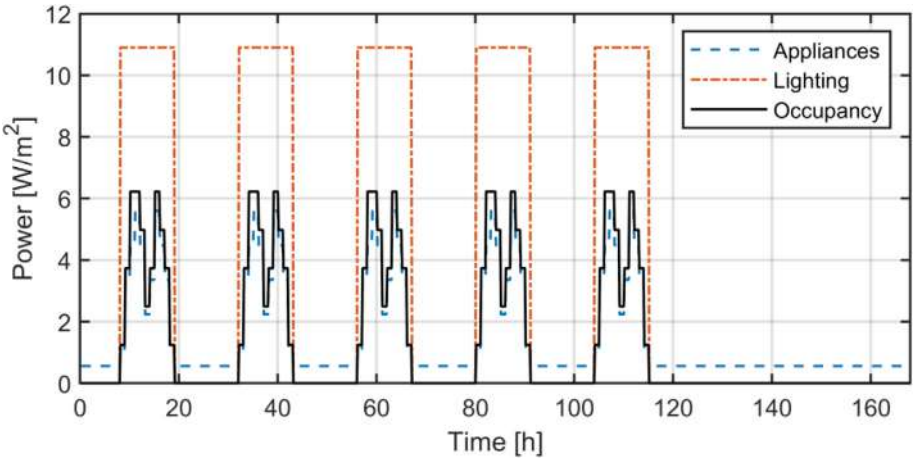

Figure 2.2. Internal gains due to appliances, lighting and occupancy.

(Table 2.4: C1/C2) and equation-based (Table 2.4: C3) calculation. The radiative exchange coefficient can be:

- Constant when an overall HTC is considered (Table 2.4: R1);
- Linearized (Table 2.4: R2);
- Proportional to the temperature difference at the fourth power (Table 2.4: R3); and
- Calculated considering the view factors between the surfaces (Table 2.4: R4).

Different window models are implemented in the analysed tools, in particular, EP, TRN, SIM_BO, IDA and MOD perform a thermal balance over each pane of the window (see Figure 2.4a), while DAL, SIM_IBK and PHPP are based on a simplified window thermal model where the transmission losses are calculated by using a constant heat transfer coefficient (see Figure 2.4b).

EP, TRN, SIM_BO, IDA, MOD consider the solar transmittance and the distribution of absorbed solar radiation across the multi-layer glazing system as a function of the angle of incidence. EP, IDA, MOD explicitly describe this behaviour by recursively solving the transmittance, reflectance and absorptance of solar radiation through each layer, while TRN and SIM_BO by using pre-processed data of multi-layer window system from the LBNL-Window software [72] (see [73] for the WINDOW technical documentation). A description of the implementation of the detailed window modelling approach in EP can be found in [74] and [75]. EP, MOD and IDA ease the investigation of particular fenestration systems (e.g. including glass coatings) and require more detailed input. SIM_IBK uses a standard correction function (different for single, double and triple panes windows) of the SHGC at normal incidence, to different incidence angles. DAL discretizes the sky into 145 patches and, for every patch applies a pre-calculated correction factor to the SHGC at normal incidence given by the user (see [20]).

EP and TRN model the opaque structures with the transfer function method, whereas both Simulink libraries, IDA and MOD implement the finite difference method. For more details about these different approaches see: [69] where the theory behind these methods is explained and [76], which provides a detailed comparison between transfer function and finite difference methods. DAL and PHPP implement a simplified model of the walls, based on the HTC of the structures. PHPP is a quasi-steady-state calculation tool where the capacity of the building is used only to calculate the utilization factor of the internal and solar gains as described in the Standard ISO 13790:2008 [71]. In DAL the mass of the building is lumped in one capacity as described in the Standard ISO 13790:2008 [71].

The model used for the adiabatic structures influences the active capacity of the building. Both Simulink libraries and IDA apply the same boundary conditions (BC) to both sides of the structure, TRN additionally applies the same thermal resistance between the surface and the air and radiative nodes on both sides. EP implements a null thermal flux on the external side of the adiabatic structure and MOD in the middle of the structure. PHPP and DAL consider the thermal mass in one unique node belonging to the Thermal Zone (TZ).

The isotropic sky model, used in DAL [58], assumes that the diffuse radiation from the skydome is uniform across the sky and predicts lower solar radiation availability on the south façade (see Figure 2.5), compared to the other tools implementing the Perez sky model (see Section 2.1).

The internal gain can be defined as an hourly profile in almost all tools except for PHPP where the internal gain is considered as a constant and in DAL where the internal gain can be defined with a constant value throughout the day, as shown in Figure 2.6.

The control status of the shading and ventilation bypass is defined in every time step for all tools except for PHPP where constant shading and ventilation rate are applied for the summer and winter balance calculation (see Section 2.4, Table 2.7 and Table 2.8). To clarify this aspect, the control status of the shading simulated with SIM_BO for the climate of Stockholm together with the sunset and sunrise time for each day of the year is reported in

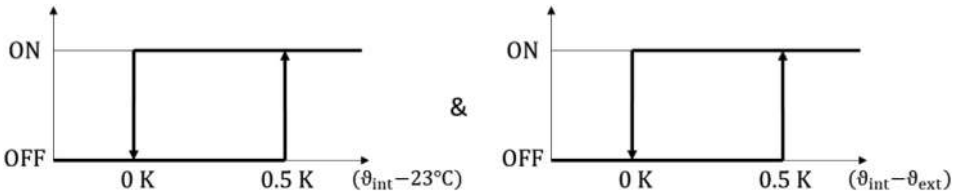

Figure 2.3. Control logic of the ventilation bypass.

Table 2.3
Summary of the features of the mathematical models employed in each tool within this case study (black points) or are available (grey points).

		EP	TRN	SIM_IBK	SIM_BO	IDA	MOD	DAL	PHPP
Thermal zone model	Standard ISO 13790 (monthly)								●
	Standard ISO 13790 (hourly)							●	
	Star node model			○					
	Star network		●						
	Two-star node model			●	●	○			
	One convective node and surf. to surf. radiative exchange	●	○		○	●	●		
	More convective nodes and surf. to surf. radiative exchange				○	○	○		
Convective heat transfer	Constant (see Table 2.4 line C1)	○	○		○		○	●	●
	Internal const.; External prop. to wind speed (see Table 2.4 line C2)		○		○		○		
	Internal f(ΔT) (Eq. (2-5)); External Constant (Eq. (2-2))		○				○		
	Internal f(ΔT); External prop. to wind speed (see Table 2.4 line C3)	●	●	●		●	●		
Radiative exchange	Radiative node - Constant (see Table 2.4 line R1)	○	○					●	●
	Radiative node - Linearized (see Table 2.4 line R2)				○				
	Radiative node - Proportional to ΔT^4 (see Table 2.4 line R3)		●	●		○			
	Surf. to Surf. - Based on view Factor (see Table 2.4 line R4)	●	○		○	●	●		
Window thermal model	Constant HTC							●	●
	Constant thermal resistance (see Figure 2.4b)			○		●			
	Thermal balance of each pane (see Figure 2.4a)	●	●		●	○	●		
Window optical model (short wave radiation)	Isotropic SHGC (see Figure 2.4b)								●
	Anisotropic SHGC (see Figure 2.4b)			●		●		●	
	Anisotropic optics + solar absorption at each pane (see Figure 2.4a)[1]	●	●		○	●	●		
Shading thermal model	No interaction with the window		●	●	●	●	●	●	●
	Constant additional thermal resistance					○			
	Thermal balance of the air gap (shading - glass)	●	○			○	○		
Shading optical prop (short wave radiation)	Constant reduction factor		●	●	●	●	●	●	●
	Optical properties of the shading layer	●	○			○	○	○	○
Distribution of the solar gains in the TZ	Added directly to the capacity of the TZ		○					●	●
	Proportional to the surface area		○	●					
	Complex calculation based on the reflection of the surfaces	●	●		●	●	●		
Wall model	Constant HTC (no capacity)	○		○				●	●
	Transfer function	●	●			○			
	Finite difference	○		●	●	●	●		
	Hygrothermal model	○		○		○			
Adiabatic structure model	Capacity of the adiabatic structure added to the building node							●	●
	Null thermal flux outside	●					○		
	Null thermal flux in the middle						●		
	Same BC inside and outside and same heat exchange coeff.		●						
	Same BC inside and outside			●	●	●	○		
Sky model	Isotropic			○	○	○	○	●	○
	Perez	●	●	●	●	●	●		●
Internal gain	Constant	○	○	○	○	○	○		●
	Daily profile	○	○	○	○	○	○	●	
	Hourly profile	●	●	●	●	●	●		
Control of shading and ventilation bypass	Constant	○	○	○	○	○	○	○	●
	Dynamic	●	●	●	●	●	●	●	
Calculation time step	Constant	●	●	○	○	○	○	●	●
	Variable			●	●	●	●		

[1] EP, IDA and MOD require as inputs the solar reflectance for each side of each pane and the solar transmittance of each pane, while TRN and SIM_BO require only the solar absorption on each pane and the overall solar transmittance calculated using an external subsystem simulation (LBNL-Window [72]).

Figure 2.7. PHPP performs only monthly balances and the shading coefficient can be given only as a constant that might be different for the summer and winter balance (see Table 2.8). Therefore, the graph reported in Figure 2.7 would be completely black for the PHPP and the value represented by the black colour would be the constant shading coefficient given as input to the PHPP. The same applies to the control of the bypass of the ventilation heat recovery.

Concerning the solver settings, the calculation time step can be defined as constant or can be variable in Simulink, MOD and IDA while it is fixed with the time length defined by the user in TRN and EP. Whereas DAL and PHPP are based on a fixed-time interval of one hour and one month, respectively.

Subportions of the models of the two Simulink libraries could be quite easily exchanged even when this is not foreseen from the structure of the tool itself. The SIM_BO library contains a detailed window model, which is missing in the original SIM_IBK library that has only a simplified model with constant thermal resistance. Therefore, in the current work the complex window model developed in SIM_BO (see Table 2.3, lines: Window thermal model and Window optical model, column SIM_BO) has been used also in the SIM_IBK model and the convective and radiative exchange coefficients of SIM_IBK

Table 2.4
Internal and external convective (subscripts ci and ce) and radiative (subscripts ri and re) exchange equations where: K is a constant heat exchange coefficient [W/(m^{2}K)], v is the wind speed [m/s], T and ϑ are temperatures in K and °C respectively, F_{ij} is a view factor between the surfaces i and j, H is the radiosity [W/m^2], ε is the emissivity and σ the Stefan–Boltzmann constant 5.670 373 (21) × 10–8 [W/(m^2 K^4)]. The subscripts C and R mean convective and radiative, si and se are the internal and external surfaces, amb is ambient and gnd is ground.

	Internal side	Eq.	External side	Eq.
C1	$q_{ci} = K_{ci}(\vartheta_{si} - \vartheta_C)$	2-1	$q_{ce} = K_{ce}(\vartheta_{se} - \vartheta_C)$	2-2
C2	$q_{ci} = K_{ci}(\vartheta_{si} - \vartheta_C)$	2-3	$q_{ce} = (4v + 4)(\vartheta_{se} - \vartheta_C)$	2-4
C3	$q_{ci} = K_{ci}\lvert_{si} - c\rvert(_{si} - c)$	2-5		
R1	$q_{ri} = K_{ri}(\vartheta_{si} - \vartheta_R)$	2-6	$q_{re} = K_{re}(\vartheta_{se} - \vartheta_{amb})$	2-7
R2	$q_{ri} = 4\varepsilon\sigma T_R^3(\vartheta_{si} - \vartheta_R)$	2-8	$q_{re} = \left[T_{amb}^3 4\varepsilon\sigma(\vartheta_{amb} - \vartheta_{se})\right] + \left[(T_{sky}^4 - T_{se}^4)F_{sky}\varepsilon\sigma\right]$	2-9
R3	$q_{ri} = \varepsilon\sigma(T_{si}^4 - T_R^4)$	2-10	$q_{re} = \varepsilon\sigma\left[F_{gnd}\left(T_{gnd}^4 - T_{se}^4\right) + F_{sky}\left(T_{sky}^4 - T_{se}^4\right) + F_{amb}\left(T_{amb}^4 - T_{se}^4\right)\right]$	2-11
R4	$q_{ri} = \sum_j F_{ij}(H_i - H_j)^{(1)}$	2-12		

[1]Different methods are applied for the detailed radiative model within the different tools. TRN implements the Gebhart matrix, EP the ScriptF method similarly, in IDA a longwave absorption matrix is used to calculate the net absorbed longwave radiation (these approaches are reported in [16]) and MOD [83] and SIM_BO [15] are using the radiosity approach.

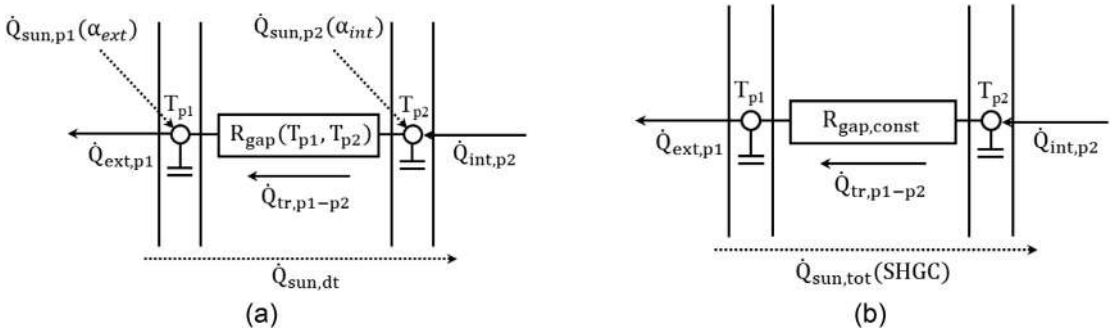

Figure 2.4. Sketch of the window models addressing the solar distribution and the thermal resistance between the panes. In (a) a thermal balance over each pane is performed and the solar gains are distributed over each pane and in (b) a constant thermal resistance is used and the total solar gains are calculated using the SHGC.

Table 2.5
Parameter set that needed to be adapted for each tool.

	EP	SIM_IBK	SIM_BO	IDA	MOD	DAL	PHPP
Window optical properties	●				●		
Window HTC				●		●	●
Building Capacity				●		●	
Ventilation Rate	●[1]			●		●	●
Internal Gain						●	●
Shading control						●	●

[1] In this case study the ideal loads air system model is used in EP. In this model heating and cooling energy are convectively supplied in sufficient quantity to meet zone loads. This model offers default controls for heat recovery and outdoor air delivery that differ from the controls described for this case study (see Section 2.1). EMS scripts were therefore used in EP to control heat recovery bypass and heat gains from ventilation frost protection. More detailed HVAC models could have been selected in EP. However, these would have required further estimation of unknown input parameters.

(see Table 2.3, lines: Convective heat transfer and Radiative exchange, column SIM_IBK) have been used in SIM_BO.

2.4. Parametrization process

Unfortunately, the building description, written using the input required by TRN [57], is either too detailed (this is the case for DAL and PHPP) or too simplified (for EP, IDA, MOD) and therefore equivalent inputs had to be found. The list of inputs that had to be adapted is reported in Table 2.5. Since SIM_BO uses the same input as TRN both tools do not need any parametrization.

As reported in [77] the window properties and heat transfer model have a substantial influence on the results, which is particularly evident in this case study. The model of the

Table 2.6
HTC glass and façade reported in the report, calculated with SIM_BO and used in DAL, PHPP and IDA.

	REPORT		SIM_BO		IDA	DAL	PHPP
	HTC-glass [W/(m^{2}K)]	HTC-façade [W/(m^{2}K)]	HTC-glass [W/(m^{2}K)]	HTC-façade [W/(m^{2}K)]	HTC-glass [W/(m^{2}K)]	HTC-façade [W/(m^{2}K)]	HTC-façade [W/(m^{2}K)]
Rome	1.29	1.08	1.30	1.08	1.21	0.97	1.08
Stuttgart	1.40	0.97	1.59	1.05	1.45	0.98	1.03
Stockholm	0.81	0.66	1.29	0.88	1.22	0.87	0.85

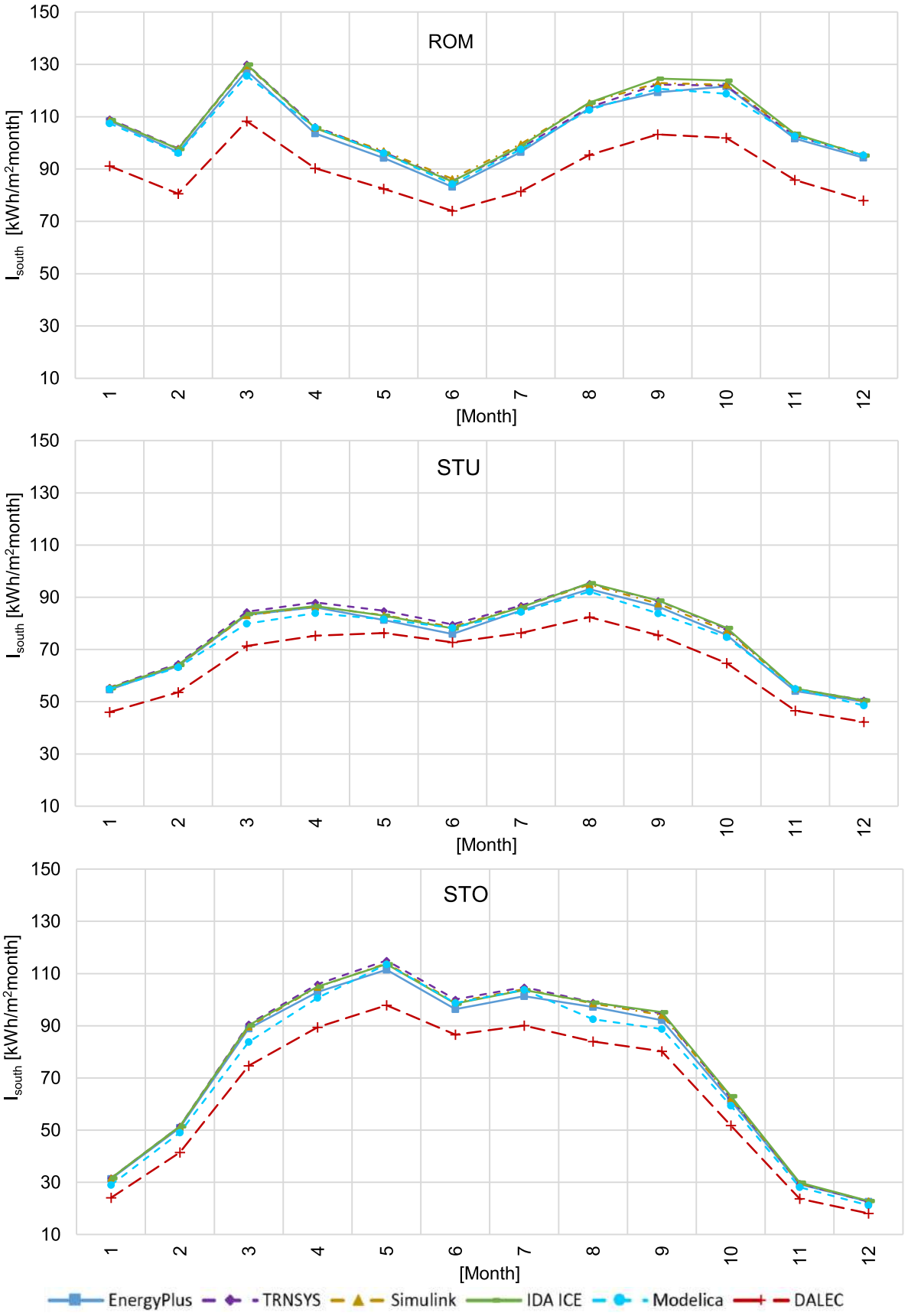

Figure 2.5. Solar irradiation on the south-oriented facade for the climate of Rome (ROM), Stuttgart (STU) and Stockholm (STO).

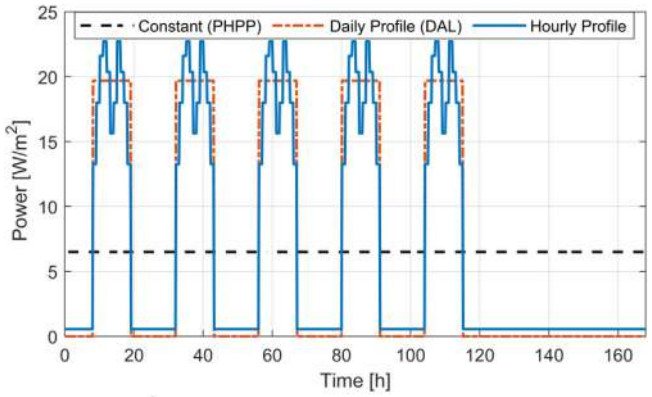

Figure 2.6. Total internal gain profiles, including occupancy, lighting and appliances, used in the PHPP (as a constant average value), in DAL (as a daily profile) and all the other dynamic simulation tools (as hourly profiles).

fenestration system in EP and MOD requires optical and thermal properties to be assigned for each glazing pane. Yet, the description of the input, defined for TRN [57], only describes the optical behaviour of the overall glazing system as a function of the angle of incidence. To obtain the detailed glazing properties for EP and MOD, the solar transmittance and reflectance of the glazing panes were varied and the results were compared with SIM_BO, which uses the same input as TRN. In EP this was done using an exhaustive search approach and in MOD a trial and error process was followed. The detailed glazing properties were then selected that gave the smallest difference ($\leq$0.1 kWh/m^2) in terms of the predicted annual sums of the solar energy that is transmitted by the glazing system, and the energy that is absorbed at each of the two panes. The resulting inputs that were found for the window models in MOD and EP are the same for ROM while small differences for the window properties in STO and STU are present, as reported in the appendix (see Figure A1).

Table 2.6 reports the HTC of the glass and façade, defined in a report from the current study [57], derived from SIM_BO and the one used in IDA, DAL and PHPP. SIM_BO dynamically calculates the HTC of the window since it depends on the boundary conditions, therefore, the constant HTC reported in Table 2.6, for SIM_BO, is calculated by finding a constant HTC of the glass, which delivers the same annual thermal losses calculated with the dynamic HTC. The discrepancy between the HTC calculated by Simulink and the one indicated in the report [57], which is especially high in Stockholm, is caused by the fact that the report gives this input considering fixed boundary conditions (i.e., ϑ_{amb} = 26.7 °C, no solar irradiation, Wind speed = 6.71 m/s, Internal temperature = 21 °C).

In IDA, both complex and simplified window models could be used. However, the complex window model has to be used with a complex shading model involved in the thermal balance of the window while the simplified window model can be used with a simplified shading model that does not affect the thermal balance of the window. The shading device is described just as a reduction factor of the incoming solar radiation impinging the window in this case study [57]. Therefore, all the tools except for EP (where this was not easily modified), do not consider the thermal effect of the shading layer on the thermal balance of the window. Hence, in IDA the simplified approach was used too due to this strong simplification of the fixed shading factor. IDA uses a simplified window model with two panes that use a constant thermal resistance (the fenestration system is always simplified as two-pane glazing). The value of this constant has been derived from the annual dynamic simulation of SIM_BO.

In IDA it is not possible to increase the capacity of the air node (as suggested in [57]) therefore the thermal mass was artificially increased by adding a wall (i.e., area: 20 m^2; thickness: 0.05 m; density: 900 kg/m^3; specific heat capacity: 987 J/kgK) with high thermal conductivity (i.e. 10000 W/mK) and heat transfer coefficient (i.e., 20000 W/m^{2}K). Moreover, IDA controls the mass flow rate of the supply and exhaust air while in [50] the volume flow rate is given and specified as constant. Therefore, the efficiency of the heat recovery system was adjusted (+4% compared to [50]) to compensate for the slightly unbalanced volume flows of the supply and exhaust air.

DAL is an open-access online tool where the code cannot be modified by the user. To adapt the DAL calculation to the building description, an unpublished Matlab version of the code was used. The results of the original web DALEC and the calibration process are reported in Section 3.4. Concerning the online version the following parts have been modified:

- The lumped capacity of the model was calibrated by comparing the hourly heating and cooling demand with SIM_BO;
- Ventilation rate: in the original calculation the ventilation system is always active, while in the calibrated version it is active only during the presence of people (as described in [57]);
- Shading model: in the original version, the shading is modelled considering optical properties dependent on the solar incident angle while in the calibrated version a constant reduction of the incoming solar gain was applied. Given the fact that DAL applies an isotropic sky model, resulting in lower solar irradiation toward the south façade, the shading threshold is modified to make the solar gain comparable; and
- The overall HTC of the window and wall is selected to minimize the difference in transmission losses between DAL and SIM_BO.

PHPP and DAL base their calculation on a constant HTC for the wall and window therefore, especially for Stockholm, it was necessary to parametrize the (Table 2.6).

Table 2.7 documents the effective volume flow (considering the 70% efficiency of the heat recovery) elaborated by the ventilation unit during the occupied time (from 8 until 18 see Figure 2.2) and the increased volume flow when the bypass is activated. The values used in DAL are found by minimizing the deviation in terms of cooling demand and ventilation losses with SIM_BO.

PHPP calculation is based on monthly balances therefore only one constant ventilation value for the summer and one for the

Table 2.7
Effective volume flow of the mechanical ventilation system and volume flow when the bypass is activated described in the report and used in DAL and the average volume flow used in PHPP for the winter and summer balance.

	Report / SIM_BO		DAL		PHPP	
	Effective volume flow [m^3/h$_{presence}$]	Volume flow bypass [m^3/h]	Effective volume flow [m^3/h$_{presence}$]	Volume flow bypass [m^3/h]	Winter [m^3/h]	Summer [m^3/h]
Rome	0.44	1.48	0.50	1.46	0.20	0.40
Stuttgart			0.42	1.57	0.15	0.41
Stockholm			0.40	1.48	0.15	0.41

Table 2.8
Winter and summer ratio between solar gains and incident solar radiation derived from Simulink and applied in PHPP.

	SIM_BO		PHPP	
	Winter	Summer	Winter	Summer
	[$kWh_{solargain}/kWh_{incident}$]		[$kWh_{solargain}/kWh_{incident}$]	
Rome	0.112	0.120	0.107	0.112
Stuttgart	0.254	0.315	0.238	0.295
Stockholm	0.277	0.291	0.265	0.280

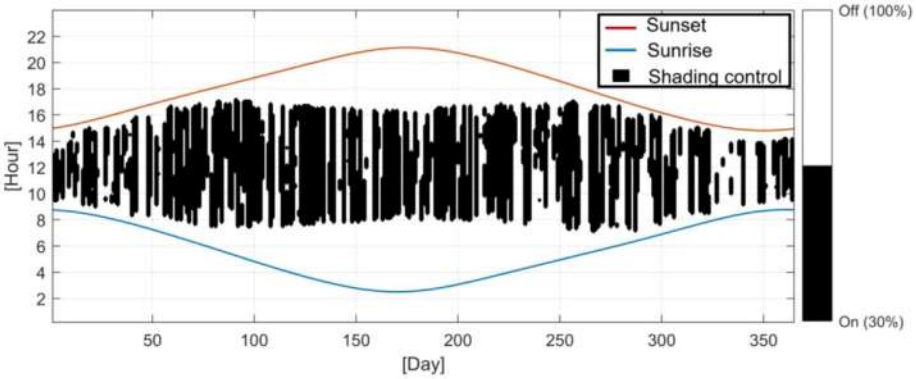

Figure 2.7. Hourly shading control simulated with SIM_BO for the climate of Stockholm. The blue and red lines represent sunrise and sunset time, respectively. (For interpretation of the references to colour in this figure legend, the reader is referred to the web version of this article.)

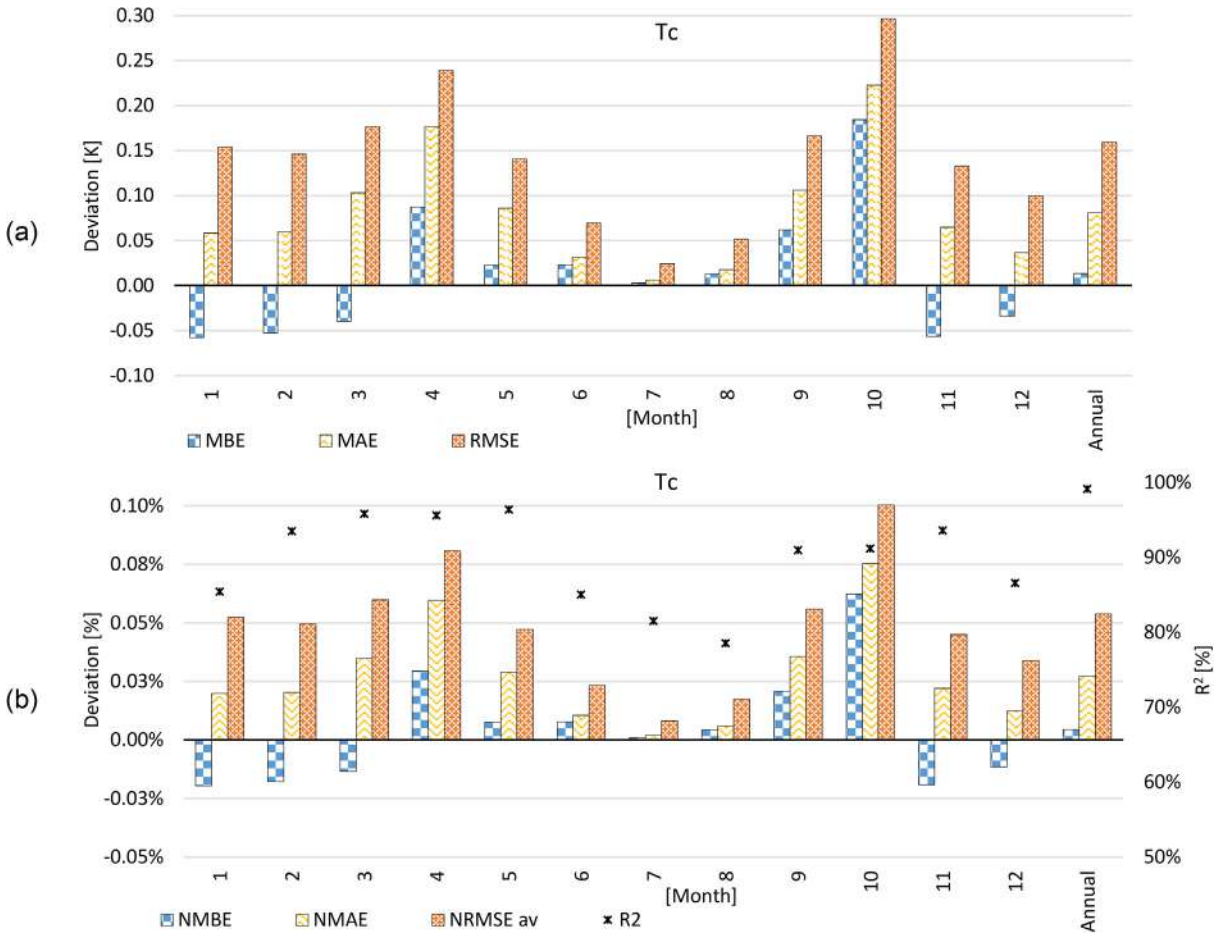

Figure 3.1. Non-normalized (a) and normalized (b) statistical indices applied for the calculation of the deviation between the simulated convective temperature with SIM_IBK and the reference convective temperature calculated as the median value of all tools for each time step, for the climate of Stockholm.

winter can be used, disregarding the occupancy schedule. In practice, describing the ventilation with detailed characteristics (e.g. mechanical ventilation with heat recovery of this case study) might be not possible because it is extremely complicated to guess the corresponding ventilation rates without the results of the dynamic simulation as a reference. On the contrary, if the mechanical ventilation system is not yet defined it might be easier to model it with PHPP instead of tools requiring detailed inputs.

Table 2.8 reports the ratio between the solar gain and the solar radiation impinging the south glass area as a result of the SIM_BO simulation and the input used in PHPP. The SHGC of the window, as well as the shading and dirt factor, are included in this ratio. The shading coefficient in PHPP is during the winter period 0.60, 0.50, 0.48 in Rome, Stuttgart and Stockholm, respectively and during the summer period 0.58, 0.38, 0.45 in Rome, Stuttgart and Stockholm, respectively.

2.5. Statistical indices

In this work, statistical indices were used to quantify the deviations between the results of the different tools. This evaluation was conducted using monthly and hourly datasets for all the components of the energy balance (heating, cooling, ventilation plus infiltration, transmission losses and solar gain) as well as for the convective temperature. Since no absolute reference such as measurements is considered within this work, it is important to define a benchmark against which the results can be compared and the median value of all tools will be used for each parameter.

ASHRAE Guideline 14-2014 [42], FEMP [43] and IPMVP [44], describe a method for the validation of the building model against measurement and suggest limits for the NMBE shown in Eqs. 2-14, NRMSE (using the average as a normalization means) in Eqs. 2-18 and the R^2 in Eqs. 2-19 to verify the accuracy of the models. The calibration criteria given by these standards are: ±5% for the monthly NMBE, 15% for the monthly NRMSE, ±10% for the hourly NMBE, 30% for the hourly NRMSE and > 0.75 for the R^2 ([47], Table 1).

In Eqs. (2-13) to (2-19) r_i represents the reference value for the i^{th} time step, calculated as the median of the results of all the tools in each considered time step (i.e. hourly or monthly), while s_i is the simulated value for a particular tool at the i^{th} time step, N is the number of considered data, $\bar{r}$ is the average of the reference values (i.e., median of all the tools for each time step) and nm is a normalization means. All the indices reported in Table 2.9 are calculated for each tool using hourly or monthly data. The MBE and its normalized value NMBE are good indicators of the overall bias but suffer from the cancellation effect, therefore at least one additional index is needed. ASHRAE Guideline 14-2014, FEMP and IPMVP suggest using the NRMSE based on the average value as a normalization means. The Mean Absolute Error (MAE) also provides analogous information as the RMSE, but is easier to interpret since each deviation influences linearly the MAE while the RMSE is more sensible to the outliners.

The RMSE is scale-dependent [78] therefore can be used as a measure of accuracy for a specific dataset but not between different datasets. The normalization of the RMSE eases the comparison between datasets with different scales but it should be computed only for data based on a scale with an absolute zero (e.g., Kelvin, not Celsius or Rankine, not Fahrenheit). Although the average has been commonly used and is suggested by [42,43] and [44] as a normalization means, this is not an appropriate method when the dataset contains a large number of zeros since the average is then close to zero and the NRMSE is no longer meaningful as highlighted in [78]. Therefore, it is noteworthy to mention that the normalization process may be based on different normalization means, such as average, range, interquartile range (not affected by outliners) or standard deviation (affected by outliners). Inconsistencies and problematics related to the application of statistical indices are explained in detail in Section 3.1.

Table 2.9
non-normalized (Mean Bias Error, Mean Absolute Error, Root Mean Square Error) and normalized statistical indices (Normalized Mean Bias Error, Normalized Mean Absolute *Error, Normalized Root Mean Square Error, Coefficient of Determination).*

Non-normalized indices		Normalized Indices	
$MBE = \frac{\sum_{i=1}^{N}(s_i - r_i)}{N}$	(2-13)	$NMBE = \frac{\sum_{i=1}^{N}(s_i - r_i)}{\sum_{i=1}^{N} r_i}[\%]$	(2-14)
$MAE = \frac{\sum_{i=1}^{N}\lvert s_i - r_i\rvert}{N}$	(2-15)	$NMAE = \frac{\sum_{i=1}^{N}\lvert s_i - r_i\rvert}{\lvert\sum_{i=1}^{N} r_i\rvert}[\%]$	(2-16)
$RMSE = \sqrt{\frac{\sum_{i=1}^{N}(s_i - r_i)^2}{N}}$	(2-17)	$NRMSE = \frac{1}{\lvert nm\rvert}\sqrt{\frac{\sum_{i=1}^{N}(s_i - r_i)^2}{N}}[\%]$	(2-18)
		$R^2 = 1 - \frac{\sum_{i=1}^{N}(s_i - r_i)^2}{\sum_{i=1}^{N}(r_i - \bar{r})^2}$	(2-19)

2.6. Evaluation of the computational cost

For the evaluation of the computational cost, each tool runs the corresponding model on the same local workstation with the following specifications:

- Processor: Intel® Core™ i5-8350U CPU @ 1.7 GHz;
- 4 physical cores;
- 8 logical processors;
- RAM: 16.0 GB;
- OS: Windows 10, 64 bit.

During the simulation, no other applications were running in the background except the operating system. Each computation was repeated 10 times and the median value of the CPU times was used for the comparison. Since the outputs are treated differently in each tool, the computational cost was evaluated including and excluding the processing of the output to analyse the computational cost of the model itself and to be able to address the additional time needed for the preparation of the output. 28 days of pre-simulation time is considered for all the tools. Table 2.10 reports the simulation set-up used in each tool. Figure 3.7 shows the comparison of the runtimes.

3. Results and discussion

In this section, inconsistencies and problems related to the application of statistical indices are explained and the monthly and hourly results of all the tools are reported together with their deviations. In addition, the results of the computational cost are presented. Furthermore, the influence of the parametrization process on the results of IDA and PHPP is reported.

3.1. Challenges related to the usage of statistical indices

The statistical indices introduced in Section 2.5 were analysed to explain their limits and their application within this work. The literature review highlighted that different approaches are applied for the determination of deviations in the building calibration and validation field and they differ mainly by the statistical indices that are used, and the time frame and reference variables on which they are calculated. Another aspect that is not often mentioned is the normalization of the statistical indices, which can be problematic especially when the normalization approaches zero. To show these aspects, the statistical indices were calculated using the deviations of the convective temperatures and heating power between the

Table 2.10
Simulation settings for the different tools.

	EP (TZ)[1]	TRN	SIM_IBK	SIM_BO	IDA	MOD	DAL
Time step	Fixed	Fixed	Variable	Variable	Variable	Variable	Fixed
Maximum time step [min]	10	10	10	10	10	10	60
Solver	Third-order finite difference approximation	Modified-Euler method	implicit Runge-Kutta (ode23tb)	implicit Runge-Kutta (ode23tb)	See [79]	Cvode	Crank-Nicholson

[1] EP implements different algorithm for the numerical solution of the thermal zone and of the HVAC system. The time step is fixed for zone heat balance calculation and variable for HVAC system simulation.

hourly results of SIM_IBK and the median of the hourly results of all the tools. The MBE in Eq. (2-13), and MAE in Eq. (2-15), and the RMSE Eq. (2-17) were calculated based on the deviations for the climate for Stockholm; the hourly results of SIM_IBK with respect to the reference results concerning the convective temperature (see Figure 3.1a); and the heating power (see Figure 3.2a). While the normalized statistical indices such as the NMBE in Eq. 2(-14), the NMAE in Eq. (2-16) and the NRMSE in Eq. (2-18) and the R^2 in Eq. (2-19) were reported in Figure 3.1b applied to the convective temperature, and Figure 3.2b as applied to the heating power.

The normalization of the RMSE was calculated using the average *(av)*, average of the absolute value higher than zero *(av > 0)*, the range, the interquartile range *(iqr)* and the standard deviation *(std)*. In addition, the statistical indices were calculated across different time periods using an hourly resolution. These time periods can vary from a few days (e.g., periods in which measurements are available) [16], to a month [46] to a year [5]. Here the results are presented considering monthly and annual time frames.

Figure B.4 shows the distribution of the absolute deviation of the internal convective temperature for all the tools considering hourly data for a one-year simulation. It can be noticed that the deviation range for SIM_IBK is ± 0.5 K and only for 2% of the time which can be considered as a good agreement. Figure 3.5b shows a box plot of the reference convective temperature distribution for each month and considers the data set of the whole year. Figure 3.1a shows the MBE, MAE and RMSE for each month and also considers the data for the whole year. It can be noticed that the MBE is the only indicator giving information about the sign of the deviation and that the MAE and RMSE follow the same trend but the RMSE is always higher than MAE since it is more sensible to the outliners. Figure 3.1b reports the normalized indices and the R^2, in this case, NMBE, NME and NRMSE_av are ranging between −0.02% and + 0.1%. The same indices calculated using the temperature in Celsius would vary between −0.27% and + 1.3%. Since the internal convective temperature is always higher than zero, NRMSE_av is equal to NRMSE_av > 0. In this case, it is not possible to normalize the RMSE for the iqr or std during the winter and summer months since the temperature is close to the set point most of the time (as highlighted in Figure 3.5) therefore iqr and std are set equal to zero. These normalizations could only be used when the hourly data of the whole year were considered. The NRMSE_range can also be misleading since this index would be higher in months where the temperature is constant (i.e., range close to zero). The R^2 is lower in the months where the temperature is close to the set point (January, June, July, August and December) since in these periods the reference temperature is always near to the average temperature (see Eq. (2-19)).

Figure 3.5 shows the distribution of the reference heating power used for the calculation of the SIM_IBK deviation.

Figure 3.2 shows the indices considering the hourly data of heating power on monthly and yearly time frames. In addition, one additional column is added considering hourly data for the whole year only when the heating system is active. The monthly absolute deviation indices (i.e, MAE and RMSE) tend to be lower in April and May where the heating system is working less. The normalization of the statistical indices is also non-trivial for the heating power, in fact in April and October (see Figure 3.2b) where the heating power trends toward zero almost all the normalization means trend to zero as well (std, iqr, and av). This leads to really high relative deviations. The only normalization means that allow a stable evaluation of the deviation with relative indices is the range and av > 0. Another reasonable option might be to exclude transition periods (i.e. April and October) but this would require a subjective definition of the threshold under which the heating demand is too low for the calculation of the deviations. This problem arises also when a building has either a high envelope quality or is placed in a warm climate, i.e. if it has a really low heating demand (e.g. in this study for the climate of Rome).

By considering the whole year as a time frame, the NRMSE_av is 31.1% which would even be outside the thresholds suggested by ASHRAE Guideline 14-2014 [42] even though looking at Figure B.3a it can be noticed that SIM_IBK records deviations in heating power only 1% of the time of the whole year simulations and the deviation range between ± 5 W/m^2. The problem, in this case, is that the average heating power for the whole year trends towards zero since in many periods the building does not need any heating power (see Figure 3.5a). Calculating the deviation including only the heated periods (annual > 0), leads to a much lower NRMSE_av (18.2%), thanks to a higher mean value (see Figure 3.5a), even though the RMSE is higher since the number of samples is lower (see Figure 3.2a).

This approach would require selecting the periods over which the deviations are calculated leading to a subjective decision process. Another possibility is to consider all the available data and normalize the sum of the squared errors with the average of the reference values including only reference data higher than zero (NRMSE_av > 0).

The NMBE is not influenced by this problem since the sum of the reference values (i.e. in this case reference heating powers) at the denominator does not change considering or not values equal to zero.

After this analysis, it can be stated that:

- The MBE/NMBE is needed to show the sign of the deviation, but another index has to be used since the MBE suffers from the cancellation effect;
- The RMSE and MAE provide similar information but the RMSE is more sensitive to the outliners than MAE where each error increases linearly the MAE;
- The R^2 is not a good index when the analysed variable is mainly constant;
- The normalization of the statistical indices is a complex step and has to be performed carefully. In the current work this work the NRMSE_av > 0 will be used for the analysis of temperatures, power and energy;
- Having a larger dataset (hourly data for the whole year) makes the evaluation of the deviations more robust. Therefore when hourly data are considered the indices should be calculated over the whole year;

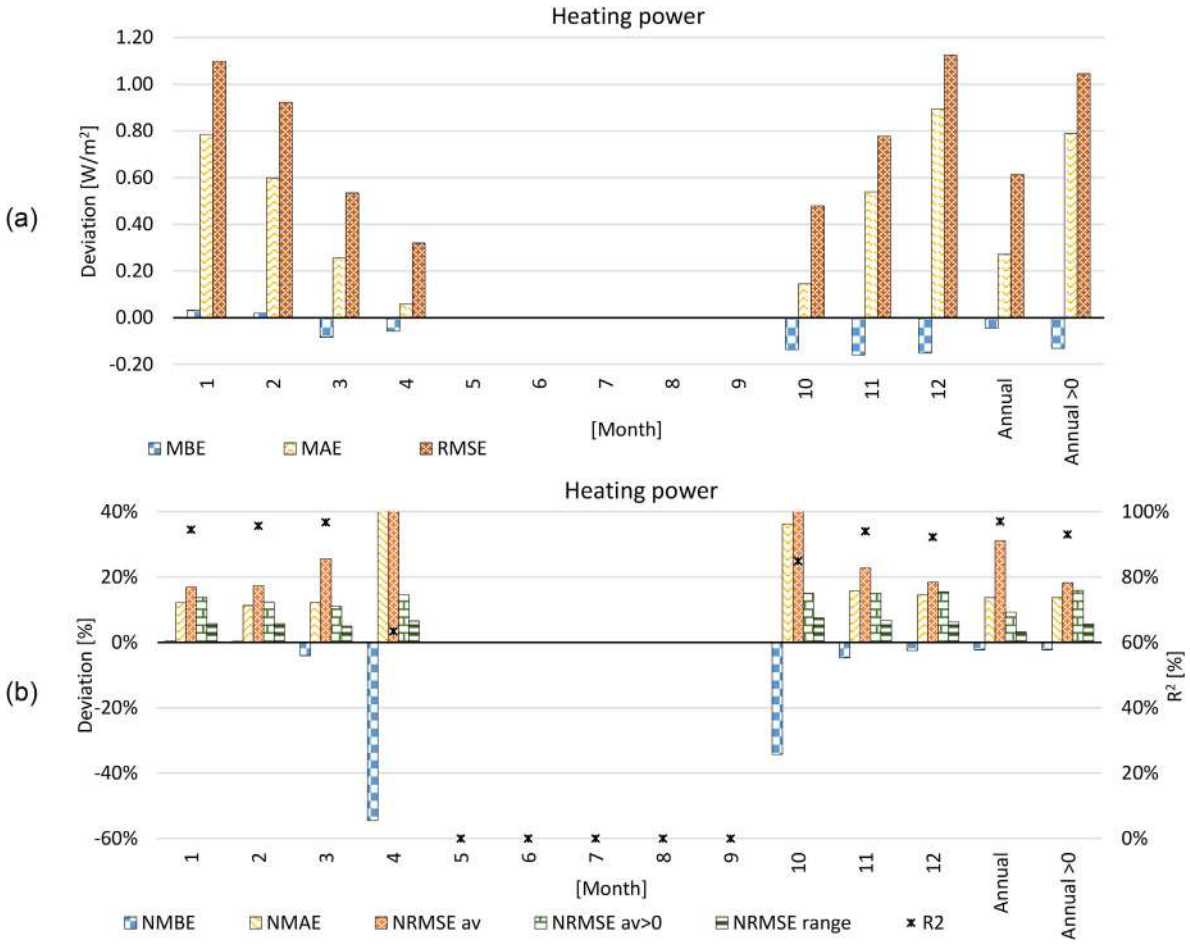

Figure 3.2. Non-normalized (a) and normalized (b) statistical indices applied for the calculation of the deviation between the simulated heating power with SIM_IBK and the reference heating power calculated as the median value of all tools for each time step, for the climate of Stockholm.

- The absolute thresholds suggested by ASHRAE Guideline 14–2014 can lead to unjust conclusions regarding the validity of cases with low energy demand (i.e. high-quality buildings or warm climates).

3.2. Results of the tool Cross-Comparisons

In this section, the monthly and hourly results of all the tools is presented that considers all the climates (i.e. Rome, Stuttgart and Stockholm) and the corresponding deviations.

3.2.1. Monthly results

Figure 3.3 shows the monthly heating (HD) and cooling (CD) demands, solar gain (SOL), ventilation summed with the infiltration (INF + VENT) and transmission (TR) losses for all the tools except for the PHPP where only HD and CD are reported, for climates of Stockholm, Stuttgart and Rome. The median value of each component of the thermal balance is presented in Figure 3.3 as a solid black line. The monthly values of the internal gains are excluded from the figure because all the tools consider the same monthly energy. Figure 3.3 shows that an overall good agreement between all the tools is reached, after the parametrization phase (see Sections 2.4 and 3.4). The PHPP was aligned with the other tools in the coldest winter and hottest summer months, but it could not exactly predict the HD and CD during the interim season. In all the locations, SIM_IBK had slightly lower infiltration and ventilation losses during the first part of the year. Considering the climate of Stockholm, DAL and EP had slightly higher solar gains and MOD slightly lower than the median value. Regarding the ventilation and infiltration losses, EP recorded lower losses in winter and slightly higher in summer, while IDA had higher ventilation losses in summer with respect to the median value. The effect of the capacity of the adiabatic structures generated deviations in the transmission losses in spring and autumn especially for the climate of Stockholm. In Stuttgart, EP was slightly above the median value concerning the solar gains, while IDA lower. MOD had slightly higher solar gains during winter and DAL during the summer with respect to the median value. Regarding the climate of Rome, IDA had higher solar gains during the whole year compared to the other tools and DAL only during summer.

All the component of the thermal balance are acting together and the results are the heating and cooling demands. In this specific case study, the control of the ventilation system allows to reduce the overheating problem (or cooling demand) compensating higher solar gains with increased ventilation losses.

3.2.2. Hourly results

Figure 3.4 shows the hourly average convective temperature (ϑ_c), ventilation and infiltration losses ($\dot{Q}_{Inf+Vent}$), solar gain ($\dot{Q}_{SOL}$), heating ($\dot{Q}_{HD}$) and cooling power ($\dot{Q}_{CD}$) for all the dynamic simulation tools for climate of Stockholm, for four different periods (48 h each) to represent the typical behaviour in all the seasons. From the convective temperature plots, it can be noticed that DAL is responding slower than the other tools in the free-floating periods since it considers only one lumped capacity. The

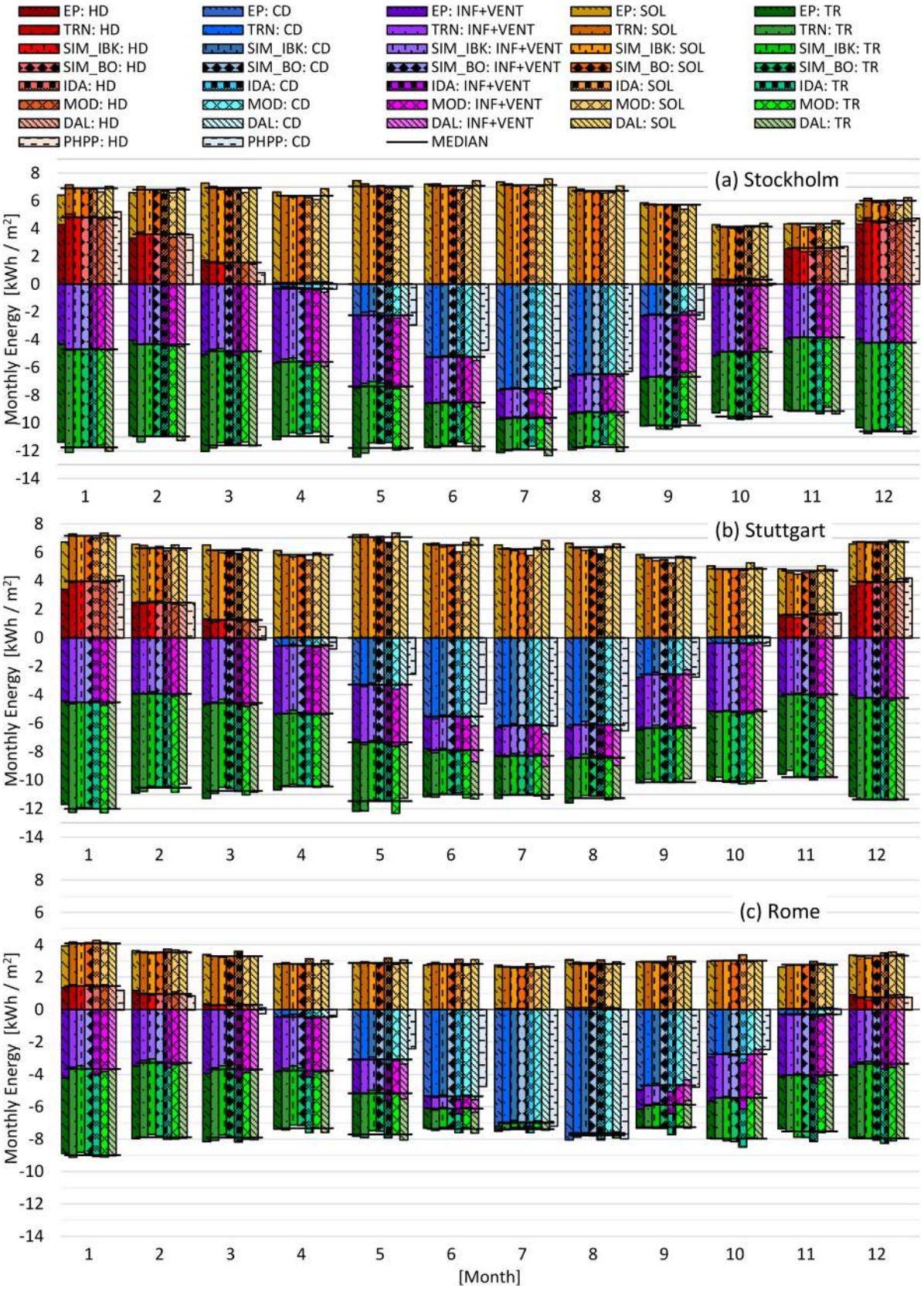

Figure 3.3. Monthly heating (HD) and cooling demand (CD), ventilation and infiltration losses (VV), transmission losses (TR), solar gains (SOL) and median values for the climates of Stockholm (a), Stuttgart (b) and Rome (c) for all the tools.

convective temperature in IDA is reacting faster than other tools and in MOD it is rising slightly earlier than other tools during the reported spring period (this is not happening systematically every day). Regarding the ventilation losses it can be noticed that DAL and IDA are starting one hour earlier than other tools in spring, summer and autumn since they consider the daylight-saving time.

In addition, EP has a slightly different control of the ventilation heat recovery bypass, which is activated slightly later than other tools in autumn and spring. The results show that solar gains are in good agreement as well as the cooling demand, even though DAL has sometimes higher peaks of the solar gains compared to the other tools due to the different sky model and shading control. Figures for the climates of Stuttgart (STU) and Rome (ROM) are reported in Appendix B (Figures B.1 and B.2).

Figure 3.5 shows boxplots[5] of the reference (i.e., median) heating power (a) and convective temperature (b) for the climate of Stock-

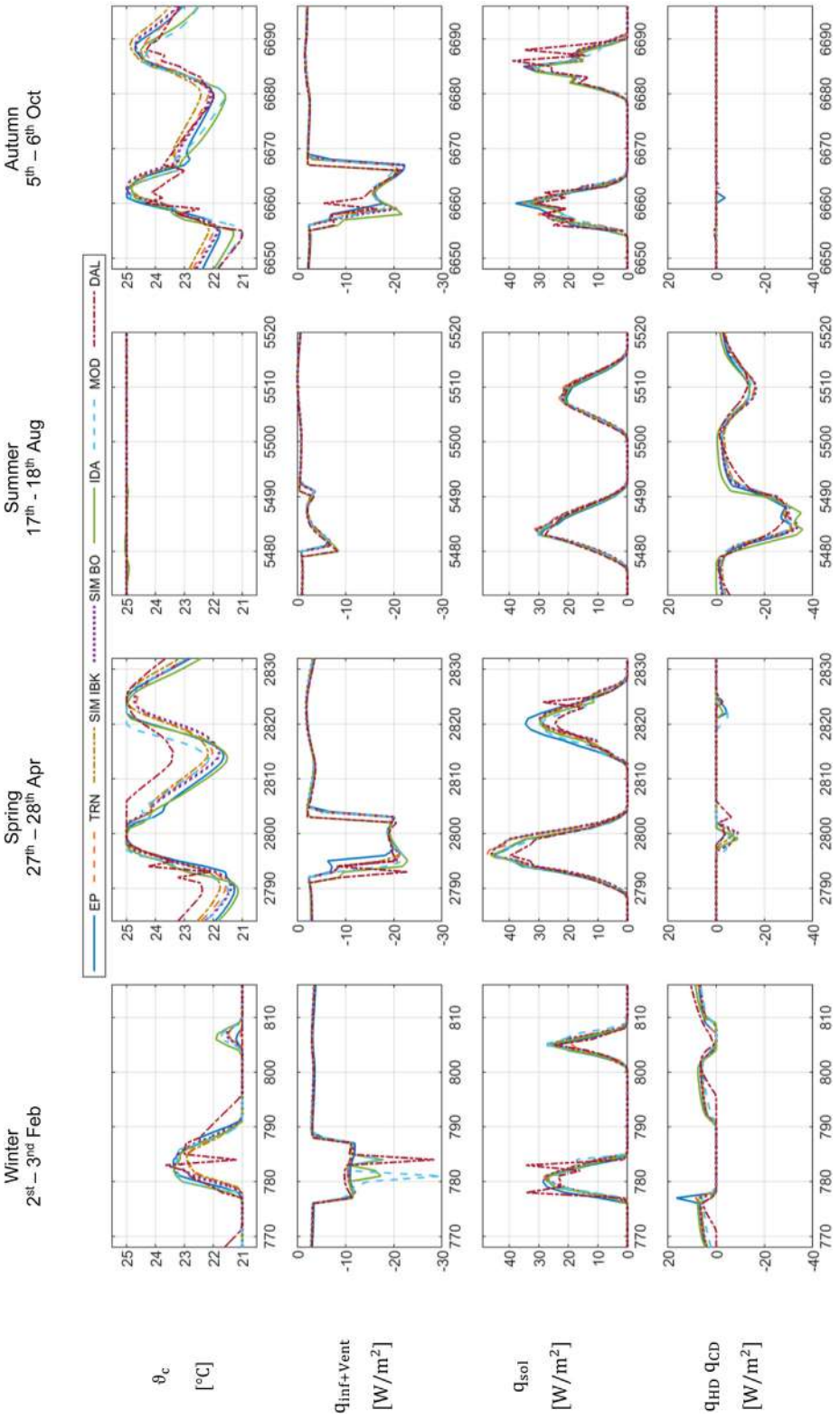

Figure 3.4. Hourly results (i.e., convective temperature, ventilation plus infiltration losses, solar gain, heating and cooling power) for all the dynamic simulation tools for the climate of Stockholm for winter, spring, summer and autumn periods (x-axis is hour of the year).

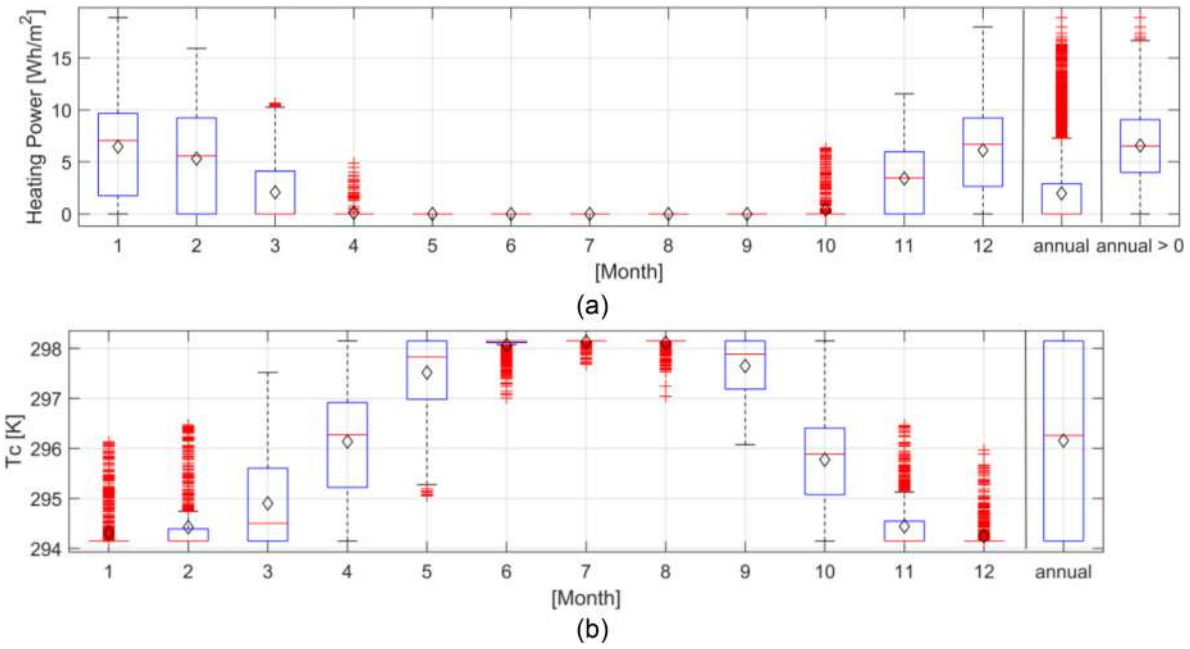

Figure 3.5. Box plot of the reference (i.e. median value of all tools for each time step) (a) heating power on monthly basis, for the whole year (i.e., "annual") and for the whole year considering only periods where the heating system is switched on (i.e. "annual > 0"); (b) convective temperature on monthly basis and for the whole year (i.e., "annual"). The red lines represent the median and the black rhombuses the mean. (For interpretation of the references to colour in this figure legend, the reader is referred to the web version of this article.)

holm considering monthly and annual data. In Figure 3.5a there is an additional box plot of the heating power considering the whole year, for those periods when only the heating system is activated ("annual > 0"). It can be noticed that the median heating power is equal to zero and the mean is close to zero if the whole year is considered (i.e., "annual") while excluding the periods in which the heating system is switched off (i.e., "annual > 0") the median is close to the mean value and they are both higher than zero. Problems might arise from this aspect concerning the normalization of the statistical indices as reported in Section 3.1 in more detail.

3.2.3. Deviations

Figure 3.6 presents the NMBE and NRMSE_av > 0 calculated on an hourly (h) and monthly (m) basis using the energy gain and losses associated with heating, cooling, infiltration, ventilation for the climate of Stockholm (a), Stuttgart (b) and Rome (c). The thresholds[6] for the NMBE and NRMSE are reported in Section 2.5 and are shown in Figure 3.6 using dot-dash lines. It is noteworthy, that PHPP only calculates heating and cooling demand on a monthly basis as standard output.

For the climate of STO and STU (see Figure 3.6a and b) DAL exceeds the threshold of 30% for the hourly NRMSE calculated on the solar gains, though the other indices are clearly within the thresholds. This is due to the combined effect of the different sky model used in DAL and the calibration of the shading threshold which allow reaching the same solar gain from the energy point of view, but with a different hourly distribution with respect to the other tools (see Figure 3.4 and Figure B.1). IDA slightly exceeds the solar gains NMBE_m in STU even though the other components of the thermal balance remain acceptable, while in ROM the higher solar gains also cause high ventilation losses and cooling demand, which leads to the thresholds (i.e., NMBE_m for solar gains and cooling demand and NMBE_m/h, NRMSE_av > 0_m/h for the ventilation losses) being exceeded. In ROM also SIM_IBK slightly exceeds the NMBE_m for the ventilation losses, even though all the other components of the balance are within the thresholds.

The results for monthly heating demand in ROM show that TRN, SIM_BO and IDA are within the thresholds while EP, DAL, SIM_IBK, MOD, DAL and PHPP are not. However, the HD in ROM is so low that it could be disregarded. In most cases, the hourly NRMSE_av > 0 is higher than the monthly value, while the hourly and the monthly NMBE deliver the same information. The results show that it is important to take both the NMBE and the NRMSE into consideration since in some cases the overall annual energy gains and losses might be in agreement, but the deviations considering hourly data are not. For example, the calculation of these indices for the solar gain in DAL can be observed. The hourly NRMSE_av > 0 calculated for the ventilation losses is particularly high for IDA and DAL because these two tools are the only two considering the shift between the daylight saving time and summer time, which leads to a shift in the schedule of the ventilation system (as can be seen in Figure 3.4, Figure B.1 and Figure B.2). For sake of better readability, R^2 was not reported in the graph but is always above 75%, (the minimum required by ASHRAE Guideline 14-2014), except for the heating demand in ROM for DAL where it is equal to 61% and for the ventilation losses of DAL in Stockholm, Stuttgart and Rome where it is equal to 67%, 64% and 72%, respectively. Concerning the convective temperature, the agreement between the tools is always within the thresholds in all the climates.

Overall, it can be stated that a good agreement between the tools is reached and that all the models are quite reliable after the parametrization process.

3.3. Computational cost

In Section 2.6 the boundary conditions in which the computational cost of each tool is calculated are defined. The PHPP is an instantaneous calculation tool therefore the fastest and is not included within this comparison. Figure 3.7 shows the computational cost for each tool without the post-processing of the output (in blue) and including it (in red). The filled diamond represents

[6] ±5% for the monthly NMBE, 15% for the monthly NRMSE, ±10% for the hourly NMBE, 30% for the hourly NRMSE and >0.75 for the R^2 [47].

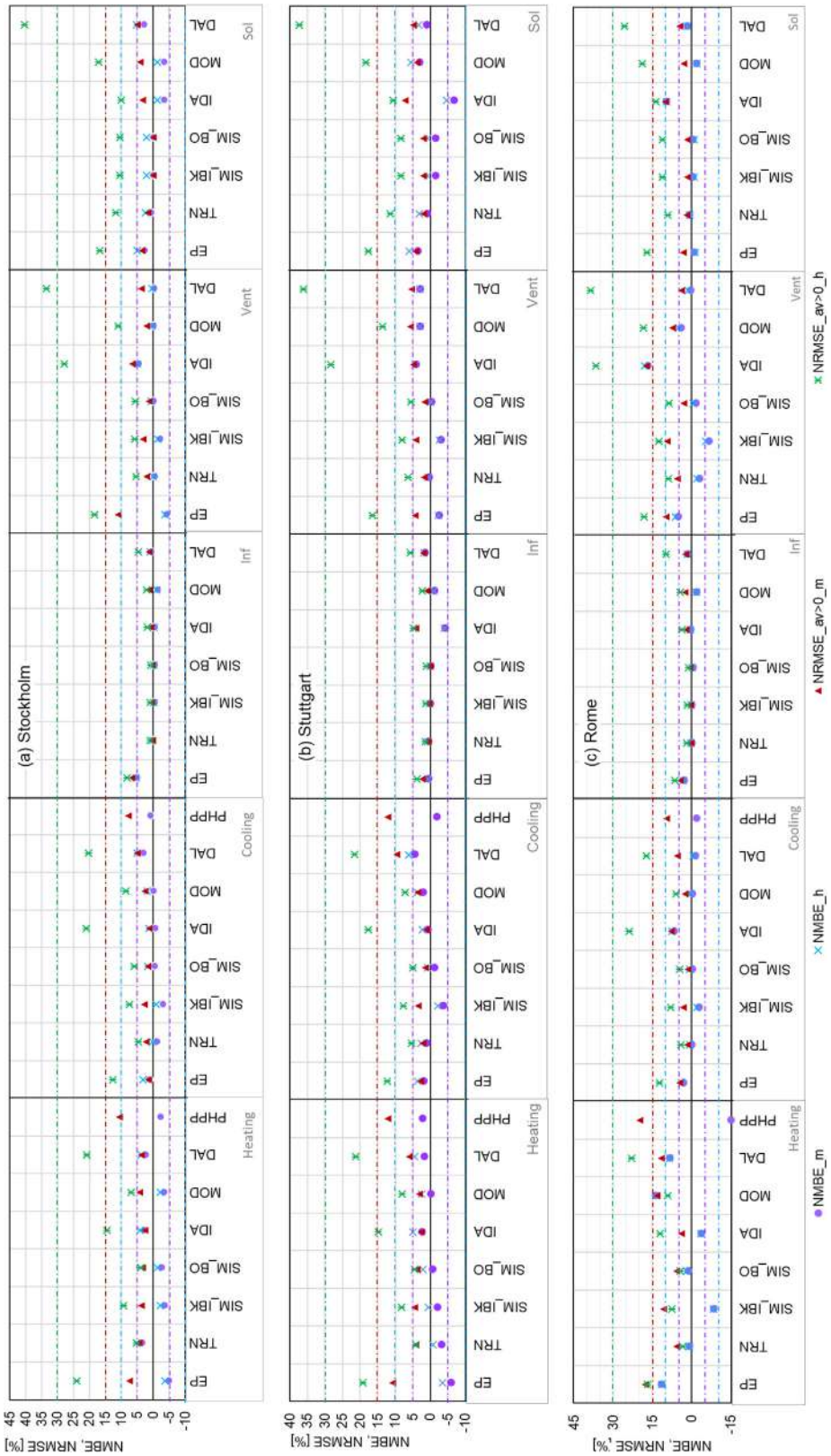

Figure 3.6. Hourly (h) and Monthly (m) NMBE and NRMSE_av > 0 calculated for Heating and cooling demand, ventilation and infiltration losses and solar gains considering the climate of Stockholm (a), Stuttgart (b) and Rome (c). The horizontal dot-dash lines represent the calibration criteria suggested by [42]: ±5% for the monthly NMBE, 15% for the monthly NRMSE, ±10% for the hourly NMBE, 30% for the hourly NRMSE.

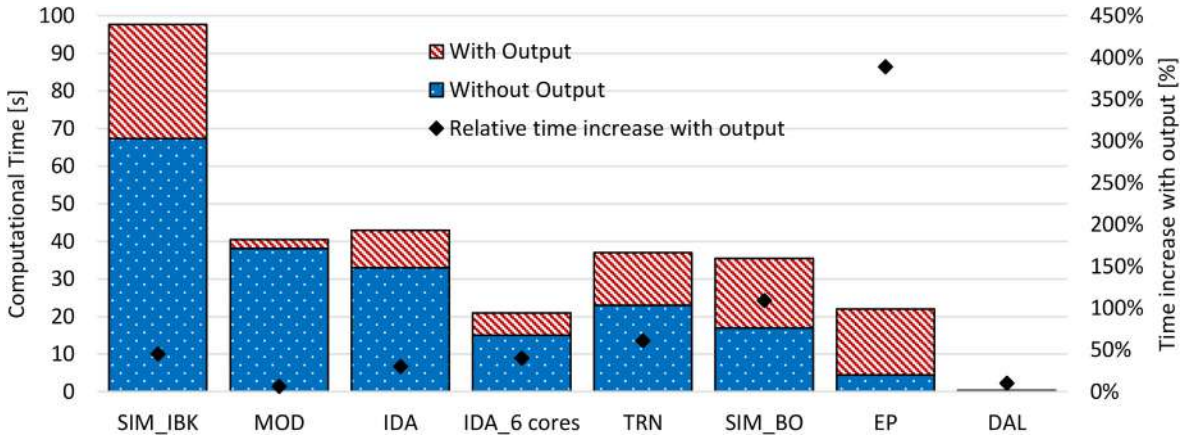

Figure 3.7. Computational time of each tool without the processing phase of the output (in blue) and the additional time required for the output preparation (in red). The dots represent the relative additional time when the outputs are prepared. (For interpretation of the references to colour in this figure legend, the reader is referred to the web version of this article.)

the relative additional time required when the output file needs to be prepared. The number and format of the outputs are different in the different tools. This is important to consider because the number of outputs considered is a user-defined variable that depends on the level of detail the user needs to analyse the results. For these reasons, the computational time is shown with and without output-processing to make a fair comparison of the calculation effort required by the model itself and, at the same time, to give an insight into the time required for the simulation to generate the output file.

The computational time of MOD is comparable with IDA, while EP and DAL can run an annual simulation in only a few seconds. IDA ICE can decrease to half the simulation time by splitting the annual simulation into various time slices, assigning them to different processing cores in the computer, while the other tools (TRNSYS, Simulink, Modelica and EnergyPlus) can profit from the multiple cores when more simulations run simultaneously (e.g., parametric sweep), but not on a single simulation for this model configuration. Among the investigated tools, DAL is the fastest but it must be highlighted that is the only tool based on an hourly time step and can be used only for predefined simple geometries (i.e., a shoebox) for which the view factor- and daylight matrices are pre-calculated. Although EP is one of the fastest tools, it requires a similar amount of time, for the elaboration of the output, than TRN and SIM_BO. The MOD and IDA simulations are faster than the other tools for the preparation of the output file.

Another aspect that is not depicted in Figure 3.7 is the time required for setting up the model. TRNSYS, IDA ICE, user interfaces for EnergyPlus, both Simulink libraries and PHPP can import the geometry information from a 3D drawing (i.e., gbXML, idf, dxf, IFC, etc. . .), easing the definition of the building model. For Modelica/Dymola such features are currently being developed within IBPSA project 1 [80]. Nevertheless, the requirements of the 3D drawing are different for the different tools therefore the interoperability is not straightforward. Though, this problem is supposed to be addressed by the improvements in the field of BIM to BEM in the near future.

3.4. Results pre and post-parametrization for DAL and PHPP

This section describes the effects of the parametrization process (see Section 2.4) on the results of PHPP and DAL, reporting the results of the non-parametrized simulation (i.e., DAL_online and PHPP_nonpar) and of the parametrized simulation (i.e. DAL_par and PHPP_par), which correspond to the final results of DAL and PHPP reported in Sections 3.2.1, 3.2.2 and 3.2.3.

With pre-design tools, it is not straightforward to model aspects such as hourly internal gain profiles, dynamic shading and ventilation bypass control as required by the description of this case study. The average value of the power due to the internal gain (see Figure 2.6) can be easily determined by averaging the hourly profile over the day for DAL (19.7 W/m^2) and over the week for the PHPP (6.5 W/m^2). The standard effective ventilation rate needs to also be recalculated for both PHPP and DAL online since both tools are based on a constant rate while, according to the description of the building the ventilation system, is switched on only during the working time. The additional ventilation rate due to the dynamic control of the bypass is considered in DAL online while in PHPP it is only possible to set this option for the summertime since the control is based on monthly ambient temperature instead of hourly as in DAL. The shading can be controlled as required by this case study in DAL online but the solar irradiation on the south facade used by DAL is different from the other tools since an isotropic sky model is applied instead of the Perez model, therefore the solar gains are also different. In PHPP only a summer and winter shading value can be given as input and in this case study, it would be difficult to guess this constant without knowing the results of the other dynamic simulation tools.

In PHPP_nonpar the standard assumptions are used during winter (25% reduction) and the reduction factor described in the report (70% reduction) is used for the summertime as temporary sun protection. In DAL online and PHPP_nonpar, the HTC of wall and window described in the report are used. DAL_par compared to DAL_online implements an improved ventilation model where only during the occupied time the ventilation system works, moreover the shading control threshold, the HTC of the façade and the building capacity are parametrised against the results of the other dynamic simulation tools.

PHPP_par implements a parametrized shading coefficient for summer and winter, ventilation rate and HTC (see Table 2.8). Table 3.1 reports the annual heating demand (HD) and cooling demand (CD) of PHPP and DAL pre and post parametrization, showing the relative deviation against the reference HD and CD (median of the results of all the tools). Figure 3.8 shows the monthly heating and cooling demand, infiltration plus ventilation and transmission losses, solar gains and average convective temperature simulated with DAL and PHPP pre and post parametrization and the reference value derived as a median of the results of all the tools for the climate of Stockholm. PHPP delivers only monthly heating and cooling demand, all the other components of the energy balance can be extrapolated by the user, but especially in spring and autumn, this process is non-trivial. Therefore,

Table 3.1
Annual Heating and Cooling demand (HD, CD) calculated with DALEC and PHPP pre and post parametrization compared against the reference heating and cooling demand (median of all the tools), for the climate of Stockholm.

	HD [kWh/(m²)]	ΔRef [%]	CD [kWh/(m²)]	ΔRef [%]
DAL_online	17.8	1%	−17.0	−30%
DAL_par	18.0	2%	−24.9	3%
PHPP_nonpar	6.3	−64%	−21.5	−11%
PHPP_par	17.2	−2%	−24.3	1%
Reference	**17.5**	**–**	**−24.1**	**–**

these months are not reported in Figure 3.8. It can also be noticed that the HTC of the window plays an important role in the transmission losses and that after the parametrization both tools are in agreement with the reference results. The standard assumptions of PHPP lead to an overestimation of the solar gain in winter and an underestimation in summer and to underestimate the ventilation losses, especially during summer. All these components lead to lower CD and HD of the PHPP_nonpar. DAL_online underestimates the solar gain throughout the year because of the different calculation of the solar radiation impinging the south façade (see Figure 2.5), this is improved in DAL_par by modifying the threshold of the shading control. The ventilation losses in DAL_par are fitting the results of SIM_BO since a schedule for the activation of the mechanical ventilation is introduced. It is also noteworthy to mention that in DAL_online the lower losses (transmission and ventilation) are compensated by lower solar gains resulting in an HD matching with the reference HD (see Table 3.1).

4. Lessons learned

Numerous iterations were necessary to reach a good agreement among the different tools even though the case study is well described in a comprehensive report and the reference building is geometrically simple. The challenges encountered in this process are only partly avoidable since user mistakes are difficult to foresee. Part of the challenge could be prevented by having a more detailed description of the building, avoiding misinterpretation and the entire parametrization process. An important issue that must also be highlighted is that since the tools implement different models, the outputs and the required inputs are defined differently. Defining equivalent input parameters for each model is a non-trivial task considering that different models describe physical phenomena using different levels of abstraction and at different levels of scale. A lesson that the authors derived from the parametrization process is that it is recommended to define input

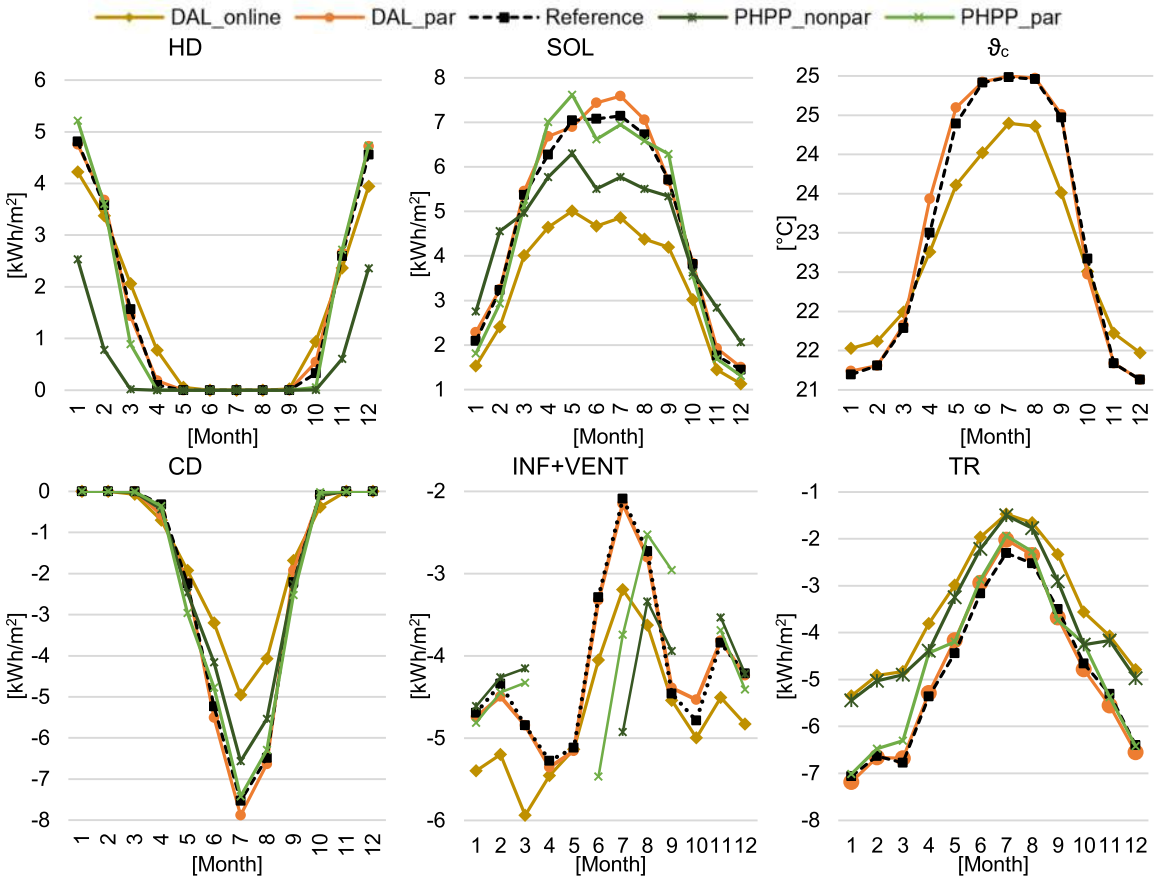

Figure 3.8. Monthly heating (HD) and cooling (CD) demand, infiltration plus ventilation (Inf + Vent) and transmission (TR) losses, solar gain (SOL) and convective temperature (ϑ_c) simulated with DAL online, DAL parametrized (DAL_par), PHPP non parametrized (PHPP_nonpar) and parametrized (PHPP_par) compared against the reference results for the climate of Stockholm.

parameters starting at the most detailed scale and the lowest level of abstraction amongst the tools that are going to be compared. Using the window system as an example, the process started with a reference office description where the window was described using properties at the level of the glazing system (TRN, SIM_BO) and detailed properties at the level of the individual window pane (EP, MOD) had to be derived through an exhaustive search process. The process of defining equivalent input parameters could have proceeded faster, however, if properties were originally defined at the window pane level and then used to derive equivalent properties at a higher level of abstraction based on subsystem simulation.

The window example also illustrates the problem of aligning simulation outputs. In tools with a simplified window, only the total solar gain can be given as output, while in other tools solar gains are reported using only directly transmitted solar radiation or the solar radiation absorbed at interior surfaces. Here, clearly defining the boundary conditions of different energy contributions was an essential part of aligning the simulation results of the different tools. The following paragraphs will give an overview of the user-related input errors and modelling decisions that were identified throughout the calibration process as sources of discrepancies between the different tools. Additionally, the magnitude of these discrepancies at different stages of calibration will be presented.

User mistakes experienced within this case study, were as follows:

- Flipped order of the layers of surface constructions;
- Wrong interpretation of the HTC of the window (HTC-glass instead of HTC-window). HTC-window is the results of the area-weighted HTC of the frame and the glass;
- Wrongly selected weather file where different data for the same location is used;
- Wrong starting day of the internal gain profile; and
- Wrong wall thermal capacity.

Wrong interpretations of the office description that could have been prevented by a more detailed description were made regarding the:

- Control of the mechanical ventilation;
- Control of the shading;
- Ventilation air volume flow;
- Heat recovery from fans of the ventilation system; and
- Control of the pre-heater used to avoid ice formation in the ventilation heat recovery system.

Moreover, information that was initially missing in the report were implemented differently in the different tools, i.e.:

- Air density (as a function of temperature or constant);
- Absorption and emission coefficient of opaque structures; and
- The convective exchange coefficients (as a constant or function of the temperature difference);

Comparing only the modelled heating and cooling demand, was not enough to find the reasons for the deviations between the tools. Often, higher gains might be balanced by higher losses hardly affecting the heating and cooling demand and therefore the zone heat balance was investigated. Additionally, isolating particular heat transfer phenomena assisted in identifying the cause of deviations. For instance, simulations were executed:

- Without solar radiation;
- Without windows;
- With a permanently activated, or no shading device;
- Using constant convective heat transfer coefficients, identical in all models, rather than the detailed algorithms available in some tools;
- Without internal gains;
- With different modelling approaches of the adiabatic structures;
- Without ventilation system.

All these cases were not executed with all the tools, but only where deviations needed to be identified with further analysis. Along with the different tests, an increasing number of outputs were analysed and compared (e.g., Internal surface temperatures, all the details of the balance of windows and walls, all the components of the weather data, distribution of the internal gains and solar gains, ventilation and infiltration losses, etc. . .).

The window model has a key role, in this case study, since it represents the main source of transmission losses. Therefore, the parametrization of the input for both simplified and detailed window models was a time-consuming process. Within this work, using the given constant HTC for the window in Stockholm deliver an HD 37% lower than using the detailed window model.

Table 4.1 reports the annual heating (HD) and cooling (CD) demand of each tool for the climates of Rome (ROM), Stuttgart (STU) and Stockholm (STO) in the initial iteration (V1), an intermediate step (V2) and the final results presented in this paper (V3). For each case, the maximum and minimum annual NMBE are reported and on the right-hand side, the dispersion of the annual HD and CD is represented by box plots for each iteration. The first iteration is represented by V1, here the dispersion of the results is important since many user mistakes and wrong interpretation of the office description are present. Within the V2 the situation is improved, but still not acceptable since the spread of the results is still high.

With V3 a good agreement is reached thanks to the recognition of the user mistakes and the parametrization of the window model. From V1 to V2 the window properties were parameterized in EP, the set point of the anti-freezing was corrected in TRN, the shading model, the volume of the TZ, the starting day of the occupancy profile, the adiabatic model of the opaque structure and the weather file were corrected in SIM_IBK, and the HTC of the window in DAL. From V2 to V3 an improved parameterization of the window properties was carried out for MOD and EP, the convective coefficient calculation was modified to use the same equations in EP, TRN and MOD. In SIM_IBK was introduced the window model from the library of SIM_BO and the order of the construction layers of the adiabatic ceiling and floor was corrected in MOD and TRN.

5. Conclusions

In this work, the modelling approaches of well-known dynamic simulation tools, EnergyPlus, TRNSYS, IDA ICE, Modelica/Dymola the new Matlab/Simulink libraries, CarnotUIBK and ALMABuild as well as the predesign tools DALEC and PHPP were described and the tools compared against each other using a typical office cell located in Rome, Stuttgart and Stockholm as a reference building. To compare the results of the different tools, commonly used statistical indices and normalization means were analysed and finally the Normalized Mean Bias Error and Normalized Root Mean Square Error were used to assess the degree of agreement of the results with the median value used as a reference. The thresholds suggested by ASHRAE Guideline 14–2014 were used as a basis for this evaluation. The normalization process of the statistical indices was non-trivial and the encountered challenges were presented and thoroughly highlighted within this paper.

Table 4.1
Annual Heating and Cooling demand for each tool in the climate of ROM, STU and STO through the different iteration rounds (V1, V2 and V3) required to reach a good agreement.

		V1 (04/2018) HD	V1 (04/2018) CD	V2 (04/2019) HD	V2 (04/2019) CD	V3 (04/2021) HD	V3 (04/2021) CD
		[kWh/m²]					
ROM	EP	1.0	-51.2	3.6	-36.4	3.9	-32.3
	TRN	3.4	-32.4	3.5	-33.3	3.5	-31.4
	SIM_IBK	7.9	-29.9	5.8	-38.2	3.2	-30.5
	SIM_BO	-	-	3.1	-33.4	3.5	-31.3
	IDA	-	-	-	-	3.4	-33.5
	MOD	-	-	7.1	-34.0	4.0	-31.3
	DAL	6.1	-31.0	5.9	-35.9	3.8	-31.0
	PHPP	-	-	5.7	-37.9	3.0	-30.8
	MEDIAN	**4.7**	**-31.7**	**5.7**	**-35.9**	**3.5**	**-31.3**
	Max NMBE	67%	61%	25%	6%	12%	7%
	Min NMBE	-79%	-6%	-46%	-7%	-16%	-2%
STU	EP	11.4	-32.3	15.8	-28.1	12.5	-25.2
	TRN	18.0	-22.6	18.7	-23.2	12.9	-24.9
	SIM_IBK	18.5	-22.6	16.0	-31.7	13.0	-23.8
	SIM_BO	-	-	13.2	-23.9	13.2	-24.4
	IDA	-	-	-	-	13.7	-24.9
	MOD	-	-	17.1	-27.9	13.3	-25.2
	DAL	16.4	-22.6	18.2	-28.4	13.6	-25.8
	PHPP	-	-	14.5	-27.6	13.6	-24.2
	MEDIAN	**17.2**	**-22.6**	**16.0**	**-27.9**	**13.3**	**-24.9**
	Max NMBE	8%	43%	17%	13%	3%	4%
	Min NMBE	-34%	0%	-17%	-17%	-5%	-5%
STO	EP	13.5	-34.6	17.0	-32.2	16.7	-24.4
	TRN	20.4	-23.3	21.3	-23.8	18.2	-23.8
	SIM_IBK	15.0	-23.8	14.5	-31.0	16.9	-23.4
	SIM_BO	-	-	17.4	-23.6	17.1	-24.0
	IDA	-	-	-	-	18.1	-24.0
	MOD	-	-	14.5	-30.0	16.9	-24.1
	DAL	14.2	-21.8	16.9	-28.2	18.0	-24.9
	PHPP	-	-	14.6	-31.0	17.1	-24.3
	MEDIAN	**14.6**	**-23.5**	**16.9**	**-30.0**	**17.1**	**-24.1**
	Max NMBE	40%	47%	26%	7%	6%	3%
	Min NMBE	-7%	-7%	-14%	-21%	-2%	-3%

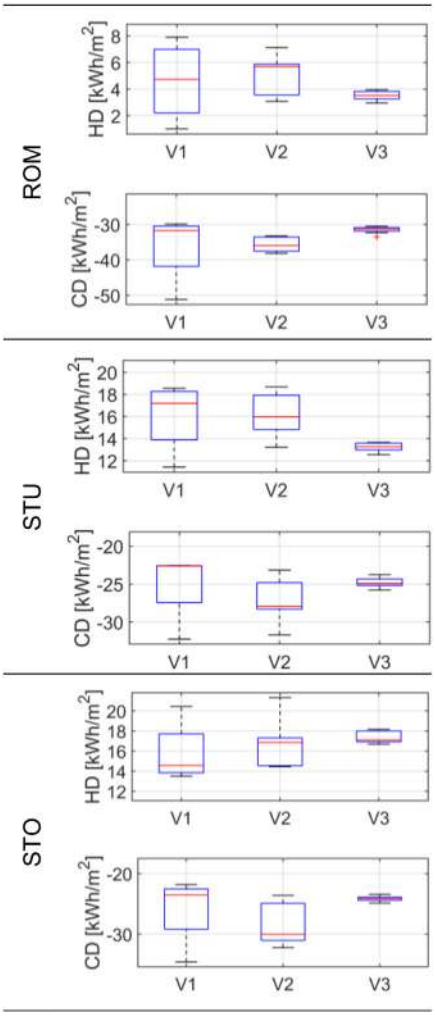

After many iterations, it can be stated that overall a good agreement between all the dynamic tools was reached. The annual results from the PHPP program was also aligned with the annual results of all the other tools. At the beginning of this process, the relative deviation of the heating and cooling demands predicted by the different tools was from + 61% to −34%, which was reduced to + 7% to −5% after many simulation rounds (excluding the heating demand in Rome which is almost negligible). The deviations that were experienced were mainly due to difficulties in defining equivalent input parameters for the models based on different approaches; user mistakes; and misinterpretation of the building description. User mistakes were clearly difficult to avoid, while different interpretations of the building description were mainly caused by an insufficient description. At the same time a tedious parametrization phase was required for those tools which were either more simplified (e.g., PHPP and DALEC) or more complex (e.g. Modelica and EnergyPlus) compared to the building description that was written using TRNSYS as a reference. The parametrization of inputs such as the ventilation rate and constant shading allowed the comparison to reach a good agreement even for simplified tools like PHPP, where dynamic control logics (i.e., shading and ventilation control) required for this case study, cannot be modelled. The results of DALEC and PHPP pre and post-parametrization for the climate of Stockholm were reported and the deviation of PHPP annual heating demand compared to the reference median value was reduced from −64% to −2% and from −11% to 1% for the cooling demand. The different tools involved in this study allow analysis with different degrees of detail and at the same time, they have very different computational costs. An overview of the modelling approaches available within the different software packages was given and the computational time required by each model used for this case study was reported, to support users in choosing a simulation tool that fits their purpose.

The computational cost was quantified by running the simulations using the different tools on the same computer. DALEC and PHPP were both almost instantaneous. However, these were also simplified compared to the other simulation software packages. EnergyPlus ran for about 5 sec and was faster compared to the other tools. TRNSYS and ALMABuild were in the same range around 20 sec, whereas Modelica/Dymola and IDA ICE were slightly slower with 38 and 33 sec respectively. CarnotUIBK was the slowest with 67 sec.

CRediT authorship contribution statement

Mara Magni: Conceptualization, Methodology, Software, Validation, Formal analysis, Investigation, Data curation, Writing - original draft, Visualization. **Fabian Ochs:** Supervision, Project

administration, Funding acquisition, Writing - review & editing. **Samuel de Vries:** Software, Validation, Writing - review & editing. **Alessandro Maccarini:** Software, Writing - review & editing. **Ferdinand Sigg:** Software, Writing - review & editing.

Declaration of Competing Interest

The authors declare that they have no known competing financial interests or personal relationships that could have appeared to influence the work reported in this paper.

Acknowledgements

This work was performed within the framework of IEA SHC Task 56 international project.

We thank Abdulrahman Dahash and Shandilya Apeksha for an internal review of the paper, Hauer Martin and Plörer Daniel for supporting the simulations with DALEC, EURAC for the collaboration within the IEA SHC Task 56 project. Thanks to the University of Bologna for allowing us to use ALMABuild, Nicola Franzoi for the fruitful discussion about the statistical indices, Toni Calabrese and Ellika Taveres-Cachat for contributing in creating the TRNSYS and IDA ICE models.

Appendix

A. Detailed window properties

In Figure A.1 the window properties used in MOD and EP in the climates of Rome, Stuttgart and Stockholm are reported.

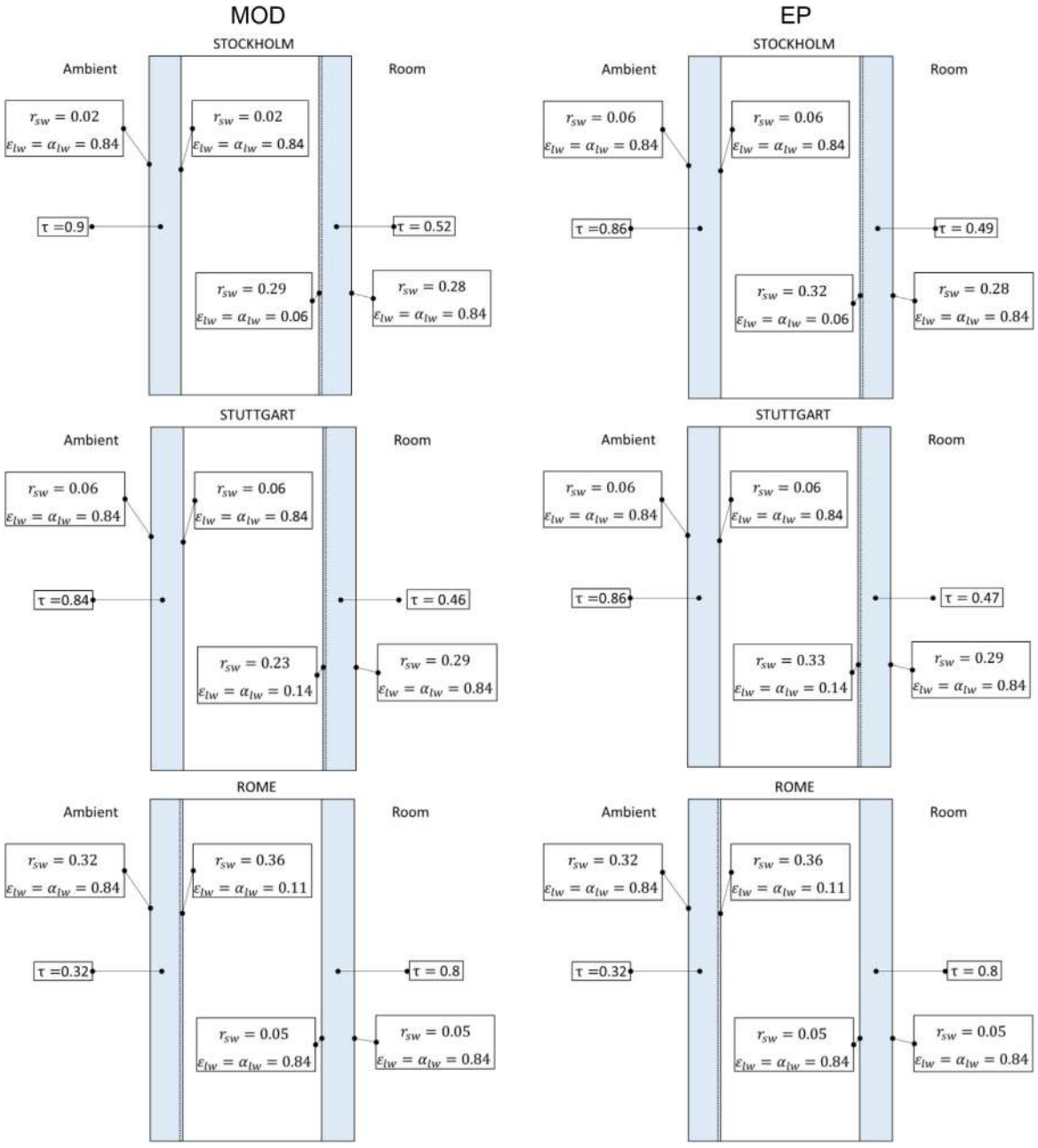

Figure A1. Detailed optical window properties used in EP and MOD in each climate.

B. Hourly plot

Figure B.1 and Figure B.2 show the hourly average convective temperature (ϑ_c), ventilation and infiltration losses ($\dot{Q}_{Inf+Vent}$), solar gain ($\dot{Q}_{SOL}$), heating ($\dot{Q}_{HD}$) and cooling power ($\dot{Q}_{CD}$) in 4 representing periods for winter, spring, summer and autumn for all the dynamic simulation tools considering the climate of Stuttgart and Rome, respectively. In Figure B.1 and Figure B.2 can be noticed that:

- DAL is responding slower than the other tools in the free-floating periods since it considers only one lumped capacity;

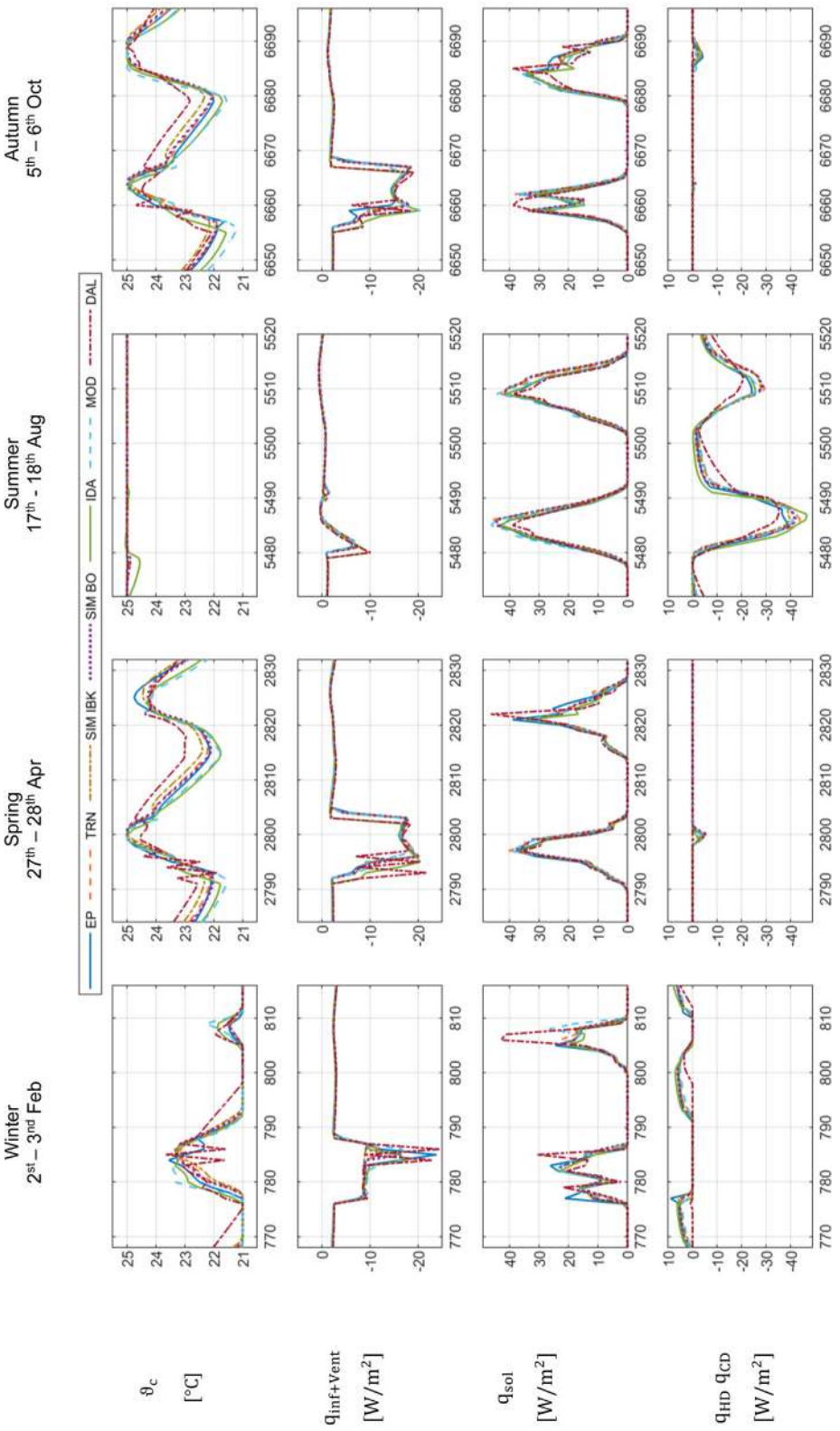

Figure B1. Hourly results (i.e. convective Temperature, ventilation plus infiltration losses, solar gain, heating and cooling power) for all the dynamic simulation tools considering the climate of Stuttgart and 4 representing periods for winter, spring, summer and autumn.

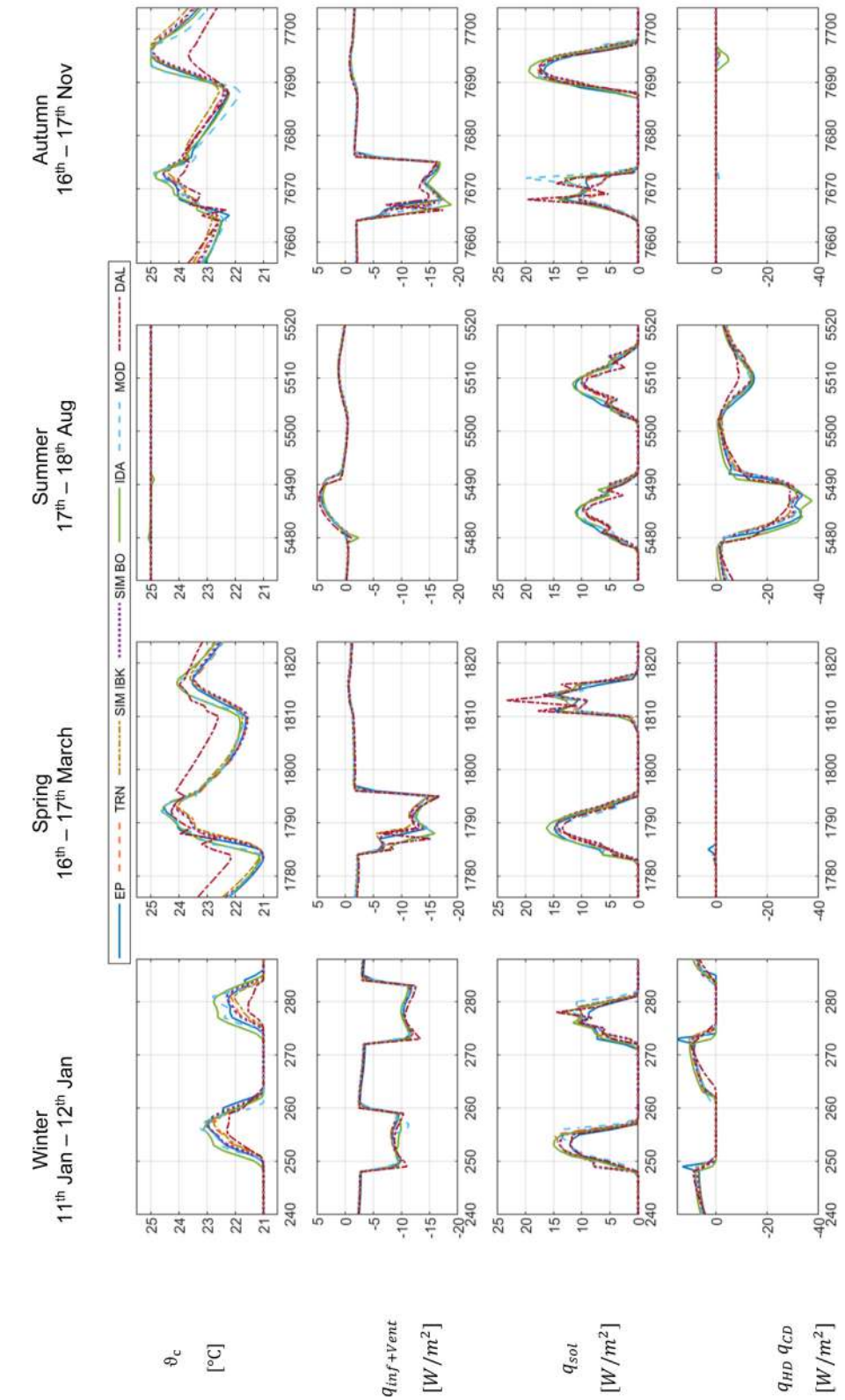

Figure B2. Hourly results (i.e. convective Temperature, ventilation plus infiltration losses, solar gain, heating and cooling power) for all the dynamic simulation tools considering the climate of Rome and 4 representing periods for winter, spring, summer and autumn.

- The convective temperature in IDA and MOD is reacting faster than other tools;
- The ventilation system is starting one hour earlier in DAL and IDA than other tools in spring, summer and autumn since DAL and IDA consider the daylight-saving time;
- DAL has sometimes higher peaks of the solar gains compared to the other tools due to the different sky model and shading control;
- In winter EP has heating power peaks due to non-completely ideal control.

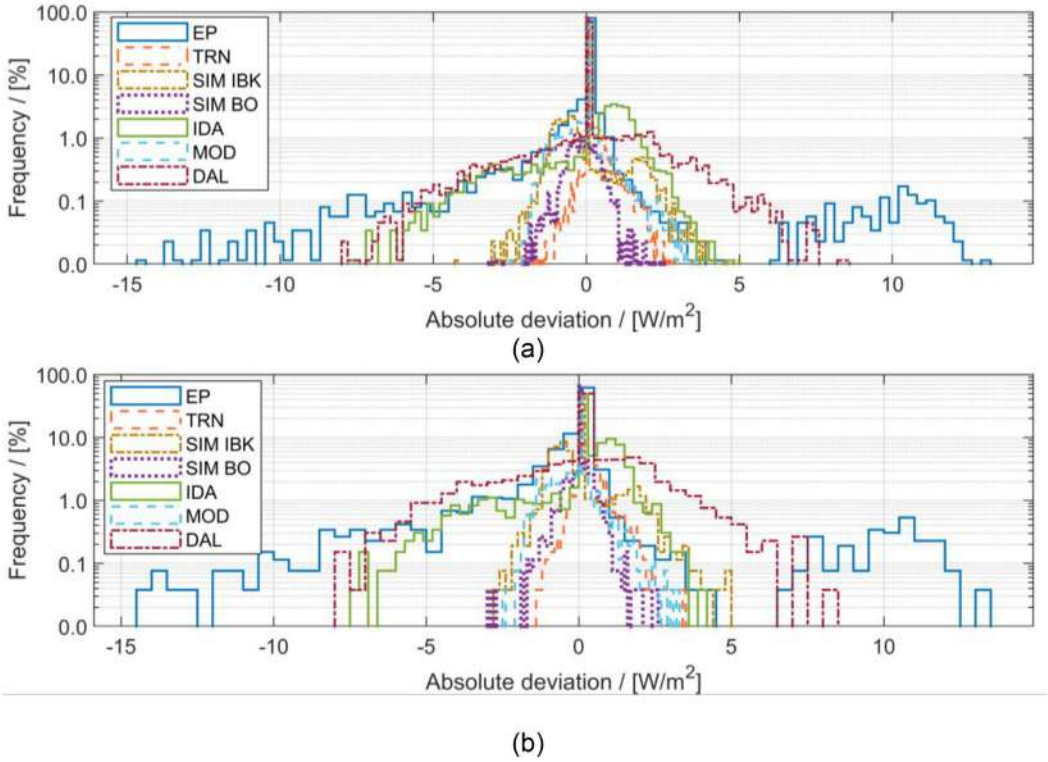

Figure B3. Absolute deviation of the hourly heating power for all the tools for one-year simulation in the climate of Stockholm, (a) considering the whole year, (b) considering only periods in which the heating system is working. The deviation is calculated as the hourly heating power of the tool minus the hourly reference power (median of all the tools).

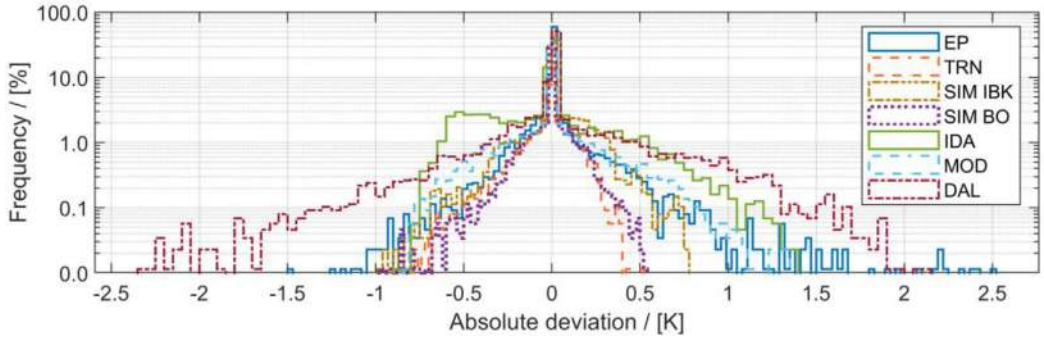

Figure B4. Absolute deviation of the hourly convective temperature for all the tools for one-year simulation in the climate of Stockholm. The deviation is calculated as the hourly convective temperature of the tool minus the hourly reference convective temperature (median of all the tools).

The histogram reporting the distribution of the deviations can give precious information regarding the sign of the deviation and how often it occurs.

Figure B.3 shows the distribution of the absolute deviations of the heating power for all the tools considering the climate of Stockholm including the whole year (a) and only periods in which the heating system is active (b). It can be noticed that the distribution of the deviations for the different tools is the same in graphs a and b but the frequency of the deviation is drastically higher when only periods in which the heating system is working are considered.

Figure B.4 shows the distribution of the absolute deviations of the convective temperature for all the tools considering the climate of Stockholm.

From Figures B.3 and B.4 it can be easily noticed that IDA and EP reported a non-symmetrical distribution of the deviations. In particular, IDA reported a lower convective temperature (−0.5 K) more often than other tools. Starting from this information and analysing the hourly plot for the whole year, it was possible to see that the convective temperature of IDA in summer during the night is decreasing slightly faster than the other tools. For EP it can be noticed that the distribution of the convective temperature deviation (see Figure B.4) is shifted towards the positive side and the distribution of the deviation of the heating power is shifted towards the negative side (see Figure B.3). Analysing the hourly plot for the whole year, it was possible to notice that the ventilation control of EP on some days during winter caused lower ventilation losses with respect to the other tools. The peaks of the heating power of EP, visible in Figure 3.4 (hour 775), caused the frequency peak correspondent to 10 W/m2 in Figure B.3. The high dispersion in both convective temperature and heating power deviations for DAL is due to the simplified capacity model used within this tool (see Sections 2.3, 2.4, and 3.2.2).

C. Summary of reference office cell description and boundary conditions

In Table C1 a short description of the office building inputs and of the applied boundary conditions is provided.

Table C1
Summary of reference office cell description and boundary conditions.

Geometry	Dimensions	width: 4.5 m; depth: 6 m; height: 3 m (27 m^2)
	Facade orientation	South
	Window to wall ratio:	60%
	Frame to window ratio:	25%
Fenestration	Stockholm:	HTC_{gl}: 0.81 W/(m^2 K), HTC_{frame}: 1.18 W/(m^2 K), τ_{sol}: 0.46, SHGC: 0.63, CEN
	Stuttgart:	HTC_{gl}: 1.40 W/(m^2 K), HTC_{frame}: 1. 18 W/(m^2 K), τ_{sol}: 0.43, SHGC: 0.59, CEN
	Rome:	HTC_{gl}: 1.29 W/(m^2 K), HTC_{frame}: 1. 18 W/(m^2 K), τ_{sol}: 0.26, SHGC: 0.33, CEN
Shading		Active when direct solar radiation on the south façade is higher than 120 W/m^2
Facade	Stockholm:	HTC_{wall} = 0.3 W/m^2K
	Stuttgart:	HTC_{wall} = 0.4 W/m^2K
	Rome:	HTC_{wall} = 0.8 W/m^2K
Ceiling, walls, floor		Mixed: heavy weight floor/ceiling, lightweight walls
Internal gains	People:	3 (variable occupancy). 120 W/pers.
	Occupancy:	Weekdays: 8:00–19:00, 3 people (variable occupancy), 120 W per person
	Lighting:	10.9 W/m^2 (hourly profile)
	Equipment:	7.0 W/m^2 (hourly profile)
HVAC and settings	Infiltration:	ACH: 0.15
	Ventilation:	Constant during occupied hours, 40 m^3/(h*pers.)
		Sensible heat recovery with controlled bypass, efficiency: 70%
	Set points:	Lower set point: 21 °C, Upper set point: 25 °C (constant)
Weather		TMY2, Stockholm, Stuttgart, Rome

References

[1] H. Wang, Z. Zhai, Advances in building simulation and computational techniques: a review between 1987 and 2014, Energy Build. 128 (2016) 319–335, https://doi.org/10.1016/j.enbuild.2016.06.080.

[2] V.S.K.V. Harish, A. Kumar, A review on modeling and simulation of building energy systems, Renew. Sustain. Energy Rev. 56 (2016) 1272–1292, https://doi.org/10.1016/j.rser.2015.12.040.

[3] D.B. Crawley, J.W. Hand, M. Kummert, B.T. Griffith, Contrasting the capabilities of building energy performance simulation programs, Build. Environ. 43 (4) (2008) 661–673, https://doi.org/10.1016/j.buildenv.2006.10.027.

[4] Building Energy Software Tools, Best Directory | Building Energy Software Tools, (2020). https://www.buildingenergysoftwaretools.com/?__cf_chl_jschl_tk__=333a9062c0deb41f0aedbc09d4de96cab9d74a2d-1595925926-0-Ac80m_md0jCDx9IWiUyqe8WYrQij-imLS12aG2ZaEQAA0YJNQ0m3L4gPuZsqdDSQfZjPvfeemai8Is_wyDsp2znHqB0uwrDsw9iKK61KqCSarbSfBzG2zeBoLKS2ww74sxIaBbi7 (accessed July 28, 2020).

[5] T. Zakula, M. Bagaric, N. Ferdelji, B. Milovanovic, S. Mudrinic, K. Ritosa, Comparison of dynamic simulations and the ISO 52016 standard for the assessment of building energy performance, Appl. Energy 254 (2019) 113553, https://doi.org/10.1016/j.apenergy.2019.113553.

[6] M. Trčka, J.L.M. Hensen, Overview of HVAC system simulation, Autom. Constr. 19 (2) (2010) 93–99, https://doi.org/10.1016/j.autcon.2009.11.019.

[7] S. Kota, F.J.F. Stipo, W. Jeong, J.B. Kim, J.L.B. Alcocer, M.J. Clayton, W. Yan, J.S. Haberl, Development of a reference building information model for thermal model compliance testing-part I: Guidelines for Generating Thermal Model Input Files, ASHRAE Trans. 122 (2016) 256–266.

[8] F. Farias, S. Kota, W. Jeong, J.B. Kim, J.L.B. Alcocer, J.S. Haberl, M.J. Clayton, W. Yan, Development of a reference building information model (BIM) for thermal model compliance testing-part ii: test cases and analysis, ASHRAE Trans. 125 (2019) 750–764.

[9] CARNOT Toolbox - File Exchange - MATLAB Central, (2020). https://de.mathworks.com/matlabcentral/fileexchange/68890-carnot-toolbox (accessed August 19, 2020).

[10] D. Siegele, E. Leonardi, F. Ochs, A new MATLAB Simulink Toolbox for Dynamic Building Simulation with B.I.M. and Hardware in the Loop compatibility, Proc. Build. Simul. 2019 16th Conf. IBPSA. (2019) 2651–2658. https://doi.org/10.26868/25222708.2019.210641.

[11] J.P. Campana, G.L. Morini, BESTEST and EN ISO 52016 benchmarking of ALMABuild, a new open-source simulink tool for dynamic energy modelling of buildings, Energies 12 (2019) 2938, https://doi.org/10.3390/en12152938.

[12] Berkeley National Laboratory, Open source library for building and district energy and control systems, (2020). https://simulationresearch.lbl.gov/modelica/ (accessed November 30, 2020).

[13] Bartenbach, University, of Innsbruck, DALEC, Zubotel Lighting, 2020, http://dalec.uibk.ac.at/#room (accessed November 30, 2020).

[14] Passivhaus Institut, (2020). https://passiv.de/en/04_phpp/04_phpp.htm (accessed August 25, 2020).

[15] Mara Magni, Jean Pierre Campana, Fabian Ochs, Gian Luca Morini, Numerical investigation of the influence of heat emitters on the local thermal comfort in a room, Build. Simul. 12 (3) (2019) 395–410, https://doi.org/10.1007/s12273-019-0506-8.

[16] D. Mazzeo, N. Matera, C. Cornaro, G. Oliveti, P. Romagnoni, L. De Santoli, EnergyPlus, IDA ICE and TRNSYS predictive simulation accuracy for building thermal behaviour evaluation by using an experimental campaign in solar test boxes with and without a PCM module, Energy Build. 212 (2020) 109812. https://doi.org/10.1016/j.enbuild.2020.109812.

[17] L. Giraud, R. Bavière, C. Paulus, Modeling of solar district heating: a comparison between TRNSYS and MODELICA, in: EuroSun, Aix-les-Bains, 2014: p. 11. https://doi.org/10.18086/eurosun.2014.19.06.

[18] W. Tian, A review of sensitivity analysis methods in building energy analysis, Renew. Sustain. Energy Rev. 20 (2013) 411–419, https://doi.org/10.1016/j.rser.2012.12.014.

[19] A.S. Solmaz, A critical review on building performance simulation tools, Int. J. Sustain. 12 (2019) 7–21.

[20] Matthias Werner, David Geisler-Moroder, Bert Junghans, Oliver Ebert, Wolfgang Feist, DALEC–a novel web tool for integrated day- and artificial light and energy calculation, J. Build. Perform. Simul. 10 (3) (2017) 344–363, https://doi.org/10.1080/19401493.2016.1259352.

[21] Hema Sree Rallapalli, A Comparison of EnergyPlus and eQUEST Whole Building Energy Simulation Results for a Medium Sized Office Building, Arizona State University, 2010.

[22] Tianzhen Hong, Fred Buhl, Philip Haves, Stephen Selkowitz, Michael Wetter, Comparing computer run time of building simulation programs, Build. Simul. 1 (3) (2008) 210–213, https://doi.org/10.1007/s12273-008-8123-y.

[23] D. Kim, W. Zuo, J.E. Braun, M. Wetter, Comparisons of building system modeling approaches for control system design, in, Build. Simul. (2013) 3267–3274.

[24] A.T. Nguyen, S. Reiter, P. Rigo, A review on simulation-based optimization methods applied to building performance analysis, Appl. Energy. 113 (2014) 1043–1058, https://doi.org/10.1016/j.apenergy.2013.08.061.

[25] W. Feist, Thermische Gebäudesimulation: kritische Prüfung unterschiedlicher Modellansätze, Müller Jur Verl, Heidelberg, 1994.

[26] R. Judkoff, D. Wortman, J. Burch, Empirical Validation of Building Analysis Simulation Programs: A Status Report, Solar Energy Research Institute, Golden, Colorado, 1982.

[27] R. Judkoff, D. Wortman, B. O'Doherty, J. Burch, A methodology for validating building energy analysis simulations, NRELTechnical Rep. 550–42059 (2008) 1–192.

[28] Paul Strachan, Katalin Svehla, Ingo Heusler, Matthias Kersken, Whole model empirical validation on a full-scale building, J. Build. Perform. Simul. 9 (4) (2016) 331–350, https://doi.org/10.1080/19401493.2015.1064480.
[29] P. Nageler, G. Schweiger, M. Pichler, D. Brandl, T. Mach, R. Heimrath, H. Schranzhofer, C. Hochenauer, Validation of dynamic building energy simulation tools based on a real test-box with thermally activated building systems (TABS), Energy Build. 168 (2018) 42–55, https://doi.org/10.1016/j.enbuild.2018.03.025.
[30] G. Dermentzis, F. Ochs, M. Gustafsson, T. Calabrese, D. Siegele, W. Feist, C. Dipasquale, R. Fedrizzi, C. Bales, A comprehensive evaluation of a monthly-based energy auditing tool through dynamic simulations, and monitoring in a renovation case study, Energy Build. 183 (2019) 713–726, https://doi.org/10.1016/j.enbuild.2018.11.046.
[31] Y.J. Kim, S.H. Yoon, C.S. Park, Stochastic comparison between simplified energy calculation and dynamic simulation, Energy Build. 64 (2013) 332–342, https://doi.org/10.1016/j.enbuild.2013.05.026.
[32] S.A. Brideau, I. Beausoleil-Morrison, M. Kummert, A. Wills, Inter-model comparison of embedded-tube radiant floor models in BPS tools, J. Build. Perform. Simul. 9 (2) (2016) 190–209, https://doi.org/10.1080/19401493.2015.1027065.
[33] ANSI/ASHRAE 140-2017, Standard method of test for the evaluation of building energy analysis computer programs, American Society of Heating, Refrigerating and Air-Conditioning Engineers, Atlanta, 2017.
[34] J. Neymark, R. Judkoff, M. Kummert, R. Muehleisen, A. Johannsen, N. Kruis, J. Glazer, R. Henninger, M. Witte, E. Ono, H. Yoshida, Y. Jiang, X. Zhou, T. McDowell, M. Hiller, J. An, D. Yan, J. Allison, P. Strachan, Update of ASHRAE Standard 140 Section 5.2 and Related Sections (BESTEST Building Thermal Fabric Test Cases), Argonne National Laboratory, ANL-20/26 158451, Argonne, 2020. https://doi.org/https://doi.org/10.2172/1643690.
[35] EN, 15225:2007, Energy performance of buildings - Sensible room cooling load calculation - General criteria and validation procedures 2007 European Committee for standardization Brussels
[36] EN 15265:2007, Thermal performance of buildings - Calculation of energy needs for space heating and cooling using dynamic methods - General criteria and validation procedures, European Committee for standardization, Brussels, 2007.c
[37] VDI-Richtlinien 6020:2016-09, Anforderungen an thermisch-energetische Rechenverfahren zur Gebäude- und Anlagensimulation, VDI-Gesellschaft Bauen und Gebäudetechnik, Düsseldorf, 2016.
[38] VDI-Richtlinien 2078:2015-06, Berechnung der thermischen Lasten und Raumtemperaturen, VDI-Gesellschaft Bauen und Gebäudetechnik, Düsseldorf, 2015.
[39] VDI-Richtlinien 6007:2015, Berechnung des instationären thermischen Verhaltens von Räumen und Gebäuden, VDI-Gesellschaft Bauen und Gebäudetechnik, Düsseldorf, 2015.
[40] R. Judkoff, J. Neymark, Model validation and testing: the methodological foundation of ASHRAE standard 140, ASHRAE Trans. 112 (2006) 367–376.
[41] K. Agnew, M. Goldberg, Chapter 8: Whole-Building Retrofit with Consumption Data Analysis Evaluation Protocol, The Uniform Methods Project: Methods for Determining Energy- Efficiency Savings for Specific Measures, National Renewable Energy Laboratory, NREL/SR-7A40-68564, Golden, CO, 2017.
[42] ASHRAE Guidelines 14-2014, Measurement of energy and demand savings, American Society of Heating Refrigerating and Air-Conditioning Engineers, Atlanta, 2014.
[43] U.S. Department of Energy, M&V Guidelines: Measurement and Verification for Performance-Based Contracts Version 4.0, Federal Energy Management Program, 2015.
[44] International Performance Measurement & Verification Protocol Committee, International Performance Measurement & Verification Protocol (IPMVP): Concepts and Options for Determining Energy and Water Savings Volume I, (2002).
[45] E. Fabrizio, V. Monetti, Methodologies and advancements in the calibration of building energy models, Energies 8 (2015) 2548–2574, https://doi.org/10.3390/en8042548.
[46] M. Royapoor, T. Roskilly, Building model calibration using energy and environmental data, Energy Build. 94 (2015) 109–120, https://doi.org/10.1016/j.enbuild.2015.02.050.
[47] G.R. Ruiz, C.F. Bandera, Validation of calibrated energy models: common errors, Energies. 10 (2017) 1587, https://doi.org/10.3390/en10101587.
[48] M.J. Witte J. Glazer D.B. Crawley R.H. Henninger J. Glazer GARD Analytics, Testing and Validation of a New Building Energy Simulation Program, in Seventh Int. IBPSA Conf., Rio de Janeiro 2001 9
[49] TRNSYS 18: A Transient System Simulation Program, Solar Energy Laboratory - University of Wisconsin, (2021). http://sel.me.wisc.edu/trnsys. (accessed April 7, 2021).
[50] M. Wetter, W. Zuo, T.S. Nouidui, X. Pang, Modelica buildings library, J. Build. Perform. Simul. 7 (2014) 253–270, https://doi.org/10.1080/19401493.2013.765506.
[51] IDA ICE - Simulation Software | EQUA, (2020). https://www.equa.se/en/ida-ice (accessed July 20, 2020).
[52] Testing and Validation | EnergyPlus, (2020). https://energyplus.net/testing (accessed August 3, 2020).
[53] T. Stephane Nouidui, K. Phalak, W. Zuo, M. Wetter, Validation and Application of the Room Model of the Modelica Buildings Library, in: 9th Int. Model. Conf., Munich, 2012: p. 9.
[54] EQUA Simulation AB, Technical report: Validation of IDA Indoor Climate and Energy 4.0 build 4 with respect to ANSI/ASHRAE Standard 140-2004, 2010.
[55] P. Voit, T. Lechner, M. Schuler, Common EC validation precedure for dynamic building simulation programs - application with TRNSYS, in: Conf. Int. Simul. Soc., TRANSSOLAR GmbH, Zurich, 1994.
[56] M. Kottek, J. Grieser, C. Beck, B. Rudolf, F. Rubel, World Map of the köppen-geiger climate classification updated, Meteorol. Zeitschrift. 15 (2006) 259–263, https://doi.org/10.1127/0941-2948/2006/0130.
[57] F. Ochs, M. Magni, P. Bonato, M. D'Antoni, D. Geisler-Moroder, M. Hauer, S. de Vries, R. Loonen, IEA SHC TASK 56 | Building Integrated Solar Envelope Systems for HVAC and Lighting: System Simulation Models, Solar Heating & Cooling Programme International Energy Agency, 2020. https://doi.org/10.18777/ieashc-task56-2020-0004.
[58] M. Werner Dissertation: Gekoppelte lichttechnische und thermische Methoden zur Ganzjahresbewertung von Fassadensystemen für die Planungspraxis 2017 Universität Innsbruck
[59] R. Perez, P. Ineichen, R. Seals, J. Michalsky, R. Stewart, Modeling daylight availability and irradiance components from direct and global irradiance, Sol. Energy 44 (1990) 271–289, https://doi.org/10.1016/0038-092X(90)90055-H.
[60] TRNSYS 18: Programmer's Guide, Solar Energy Laboratory, University of Wisconsin-Madison, 2017.
[61] SIA 2024:2015 Bauwesen: Raumnutzungsdaten für die Energie- und Gebäudetechnik, Schweizerischer Ingenieur- und Architektenverein, Zürich, 2015.
[62] U.S. Department of Energy's (DOE) Building Technologies Office, EnergyPlus, (2020). https://energyplus.net/ (accessed November 30, 2020).
[63] EQUA, IDA ICE, (2020). https://www.equa.se/en/ida-ice (accessed November 30, 2020).
[64] P. Sahlin, A. Bring, E.F. Sowell, The Neutral Model Format for Building Simulation, in: IBPSA Build. Simul., Vancouver, 1989: pp. 1–11.
[65] S. Lohmann, Einführung in die Software MATLAB® - Simulink®und die Toolboxen CARNOT und Stateflow® zur Simulation von Gebäude- und Heizungstechnik, Düsseldorf, Germany, 2013.
[66] K.N. Rhee, K.W. Kim, A 50 year review of basic and applied research in radiant heating and cooling systems for the built environment, Build. Environ. 91 (2015) 166–190, https://doi.org/10.1016/j.buildenv.2015.03.040.
[67] W. Zuo, Advanced simulations of air distributions in buildings, Purdue University, 2010.
[68] L. Eriksson, G. Grozman, P. Grozman, M. Havgaard Vorre, L. Ålenius, CFD-Free, Efficient, Micro Indoor Climate Prediction in Buildings, in: Build. Simul. Optim. Conf. 12, Loughborough, UK, 2012: p. 8.
[69] D. Morries Grenfell, Buillding Heat Transfer, John Wiley & Sons, Ltd, 2004.
[70] TRNSYS 18 User Manual: Multizone Building modeling with Type56 and TRNBuild, Solar Energy Laboratory, University of Wisconsin-Madison, 2017.
[71] ISO 13790:2008, Energy performance of buildings — Calculation of energy use for space heating and cooling, 2008.
[72] D. K Arasteh, E. U Finlayson, C. Huizenga, WINDOW 4.1: Program Description, Lawrence Berkeley Laboratory, 1994.
[73] C. Curcija, S. Vidanovic, R. Hart, J. Jonsson, R. Mitchell, WINDOW Technical Documentation, Windows and Envelope Materials Group, Lawrence Berkeley National Laboratory; Windows and Envelope Materials Group, Berkeley, 2018.
[74] E.U. Finlayson, D.K. Arasteh, C. Huizenga, M. Rubin, S.M. Reilly, Window 4.0: Documentation of Calculation Procedures, Lawrence Berkeley National Laboratory, Berkeley, 1993.
[75] D.K. Arasteh, S.M. Reilly, M.D. Rubin, A versatile procedure for calculating heat transfer through windows, ASHRAE Trans. 95 (1989).
[76] L. Mazzarella, M. Pasini, CTF vs FD based numerical methods: accuracy, stability and computational time's comparison, Energy Procedia 78 (2015) 2620–2625, https://doi.org/10.1016/j.egypro.2015.11.324.
[77] M. Magni, F. Ochs, P. Bonato, M. D'Antoni, D. Geisler-moroder, S. De Vries, Comparison of Simulation Results for an Office Building Between Different BES Tools – The Challenge of Getting Rid of Modeller Influence and Identifying Reasons for Deviations, in: Proc. 16th IBPSA Conf., Rome, 2019: pp. 1475–1482. https://doi.org/https://doi.org/10.26868/25222708.2019.210834.
[78] R.J. Hyndman, A.B. Koehler, Another look at measures of forecast accuracy, Int. J. Forecast. 22 (2006) 679–688, https://doi.org/10.1016/j.ijforecast.2006.03.001.
[79] P. Sahlin, P. Grozman, IDA Simulation Environment a tool for Modelica based end-user application deployment, in: 3rd Int. Model. Conf., Linköpings, Sweden, 2003: p. 11.
[80] M. Wetter, C. Van Treeck, L. Helsen, A. Maccarini, D. Saelens, D. Robinson, G. Schweiger, IBPSA Project 1: BIM/GIS and Modelica framework for building and community energy system design and operation - Ongoing developments, lessons learned and challenges, in: IOP Conf. Ser. Earth Environ. Sci., Graz, 2019: p. 9. https://doi.org/10.1088/1755-1315/323/1/012114.
[81] G. Serale, M. Fiorentini, A. Capozzoli, D. Bernardini, A. Bemporad, Model predictive control (MPC) for enhancing building and HVAC system energy efficiency: Problem formulation, applications and opportunities, Energies 11 (2018) 631, https://doi.org/10.3390/en11030631.
[82] F. Ochs, M. Magni, M. Hauer, D. Geisler-Moroder, P. Bonato, S. de Vries, R. Loonen, D. Venus, N. Abdelnour, T. Calabrese, E. Venturi, A. Maccarini, S. Häringer, B. Bueno, Z. Ioannidis, R. Efstratios, IEA SHC T56 - System Simulation Models System Simulation Models, Solar Heating & Cooling Programme International Energy Agency, 2020. https://doi.org/10.18777/ieashc-task56-2020-0005.
[83] M. Wetter, W. Zuo, T. Stephane Nouidui, Modeling of Heat Transfer in Rooms in the MODELICA "Buildings" Library, in: Proc. Build. Simul., 2011: pp. 1096–1103.

5.2 Publication B

Title

Comprehensive analysis of the influence of different building modelling approaches on the results and computational time using a cross-compared model as a reference

Authors

Mara Magni, Fabian Ochs, Wolfgang Streicher

Published in

Energy & Buildings 259 (2022) 111859
https://doi.org/10.1016/j.enbuild.2022.111859

Own contribution

The second and third authors supported this work with fruitful discussion and reviewing the manuscript. The first author developed the methodology, made the analysis of the results, and wrote the paper.

Energy & Buildings 259 (2022) 111859

Contents lists available at ScienceDirect

Energy & Buildings

journal homepage: www.elsevier.com/locate/enb

Comprehensive analysis of the influence of different building modelling approaches on the results and computational time using a cross-compared model as a reference

Mara Magni *, Fabian Ochs, Wolfgang Streicher

University of Innsbruck, Unit for Energy Efficient Buildings, Innsbruck, Austria

ARTICLE INFO

Article history:
Received 15 October 2021
Revised 22 December 2021
Accepted 12 January 2022
Available online 19 January 2022

Keywords:
Building Energy Simulation
Modelling approaches
Sensitivity analysis
Radiative exchange
Goodness of Fit

ABSTRACT

A large number of Building Energy Simulation (BES) tools with a different focus and degree of detail are available however, increasing the model complexity usually increases the modelling time and the number of required inputs, not always leading to better accuracy. Therefore it is important to find the trade-off between model complexity and computational time having in mind the purpose and goal of the simulation study and the available inputs. To shed some light on these aspects, different modelling approaches (i.e. thermal zone model, window model, thermal mass, etc...) are implemented using a cross-validated Simulink model of an office cell and the influence of each analysed aspect on the hourly results is addressed using the Goodness-of-fit and the computational time. As a result, it is observed that modelling the thermal zone with a two-star model leads to a good agreement with the surface-to-surface detailed radiation model in terms of energy balance and operative temperature in the centre of the room, but deviations are present when the temperature in a specific location of the room (e.g. near the window) has to be evaluated. In addition, it is found that a simplified thermal zone model such as one-star model allows important savings in terms of computational time, but leads to deviations in the dynamic behaviour. However, the energy balance can have an acceptable accuracy for specific applications when the inputs are calibrated. Regarding the window model, the results show that it strongly affects the accuracy of the simulation. Furthermore, many aspects that are often overlooked, such as the models of the adiabatic structure, sky model, capacity of the air node, distribution of the radiative gains to the surfaces of the enclosure and convective and radiative exchange coefficients, influence both the accuracy of the results and the computational time.

1. Introduction

Building Energy Simulation tools (BES) are a useful means to accelerate and improve the design and planning process and to optimize the building performance in order to reduce the energy consumption of the building sector and achieve the climate protection targets limiting global warming. Thus, BES tools have been characterised by a significant development in recent decades as highlighted in [1,2] and [3]. A large number of BES tools is available (an extensive list is provided in [4;5]) and they differ from one another for the focus, degree of detail, capabilities, accessibility of the source code, user-friendliness and required inputs. Building Information Modelling (BIM) aims to enhance the automation of the building modelling process, supporting the user from the design to the optimisation phase. Yet, further development is necessary before BIM to BES can be used in practice (see [6,7]).

Increasing the model complexity allows a detailed analysis but at the same time requires user skills and the knowledge of many input parameters leading to higher modelling effort and often higher computational time. As demonstrated in [8] user mistakes and input uncertainty can highly influence the results compensating the benefits of using a detailed model. Therefore, it is important to find the trade-off between the computational and modelling load and the degree of detail, which must be adequate to the goals of the simulation study and input availability. To accomplish this, it is of great importance to analyse the impact that model simplifications have on the accuracy of the results and computational time, as highlighted in [9]. Furthermore, the definition of a robust method for the objective evaluation of deviations introduced in the results with model simplifications is necessary.

* Corresponding author at: Technikerstraße 13, 5. Stock, A-6020 Innsbruck, Austria.
E-mail address: Mara.Magni@uibk.ac.at (M. Magni).

https://doi.org/10.1016/j.enbuild.2022.111859
0378-7788/

Nomenclature

Acronyms and abbreviations

BES	Building Energy Simulation
BIM	Building Information Modelling
CD	Cooling Demand
CF	Correction Factors
GOF	Goodness Of Fit
HD	Heating Demand
HTC	Heat Transfer Coefficients
HVAC	Heating Ventilation and Air Conditioning
Inf	Infiltration losses
MAE	Mean Absolute Error
MBE	Mean Bias Error
MRT	Mean Radiant Temperature
NMBE	Normalized Mean Bias Error
NRMSE	Normalized Root Mean Square Error
REF	Reference
ROM	Rome
s	simulated value
SHGC	Solar Heat Gain Coefficients
Sol	Solar Gains
STO	Stockholm
STU	Stuttgart
Vent	Ventilation losses

Variables and Parameters

$\Delta\lambda$	Derivative of thermal conductivity to the temperature [W/mK^2]
σ_0	Stefan–Boltzmann constant 5.670 373 (21) × 10–8 [W/(m^2 K^4)]
A	Area [m^2]
C	Capacity [J/K]
d	Characteristic length [m]
F	Distribution factor [–]
H	Radiosity [W/m^2]
I	Solar irradiation [W/m^2]
K	Constant coefficient [–]
$\overline{m}$	Average of the reference results
N	Total number of time steps [–]
Nu	Nusselt [–]
Q	Heat flux [W]
$\dot{q}$	Specific heat flux [W/m^2]
R	Thermal Resistance [m^2 K/ W]
Ra	Rayleigh number [–]
t	Time [s]
T	Temperature [K]
v	Wind speed [m/s]
VF	View Factor [–]
α	Absorption factor [–]
β	Constant coefficient [–]
γ	Surface inclination [°]
ε	Emissivity factor [–]
ϑ	Temperature [°C]
λ	Thermal conductivity [W/mK]
τ	Transmission factor [–]

Subscripts

amb	ambient
av	average
c	convective
ce	convective external
ci	convective internal
diff	diffuse
dir	direct
ext	external
f	frame
g	global
G	variable
gnd	ground
hor	horizontal
i	ith
IG	internal gains
int	internal
ma	modeling approach
p	pane
r	radiative
re	radiative external
ri	radiative internal
S	surface
se	surface external
si	surface internal
sol	Solar
tot	total
tr	transmission
vent	ventilation
win	window

There exist many sensitivity analysis studies concerning the influence of the input parameter on the results of building and HVAC simulations. For instance, [10,11] are comprehensive reviews on this topic, which show the applied methods and the selection of the inputs under analysis. Only a few studies, however, investigate the impact of the degree of detail of the model on the simulation results. In this regard, the work of Gilani et al. [12] gives noteworthy attention to the influence of the user behaviour model, whereas [9,13,14,15] focus more on the influence of the zoning and shading simplification. In particular, M. Klimczak et al. in [9] analyse the effect of a gradual simplification of the building geometry on the results by disregarding shading elements and stepwise reducing the number of thermal zones, highlighting that shading elements on the south façade highly influence the results. The analysed variants are simulated using EnergyPlus and compared against a reference case and the deviations are evaluated in terms of heating demand and heating load. Similarly, the work of S. Elhadad et al. [13] shows the effect of progressive thermal zoning simplification (i.e. reducing the number of thermal zones) on the results and calculation time using IDA ICE as simulation software. The deviations are calculated in terms of percentage deviation comparing each analysed case against the results of the reference model in terms of heating and cooling demand, predicted mean vote, CO_2 concentration, daylight factor and save in simulation time. The conclusion highlights that merging rooms with similar orientations and end-use leads to high computational time savings with an acceptable loss in accuracy. However, the decision of whether to use or not a simplified model highly depends on the simulation goals.

The work of M. Martin et al. [14] focuses on the study of the impact of the EnergyPlus model simplification on the cooling demand using a shoebox model considering the interaction with the urban canopy. The model simplifications introduced in [14] mainly regard thermal zoning. The detailed model is used as a ref-

erence for the calculation of the deviations in terms of Root Mean Square Error on hourly bases and Mean Absolute Percentage Error on monthly bases. Aside from the evaluation of the deviations introduced with stepwise model simplifications also the computation time difference is reported. Concluding that the simplified model provides acceptable results in terms of cooling demand allowing important computational time savings and that the accuracy of the simplified model has to be assessed according to the requirements of the specific case study. M. Shin et al. [15] provides a literature review of building thermal zoning strategies and methods for building energy simulation and heating ventilation and air conditioning (HVAC) system design highlighting the lack of guidelines for the thermal zoning strategies.

The results of a quasi-steady-state calculation tool (i.e. PHPP) against the results of dynamic simulations carried out with TRNSYS are compared by G. Dermentzis et al. in [16] using the relative deviation as an index. The conclusion of this work is in agreement with what is reported in [8], i.e. that satisfactory results can be obtained with simplified tools such as PHPP, but it is very important to introduce the correct assumptions, which are not always known.

The influence of the thermal inertia of furniture or phase change material on the energy flexibility[1] is addressed by H. Johra et al. [17] where Matlab-Simulink is used to simulate the multi-zone building model. In [17] it is concluded that the empty room assumption in low thermal mass buildings leads to deviations in energy flexibility up to 21%.

In H. Karlsson et al. [18] two different approaches (i.e. star model and net radiation exchange model) for modelling the longwave radiation exchange in enclosures are compared, considering the influence on the accuracy of the internal surface temperatures. This work highlights that the star approach is not as accurate as the net radiation exchange approach and that the star approach in some cases could lead to inaccuracies in the evaluation of the building energy demand when for example the heating system is controlled according to the operative temperature and inaccurate evaluation of the thermal comfort. The work of M. Camci et al. [19] compares different formulations for the calculation of the internal convective heat transfer coefficients assessing that noteworthy differences are present between the equations presented in the literature. A review of the models for the external convective heat transfer coefficients is proposed by M. Mirsadeghi et al. [20], where it is highlighted that different models can lead to deviations up to ± 30% in cooling demand and up to ± 6% in heating demand in relation to the average results. M. Thalfeldt et al. [21] and M. K. Urbikain et al. [22] analyse the effects of different windows models (from simplified such as single layer to detailed including an energy balance over each pane and cavity) on the building energy balance highlighting the high influence that the window model has on the simulated energy demand of the building. T. Zakula et al. [23,24] present an extensive comparison between the simplified approach proposed by ISO 52016-1:2017 and the dynamic simulation model implemented in TRNSYS highlighting that the main cause for deviations lies on the constant parameters (i.e. thermal resistance and solar heat transfer coefficient) used by the standard ISO 52016-1:2017 for the window model. The differences between the two methods in the annual energy needs are up to 40% for heating and up to 18% for cooling.

Yet, each of these studies tackles only one section of the model (e.g. convective coefficients) or only one modelling problem (e.g. thermal zoning) and applies different statistical indices and methods to evaluate the influence of the introduced simplifications on the results of the building simulation.

M. Magni et al. [8] provides an overview of the available mathematical approaches, for each section of the building model, supported by some of the widely used BES tools (i.e. EnergyPlus, TRNSYS, Simulink libraries ALMABuild and CarnotUIBK, IDA ICE, Modelica building library, DALEC and the predesign tool PHPP). Within this work the Simulink model of a typical office cell located in Rome, Stuttgart and Stockholm, validated through a cross-comparison with other dynamic simulation tools in [8] is used as a basis for the analysis of the influence on the results and computational cost of different modelling approaches concerning the following aspects of the model: Thermal zone model, thermal mass, solar and internal gains distribution between the different surfaces of the enclosure, convective and radiative heat transfer coefficients, window model, adiabatic structure model, sky model, pre-runtime and solver settings. The influence of the different modelling approaches on the results is presented using the Goodness of Fit [25] calculated for both heating and cooling demand together with the computational time. The detailed model for the radiative exchange implemented in Simulink and proposed in [26] is cross-compared against a modified version of the TRNSYS model used in [8], where the detailed model for the radiative exchange is used instead of the star network approach (see [27] chapter 5.4.1.6). The cross-compared Simulink model implementing the detailed longwave radiative exchange is then used within this work in order to analyse the accuracy, in terms of temperature prediction, of simplified models such as two-star or one-star approaches.

2. Methodology

In this section, the office building used for this case study is shortly described, as well as the analysed modelling approaches. Moreover, the used accuracy indices are introduced and conditions for the evaluation of the computational cost are reported.

2.1. Boundary conditions and building description

The reference office building introduced by IEA SHC Task 56 [28] as a typical European office cell located on the middle floor of a high-rise building for the climate of Rome, Stuttgart and Stockholm is used as a basis for this case study. A complete description of the building inputs can be found in the project report of IEA SHC Task 56 [28] and within this section, only the main building characteristics are resumed. Fig. 2-1 shows the office cell, characterized by a heated area of 27 m^2 and a volume of 81 m^3. All the surfaces are considered adiabatic, except for the façade oriented towards the South (with a window-to-wall ratio of 60 %). External movable

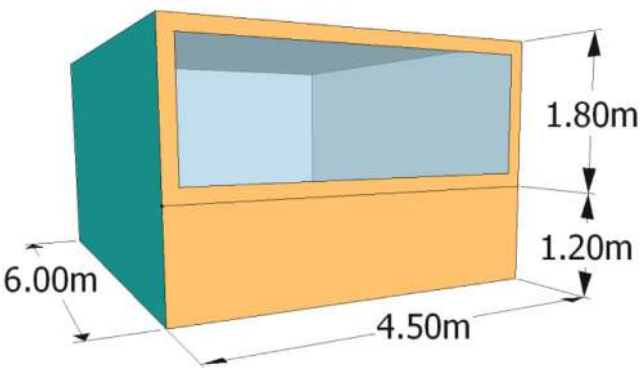

Fig. 2-1. Representation of the reference office zone from [8].

[1] The energy flexibility of a building is defined, in [17], as its capacity to reduce heating need during medium and high electricity price periods by storing heat during low electricity price periods.

shadings, able to block 70 % of the incoming radiation, are activated when direct solar radiation impinging the south façade is higher than 120 W/m^2, whereas shadings from adjacent obstacles are not considered.

The heat transfer coefficient (HTC) of the opaque wall element and the characteristics of the windows such as HTC, Solar Heat Gain Coefficient (SHGC) and the solar transmittance (τ_{sol}) for the three considered climates are reported in Table 2-1.

Hourly resolution profiles that show different user behaviour for weekdays and weekends [29] are implemented to account for user behaviour (e.g., occupancy, appliances and lighting), (see Fig. 2-2).

A constant air change per hour is set to 0.15 ACH to account for natural infiltration. A mechanical ventilation system, with a sensible heat recovery of 70 % efficiency, providing a fresh air supply of 40 m^3/h per person is considered. When the temperature of the zone is higher than 23 °C and the ambient temperature is lower than the indoor temperature, the bypass of the heat recovery is activated.

Ideal heating and cooling systems are implemented using a set-point for the indoor convective temperature of 21 °C and 25 °C, for heating and cooling respectively.

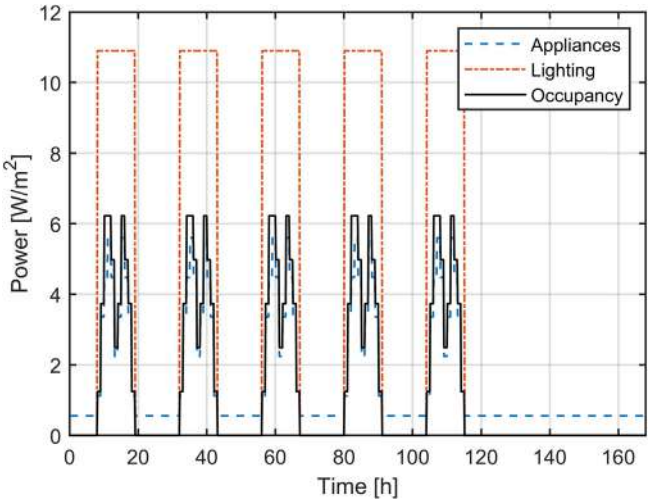

Fig. 2-2. Internal gains due to appliances, lighting and occupancy [8].

2.2. Description of the analysed building modelling approaches

The analysis carried out within this work aims at showing the influence of different modelling assumptions and simplifications on the results in terms of accuracy and computational time. For this purpose, the Simulink model cross-compared in [8] is used as a reference (REF) model and the different subsections of the model are modified one at a time. Table 2-2 provides an overview of all the analysed cases. The first column of Table 2-2 describes the sections of the model where variations are implemented and the second column provides a short description of the different sub-variants (a detailed description is provided in Sections 2.2.1–2.2.10). Each column on the right-hand side represents one specific case and the black dots give an overview of the components/settings used to create the building model for that specific case. In bold is the description of the sections of the model used in the REF case. In total 22 different variations have been performed and each evaluated for the climate of Rome, Stuttgart and Stockholm.

2.2.1. Thermal zone model

The heat exchange (i.e. convective and radiative) within the thermal zone can be modelled with a thermal electric circuit applying different levels of detail. Figs. 2-3 and 2-4 show the sketches of the different models analysed in the current work. The most simplified approach is the one-star model (see Fig. 2-3a) where the walls are modelled with a constant heat transfer coefficient without capacities and the whole building thermal mass (i.e., air and walls) is represented by one unique capacity ($C_{building}$). The scheme of Fig. 2-3b depicts a variation of case (a) where the walls are modelled with a finite difference approach (i.e. the mass of the wall is modelled within the wall component) and the only one node of the thermal zone represents only the capacity of the air mass and furniture. Having only one node, both models represented in Fig. 2-3 are able to simulate only one temperature of the thermal zone, which can be considered as the operative temperature.

The model (a) in Fig. 2-4, the so-called two-star model, includes two nodes in the thermal zone: one representing the air and furniture and the other one representing the mean radiant temperature. In this model, the internal surfaces of each component are connected with both the convective and the radiative nodes by means of the thermal resistances representing the convective and radiative exchange coefficients respectively (see Section 2.2.5). The last and most detailed thermal zone model is reported in Fig. 2-4b where the air and furniture temperature are represented by only one node (as in scheme Fig. 2-4a and Fig. 2-3b) but the longwave radiative exchange is modelled considering the detailed surface to surface radiative exchange (also called net radiation exchange model) instead of the simplified star approach.

Another variant of the two-star model, represented in Fig. 2-5, is the starnode approach, as for example implemented in TRNSYS (see Fig. 5.4.1-7 in [30]). The TRNSYS model, implementing the starnode approach, is compared against the Simulink model implementing the two-star approach in [8] showing a good agreement, therefore the starnode approach is not included in the present study.

The reference (**REF**) case is based on a two-star approach (see Fig. 2-4a). The REF model can be simplified by implementing a one-star approach, this is the case called **TZ1s** (see Fig. 2-3b) and further simplified by lumping the capacities of the walls in the unique node of the thermal zone, to reduce the number of integrators and achieve lower computational time (case **TZ1s_UA_Ccal** where the building capacity is calibrated and **TZ1s_UA_Cnoncal** where the building capacity is not calibrated, see Fig. 2-3a for the thermal circuit and Section 3.1.1 for the parametrization process). This approach could be beneficial when many simulations need to be run (e.g. multi-objective simulation-based optimization).

The **RM** model (see Fig. 2-4b), where a surface to surface radiative exchange is implemented, introduces a higher level of detail and complexities with respect to the REF model since additional

Table 2-1
Main properties of the south-oriented façade and weathers characteristics (yearly average ambient temperature ($\bar{\vartheta}_{amb,av}$), yearly global irradiation on a horizontal surface ($I_{g,hor}$) and yearly irradiation on a south- oriented vertical surface (I_{south}).

Properties	Rome (Italy)	Stuttgart (Germany)	Stockholm (Sweden)
$HTC_{ext,wall}$ [W/(m^{2}K)]	0.80	0.40	0.30
HTC_{win} [W/(m^{2}K)]	1.26	1.35	0.90
SHGC [%]	0.33	0.59	0.63
τ_{sol} [%]	0.26	0.43	0.46
$\bar{\vartheta}_{amb,av}$ [°C]	15.8	9.9	7.8
$I_{g,hor}$ [kWh/m^2]	1632	1101	952
I_{south} [kWh/m^2]	1253	889	884

Table 2-2
Overview of the sensitivity analysis variants.

	Variant Name	REF	TZ1s_UA	TZ1s	RM	AC	RG_distr	SD	Win_Rcalc	Win_Rcal	Win_Rcal_gcal	R_now	Rlin	Rlin_now	Rconst	Ad_nm	Ad_no	Ad_sb	Iso_Sky	Noprerunt	Sol_23s	Sol_23t	Sol_15s
Thermal zone model	One-star model – Constant HTC wall (see Figure 2-3a)		•																				
	One-star model – Finite difference wall (see Figure 2-3b)			•																			
	Two-star model (see Figure 2-4a)	•				•	•	•	•	•	•	•	•	•	•	•	•	•	•	•	•	•	•
	One convective node and surf. to surf. radiative exchange (see Figure 2-4b)				•																		
Air Capacity	Incl. in the lumped capacity of the building		•																				
	Only capacity of the air mass					•																	
	Capacity of the air mass increased by 10 to consider furniture	•		•	•		•	•	•	•	•	•	•	•	•	•	•	•	•	•	•	•	•
Distribution of the internal radiative gains	To the building star node		•	•																			
	To the radiative node	•				•		•	•	•	•	•	•	•	•	•	•	•	•	•	•	•	•
	Distributed to the internal surfaces				•		•																
Distribution of the solar gains in the TZ	Added directly to the capacity of the TZ		•																				
	Proportional to the surface area							•															
	Complex calculation based on the reflection of the surfaces	•		•	•	•	•		•	•	•	•	•	•	•	•	•	•	•	•	•	•	•
Convective heat transfer (see Table 2-5 and Table 2-6)	Constant (see Table 2-5 line C1)		•											•	•								
	Internal const.; External prop. to wind speed (see Table 2-5 line C2)												•										
	Internal f(ΔT) (Eq. 2-6); External Constant (Eq. 2-3)											•											
	Internal f(ΔT); External prop. to wind speed (see Table 2-5 line C3)	•		•	•	•	•	•	•	•	•					•	•	•	•	•	•	•	•
Radiative exchange (see Table 2-5 and Table 2-6)	Radiative node - Constant (see Table 2-5 line R1)		•												•								
	Radiative node - Linearized (see Table 2-5 line R2)												•	•									
	Radiative node - Proportional to ΔT^4 (see Table 2-5 line R3)	•		•		•	•	•	•	•	•	•				•	•	•	•	•	•	•	•
	Surf. to Surf. - Based on view Factor (see Table 2-5 line R4)				•																		
Window thermal model	Constant thermal resistance and SHGC								•														
	Calibrated const. thermal resis. Rcal and const. SHGC									•													
	Calibrated constant thermal resis. Rcal and SHGC		•								•												
	Thermal balance of each pane	•		•	•	•	•	•				•	•	•	•	•	•	•	•	•	•	•	•
Adiabatic structure model	Capacity of the adiab. structure added to the building node		•																				
	Null thermal flux outside															•							
	Null thermal flux in the middle																•						
	Same BC inside and outside and same heat exchange coeff.																	•					
	Same BC inside and outside	•		•	•	•	•	•	•	•	•	•	•	•	•				•	•	•	•	•
Sky model	Isotropic																		•				
	Perez	•		•	•	•	•	•	•	•	•	•	•	•	•	•	•	•		•	•	•	•
Preruntime	No preruntime																			•			
	1 month preruntime	•		•	•	•	•	•	•	•	•	•	•	•	•	•	•	•	•		•	•	•
Solver	**ode23tb implicit Runge-Kutta**	•		•	•	•	•	•	•	•	•	•	•	•	•	•	•	•	•	•			
	Ode15s variable-order solver based on the numerical differentiation formulas																						•
	ode23s modified Rosenbrock formula of order 2																				•		
	ode23t trapezoidal rule using a free interpolant																					•	

geometrical information (i.e. coordinates of each envelope element) is required and the calculation of the view factors is necessary. The RM implemented in Simulink [26] is cross-validated with the TRNSYS model implementing the Detailed Radiation Transfer Model (see Appendix 5) and then used as a reference to assess the accuracy of simplified models (i.e. one-star and two-star) in predicting the temperature of the thermal zone (see Section 3.2.2).

It is noteworthy to mention that using a one-star model, only the operative temperature can be simulated, while in this case study the heating and cooling systems are controlled using the convective temperature leading to higher deviations. The building capacity of the one-star approach is a lumped parameter that should include only the effective capacity of the building, therefore it is not known as input from the office description. The capacity used in the case called **TZ1s_UA_Ccal** is found by trying to minimize the deviation in terms of annual heating and cooling demand with the REF case minimizing the value of the function described in equation (2-1) (see Section 3.1 for the results of the calibration process). This procedure leads to find a $C_{building}$ that compensates for the differences due to control of the heating and cooling systems over the operative temperature instead of the convective temperature as done in the REF case.

$$f = |HD_{TZ1sUACcal} - HD_{REF}| \frac{HD_{REF}}{HD_{REF} + |CD_{REF}|} + |CD_{TZ1sUACcal} - CD_{REF}| \frac{|CD_{REF}|}{HD_{REF} + |CD_{REF}|} \quad (2\text{-}1)$$

Since the calibration process is time-consuming and not always possible (e.g. due to a lack of reference results) the case **TZ1s_UA_Cnoncal** is also included in the comparison. The lumped

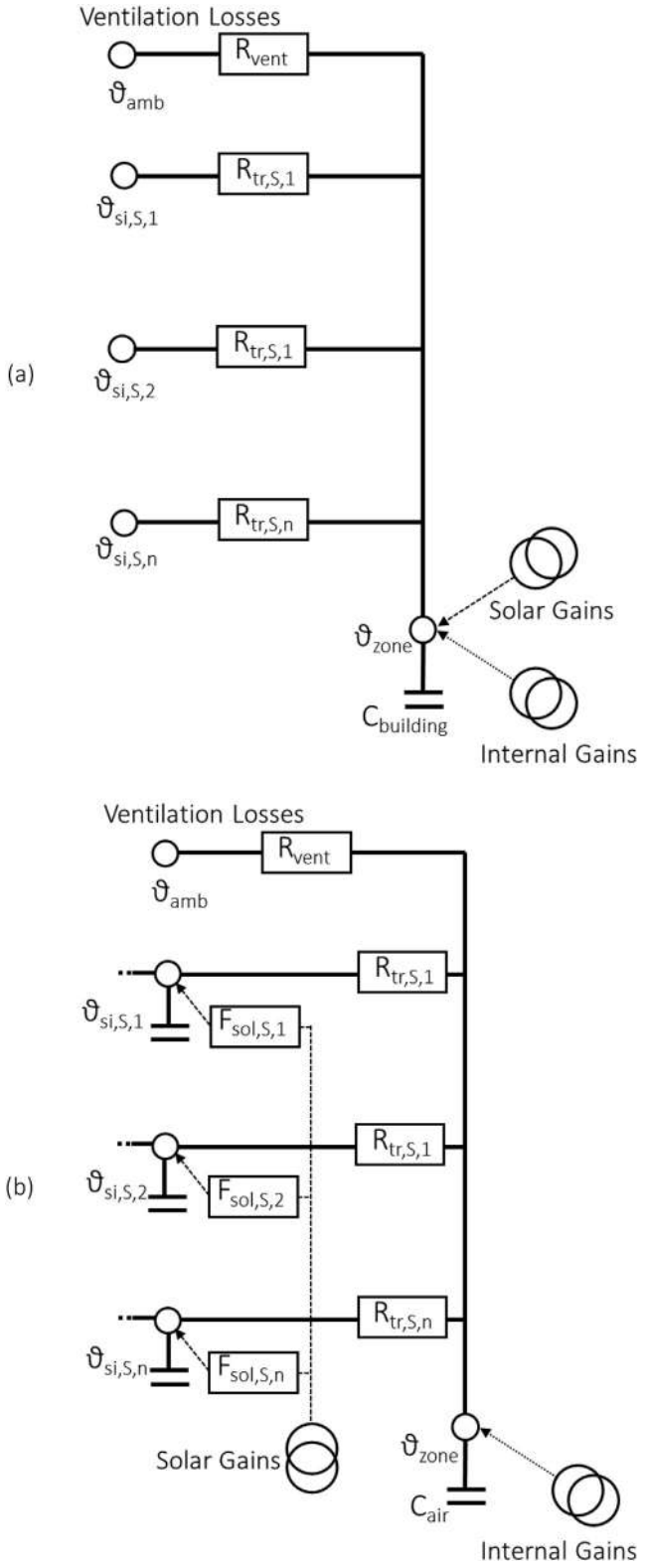

Fig. 2-3. Thermal circuit of two different thermal zone models: (a) One-star model combined with constant Heat Transfer Coefficient wall model (cases**: TZ1s_UA_Ccal** and **TZ1s_UA_Cnoncal**); (b) One-star model combined with finite-difference wall model **TZ1s.**

capacity used in **TZ1s_UA_Cnoncal** is calculated using the equation for the effective internal capacity suggested by PHPP [31] (see Equation (2-2)).

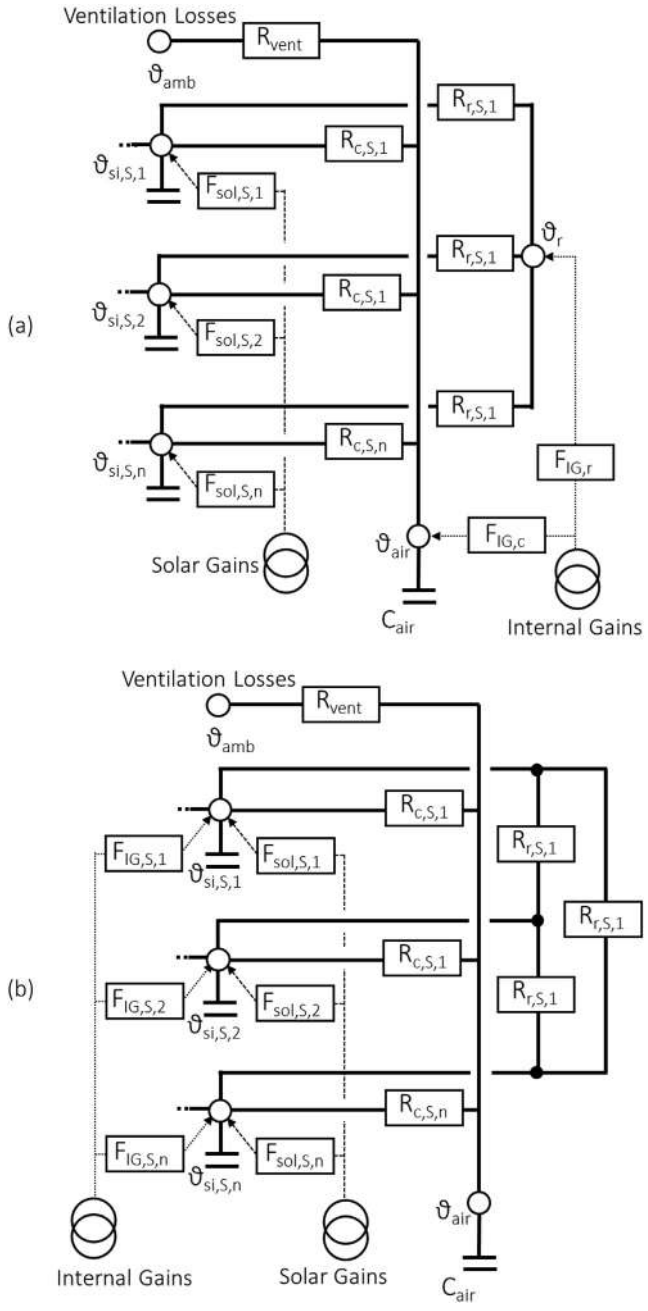

Fig. 2-4. Thermal circuit of two different thermal zone models: (a) Two-star model **REF**; (b) One convective node and surf. to surf. radiative exchange **RM.**

$$C_{building} = (60 + n_{tm}\ 8 + n_m\ 24)\ 3600\ A_{floor} \quad (2\text{-}2)$$

Where $C_{building}$ is the building capacity in [J/K], n_{tm} represents the number of partly massive and n_m the number of massive envelope areas. For the current case study, floor and ceiling are massive while all the other structures are considered as partly massive, resulting in a capacity of 1.3608 10^7 J/K.

To further analyse the influence of the building capacity and of the control strategy of the heating and cooling systems on the results of the one-star model, additional cases are analysed in Appendix 4. Here, another method for the calculation of the internal effective heat capacity is applied (i.e. EN ISO 13786 [32]) and the REF and RM are simulated controlling the heating and cooling systems according to the operative temperature and assigning half of the heating and cooling power to the convective node and half to

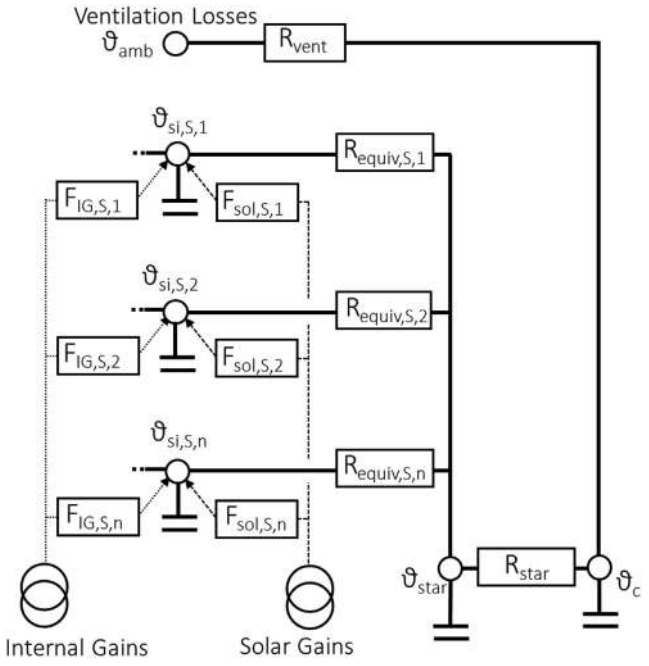

Fig. 2-5. Thermal circuit of the star network approach see Fig. 5.4.1-7 in [26].

the radiative node (case Ref2) or to the internal side of the surfaces of the enclosure based on the area fraction (case RM2). The building capacity of the one-star model (TZ1s_UA_Ccal_Ref2) is calibrated using the annual heating and cooling demand of the case Ref2 and the results are compared in Appendix 4.

A comparison of the operative temperatures simulated by the REF, Ref2, RM, RM2, TZ1s, TZ1s_UA_Ccal and TZ1s_UA_Ccal_Ref2 are additionally reported in Section 3.2.2 to show the impact of the model simplifications on the simulated temperature of the thermal zone.

2.2.2. Capacity of the convective node

The capacity of the air node (see Fig. 2-3b and Fig. 2-4a and b) needs to be increased with respect to the capacity of the pure air in order to account for the thermal mass of the furniture located in the room. In the reference case (REF) the air capacity is multiplied by 10 to consider the additional capacity given by the furniture in the room (see Table 2-3), which, represents a medium furnished single office building according to [17]. While the case called **AC** shows how the results vary when the capacity assigned to the air node does not consider the furniture capacity. In Table 2-3 the air properties used in the simulations are listed.

2.2.3. Distribution of the radiative fraction of the internal gains within the thermal zone

The radiative part of the internal gain (i.e. 34 % of the total internal gains for this case study) can be assigned directly to the radiative node (see Fig. 2-4a) or to the internal node of the surfaces (see Fig. 2-4b) using a distribution factor based on the area ratio between the considered surface and the total surface area of the enclosure. In the case called **RG_distr** the latter approach is used while in the REF case the internal gains are assigned to the radiative node.

Table 2-3
Properties of the air volume of the considered thermal zone.

Volume [m^3]	81
Density of the air [kg/m^3]	1.204
Specific heat of the Air [J/(kg K)]	1012
Room floor area [m^2]	27
Air Capacity [$kJ/(m^2K)$] (AC case)	3.7
Additional capacity representing furniture [$kJ/(m^2K)$] (used in REF case)	32.9

2.2.4. Solar gain distribution

The distribution of the incoming solar gains in the thermal zone depends on the level of detail of the used thermal zone model. The solar gain can be assigned directly to the whole building capacity (e.g. when a one-star approach is used, see Fig. 2-3a) or distributed to the surfaces of the enclosure (see Fig. 2-3b and Fig. 2-4). In the latter case, the distribution factors can be calculated proportionally to the internal surface area of each component of the enclosure, as reported in Equation (2-3) (i.e. case called **SD**) or considering the reflections of the incoming direct solar irradiation over the different surfaces (as implemented in case **REF**).

$$F_{dir=diff,i} = \frac{A_i}{A_{tot,opaque}} \quad (2\text{-}3)$$

The method applied in the REF (proposed by [33], Chapter 2.7.2) is described by equations A- 1 - A- 6 (see Appendix 2). Equation A-1 is used to calculate the distribution factor for the direct solar radiation while equations A- 2 - A- 6 for the calculation of the distribution factors of the diffuse solar radiation.

The resulting distribution factors used in the current analysis are reported in Table 2-4. The sum of the distribution factors for direct solar irradiations is lower than 1 and the remaining part (i.e. in this case 40%) is then treated as diffusively reflected within the enclosure. The distribution of the diffuse solar irradiation is described by Equations A- 2 - A- 6 representing the different reflection bounces. With this method, a small part of the solar radiation is transmitted back to the external ambient (reported as Losses in Table 2-4).

2.2.5. Convective and radiative heat exchange coefficients

Different equations can be applied for the calculation of the convective and radiative heat exchange of the internal and external sides of the opaque and transparent surfaces. An overview of the different approaches is reported in Table 2-5. The convective and radiative exchange coefficients can be taken as constants (see Table 2-5 lines C1 and R1) or they can be calculated as a function of the temperature difference. The **REF** model calculates the convective exchange according to equations (2-7) and (2-8) (see Table 2-5 line C3) and the values used for Kci and β are specified in Table 2-6 as suggested by [34], while the external convective heat exchange coefficient is calculated according to EN ISO 6946 [35] (see Table 2-5 line C3). The radiative exchange in REF is based on the star approach and it is calculated with equations (2-13) and (2-14) (see Table 2-5 line R3). To analyse the influence of the wind speed[2] on the external convective heat transfer coefficient the case **R_now** is simulated using Equation (2-5) instead of (2-7) on the external side (in Table 2-6 the value used for Kce is given). The effect of simplified calculation of convective and radiative heat exchange coefficient (suggested by EN ISO 6946 [35] and implemented in ALMABuild [33]) are analysed with the case **R_lin**, where the equations reported in lines C2 and R2 of Table 2-5 are applied (see Table 2-6 for the value used for K_{ci} and K_{ce}). The case **R_lin_now** uses the same equations of R_lin but on the external side, the wind speed is not considered in the calculation of the convective coefficient (lines C1 and R2 of Table 2-5, the value used for Kce is given in Table 2-6). Another considered variant is called **R_const**, here constant convective and radiative exchange coefficients are imple-

[2] The wind speed of the used weather file is measured at 10 m from the floor level.

Table 2-4
Direct and diffuse solar gain distribution factors for the reference case and for the SD variant.

		Floor	Ceiling	Ext. Wall	Int. Walls	Window	Losses
REF	F dir	0.157	0.157	0.000	0.287	0.000	0.000
	F diff	0.648	0.103	0.021	0.189	0.017	0.0218
SD	F dir = F diff	0.248	0.248	0.050	0.455	0.000	0.000

Table 2-5
Internal and external convective (subscripts ci and ce) and radiative (subscripts ri and re) exchange equations where: K is a constant heat exchange coefficient [W/(m^{2}K)], v is the wind speed [m/s], T and ϑ are temperatures in K and °C respectively, VF_{ij} is a view factor between the surfaces i and j, H is the radiosity [W/m^2], e is the emissivity and σ_0 the Stefan- Boltzmann constant 5.670 373 (21) × 10–8 [W/(m^2 K^4)]. The subscripts C and R mean convective and radiative, si and se are the internal and external surfaces, amb is ambient and gnd is ground [8].

	Internal side	Eq.	External side	Eq.
C1	$q_{ci} = K_{ci}(\vartheta_{si} - \vartheta_C)$	2–4	$q_{ce} = K_{ce}(\vartheta_{se} - \vartheta_C)$	2–5
C2	$q_{ci} = K_{ci}(\vartheta_{si} - \vartheta_C)$	2–6	$q_{ce} = (4v + 4)(\vartheta_{se} - \vartheta_C)$	2–7
C3	$q_{ci} = K_{ci}\lvert\vartheta_{si} - \vartheta_C\rvert^{\beta}(\vartheta_{si} - \vartheta_C)$	2–8		
R1	$q_{ri} = K_{ri}(\vartheta_{si} - \vartheta_r)$	2–9	$q_{re} = K_{re}(\vartheta_{se} - \vartheta_{amb})$	2–10
R2	$q_{ri} = 4\varepsilon\sigma_0 T_R^3(\vartheta_{si} - \vartheta_r)$	2–11	$q_{re} = [T_{amb}^3 4\varepsilon\sigma_0(\vartheta_{amb} - \vartheta_{se})] + [(T_{sky}^4 - T_{se}^4)VF_{sky}\varepsilon\sigma_0]$	2–12
R3	$q_{ri} = \varepsilon\sigma_0(T_{si}^4 - T_r^4)$	2–13	$q_{re} = \varepsilon\sigma_0[F_{gnd}\left(T_{gnd}^4 - T_{se}^4\right) + VF_{sky}\left(T_{sky}^4 - T_{se}^4\right) + VF_{amb}\left(T_{amb}^4 - T_{se}^4\right)]$	2–14
R4	$q_{ri} = \sum_j VF_{ij}(H_i - H_j)$	2–15		

Table 2-6
Convective and radiative exchange coefficients and equations implemented in the cases: REF, R_now, R_lin, R_lin_now and R_const.

			Equation q_{ci}	K_{ci} [W/(m^{2}K)]	β [–]	K_{ce} [W/(m^{2}K)]		q_{ri} [W/m^2]	q_{re} [W/m^2]
						Wind (Eq. 2–5)	No wind(Eq. 2–7)		
RM	Floor	If $\vartheta_{si}>\vartheta_c$	Eq. 2–8	2	0.31	–	X	Eq. 2–15	–
		If $\vartheta_{si}<\vartheta_c$		0.54	0.31	–			–
	Ceiling	If $\vartheta_{si}>\vartheta_c$		0.54	0.31	–			–
		If $\vartheta_{si}<\vartheta_c$		2	0.31	–			–
	Vertical surf			1.6	0.3	4v + 4			Eq 2–14
REF	Floor	If $\vartheta_{si}>\vartheta_c$	Eq. 2–8	2	0.31	–	–	Eq. 2–13	–
		If $\vartheta_{si}<\vartheta_c$		0.54	0.31	–	–		–
	Ceiling	If $\vartheta_{si}>\vartheta_c$		0.54	0.31	–	–		–
		If $\vartheta_{si}<\vartheta_c$		2	0.31	–	–		–
	Vertical surf			1.6	0.3	4v + 4	20		Eq 2–14
R_lin	Floor	If $\vartheta_{si}>\vartheta_c$	Eq. 2–6	5	–	–	–	Eq. 2–11	–
		If $\vartheta_{si}<\vartheta_c$		0.7	–	–	–		–
	Ceiling	If $\vartheta_{si}>\vartheta_c$		0.7	–	–	–		–
		If $\vartheta_{si}<\vartheta_c$		5	–	–	–		–
	Vertical surf			2.5	–	4v + 4	20		Eq. 2–12
R_const	Floor/Ceiling	–	Eq. 2–6	3.06	–	–	x	Eq. 2–13	–
	Vertical surf	–		3.06	–	17.78	x		Eq. 2–18

mented (lines C1 and R1 of Table 2-5 and line R_const of Table 2-6). These constant convective heat transfer coefficients are taken from the standard values suggested in TRNSYS 18 [27]. In the case 1nTZ_UA (see Section 2.2.1) constant heat transfer coefficients suggested by EN ISO 6946 [35] are used where constant internal and external thermal resistances are considered including both radiative and convective exchange (i.e. Rse_vertical = 0.04 (m^{2}K)/W, Rsi_vertical = 0.13(m^{2}K)/W).

Within the variant called "radiative model" **RM** (see Fig. 2-4b), a surface to surface radiative exchange approach is applied instead of the star equivalence as explained in [26]. This is implemented using the radiosity approach and requires the calculation of the view factor between the surfaces (see R4 of Table 2-5 and line RM of Table 2-6).

The radiosity approach method (case RM) described in [36] is implemented in Simulink [26] using the Equations (2-16)–(2-18). The radiosity H combines the radiation emitted and reflected by a surface with the surface temperature T_{si}. Using the radiosity approach it is possible to calculate the radiative heat flux emitted by a surface i by means of Equation (2-17). Combining Equations (2-16) and (2-17) it is possible to obtain Equation (2-18), with which the radiative heat flux is calculated within the model.

$$H_i = \varepsilon_i\sigma_0 T_{si,i}^4 + (1 - \varepsilon_i)\sum_j VF_{ij}H_j \tag{2-16}$$

$$Q_{ri} = A_i\left(H_i - \sum_j VF_{ij}H_j\right) \tag{2-17}$$

$$Q_{ri} = \frac{A_i\varepsilon_i}{1 - \varepsilon_i}\left[\sigma_0 T_{si,i}^4 - H_i\right] \tag{2-18}$$

Additionally to the detailed surface to surface radiative exchange, this model (RM) allows the user to calculate the view factors between all the surfaces of the enclosure and specific points where the mean radiant temperature has to be evaluated allowing the simulation of a radiant temperature field within the thermal zone. Equation (2-19) is used for the calculation of the mean radiant temperature.

$$T_r = \sqrt[4]{\sum_i VF_i\ T_{si,i}^4} \tag{2-19}$$

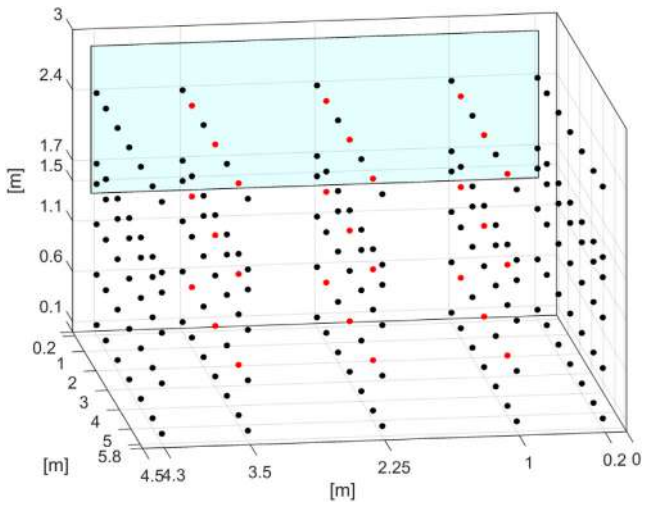

Fig. 2-6. Maps of the points where the mean radiative temperature is evaluated. The red dots represent the points where the calculation of the mean radiant temperature calculated with Simulink has been compared against the results of TRNSYS. (For interpretation of the references to colour in this figure legend, the reader is referred to the web version of this article.)

Fig. 2-6 represents the maps of the points where the mean radiant temperature is simulated using the RM model. The dynamic temperature of the red sensors (see Fig. 2-6) is additionally compared against the dynamic results of TRNSYS 18 implementing the detailed mode for modelling the radiation exchange of surfaces within a zone [30] in order to cross-compare the results of the RM model (see Appendix 5).

2.2.6. Window model

The window model highly influences the accuracy of the results especially in cases where the window to wall ratio is high as highlighted in [8]. In this work, two different window models are compared. The more detailed model is proposed by Campana in [33][3] and a scheme of the thermal circuit is reported in Fig. 2-7. In this model, the solar irradiation is absorbed in each pane and the absorption factor is given as input as a function of the solar incident angle (see appendix Appendix 1). The heat exchange between the windows panes is divided into radiative (see Equation (2-20)) and convective (see Equation (2-21)). The convective and radiative heat exchanges are a function of the temperature difference between the two panes resulting in a dynamic variable heat exchange coefficient.

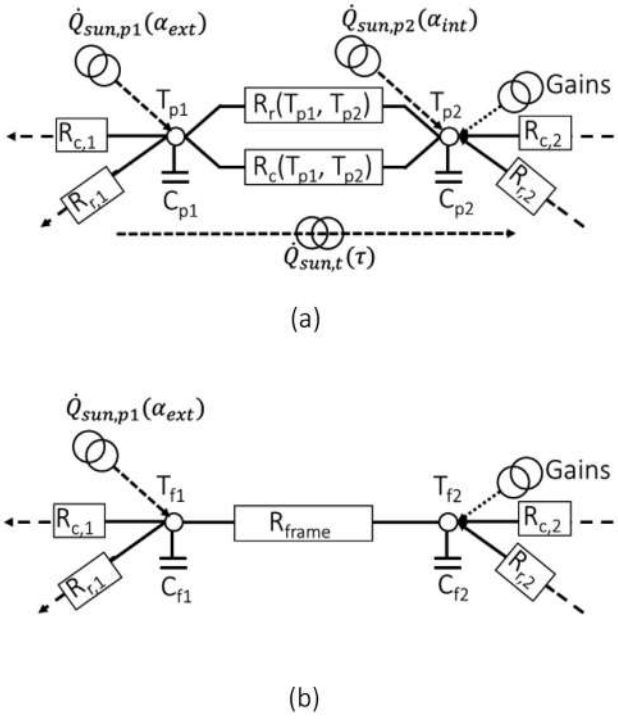

Fig. 2-7. Thermal circuit of the detailed window model for a two panes glazing system: (a) glass and (b) frame.

The frame is modelled with two separated capacities and a constant thermal resistance for the calculation of the heat conduction between the two frame capacities (see Fig. 2-7b). It is noteworthy to mention that the model implements one capacity for each pane that in this case study corresponds to two capacities as reported in Fig. 2-7a, but if three panes windows were to be analysed the model would implement three capacities.

$$\dot{Q}_{r,p1\_p2} = \frac{4\sigma_0 \left[\frac{T_{p1}+T_{p2}}{2}\right]^3}{1-\frac{1}{\varepsilon_{s1}}-\frac{1}{\varepsilon_{s2}}}(T_{p1}-T_{p2}) \tag{2-20}$$

$$\dot{Q}_{c,p1\_p2} = \left|\frac{Nu}{d}\left[\left(\frac{T_{p1}+T_{p2}}{2}\right)\lambda+\Delta\lambda\right]\right|(T_{p1}-T_{p2}) \tag{2-21}$$

$$Nu = \left[1+\left(0.0303Ra^{0.402}\right)^{11}\right]^{0.091} \text{ for } Ra < 2x10^5 \tag{2-22}$$

The thermal circuit of the simplified window model (proposed in the CARNOT Simulink library [37]) is reported in Fig. 2-8. Here both frame and glazing are lumped in the same component and a transfer function characterised by a time constant replaces the capacities. The thermal resistance of the glass is constant and given as input. The calculation of the internal and external surface temperatures is reported in equations (2-23) and (2-24).

$$\vartheta_{se} = \left(R_{win,const}\,\dot{q}_{se}+\vartheta_{si}\right)\frac{e^{\frac{t}{timeconstant}}}{timeconstant} \tag{2-23}$$

$$\vartheta_{si} = \left(R_{win,const}\,\dot{q}_{si}+\vartheta_{se}\right)\frac{e^{\frac{t}{timeconstant}}}{timeconstant} \tag{2-24}$$

Where $R_{win,const}$ [$(m^2K)/W$] is the constant thermal resistance of the window, $\dot{q}_{s,e}$ and $\dot{q}_{s,i}$ [W/m^2] are the thermal fluxes on the external and internal surface, respectively, ϑ_{se} and ϑ_{si} [°C] are the temperatures on the external and internal surface of the window, respectively, and t [s] is the time.

The solar absorption on the external side of the frame is added to the balance of the external node of the window while the solar gains are calculated based on the solar heat gain coefficient (SHGC) given as input and corrected with a standard correction function based on the solar incidence angle. The correction function,

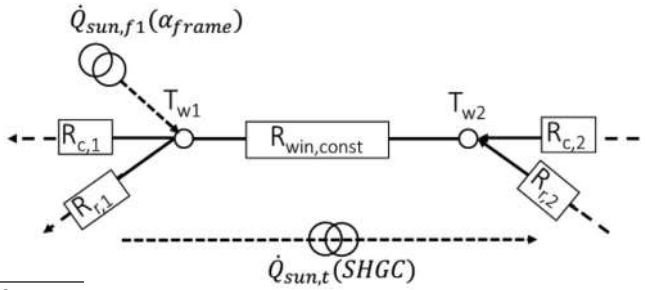

[3] This window model uses the window optical properties pre-processed by the LBNL-Window software [42] (see [43] for the WINDOW technical documentation).

Table 2-7
Correction factor (CF) of the SHGC, implemented in the simplified window model for a double pane window, as a function of the solar incident angle. For the diffuse radiation the CF at 60° is used.

ϑ	0°	10°	20°	30°	40°	50°	**60°**	70°	80°	90°
CF	1	0.99912	0.9961	0.98941	0.97519	0.94337	**0.86634**	0.67843	0.3235	0

implemented in the simplified window model, depends on the number of panes of the window and Table 2-7 reports the correction factors (CF) used for double pane windows. The diffuse solar irradiation is corrected using the CF for 60° incidence angle. As shown in Fig. 2-9 the correction function of the SHGC used in the simplified model is, for this case study, slightly different from the detailed window properties reported in Appendix 1. The deviations are particularly evident when the incidence angle is between 50° and 80°. Nevertheless, only around 20-30% of the impinging solar radiation has an incidence angle between 50° and 90° while the correction factor for the diffuse solar radiation is influencing the 30% to 60% of the impinging solar radiation. For this reason, the deviation for the diffuse solar radiation correction factor is maximum 1.7%, but it highly influences the total solar gains since this coefficient is multiplied by the whole incoming diffuse solar radiation.

The REF case implements the detailed window model (see Fig. 2-7) using the detailed window properties (see Tables A1–A9) while the cases Win_Rcalc, Win_Rcal and Win_Rcal_gcal implement the simplified window model represented by Fig. 2-8. In particular, in the case called **Win_Rcal_gcal,** the thermal resistance of the window is calibrated against the results of the REF case

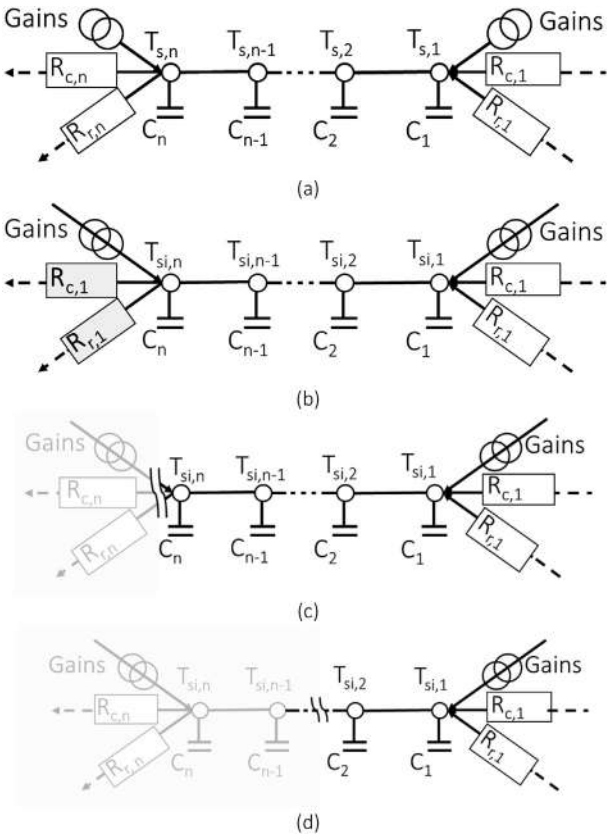

Fig. 2-10. Thermal circuit of the different models applicable for adiabatic structures. (a) **REF** same boundary conditions are applied on both sides; (b) **Ad_sb** same boundary conditions and thermal resistance are applied on both sides; (c) **Ad_no** a null thermal flux is imposed on the external side and (d) **AD_nm** where a null thermal flux is imposed in the middle of the structure.

in order to assure the same transmission losses and the resulting heat transfer coefficients. In addition, a calibrated SHGC correction coefficient for the diffuse radiation that assures the same solar gains as the REF case is applied. See Section 3.1 for the values of the calibrated HTC and SHGC. The case **Win_Rcal** implements the predefined correction function of the SHGC used in the simplified model (see "simplified window model" in Fig. 2-9), but the calibrated thermal resistance is used. The case **Win_Rcalc** is based on the window thermal resistance given as input for this case study (see Table 2-1) and the standard correction function of the SHGC (see Fig. 2-9, "simplified window model").

2.2.7. Adiabatic structure model

Although adiabatic structures do not exchange heat with the environment outside the thermal zone, they do play an important role since they represent a part of the building capacity. Different approaches can be adopted to represent an adiabatic structure:

- The same boundary conditions (i.e. solar gains and internal gains assigned to the considered surface, convective and radiative temperature) can be applied on both sides (see Fig. 2-10a) (i.e. case **REF**)
- The same boundary conditions (i.e. solar gains and internal gains assigned to the considered surface, convective and radiative temperature) and thermal resistance can be applied on both sides (see Fig. 2-10b) (i.e. case **Ad_sb**),
- A null thermal flux can be imposed on the external side (see Fig. 2-10c) (i.e. case **Ad_no**),
- A null flux in the middle of the structure can be applied (see Fig. 2-10d) (i.e. case **AD_nm**);

2.2.8. Sky model

Anisotropic sky models are typically implemented in the dynamic simulation tools and in the REF case the sky model based on Perez 1990 [38] is used. A simplified isotropic sky model can be also used and the diffuse solar radiation (I_{diff}) can be calculated by means of Equation (2-25), where: $I_{diff,hor}$ is the diffuse solar radiation on the horizontal surface and γ_s is the inclination angle of the surface (i.e. for vertical surfaces is 90°). This variant is analysed within the case called **Iso_Sky**.

$$I_{diff} = 0.5\ I_{diff,hor}\ (1 + \cos(\gamma_s)) \quad (2\text{-}25)$$

Fig. 2-11 shows the monthly solar radiation impinging the south façade calculated with the anisotropic sky model used in the REF case and with the isotropic sky model used in the case called Iso_Sky. It can be noticed that the deviations are especially important during the winter period.

2.2.9. Pre-runtime

Usually, at least one month of initialization period[4] should be added before the simulation year to start the simulation in quasi-steady-state condition correctly accounting for the energy stored in the capacities of the building (initial energy), while in this case (***Noprerunt***) only 365 days are simulated. In the variant Noprerunt the initial temperatures of the capacities of the walls are calculated

[4] The length of the pre-simulation period should be defined depending on the capacity of the simulated object and the accuracy of the imposed initial conditions.

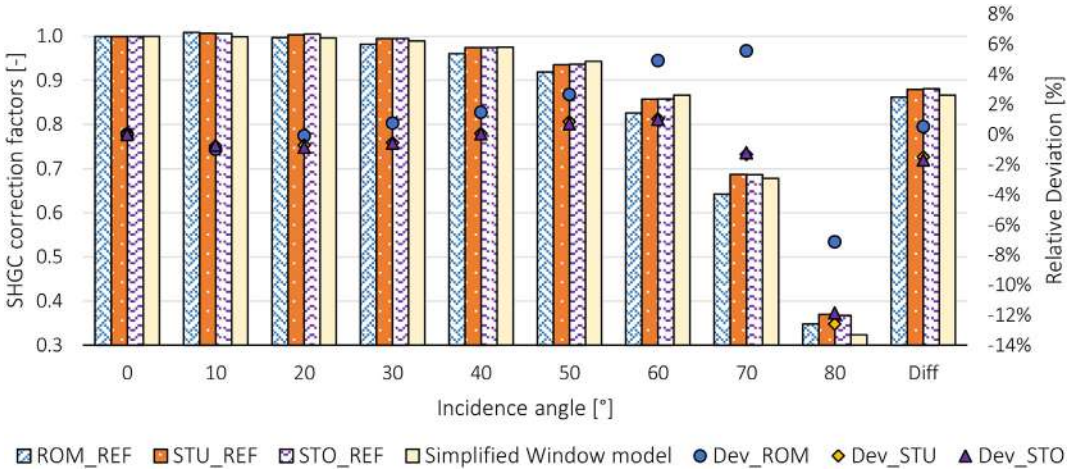

Fig. 2-9. Correction factors of the solar heat gain coefficient (SHGC) as a function of the solar incidence angle for the detailed window model for the climate of Rome Stuttgart and Stockholm and the correction function implemented in the simplified window model. On the right side of the diagram, the deviations between the correction factors used in the detailed and simplified window models are reported.

considering the steady-state temperature distribution between the initial internal convective temperature (i.e. 20 °C) and the initial ambient temperature.

2.2.10. Solver settings

Different variable-step implicit solvers can be used in Simulink, the **REF** case uses the ode23tb, which implements an implicit Runge-Kutta formula. The ode15s (***Sol_15s***) is a variable-order solver based on the numerical differentiation formulas, the ode23s (***Sol_23s***) is based on modified Rosenbrock formula of order 2, the ode23t (***Sol_23t***) implements a trapezoidal rule using a free interpolant. In all the cases the relative tolerance of the solver is set to 0.001 while the absolute tolerance is set to automatic (i.e. the absolute tolerance is reset in each state to the maximum value that the state has assumed so far, times the relative tolerance for that state). For more explanations about relative and absolute tolerances see [39]). The explicit solvers available in Simulink (i.e. ode46, ode 23 and ode 115) are not included in this comparison because they are not suitable for solving stiff numerical problems.

2.3. Statistical indices

This work aims to evaluate the influence of different modelling approaches on the results using as a reference the Simulink model already cross-compared in [8]. To achieve this goal it is necessary to define a unique index to quantify the deviation between one specific case and the reference and to select the relevant variables to be considered in this evaluation. The goodness-of-fit (GOF) [25], a function of the normalized root mean square error (NRMSE) and the normalized mean bias error (NMBE), is chosen as a compact indicator for this task. The calculations of NMBE and NRMSE are reported in Equations (2-26) and (2-27) respectively, where:

- $s_{i,ma,G}$ is the simulated value at the time step i, using the modelling approach (ma) and considering the variable G (e.g. heating or cooling power);
- $ref_{i,G}$ is the simulated value of the reference model at the time step i considering the variable G (e.g. heating or cooling power);
- N is the total number of considered time steps (i.e. hours of the year);
- $|\overline{m}|_{ref_G>0}$ is the average of the reference results considering the variable G (e.g. heating or cooling power) and including only values higher than zero as suggested by [8] to avoid normalization problems.

The NRMSE and NMBE are calculated considering the heating and cooling hourly average power[5] (i.e. G) for all the cases included in this analysis (i.e. ma). To calculate the $GOF_{ma,G}$ for each case (see Equation (2-30) and Table 2-2) and considered variable (i.e. heating and cooling powers), it is necessary to normalize the NRMSE and NRMSE in order to have these indices between 0 and 1. For this step, Equations (2-28) and (2-29) are applied. The last step regards the calculation of a unique GOF for each case averaging the GOF calculated considering the heating powers and cooling powers (i.e. G) for the same case (ma). This is done using Equation (2-31) using as weight the fraction of the energy demand for cooling or heating over the sum of energy demand for cooling and heating.

The value assumed by the GOF is limited between 0 and 1 and when the GOF is approaching 1 means that the modelling approach under consideration has the best match with the REF results between all the considered modelling approaches and vice versa when GOF is approaching 0.

In addition, to evaluate deviations in terms of temperature, the Mean Absolute Error (MAE) and the Mean Bias Error (MBE) are calculated (see Equations (2-32) and (2-33)).

$$NMBE_{ma,G} = \frac{\sum_{i=1}^{N}(s_{i,ma,G} - ref_{i,G})}{\sum_{i=1}^{N} ref_{i,G}} \ [\%] \tag{2-26}$$

$$NRMSE_{ma,G} = \frac{1}{|\overline{m}|_{ref_G>0}} \sqrt{\frac{\sum_{i=1}^{N}(s_{i,ma,G} - ref_{i,G})^2}{N}} \ [\%] \tag{2-27}$$

$$nNMBE_{ma,G} = \frac{|NMBE|^{max}_{ma,G} - |NMBE_{ma,G}|}{|NMBE|^{max}_{ma,G} - |NMBE|^{min}_{ma,G}} \tag{2-28}$$

$$nNRMSE_{ma,G} = \frac{NRMSE^{max}_{ma,G} - NRMSE_{ma}}{NRMSE^{max}_{ma,G} - NRMSE^{min}_{ma,G}} \tag{2-29}$$

$$GOF_{ma,G} = \frac{\sqrt{2}}{2} \sqrt{nNRMSE^2_{ma,G} + nNMBE^2_{ma,G}} \tag{2-30}$$

[5] The deviations in terms of other component of the energy balance (i.e. Solar gains, infiltration, ventilation and transmission losses) are also evaluated to better understand the results and assess the cases where higher/lower losses compensate higher/lower gains resulting in a similar heating and cooling demand with respect to the reference case.

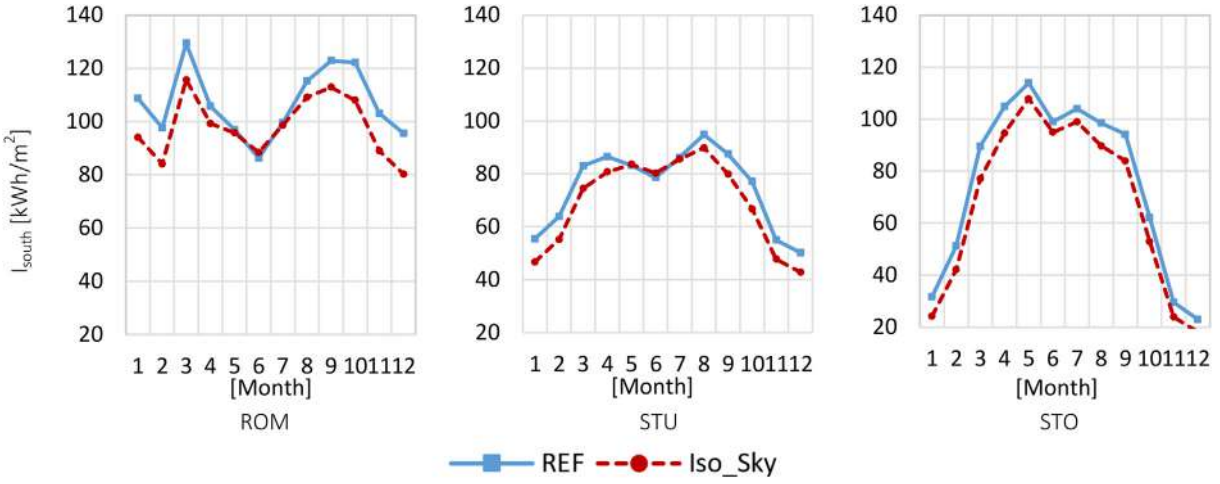

Fig. 2-11. Solar irradiation on the south-oriented facade for the climate of Rome (ROM), Stuttgart (STU) and Stockholm (STO) calculated with the anisotropic Perez model (REF) and with the isotropic model (Iso_Sky).

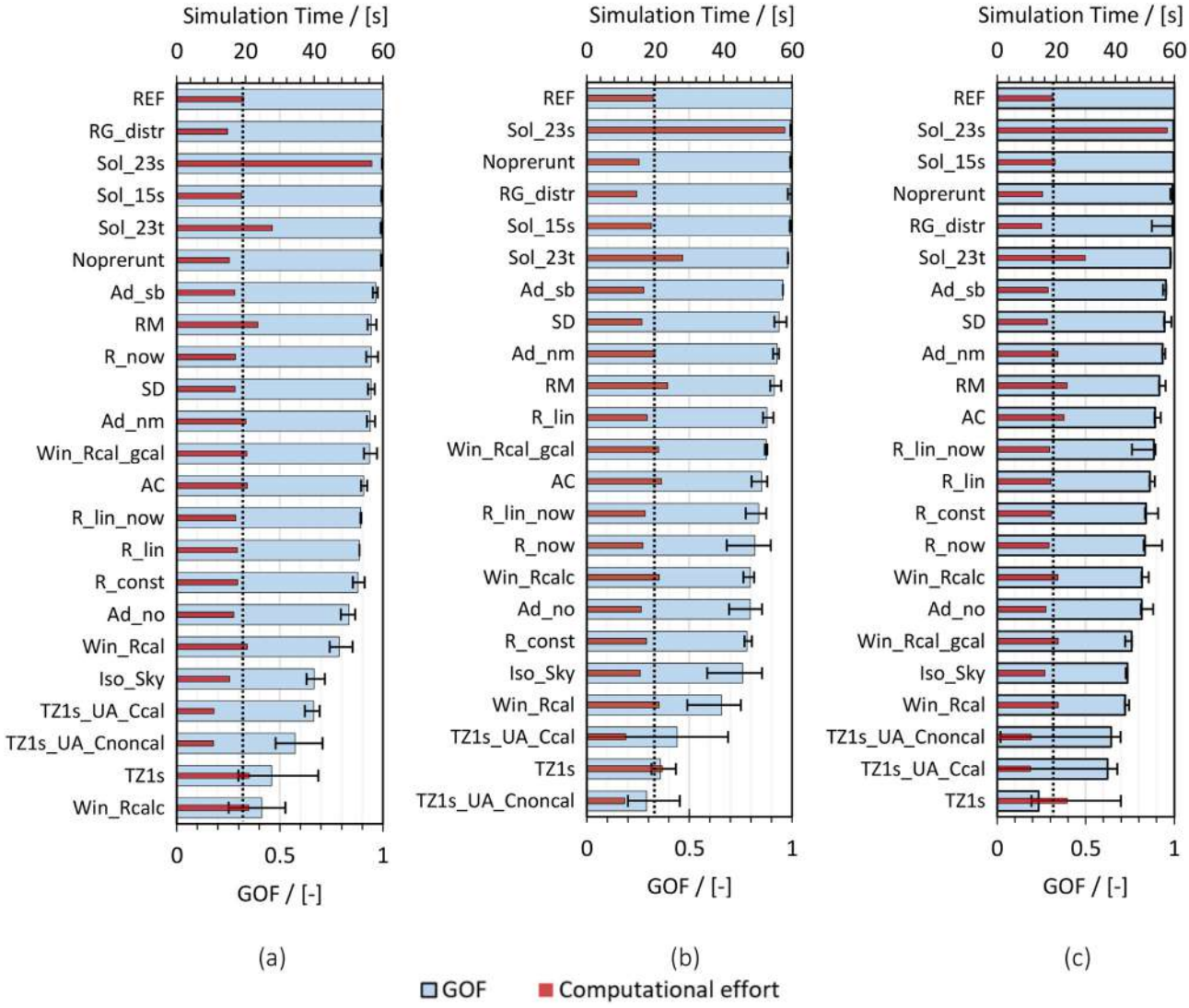

Fig. 3-1. Goodness-of-fit and computational cost for each variant considering the weathers of (a) Stockholm, (b) Stuttgart and (c) Rome. The error bars show the range of GOF calculated for the cooling and heating demands (see Section 2.3).

$$GOF_{ma} = GOF_{ma,G_1} \frac{\sum_{i=1}^{N}|ref_{i,G_1}|}{\sum_{i=1}^{N}|ref_{i,G_1}| + \sum_{i=1}^{N}|ref_{i,G_2}|} + GOF_{m,G_2} \times \frac{\sum_{i=1}^{N}|ref_{i,G_2}|}{\sum_{i=1}^{N}|ref_{i,G_1}| + \sum_{i=1}^{N}|ref_{i,G_2}|} \quad (2\text{-}31)$$

$$MAE = \frac{\sum_{i=1}^{N}|s_i - ref_i|}{N} \quad (2\text{-}32)$$

$$MBE = \frac{\sum_{i=1}^{N}(s_i - ref_i)}{N} \quad (2\text{-}33)$$

2.4. Evaluation of the computational cost

For the evaluation of the computational cost, each variant is run on the same local workstation with the following specifications:

- Processor: Intel® Core™ i5-8350U CPU @ 1.7 GHz
- 4 cores
- 8 logical processor
- RAM: 16.0 GB
- OS: Windows 10 64 bit
- GPU: Intel® UHD Graphics 620

During the simulation, no other applications were running in the background except the operative system process. Each computation is repeated 10 times and the median value of the CPU times is used for the comparison.

3. Results and discussion

The results and discussion part of this work is divided into three main sub-sections: Section 3.1 where the calibrated inputs for different analysed cases are reported and Section 3.2 where the results of all the cases included in this study are compared against the reference (REF) case to highlight the influence of each modelling approach on the results and computational cost. In Section 3.2.2 a special focus is given to the influence of the thermal zone model on the predicted temperature of the thermal zone.

3.1. Inputs calibration

The simplification of the thermal zone model from two-star node to one-star approach (see Section 2.2.1) and of the window model (see Section 2.2.6) introduces also a simplification of the input parameter (i.e. effective building capacity for the one-star model and the constant thermal resistance and solar heat gain coefficient for the window model). Introducing a pre-processing step where these inputs are calibrated leads to a better agreement between the simplified models and the reference model. For this reason in the analysis of the results both cases, i.e. using calibrated and standard inputs, are considered to show the influence of the parametrisation process on the results. The non-parametrised cases are represented by TZ1s_UA_Cnoncal for the one-star approach and by Win_Rcalc for the simplified window model. The case where the building capacity of the one-star model is calibrated is called TZ1s_UA_Ccal, where the thermal resistance of the simplified window model is calibrated is called Win_Rcal and where both the thermal resistance and the solar heat gain coefficient of the window model are calibrated Win_Rcal_gcal.

3.1.1. One-star model combined with constant heat transfer coefficient wall model

The simplified thermal zone model requires a parametrization of the building capacity (see TZ1s_UA_Ccal Section 2.2.1), which is found by trying to minimize the deviation in terms of annual heating and cooling demand with the REF case. The capacities resulting from this process are: 2.8277 10^7 J/K in Stockholm, 4.2634 10^7 J/K in Stuttgart and 1.4808 10^7 J/K in Rome. As highlighted in Section 2.2.1 this parametrisation process is compensating the different control of the heating and cooling systems used in the REF case (according to the convective temperature) and in the TZ1s_UA_Ccal case (according to the only temperature available in this model that corresponds to the operative). To clarify this aspect the calibration process of the one-star model is repeated using as a reference the annual heating and cooling demand obtained by simulating the REF model controlled with the operative temperature

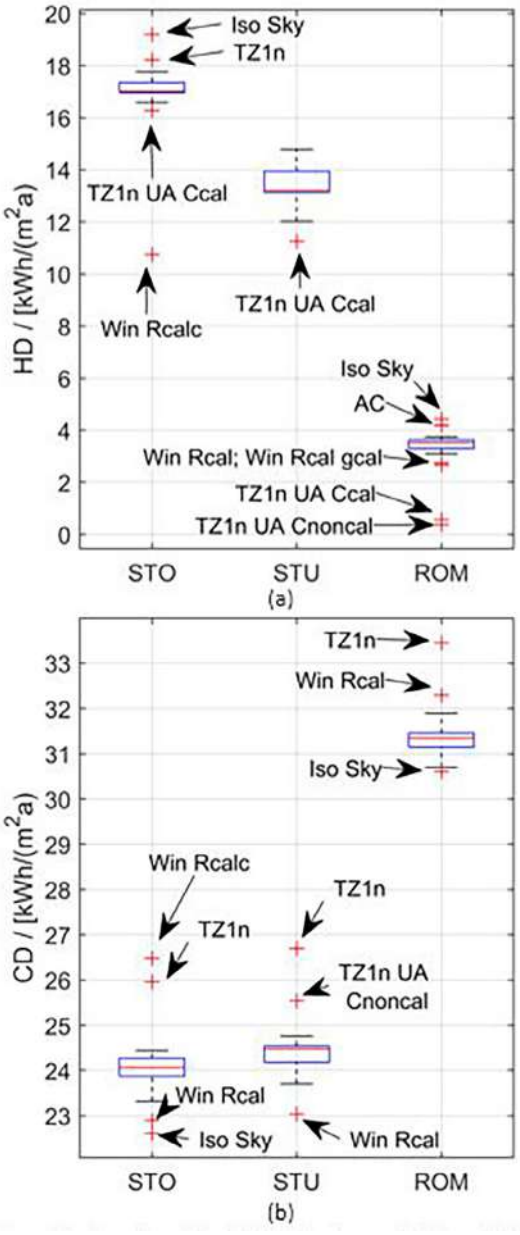

Fig. 3-2. Box plot of the Heating demand (HD) on the left and cooling demand (CD) on the right for all the cases considered in the sensitivity analysis and for the climates of Stockholm (STO), Stuttgart (STU) and Rome (ROM).

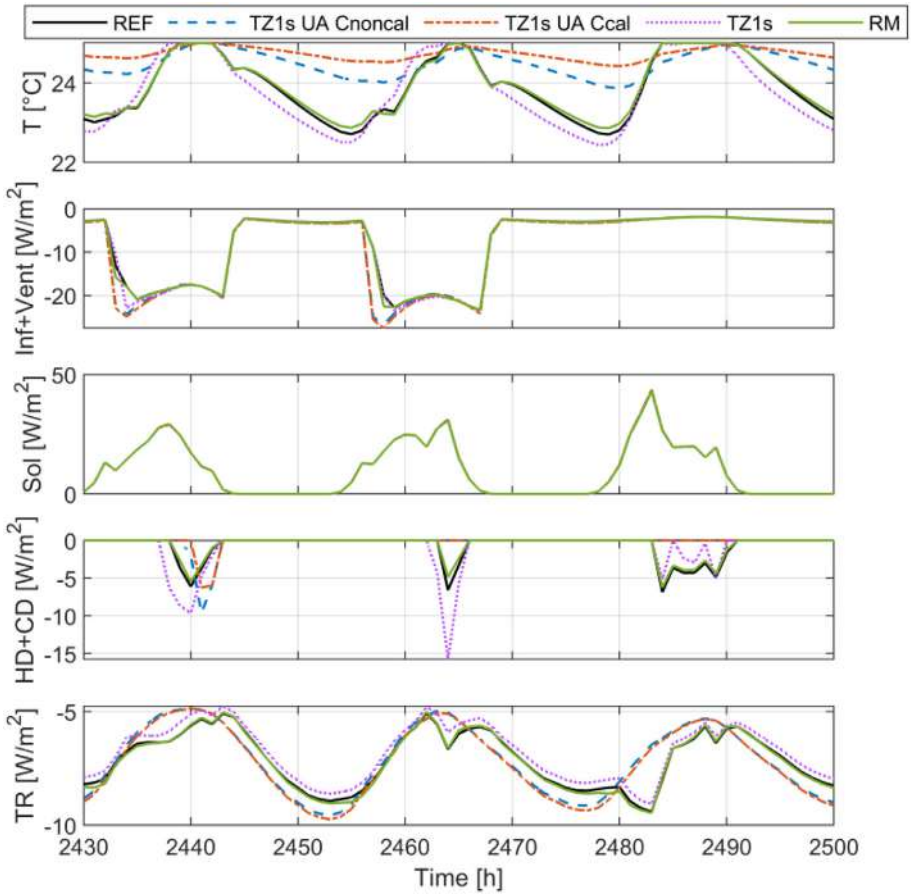

Fig. 3-3. Hourly results (i.e., convective temperature for REF and RM and thermal zone temperature for TZ1s_UA_Ccal, TZ1s_UA_Cnoncal and TZ1s, ventilation plus infiltration losses, solar gain, heating and cooling power and transmission losses) for the climate of Stockholm including the cases: REF, TZ1s, TZ1s_UA_Ccal, TZ1s_UA_Cnoncal and RM.

(Ref2) instead of the convective and the results of this in-depth analysis are presented in Appendix 4. The capacities resulting from this process are: 0.5886 10^7 J/K in Stockholm, 0.69203 10^7 J/K in Stuttgart and 0.41169 10^7 J/K in Rome.

A better agreement in terms of both heating and cooling demands between TZ1s_UA_Ccal and REF might be found by using different capacities for winter and summertime.

3.1.2. Window model

The constant heat transfer coefficient of the simplified window model (see Section 2.2.6) is calibrated against the results of the REF case to assure the same annual transmission losses and the resulting heat transfer coefficients are: (considering constant external and internal thermal resistances of 0.04 (m^2K)/W and 0.13 (m^2K)/W, respectively) 1.24 W/(m^2K) in Stockholm, 1.48 W/(m^2K) in Stuttgart and 1.15 W/(m^2K) in Rome. The calibrated HTCs are used in Win_Rcal_gcal and Win_Rcal.

In addition, a calibrated correction coefficient of the Solar Heat Gain Coefficient (SHGC) for the diffuse radiation that assures the annual same solar gains of the REF is used in the Win_Rcal_gcal case. The correction coefficient that minimizes the solar gain deviations with the REF case is 0.92 in Stockholm, 0.94 in Stuttgart and 0.73 in Rome (see Section 2.2.6).

3.2. Sensitivity analysis of the model simplifications on the results and computational cost

This Section of results is subdivided into two subparts; Section 3.2.1 where the results of all the cases described in Section 2.2 are discussed and compared with the reference case (REF) and Section 3.2.2 where the influence of the thermal zone model on the accuracy of the predicted operative temperature is presented.

3.2.1. Goodness of Fit, computational time and heating and cooling demand of all the cases

Fig. 3-1 shows the Goodness-of-fit (GOF) and computational time (red bars) for each analysed case, for the climates of Rome (ROM), Stuttgart (STU) and Stockholm (STO), where the blue bars reveal the weighted average GOF and the error bars show the discrepancies between the GOF calculated based on heating and cooling demand (see chapter 2.3). The Normalized Root Mean Square Error (NRMSE) and Normalized Mean Bias Error (NMBE) for each case and each climate used to calculate the GOF are reported in Appendix 3 (see Table A13) together with the yearly energy balance of each case for each climate (see Tables A10–12). In the following subsections, the results are discussed.

It is noteworthy to mention that the computational time is strongly affected by the choice of the solver (i.e. Sol_23s) and important model simplification (i.e. TZ1s_UA_Ccal and TZ1s_UA_Cnoncal) while all the other analysed cases influence the computational time by a maximum of ±25 %.

Fig. 3-2 shows a box plot with the yearly heating (HD) and cooling demand (CD) considering the results of all the variants analysed in the sensitivity study for all climates (i.e. Stockholm, Stuttgart and Rome). The median value represented by the red horizontal line is very close to the REF results. The models corresponding to the outliers are also indicated and it can be noticed that TZ1s has in all climates higher CD while TZ1s_UA_Ccal leads to low HD

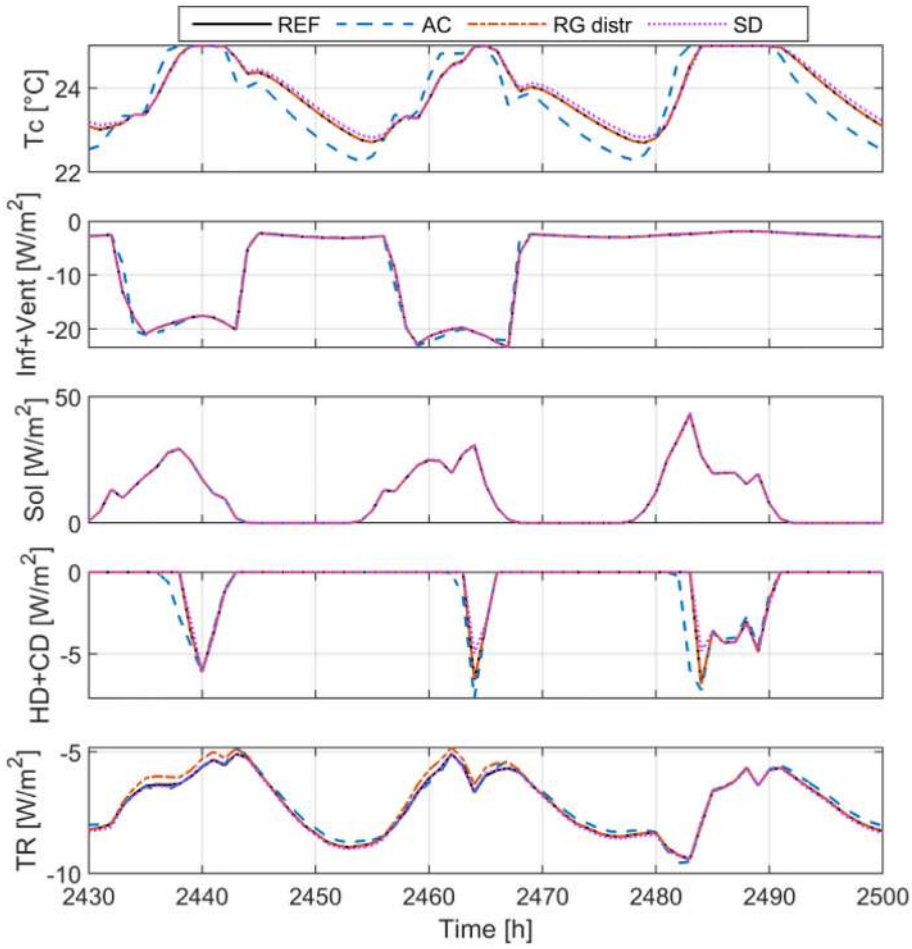

Fig. 3-4. Hourly results (i.e., convective temperature, ventilation plus infiltration losses, solar gain, heating and cooling power and transmission losses) for the climate of Stockholm including the cases: REF, AC, RG and SD.

in all climates. The Win_Rcalc model causes particularly high deviations in both HD and CD in STO and the Iso_Sky model leads to higher HD and lower CD in STO and ROM. The maximum and minimum relative deviations referred to the REF case in terms of HD are: +12% / −37% in STO, +16% / −15% in STU and +49% / −89% in ROM, while in terms of CD are: +10% / −6% in STO, +9% / −6% in STU, +7% / −2% in ROM.

3.2.2. Thermal zone model

In this case study, the heating and cooling systems that should be controlled using the convective temperature are instead controlled using the temperature of the thermal zone, which is the only one available in the cases TZ1s, TZ1s_UA_Ccal and TZ1s_UA_Cnoncal[6]. This results for the TZ1s case in higher transmission and ventilation losses in winter and lower transmission losses in summer, which increases both heating and cooling demands predicted by TZ1s in all the climates (see Tables A10 and A12) with respect to the REF case. Since in TZ1s all the powers are summed up in one node (i.e. resulting in higher and fast varying power summed up in a smaller capacity) the simulation is slightly slowed down.

The cases TZ1s_UA_Ccal and TZ1s_UA_Cnoncal implement a simplified wall and window model based on a constant heat transfer coefficient and the whole thermal mass is considered as lumped in the star node, where all the fluxes are summed up (Section 2.2.1). This solution can reduce the computational time to half, but the non-trivial parametrization of the capacity plays an important role in the accuracy of the results. Fig. 3-3 shows that the case TZ1s is better matching with REF in terms of hourly powers and temperature, compared to TZ1s_UA_Ccal and TZ1s_UA_Cnoncal as a consequence, TZ1s is characterized by a lower NRMSE compared to TZ1s_UA_Ccal (see Table A13). Anyway, since the capacity of the TZ1s_UA_Ccal is defined using a search approach aiming to reduce the difference between the heating and cooling demands of TZ1s_UA_Ccal and of REF, the NMBE of TZ1s_UA_Ccal for the cooling in ROM and STU and for both cooling and heating in STO is lower than TZ1s. For this reason, the GOF of TZ1s_UA_Ccal is higher than TZ1s (see Fig. 3-1). This conclusion is true in this case study since the same weight is given to the NRMSE and NMBE (see Section 2.3), anyway for a particular application could be more important to have a good match in terms of hourly results (in this case more weight should be given to the NRMSE) or only the final energy demand could be of importance (in this case more weight should be given to the NMBE). The model implemented in RM has a slight impact on the transmission losses of the window and wall since the radiative exchange is treated differently and on

[6] To clarify this aspect the calibration process for the TZ1s_UA_Ccal case is repeated using as a reference the annual heating and cooling demand simulated with the reference model controlled according to the operative temperature (Ref2) instead of the convective temperature and the results of this in-depth analysis are presented in Appendix 4. The main outcomes of this comparison show that, as expected, the TZ1s has a better agreement with Ref2 compared to REF and that the calibration process of TZ1s_UA_Ccal based on the results of Ref2 instead of REF leads to better agreement also in terms of dynamic behaviour.

the dynamic behaviour of the convective temperature, which slightly influences the ventilation losses (see Fig. 3-2) marginally reducing the heating and cooling demands (see Tables A10–12). The RM for this case study has a good match with the REF model (see Fig. 3-3) even though this conclusion could be different for other case studies where for example high-temperature radiative systems are used. In addition, the RM can provide the user with detailed information regarding the radiative temperature distribution (see Section 3.2.2), but also requires a higher computational time and detailed information about the building geometry.

3.2.3. Capacity of the convective node and distribution of the internal radiative gain and of the solar gain

Fig. 3-4 reports the hourly results in terms of convective temperature, infiltration and ventilation losses, solar gains, heating and cooling demands and transmission losses for the climate of Stockholm including the cases: Reference (REF), capacity of the convective node (AC), radiative gain distribution (RG_distr) and solar gain distribution (SD).

Reducing the air capacity (AC), not considering the effect of additional internal capacities such as furniture (see Section 2.2.2), leads to an increase in both heating and cooling demands in all the climates while increasing the computational time (see Tables A10–12 and Fig. 3-1). From Fig. 3-4 it is possible to notice that the lower air capacity modelled in the AC case leads to a different dynamic behaviour of the convective temperature and as a consequence of the control of the heating and cooling systems.

From Fig. 3-4 and Fig. 3-1 it can be noticed that RG_distr (see Section 2.2.3) has a minor influence on the results in all climates since the radiative heat gains are only 34% of the total internal gain for this specific case study. It is seen that distributing the radiative gains on the structure capacities instead of the radiative node helps to speed up the simulation of around 20% for this case study.

Solar gain distribution (SD) (see Section 2.2.4) has a higher impact than the radiative gain distribution since the amount of involved energy is higher. Using the SD based on weighted areas results in a reduction of the heating demand and a slight increase in cooling demand in all climates (see Tables A10–12) since the active capacities of the internal opaque structures are influenced. From Fig. 3-4 it is possible to notice that the convective temperature of the SD case slightly deviates from the convective temperature of the REF case. SD has a slightly lower computational cost than REF (see Fig. 3-1).

3.2.4. Convective and radiative heat exchange coefficients

The selection of the equations for the convective and radiative exchange between the envelope elements and the thermal zone or the ambient (see Section 2.2.5) slightly influences the calculation of the transmission losses and the exchange with the adiabatic structures leading to differences in heating and cooling demands. It is noticed that using a constant external convective coefficient (i.e. R_now, R_lin_now and R_const), in this case, leads to higher transmission losses since the used external constant convective coefficient (see Tables 2-5 and 2-6) is higher than the convective

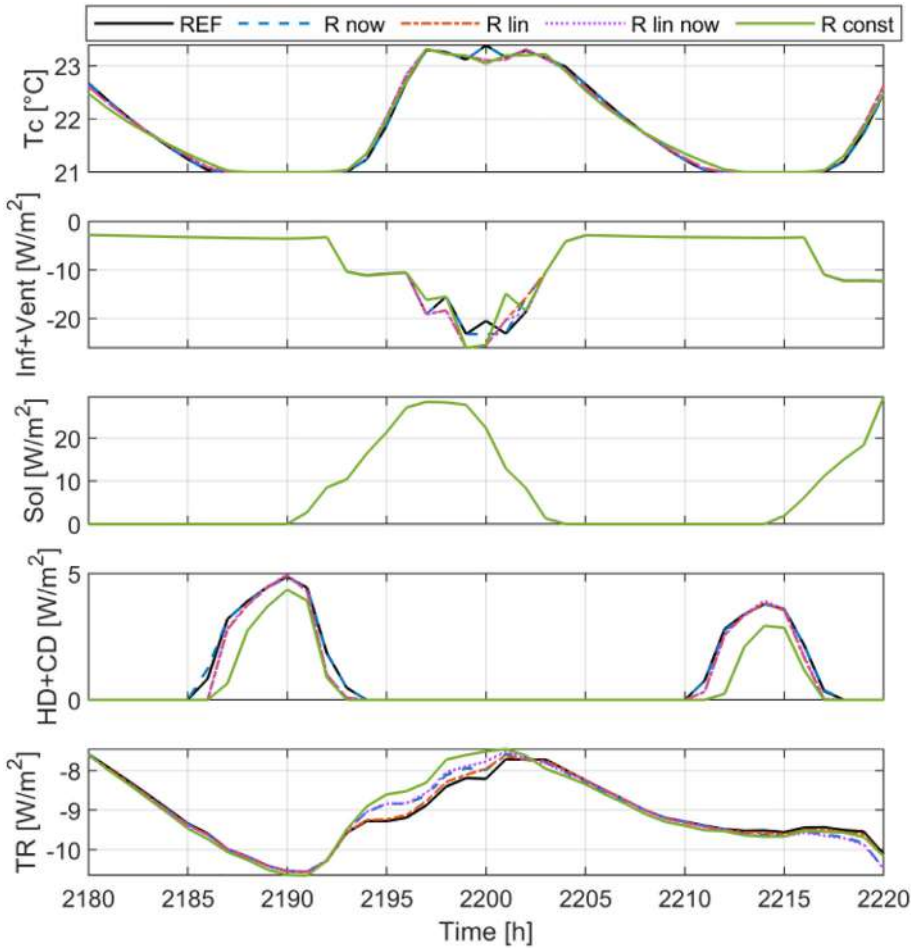

Fig. 3-5. Hourly results (i.e., convective temperature, ventilation plus infiltration losses, solar gain, heating and cooling power and transmission losses) for the climate of Stockholm including the cases: REF, R_now, R_lin, R_lin_now and R_const.

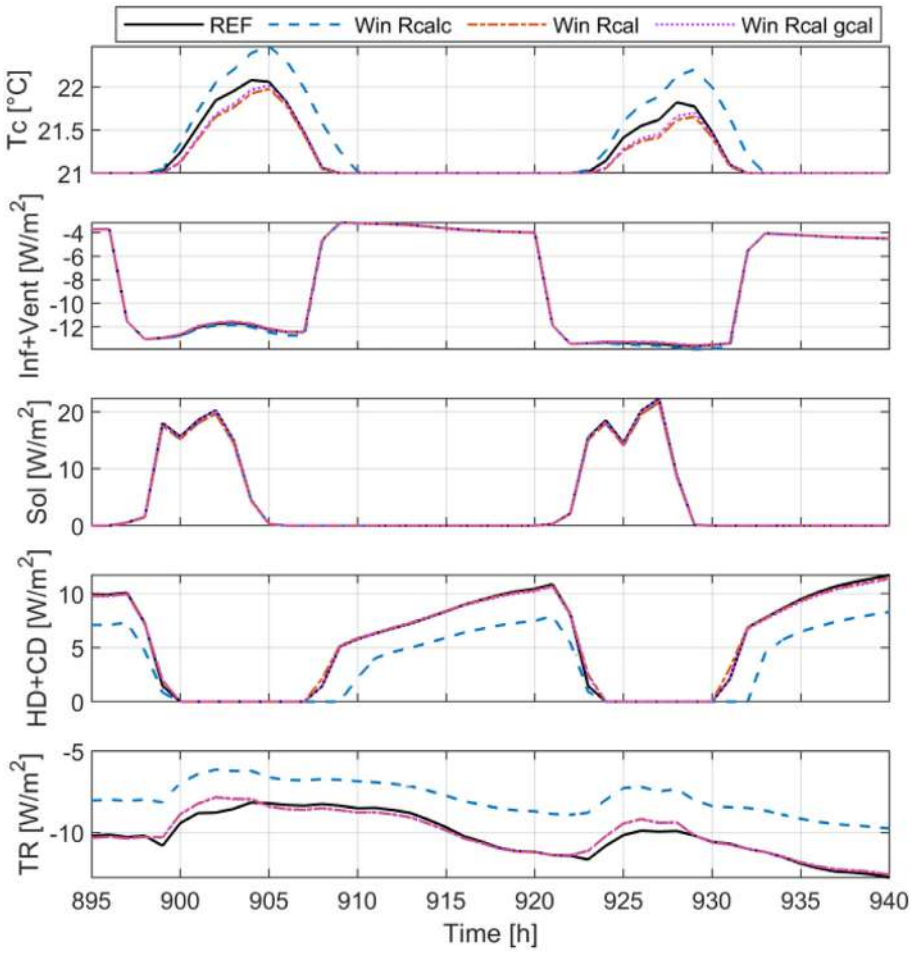

Fig. 3-6. Hourly results (i.e., convective temperature, ventilation plus infiltration losses, solar gain, heating and cooling power and transmission losses) for the climate of Stockholm including the cases: REF, Win_Rcalc, Win_Rcal, Win_Rcal_gcal.

exchange calculated as a function of the wind speed (Equation (2-5) and (2-7)) because the average wind speed in all the climates is lower than 4 m/s (constant value used in case no wind speed is considered). As a consequence, these cases (i.e. R_now, R_lin_now and R_const) have higher heating demand (see Tables A10–12). The R_lin implements linearized radiative and convective exchange coefficients, which leads to slightly higher heating and cooling demands.

The GOF is a weighted average between the GOF_ heat and the GOF_cool and each GOF is a function of the NMBE and on the NRMSE (see Section 2.3). The NRMSE represent the quality of the matching in terms of dynamic behaviour and this is always the best (i.e. lowest) for R_now (since it uses the same equation as REF apart from the external convective coefficient calculation) and increases for R_lin, R_lin_now and is the highest with R_const (see Table A13). The NMBE represents the deviation in terms of energy balance and here the different cases (i.e. R_now, R_lin_now, R_lin and R_const) are ranked differently within the different weathers. The resulting GOF as a consequence has also no clear ranking, valid in each climate, between these cases. The increased transmission losses are compensated by reduced ventilation losses maintaining the cooling demand close to the REF case, but the heating demand can increase up to 9% (e.g. R_const in Stuttgart), therefore it can be stated that the choice of the radiative and convective heat exchange coefficient highly influences the energy balance of the simulated thermal zone. The different models implementing a simplified calculation of the heat exchange coefficients (i.e. R_now, R_lin_now, R_lin and R_const) only marginally reduce the computational time (see Fig. 3-1).

3.2.5. Window model

It is seen that the case Win_Rcalc (see Section 2.2.6) highly influences the results especially in Stockholm (i.e. reducing the heating demand by 37% with respect to the REF case, see Table A10 in Appendix 3 and Fig. 3-12) since here the transmission losses are quite different due to a different heat transfer coefficient resulting from the dynamic simulation (see 2.2.6 and [8]) with the detailed window model implemented in REF and the steady-state value from the description of the window properties (see Appendix 1). Using the calibrated thermal resistance (Win_Rcal) highly reduces the inaccuracy of the results in Stockholm (see Fig. 3-1, Fig. 3-6 and Fig. 3-7 and Section 3.1.2). The simplified window model used for this case has also a simplified calculation of the solar gain, see Section 2.2.6 therefore the solar gains are different from the reference case especially in Stuttgart and Rome. Indeed, by parametrizing the solar heat gain coefficient (SHGC) and the thermal resistance of the simplified window model (Win_Rcal_gcal) (see Sections 2.2.6 and 3.1.2) the results better match the reference case in STU and STO.

Similar results are found in [23] where the results of TRNSYS, implementing a detailed windows model as it is done in the REF case, are compared against the results of the Standard ISO 52016 implementing a simplified window model with constant properties similar to the window model implemented in the case Win_Rcalc. Looking at case 4 presented in [23] (that has similar geometry,

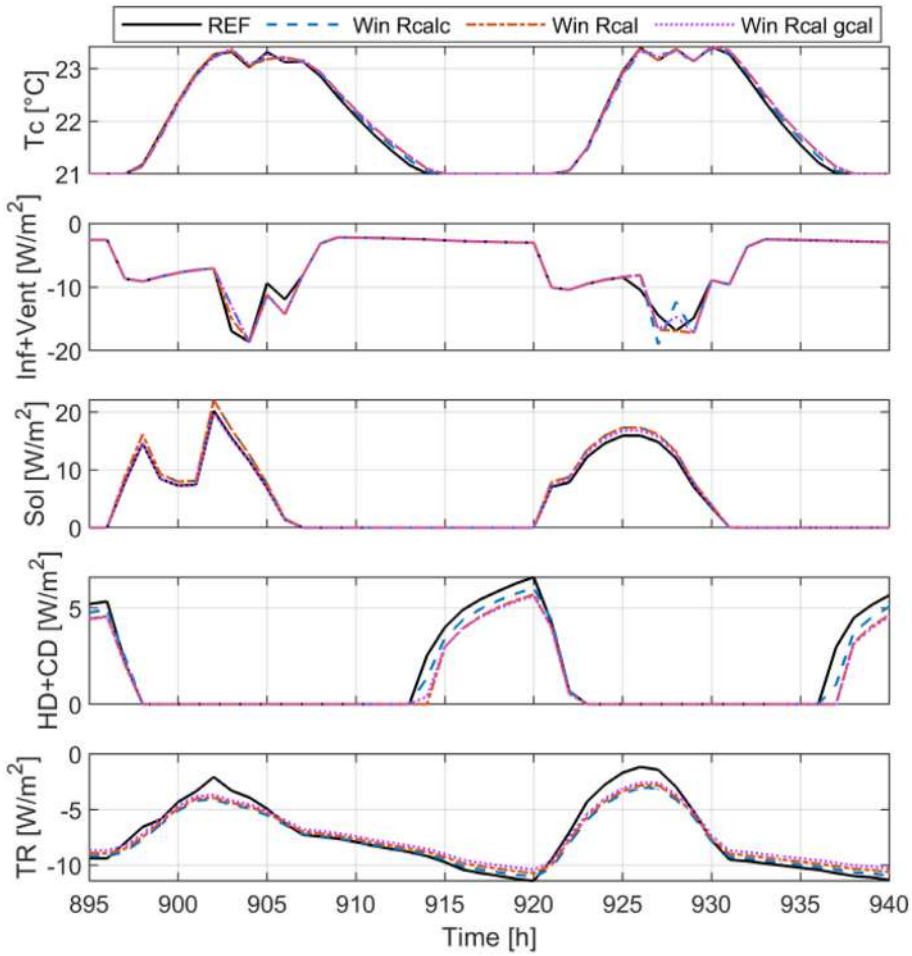

Fig. 3-7. Hourly results (i.e., convective temperature, ventilation plus infiltration losses, solar gain, heating and cooling power and transmission losses) for the climate of Rome including the cases: REF, Win_Rcalc, Win_Rcal, Win_Rcal_gcal.

envelope properties and heating demand as the simulation for the climate of Stockholm presented within this work) the deviation, for the continental climate, in terms of heating demand between the results of TRNSYS and the Standard ISO 52,016 are reduced from 40% to 5% by using, in the window model of the standard, the solar heat gain coefficient and thermal resistance of the window simulated by TRNSYS instead of constant values. This result is in agreement with the heating demand reduction of 37% obtained as a result of Win_Rcalc compared to REF for the climate of Stockholm.

The GOF of Win_Rcal is lower than Win_Rcalc in STU and ROM since the deviation in solar gains of Win_Rcalc is compensated by transmission losses keeping the total heating and cooling demand closer to the REF case concerning the Win_Rcal case (see Fig. 3-1, Tables A10–A13 and Fig. 3-7). Win_Rcalc has a better GOF in Rome than Win_Rcal_gcal due to the compensation effect between transmission losses and solar gains (see Tables A10–A13 and Fig. 3-7). It is noteworthy to mention that, with the simplified window also the solar distribution is implemented as in the SD case (see Section 2.2.4) therefore, in these specific results both the influence of the solar distribution and of the window model are combined. The simplified window model includes two transfer functions to reproduce the dynamic of the glass capacity. The small-time constant of these functions makes the model slightly slower than using the complex window model from REF (see Fig. 3-1).

3.2.6. Adiabatic structure model

The model of the adiabatic structure adopted in REF, allows the floor and ceiling to have a small heat flux through the structure since the convective coefficient are different on the internal and external sides (see Section 2.2.7). Using the same boundary conditions and the same thermal resistance (Ad_sb) between the surface and the thermal zone on each side of the adiabatic structure leads to a null annual energy balance in each structure. The variant Ad_sb has almost no influence on both dynamic and energy balance (see Tables A10–A12 and Fig. 3-8). On the contrary, the variant where a null thermal flux in the middle of the structure is imposed (Ad_nm) allows a deeper seasonal activation of the capacity and this effect is even more relevant when no flux outside is imposed (Ad_no), reducing both heating and cooling demands (see Tables A10–A12 and Fig. 3-8). For what concerns the internal walls for this case study, the REF, Ad_sb and Ad_nm cases represent the same model since in all of them the convective exchange coefficient is the same on both sides, the construction is symmetrical and also the same boundary conditions are applied resulting into a null flux in the middle of the structure. The activation of the internal wall changes only when no flux on the external side is applied (in this case more capacity is activated). Further, it is seen that the case AD_no and Ad_sb trend to reduce the computational time with respect to REF (Fig. 3-1).

3.2.7. Sky model and pre-runtime

The isotropic sky model reduces the solar irradiation impinging the windows, especially during the wintertime (see Fig. 2-11, Fig. 3-9 and Fig. 3-10) leading to a higher heating demand and a lower cooling demand in all the climates compared to the REF case (see Tables A10–A12). It can be stated that Iso_sky reduces the

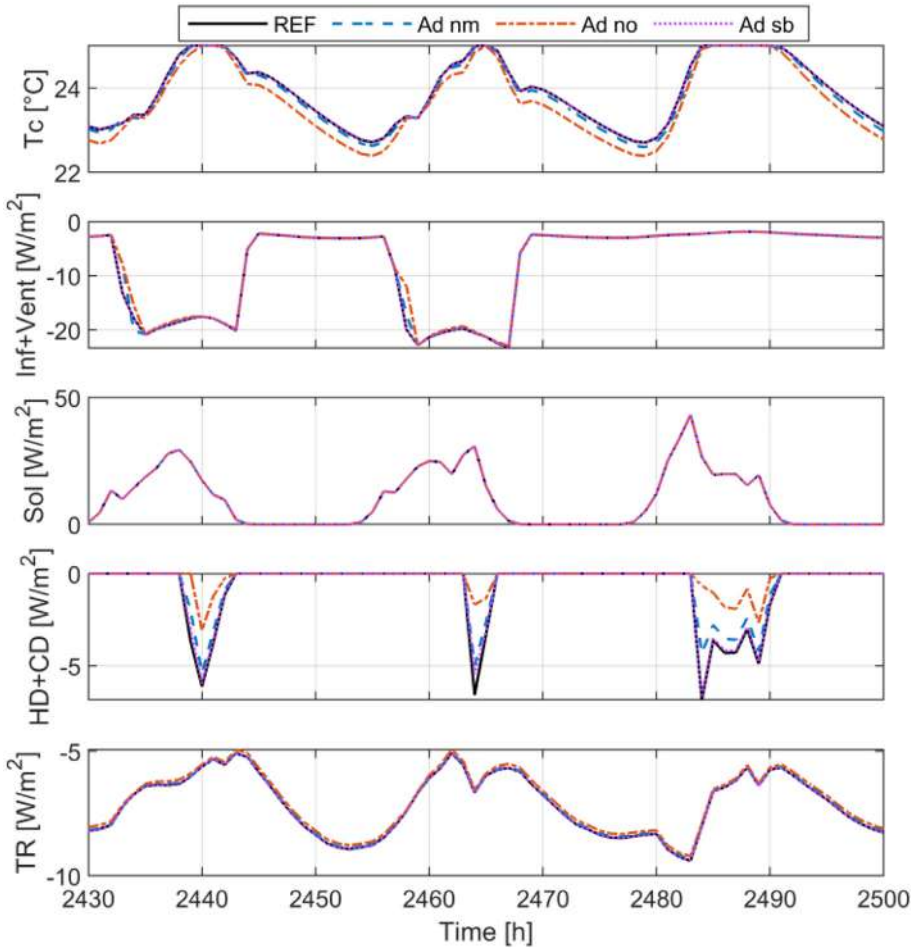

Fig. 3-8. Hourly results (i.e., convective temperature, ventilation plus infiltration losses, solar gain, heating and cooling power and transmission losses) for the climate of Stockholm including the cases: REF, Ad_nm, Ad_no and Ad_sb.

computational time reducing also the accuracy of the model (see Fig. 3-1).

Reducing the simulation period to one year (Noprerun) disregarding the pre-simulation period (as described in Section 2.2.9) leads in this case study to almost no changes in terms of yearly heating and cooling demands (see Tables A10–A12), only slight dynamic deviations within the first 8 days of simulation are visible Fig. 3-9, which leads to a good fit with the REF case (see Fig. 3-1) and a reduced computational effort. The evaluation of this specific case (Noprerun) strongly depends on the temperature selected for the initialization of the building capacities and the capacity involved in the building model (see Section 2.2.9).

3.2.8. Solver

The selected solvers (i.e. Sol_23s, Sol_23t, Sol_15s) has almost no influence on the results, but it highly influences the computational cost (e.g. see Sol_23s in Fig. 3-1).

3.2.9. Evaluation of the thermal zone temperature using different thermal zone modelling approaches

The different models have different degrees of detail and this section focuses on the prediction of the thermal zone temperature using different approaches to model the thermal zone:

- Surface to surface radiative exchange model (see Fig. 2-4b);
- Two-star model (see Fig. 2-4a);
- One-star model combined with finite-difference wall model (see Fig. 2-3b);
- One-star combined with constant heat transfer coefficient wall model (see Fig. 2-3a).

The Surface to surface radiative exchange model (see Section 2.2.1, RM) is the most detailed and it is able to model the radiative temperature distribution within the considered thermal zone. The results of the RM are reported in Fig. 3-11 showing the mean radiative temperature field in the office cell and the internal surface temperatures of the external wall and window, floor and internal wall for a critical condition in winter (left) and summer (right) for the climate of Stockholm. The window and frame internal surface temperatures are not considered in the coloured scale for sake of better readability. In winter the high mean radiant temperature (MRT) gradient in the room, of around 2.9 K, is caused by the cold ambient temperature. While in summer, a gradient of 2.2 K is generated by the high glass temperature due to high solar radiation.

The two-star model (see Section 2.2.1, REF) cannot predict the radiative temperature distribution since the radiative exchange is calculated using the star approach. As a result of this model one mean radiative temperature of the room and the average air temperature can be modelled. The one-star model combined with finite-difference wall model (TZ1s) is a simplification of the REF model where only the operative temperature is modelled and the one-star model combined with constant heat transfer coefficient

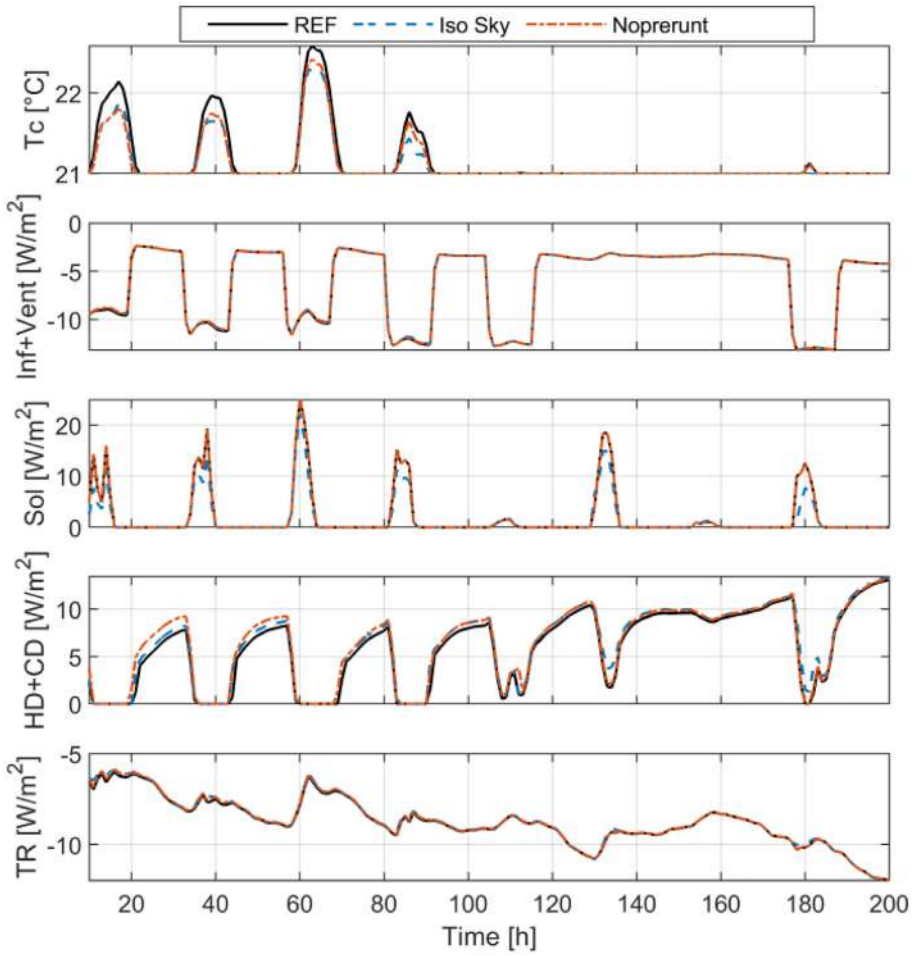

Fig. 3-9. Hourly results (i.e., convective temperature, ventilation plus infiltration losses, solar gain, heating and cooling power and transmission losses) for the climate of Stockholm during the first 8 days of the year including the cases: REF, Iso Sky and Nopreruntime.

wall model (i.e. TZ1s_UA_Ccal and TZ1s_UA_Cnoncal) is a further simplification of the TZ1s where the whole capacity of the building is lumped in one unique node.

The heating and cooling systems of the office cell under analysis are controlled using the convective temperature, however, the one-star approach allows the simulation of the operative temperature only. The calibration of the effective capacity of the one-star model (TZ1s_UA_Ccal) against the REF case compensates the differences in terms of control strategy and allows the TZ1s_UA_Ccal to deliver an annual heating and cooling demand in agreement with the REF. To give a complete overview the reference model (Ref2) and Surface to surface radiative exchange model (RM2) are simulated again controlling the heating and cooling systems according to the operative temperature instead of the convective temperature and the results are reported and described in Appendix 4. In addition, the calibration process of the one-star model combined with constant heat transfer coefficient wall model is repeated (TZ1s_UA_Ccal2) using as a reference the results of Ref2. The results of this analysis are used also in this section to show the influence of the control strategy and calibration process on the operative temperature.

Fig. 3-12A/B presents the hourly operative temperature as a result of the two-star model (REF/Ref2) on the x-axis against the operative temperature simulated with the RM/RM2 model on the y-axis in three different points (near the internal wall: blue circle [x: 2.25 m, y: 5.8 m], facing the window: red asterisk [x: 2.25 m, y: 0.2 m] and in the centre of the room: yellow plus [x: 2.25 m, y: 3 m]) at three different heights 0.6 m in a, 1.1 m in b and 1.7 m in c. At the height of 0.6 m, the effect of the window on the operative temperature is less important than at 1.7 m. In fact, at 0.6 m the results of the REF/Ref2 model are matching quite well the results of the RM/RM2 model while at 1.7 m the operative temperature of the sensor facing the window shows an important deviation with respect to the operative temperature simulated with the two-star model (REF and Ref2). Therefore, when comfort has to be analysed or when the heating and cooling control logic is influenced by the radiative temperature field, it can be important to use a model, which allows the calculation of the temperature distribution, as also concluded in [18].

In addition, from Fig. 3-12A/B it can be noticed that when the models are controlled on the air temperature (i.e. Fig. 3-12A) the operative temperature varies between 20 °C and 28 °C while when the system is controlled according to the operative temperature (i.e. Fig. 3-12B), the latter is restricted between 21 °C and 25 °C. For the RM and RM2 this is true at the centre of the room (point used for the HVAC control), but the operative temperature could be slightly higher or lower in other points due to the radiative temperature distribution (see Fig. 3-12 B c).

The same analysis presented in Fig. 3-12 is repeated in Fig. 3-13 and Fig. 3-14 comparing the detailed longwave radiation model (RM and RM2) with the one-star model (TZ1s) and the RM and RM2 with the one-star model combined with constant Heat Transfer Coefficient wall model (TZ1s_UA_Ccal and TZ1s_UA_Ccal2), respectively. Since the only temperature modelled by TZ1s, TZ1s_UA_Ccal and TZ1s_UA_Ccal2 is the operative temperature

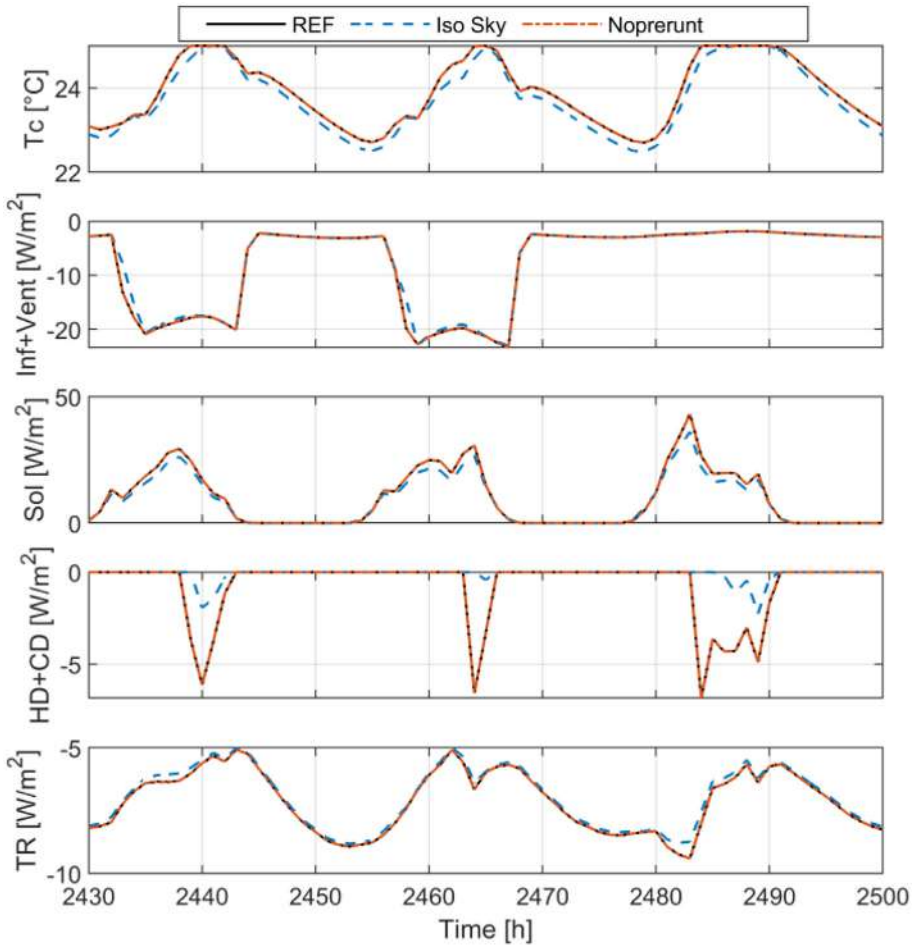

Fig. 3-10. Hourly results (i.e., convective temperature, ventilation plus infiltration losses, solar gain, heating and cooling power and transmission losses) for the climate of Stockholm (11th–14th Apr) including the cases: REF, Iso Sky and Nopreruntime.

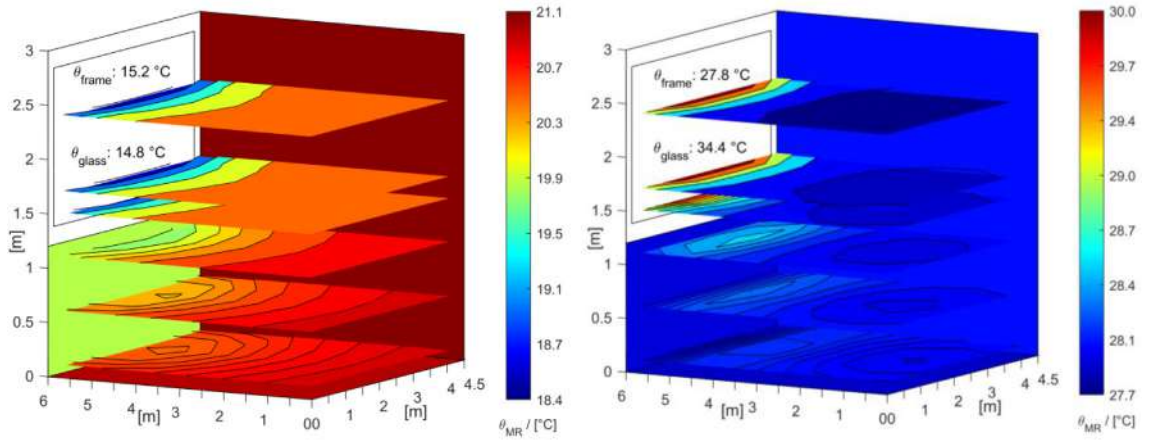

Fig. 3-11. Mean radiant temperature field calculated with Simulink (RM model) in winter (left) and summer (right) for the climate of Stockholm.

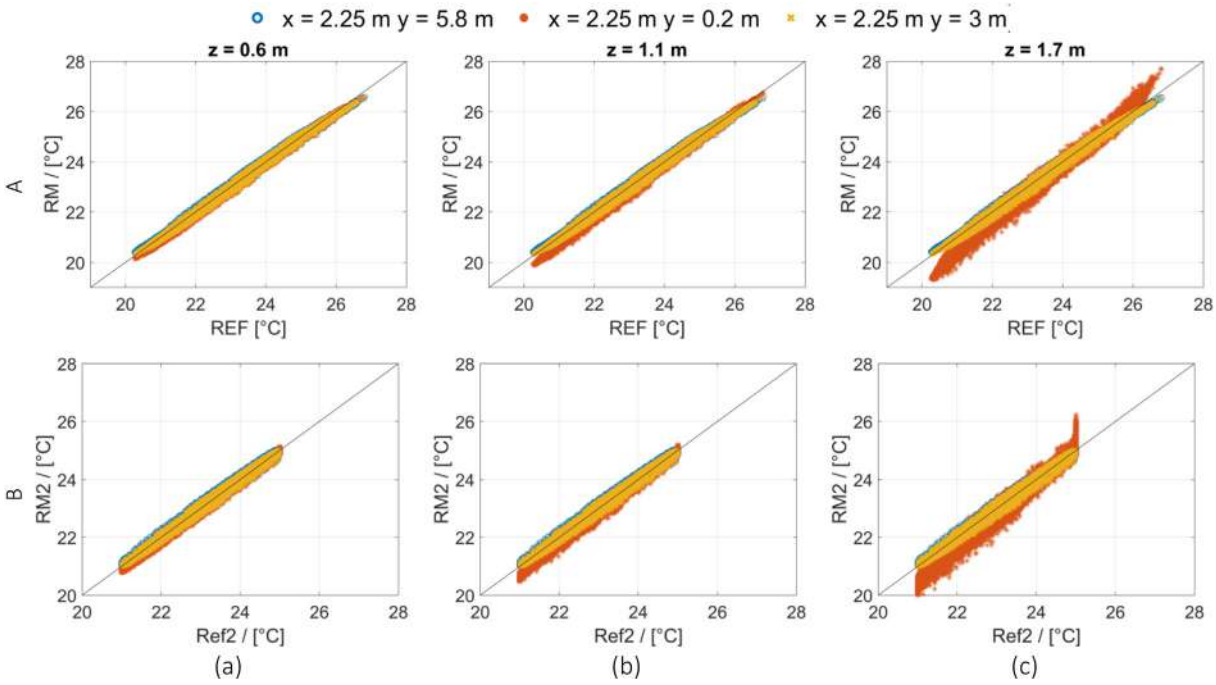

Fig. 3-12. Operative temperature of the two-star model (REF in A and Ref2 in B) vs the detailed longwave radiation model (RM in A and RM2 in B) for the climate of Stockholm at 0.6 m (a), 1.1 m (b) and 1.7 m from the floor considering different sensor positions within the room (i.e. blue circle [x: 2.25 m, y: 5.8 m], facing the window: red asterisk [x: 2.25 m, y: 0.2 m] and in the centre of the room: yellow plus [x: 2.25 m, y: 3 m]). (For interpretation of the references to colour in this figure legend, the reader is referred to the web version of this article.)

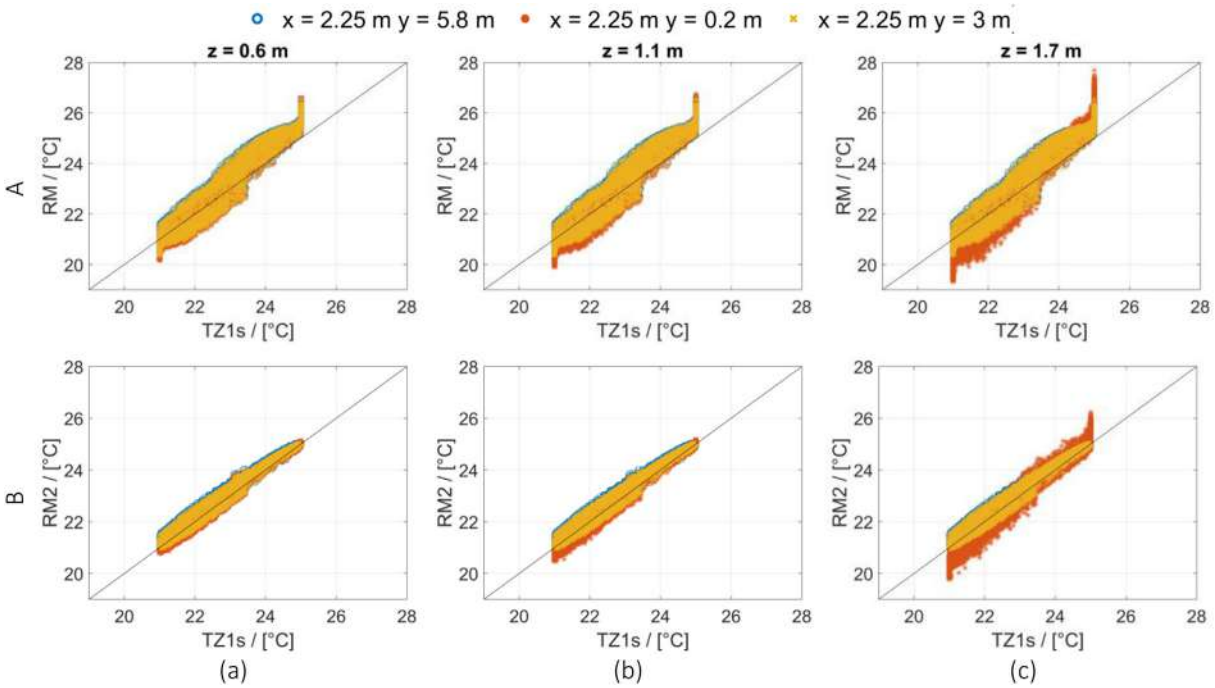

Fig. 3-13. Operative temperature of the one-star model (TZ1s) vs the detailed longwave radiation model (RM in A and RM2 in B) for the climate of Stockholm at 0.6 m (a), 1.1 m (b) and 1.7 m from the floor considering different sensor positions within the room (i.e. blue circle [x: 2.25 m, y: 5.8 m], facing the window: red asterisk [x: 2.25 m, y: 0.2 m] and in the centre of the room: yellow plus [x: 2.25 m, y: 3 m]). (For interpretation of the references to colour in this figure legend, the reader is referred to the web version of this article.)

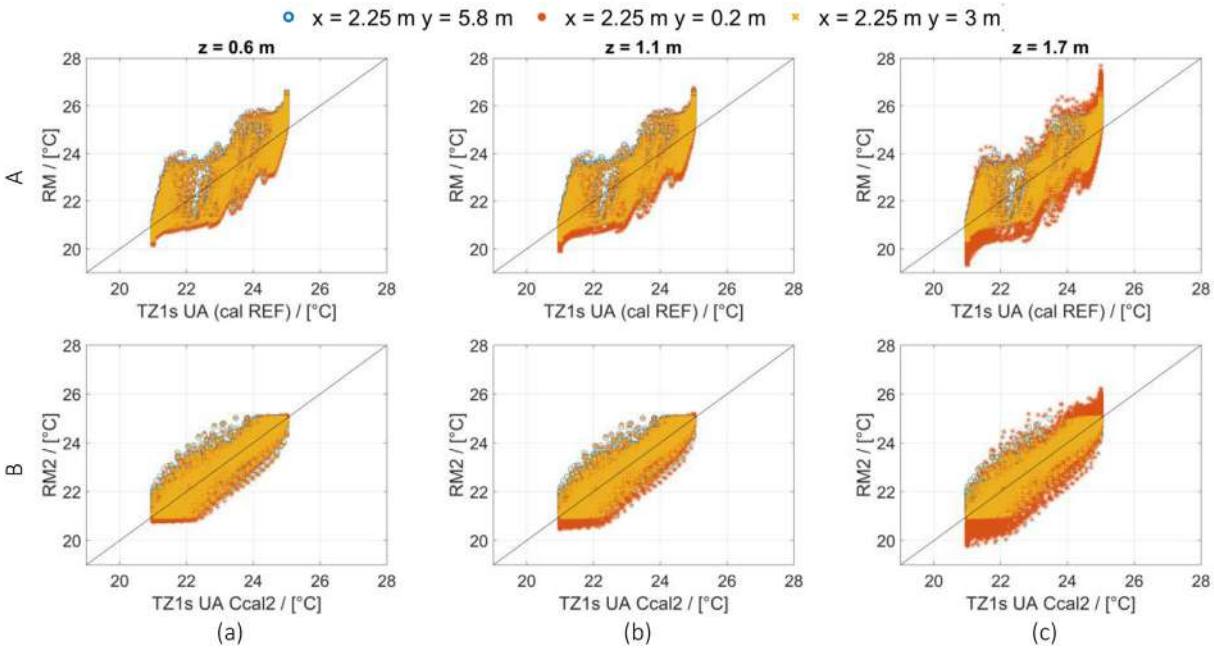

Fig. 3-14. Operative temperature of the 1 Star model combined with constant Heat Transfer Coefficient wall model (TZ1s_UA_Ccal in A and TZ1s_UA_Ccal2 in B) vs the detailed longwave radiation model (RM in A and RM2 in B) for the climate of Stockholm at 0.6 m (a), 1.1 m (b) and 1.7 m from the floor considering different sensor positions within the room (i.e. blue circle [x: 2.25 m, y: 5.8 m], facing the window: red asterisk [x: 2.25 m, y: 0.2 m] and in the centre of the room: yellow plus [x: 2.25 m, y: 3 m]). (For interpretation of the references to colour in this figure legend, the reader is referred to the web version of this article.)

this one is limited between 21 and 25 °C by the ideal heating and cooling system, leading to quite high deviations when the results are compared against RM (see Fig. 3-13A and Fig. 3-14A). When the RM2 controlled on the operative temperature is compared against the TZ1s (see Fig. 3-14B) the deviations are highly reduced. The same conclusion is applicable for the cases TZ1s_UA_Ccal and TZ1s_UA_Ccal2 (see Fig. 3-14A and B) even though the dispersions of the points is higher compared to the results reported in Fig. 3-13 for the TZ1s since here the whole building capacity is lumped in one unique node.

Fig. 3-15 reports the Mean Bias Error (MBE), Mean Absolute Error (MAE) and maximum and minimum error between the REF, TZ1s and TZ1s_UA_Ccal models and the RM model used as a reference in A and between the Ref2, TZ1s and TZ1s_UA_Ccal2 models and the RM2 model used as a reference in B considering hourly operative temperatures simulated for the whole year. These deviation indicators are calculated for different positions in the room (i.e. × = 2.25 m and y = 0.2 m, 3 m, 5.8 m) and two different heights from the floor (i.e. z = 0.6 m and z = 1.7 m). From Fig. 26A it can be noticed how the spread between the maximum and minimum error increases from the REF model to the TZ1s and TZ1s_UA_Ccal. For the points located at a height of 0.6 m (see Fig. 3-15A/B a), the deviation indicators are not strongly influenced by the position of the considered sensor within the room while at the height of 1.7 m (see Fig. 3-15A/B b) the temperature gradient within the room is more important due to the presence of the window and this results in higher deviations of all the models when y = 0.2 m compared to the other two considered points (i.e. y = 5.8 m and y = 3 m). Comparing Fig. 3-15A to Fig. 3-15B it can be seen that the agreement between RM and REF is as good as the agreement between RM2 and Ref2 while the TZ1s has a better agreement with the RM2 compared to RM. The deviations between RM2 and TZ1s_UA_Ccal2 are also strongly reduced with respect to the deviations between RM and TZ1s_UA_Ccal.

In addition, it is important to highlight that the MBE could be almost zero also when the deviations are important because of the cancellation effect (e.g. see Fig. 3-15Ab TZ1s y = 0.2 m).

4. Conclusion

In this paper, the influence of different modelling assumptions and simplifications on the results in terms of accuracy and computational time is analysed. For this purpose, the Simulink model of a typical office cell located in Rome, Stuttgart and Stockholm, cross-compared in [8] is used as a reference model (REF) and the different sections of the model (i.e. Thermal zone model, thermal mass of the furniture, solar and internal gains distribution between the different surfaces of the enclosure, convective and radiative heat transfer coefficients, window model, adiabatic structure model, sky model, pre-runtime and solver settings) are modified one at the time.

A special focus is given to the longwave radiation exchange model. The Simulink model for the detailed longwave radiative exchange (RM), proposed in [26], is cross-compared against TRNSYS 18 and used to show the influence of simplified thermal zone models on the accuracy of the predicted operative temperature.

The influence of each modelling approach applied in each section of the building model is evaluated using the Goodness-of-Fit (GOF) and the computational cost. The GOF is calculated using both the Normalized Mean Bias Error and the Normalized Root Mean Square Error considering the heating and cooling demands as reference variables. The NMBE is more sensitive to deviations related to final energy demand while the NRMSE is more sensitive to deviations in terms of dynamic behaviour. Therefore, the combination of these two indices allows an evaluation including both aspects. In this case study, the same weight is assigned to both indices, but

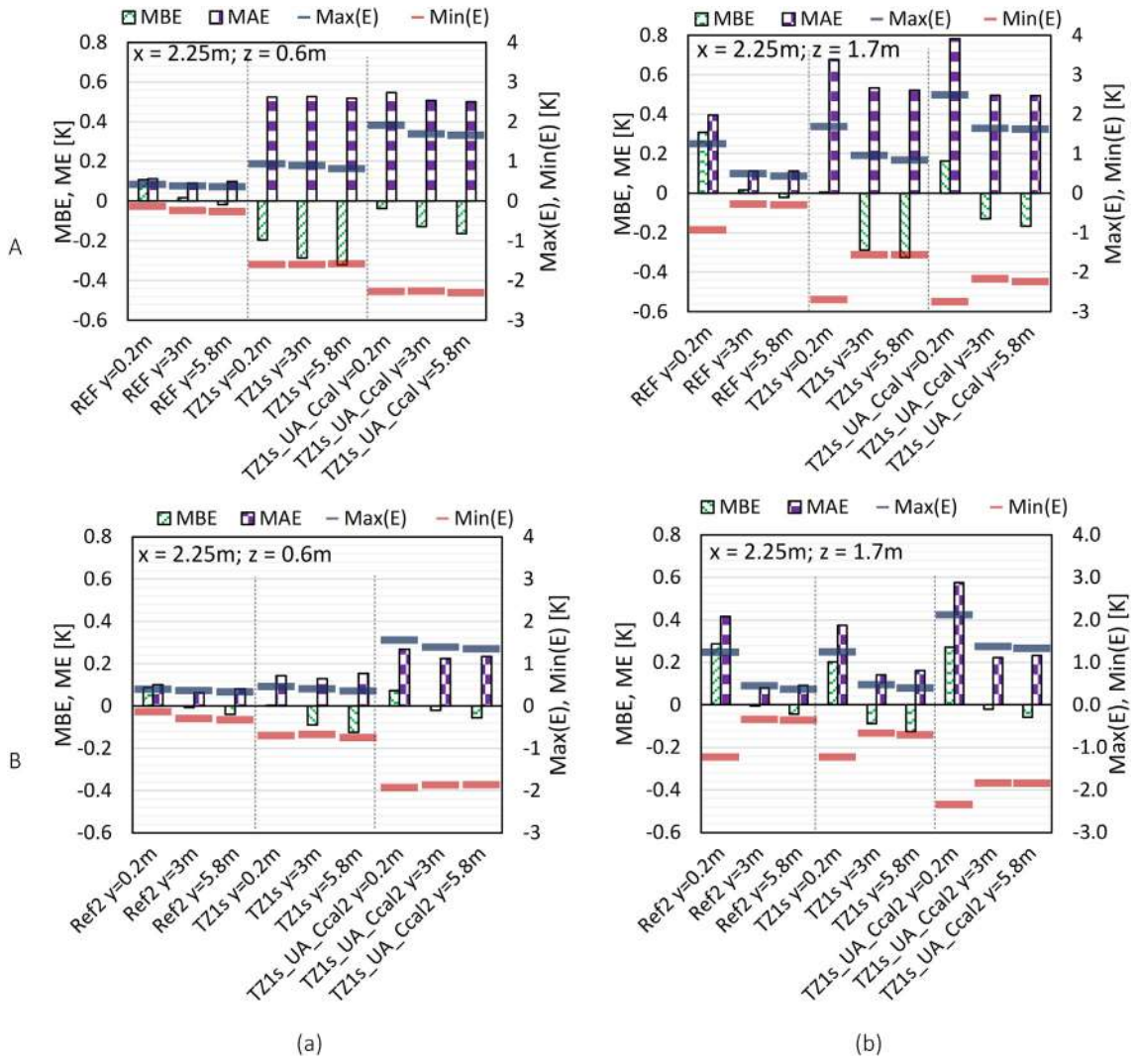

Fig. 3-15. Mean Bias Error (MBE), Mean Absolute Error (MAE), MAX and MIN error of the REF, TZ1s and TZ1s_UA_Ccal models compared vs the RM in A and of the Ref2, TZ1s and TZ1s_UA_Ccal2 models compared vs the RM2 in B considering hourly operative temperatures simulated for the whole year. These deviation indicators are calculated considering different sensor positions in the room and at different heights (a: z = 0.6 m and b: z = 1.7 m).

depending on the aim of the analysis more importance can be attributed to the overall energy balance (i.e. NMBE) or to the dynamic behaviour (i.e. NRMSE).

The main conclusions for this case study are:

- The choice of the solver, between the available solvers for stiff problems, does not influence the accuracy of the results but highly influences the computational time;
- Not always a model simplification leads to lower computational time;
- The accuracy of simplified models can be improved by calibrating the input parameters using a more complex model as a reference;
- In some analysed cases a compensation of increased thermal losses and gains leads to matching heating and cooling demands. Therefore it is important to analyse all the components of the energy balance;
- For this case study, it is shown that the two-star model (REF) presents a good agreement with the detailed longwave radiative exchange approach (RM) in terms of energy demand and operative temperature in the centre of the room but deviations are present when the operative temperature of the two-star model is compared with the operative temperature near the window of the RM. The RM is able to deliver more detailed information about the temperature distribution within the room but at the same time it requires higher computational time and detailed geometry inputs;
- The one-star model with constant Heat Transfer Coefficient (TZ1s_UA_Ccal and TZ1s_UA_Cnoncal) and the one-star model combined with finite-difference wall model (TZ1s) allow the simulation of only one temperature of the thermal zone, which can be correlated to the operative temperature. This leads to different dynamic behaviour of the operative temperature with respect to the reference model since the heating and cooling systems cannot be controlled on the convective temperature as required in this case study. Nevertheless, when the building capacity of TZ1s_UA_Ccal is calibrated using the results of the reference model, it can reproduce the energy demand of the building with an accuracy that can be acceptable for some applications and significantly reduced computational time.

The deviations between the one-star models (i.e. TZ1s and TZ1s_UA_Ccal2) and the reference model are reduced if the refer-

ence model is simulated controlling the heating and cooling systems on the operative temperature (instead of the convective).

- Many aspects, which are often overlooked (e.g., adiabatic structure model, capacity of the air node, convective and radiative exchange coefficients, sky model and distribution of the solar and internal gains over the surfaces of the enclosure) affect the energy balance of the building and do not always lead to a reduction of the computational time. As an example, increasing the capacity of the convective node including the thermal mass of the furniture reduces the computational time increasing the accuracy of the results.

In addition, the combinations of simplified assumptions for different model sections could lead to an important loss of accuracy in the results.

- The simplified window model based on a constant heat transfer coefficient (HTC) can lead to high deviations, especially when the HTC given as input to the window model is measured with boundary conditions that are different from the average conditions of the simulation study. In addition, for this case study, the simplified window model does not provide any benefit in terms of computational cost compared to the detailed window model. Nevertheless, the detailed window model requires the knowledge of a high number if inputs that are not always available.

Declaration of Competing Interest

The authors declare that they have no known competing financial interests or personal relationships that could have appeared to influence the work reported in this paper.

Acknowledgments

This work was performed within the frameworks of IEA SHC Task 56 and IEA HPT Annex 49 international projects.

Appendix 1. Detailed windows properties

In this section of the appendix the data used for modelling the windows are reported for the climates of Rome, Stuttgart and Stockholm.

Rome

WINDOW 4.1 DOE-2 Data File: Multi Band Calculation (Unit System: SI)
Window ID: 3304 (TRNSYS 15 WINDOW LIB)
Description: double glazing with Argon gap and low-SHGC coating, 6/16/6
Tilt: 90.0

Stuttgart

WINDOW 4.1 DOE-2 Data File: Multi Band Calculation (Unit System: SI)
Window ID: 2001 (TRNSYS 15 WINDOW LIB)
Description: double glazing with Argon gap and low-e coating, 4/16/4
Tilt: 90.0

Stockholm

WINDOW 4.1 DOE-2 Data File: Multi Band Calculation (Unit System: SI)
Window ID: 2206 (TRNSYS 15 WINDOW LIB)
Description: double glazing with Kripton gap and low-e coating, 4/16/4
Tilt: 90.0

Appendix 2. Equations for the calculation of the distribution of the solar gains

The method proposed by [29], Chapter 2.7.2 is applied in the reference case of this work (REF) and the equations for the calculation of the distribution factor for the direct solar radiation (A- 1) and diffuse solar radiation (A- 2 - A- 6) are reported below. It is noteworthy to mention that the sum of $F_{dir,i}$ is lower than one and that the remaining share of direct solar radiation is treated as diffuse. The distribution factor of the diffuse solar radiation is

Table A3
Properties of the panes involved in the Rome window assembly.

Glass pane	External	Internal
Emis Front (External)	0.840	0.838
Emis Back (Internal)	0.110	0.838
Thickness (mm)	6.0	6.0
Cond (W/m^2-C)	150.0	150.0

Table A1
Gap properties of the Rome window assembly.

Gap	Thick	Cond	dCond	Vis	dVis	Dens	dDens	Pr	dPr
Argon	16.0	0.0162	5.0	2.11	6.3	1.78	−0.006	0.68	0.00066

Table A2
Optical properties of the Rome window assembly.

Angle	0	10	20	30	40	50	60	70	80	90	Hemis
Tsol	0.260	0.261	0.257	0.251	0. 243	0.229	0.200	0.145	0.066	0.000	0.214
Abs1	0.470	0.474	0.480	0.482	0.480	0.477	0.477	0.460	0.351	0.001	0.464
Abs2	0.052	0.053	0.053	0.054	0.055	0.055	0.053	0.047	0.033	0.000	0.051
Rfsol	0.218	0.212	0.210	0.213	0.222	0.238	0.269	0.348	0.550	0.999	0.260
Rbsol	0.259	0.254	0.252	0.252	0.257	0.271	0.306	0.393	0.582	1.000	0.297
Tvis	0.659	0.662	0.653	0.641	0.625	0.592	0.518	0.377	0.176	0.000	0.550
Rfvis	0.119	0.112	0.109	0.112	0.124	0.147	0.192	0.294	0.523	0.999	0.176
Rbvis	0.154	0.148	0.146	0.150	0.164	0.191	0.252	0.389	0.647	1.000	0.229
SHGC	0.333	0.336	0.332	0.327	0.320	0.306	0.275	0.214	0.116	0.000	0.287

Table A4
Gap properties of the Stuttgart window assembly.

Gap	Thick	Cond	dCond	Vis	dVis	Dens	dDens	Pr	dPr
Argon	16.0	0.0162	5.0	2.11	6.3	1.78	−0.006	0.68	0.00066

Table A5
Optical properties of the Stuttgart window assembly.

Angle	0	10	20	30	40	50	60	70	80	90	Hemis
Tsol	0.426	0.428	0.422	0.413	0.402	0.380	0.333	0.244	0.113	0.000	0.354
Abs1	0.118	0.118	0.120	0.123	0.129	0.135	0.142	0.149	0.149	0.000	0.132
Abs2	0.190	0.192	0.198	0.201	0.200	0.199	0.199	0.185	0.117	0.000	0.191
Rfsol	0.266	0.262	0.260	0.262	0.269	0.286	0.326	0.422	0.621	1.000	0.314
Rbsol	0.215	0.209	0.207	0.210	0.219	0.237	0.272	0.356	0.560	0.999	0.260
Tvis	0.706	0.710	0.701	0.688	0.670	0.635	0.556	0.403	0.188	0.000	0.590
Rfvis	0.121	0.115	0.114	0.118	0.132	0.163	0.228	0.376	0.649	1.000	0.203
Rbvis	0.103	0.096	0.093	0.096	0.108	0.132	0.179	0.286	0.520	0.999	0.162
SHGC	0.589	0.593	0.591	0.586	0.574	0.551	0.505	0.405	0.218	0.000	0.518

Table A6
Properties of the panes involved in the Stuttgart window assembly.

Glass pane	External	Internal
Emis Front (External)	0.840	0.140
Emis Back (Internal)	0.840	0.840
Thickness (mm)	4.0	4.0
Cond (W/m^2-C)	225.0	225.0

calculated considering three "bounces", where the first only hit the floor.

$F_{dir,i} = \frac{A_i}{A_{tot,opaque}}\ \alpha_i$ ifsurfi has a different orientation of the considered window

$F_{dir,i} = 0$ if surf i has the same orientation of the considered window (A-1)

$$F_{diff,i} = B1_i + B2_i + B3_i + BR_i \quad \text{(A-2)}$$

$$\begin{cases} B1_i = \alpha_i \text{ if } i = \text{floor} \\ B1_i = 0 \text{ if } i \neq \text{floor} \end{cases} \quad \text{(A-3)}$$

$$\begin{cases} B2_i = 0 \text{ if } i = \text{floor;} \\ B2_i = (1-\alpha_{floor})\alpha_i \frac{A_i}{A_{tot,nofloor}} \text{ if } i \neq \text{floor and windows} \\ B2_i = (1-\alpha_{floor})\tau_{60^\circ,i} \frac{A_i}{A_{tot,nofloor}} \text{ if } i = \text{window} \end{cases} \quad \text{(A-4)}$$

$$\begin{cases} B3_i = (1-\alpha_{floor}-\sum B2)\ \alpha_i \frac{A_i}{A_{tot}} \text{if } i \neq \text{windows} \\ B3_i = (1-\alpha_{floor}-\sum B2)\ \tau_{60^\circ,i} \frac{A_i}{A_{tot}} = 0 \text{ if } i = \text{window} \end{cases} \quad \text{(A-5)}$$

$$BR_i = \left(1-\alpha_{floor}-\sum B2-\sum B3\right)\frac{B3_i}{\sum B3} \quad \text{(A-6)}$$

Appendix 3. Annual balance and deviations for all the analysed cases

Tables A10, A11 and A12, report the annual gains and losses of the reference case and the annual relative deviations of all the analysed cases for each component of the energy balance (i.e. heating demand, cooling demand, infiltration losses, ventilation losses, transmission losses and total solar gains), for the climates of Stockholm, Stuttgart and Rome, respectively.

Table A13 reports the Normalized Root Mean Square Error (NRMSE) and Normalized Mean Bias Error (NMBE) used for the calculation of the Goodness-of-Fit (GOF) for all the climates (i.e.

Table A9
Properties of the panes involved in the Stockholm window assembly.

Layer ID#	External	Internal
Emis Front (External)	0.840	0.060
Emis Back (Internal)	0.840	0.840
Thickness (mm)	4.0	4.0
Cond (W/m^2-C)	225.0	225.0

Table A7
Gap properties of the Stockholm window assembly.

Gap	Thick	Cond	dCond	Vis	dVis	Dens	dDens	Pr	dPr
Krypton	16.0	0.00860	2.800	2.280	7.500	3.740	−0.0137	0.660	0.00002

Table A8
Optical properties of the Stockholm window assembly.

Angle	0	10	20	30	40	50	60	70	80	90	Hemis
Tsol	0.462	0.465	0.458	0.448	0.436	0.412	0.360	0.263	0.121	0.000	0.384
Abs1	0.114	0.114	0.116	0.120	0.125	0.132	0.139	0.139	0.139	0.000	0.128
Abs2	0.186	0.188	0.195	0.199	0.198	0.197	0.199	0.186	0.118	0.000	0.189
Rfsol	0.237	0.232	0.231	0.233	0.241	0.260	0.303	0.406	0.614	1.000	0.289
Rbsol	0.179	0.172	0.170	0.173	0.183	0.202	0.239	0.328	0.542	0.999	0.227
Tvis	0.749	0.754	0.743	0.730	0.711	0.674	0.589	0.428	0.200	0.000	0.626
Rfvis	0.121	0.115	0.114	0.118	0.132	0.163	0.228	0.376	0.649	1.000	0.203
Rbvis	0.109	0.102	0.099	0.102	0.115	0.140	0.188	0.296	0.529	0.999	0.170
SHGC	0.632	0.636	0.635	0.629	0.616	0.592	0.542	0.434	0.232	0.000	0.557

Table A10
Annual energy balance for the climate of Stockholm of the reference (REF) case in terms of heating demand (HD), cooling demand (CD), infiltration losses (Inf), ventilation losses (Vent), transmission losses (TR) and total solar gains (SOL). For each analysed case the NMBE is reported for each component of the thermal balance considering the final annual energy.

STOCKHOLM		HD	CD	Inf	Vent	TR	SOL
REF	[kWh/m^2]	17.1	-24.0	-20.1	-29.6	-57.9	58.2
TZ1s_UA_Cnoncal		0	3	1	-3	0	0
TZ1s_UA_Ccal		-5	0	1	-3	0	0
TZ1s		6	8	0	3	-3	0
RM		-1	-1	0	0	1	0
AC		2	1	0	1	0	0
RG_distr		0	0	0	0	-1	0
SD		-2	1	0	0	0	1
Win_Rcalc		-37	10	1	6	-22	-3
Win_Rcal		2	-5	0	-1	0	-3
Win_Rcal_gcal		0	0	0	0	0	0
R_now	Annual NMBE	1	-1	0	0	1	0
R_lin	[%]	1	2	0	0	0	0
R_lin_now		3	1	0	0	1	0
R_const		4	1	0	0	1	0
Ad_nm		-1	-1	0	0	0	0
Ad_no		-3	-3	0	0	0	0
Ad_sb		0	-1	0	0	0	0
Iso_Sky		12	-6	-1	-3	-1	-9
Noprerunt		1	0	0	0	0	0
Sol_23s		-1	0	0	0	0	0
Sol_23t		-1	0	0	0	0	0
Sol_15s		-1	0	0	0	0	0

Table A11
Annual energy balance for the climate of Stuttgart of the reference (REF) case in terms of heating demand (HD), cooling demand (CD), infiltration losses (Inf), ventilation losses (Vent), transmission losses (TR) and total solar gains (SOL). For each analysed case the NMBE is reported for each component of the thermal balance considering the final annual energy.

STUTTGART		HD	CD	Inf	Vent	TR	SOL
REF	[kWh/m^2]	13.2	-24.4	-17.5	-27.8	-59.8	60.0
TZ1s_UA_Cnoncal		-5	7	1	-4	-2	0
TZ1s_UA_Ccal		-15	0	1	-3	-2	0
TZ1s		11	9	-1	4	-3	0
RM		-1	-1	0	0	1	0
AC		4	1	0	3	0	0
RG_distr		0	0	0	0	-1	0
SD		-2	0	0	0	0	1
Win_Rcalc		-8	-1	0	0	-7	-6
Win_Rcal		7	-6	0	-3	0	-6
Win_Rcal_gcal		4	1	0	-1	1	-1
R_now	Annual NMBE	5	-2	0	-2	3	0
R_lin	[%]	2	1	0	0	1	0
R_lin_now		7	0	0	-2	3	0
R_const		9	-1	0	-1	2	0
Ad_nm		-1	-1	0	0	0	0
Ad_no		-4	-3	0	0	0	0
Ad_sb		0	-1	0	0	0	0
Iso_Sky		12	-1	0	-3	-1	-5
Noprerunt		1	0	0	0	0	0
Sol_23s		0	0	0	0	0	0
Sol_23t		0	0	0	0	0	0
Sol_15s		0	0	0	0	0	0

Table A12
Annual energy balance for the climate of Rome of the reference (REF) case in terms of heating demand (HD), cooling demand (CD), infiltration losses (Inf), ventilation losses (Vent), transmission losses (TR) and total solar gains (SOL). For each analysed case the NMBE is reported for each component of the thermal balance considering the final annual energy.

ROME		HD	CD	Inf	Vent	TR	SOL
REF	[kWh/m^2]	3.5	-31.3	-10.4	-17.0	-34.2	33.3
TZ1s_UA_Cnoncal		-82	0	5	2	-10	0
TZ1s_UA_Ccal		-84	0	5	2	-10	0
TZ1s		18	7	-1	5	-6	0
RM		-4	-1	0	-1	1	0
AC		18	0	-1	6	-1	0
RG_distr		0	0	0	0	-3	0
SD		-4	0	0	0	1	0
Win_Rcalc		-13	2	1	1	7	10
Win_Rcal		-23	3	1	3	4	10
Win_Rcal_gcal		-25	-2	1	1	0	0
R_now	Annual NMBE	5	-2	0	-2	3	0
R_lin	[%]	-1	1	0	-2	1	0
R_lin_now		3	0	-1	-5	4	0
R_const		0	1	0	-3	1	0
Ad_nm		-2	-1	0	0	0	0
Ad_no		-8	-2	0	0	0	0
Ad_sb		1	0	0	0	0	0
Iso_Sky		25	-2	-1	-6	1	-8
Noprerunt		6	0	0	-1	0	0
Sol_23s		-1	0	0	0	0	0
Sol_23t		-1	0	0	0	0	0
Sol_15s		0	0	0	0	0	0

Stockholm (STO), Stuttgart (STU) and Rome (ROM)) and all the analysed cases.

Appendix 4. Influence of the building capacity and control strategy on the results of the one-star models

The one-star node model with constant Heat Transfer Coefficient wall model has only one capacity for the whole building (as described in Section 2.2.1) that represents the effective capacity of the considered thermal zone. In the current study, the building capacity is found by trying to minimize the deviation in terms of annual heating and cooling demand with the REF case (TZ1s_UA_Ccal see Sections 2.2.1 and 3.1.1). However, within the REF case, the heating and cooling systems are controlled according to the convective temperature, as required from this case study, while the TZ1s_UA_Ccal is able to model only one temperature for the thermal zone that can be related to the operative temperature. As a consequence, the calibration process of the building capacity for the one-star model includes also a compensation of the different control strategies. Within this section, this specific aspect is better explained by reporting the results of the reference model where the heating and cooling system (HVAC) is controlled according to the operative temperature (Ref2) and of the one-star model where the building capacity ($C_{building}$) is calibrated according to the results of Ref2 (TZ1s_UA_Ccal_Ref2). In addition, also the surface to surface radiative exchange model (RM) is simulated again controlling the HVAC according to the operative temperature (RM2).

The results of a reference case might not always be available, in this situation, the building capacity can be calculated using the method suggested by the standard EN ISO 13786 [32] (TZ1s_UA_Cnoncal_EN) or using the simplified equation suggested by the PHPP (see Section 2.2.1) (TZ1s_UA_Cnoncal). The one-star model with finite-difference wall model (TZ1s) does not require the calibration of the capacity of the building since the capacity of the opaque structures is already distributed in the wall model. Anyway, TZ1s is able to model only one temperature of the thermal zone that can be related to the operative temperature, therefore also the results of this model are affected by different HVAC control strategies (on the operative temperature instead of the convective).

All these results are reported in Table A14, where: $C_{building}$ is the effective capacity of the building used in the one star models, HD the heating demand, CD the cooling demand, ΔHD Ref/ΔCD Ref the relative deviation of the annual HD/CD with respect to the REF case and ΔHD Ref2/ΔCD Ref2 the relative deviation of the annual HD/CD with respect to the Ref2 case. From the results of Ref, Ref2, RM and RM2 reported in Table A14 it can be seen that the control of the HVAC leads to an approximately 4% increase in HD and 12% increase in cooling demand. The TZ1s has always a better match with the case Ref2 since both models have the HVAC controlled on the operative temperature. All the cases based on the TZ1s_UA_ model see their results directly correlated to the used capacity of the building (i.e. increasing the capacity leads to a reduction of both HD and CD and vice versa). The capacity calculated according to the standard EN ISO 13786 [32] leads to similar results (and $C_{building}$) of the case TZ1s_UA_Ccal2 calibrated according to the results of Ref_2, except of Stuttgart where higher deviations are reported. The $C_{building}$ defined according to the method proposed by PHPP leads to results aligned with the case TZ1s_UA_Ccal.

In Fig. A1 average hourly results (i.e. operative temperature and heating and cooling demands for the following cases: REF, Ref2, TZ1s, TZ1s_UA_Ccal, TZ1s_UA_Ccal2, TZ1s_UA_Cnoncal (PHPP) and TZ1s_UA_Cnoncal (EN13786), are reported for a winter period 25th-26th February (a) and a spring period 11th – 13th April (b)

Table A13
Normalized Root Mean Square Error (NRMSE) and Normalized Mean Bias Error (NMBE) and their normalized version (_norm), which range between 0 and 1 used for the calculation of the GOF for each component (heating and cooling demands). For each analysed climate (ROM, STU and STO) the weighted averaged GOF (between the GOF_Heat and GOF_Cool) is reported.

			Modelling Approaches (ma)																					
			TZ1s_UA_Cnoncal	TZ1s_UA_Ccal	TZ1s	RM	AC	RG_distr	SD	Win_Rcalc	Win_Rcal	Win_Rcal_gcal	R_now	R_lin	R_lin_now	R_const	Ad_nm	Ad_no	Ad_sb	Iso_Sky	Noprerunt	Sol_23s	Sol_23t	Sol_15s
ROME	G: Heat. demand	NRMSE	33	33	14	3	9	1	2	5	9	9	3	5	5	8	2	6	1	9	7	1	3	2
		nNRMSE	1	0	61	95	75	99	97	86	76	74	92	88	86	77	95	85	99	75	82	100	92	97
		NMBE	-82	-84	18	-4	18	0	-4	-13	-23	-25	5	-2	3	0	-2	-8	1	25	6	-1	0	0
		NMBE abs	82	84	18	4	18	0	4	13	23	25	5	2	3	0	2	8	1	25	6	1	0	0
		nNMBE	2	0	78	95	78	100	95	85	73	71	94	98	96	100	98	91	99	70	93	99	100	100
		GOF_Heat	2	0	70	95	77	99	96	86	74	72	93	93	91	89	97	88	99	73	88	100	96	98
	G: Cool. demand	NRMSE	25	25	18	2	4	1	2	3	4	4	3	4	5	5	1	3	1	5	0	0	1	0
		nNRMSE	0	0	27	92	86	98	94	88	86	83	88	83	81	78	95	88	97	81	100	100	96	100
		NMBE	0	0	7	-1	0	0	0	2	3	-2	-2	1	0	1	-1	-2	0	-2	0	0	0	0
		NMBE abs	0	0	7	1	0	0	0	2	3	2	2	1	0	1	1	2	0	2	0	0	0	0
		nNMBE	99	96	0	91	95	100	95	74	55	69	77	89	95	89	91	73	93	65	100	100	99	100
		GOF_Cool	70	68	19	91	90	99	94	81	72	76	83	86	88	84	93	81	95	74	100	100	98	100
		GOF	63	61	25	92	89	99	95	82	72	76	84	86	88	84	93	82	95	74	99	100	98	100
STUTTGART	G: Heat. demand	NRMSE	35	36	17	3	6	1	3	6	5	4	4	5	7	10	2	5	1	8	2	1	2	1
		nNRMSE	1	0	54	93	84	99	94	86	88	91	90	87	83	74	97	87	99	80	97	100	96	99
		NMBE	-6	-15	11	-1	4	0	-2	-8	7	4	5	2	7	9	-1	-4	0	12	0	0	0	0
		NMBE abs	6	15	11	1	4	0	2	8	7	4	5	2	7	9	1	4	0	12	0	0	0	0
		nNMBE	64	0	29	96	73	100	89	48	54	73	65	87	54	44	95	76	100	24	99	99	100	99
		GOF_Heat	45	0	43	95	79	99	92	69	73	83	79	87	70	61	96	82	99	59	98	100	98	99
	G: Cool. demand	NRMSE	34	35	19	3	4	0	3	5	7	5	3	4	4	5	1	4	1	6	0	1	1	1
		nNRMSE	2	0	45	93	89	99	93	84	80	86	92	89	88	86	96	90	97	84	100	98	97	98
		NMBE	7	0	9	-1	1	0	0	-1	-6	1	-2	1	0	-1	-1	-3	-1	-1	0	0	0	0
		NMBE abs	7	0	9	1	1	0	0	1	6	1	2	1	0	1	1	3	1	1	0	0	0	0
		nNMBE	28	97	0	86	89	100	97	87	35	94	75	87	95	90	85	65	90	86	100	100	99	100
		GOF_Cool	20	69	32	90	89	99	95	86	62	90	84	88	92	88	91	78	93	85	100	99	98	99
		GOF	29	45	36	91	85	99	94	80	66	88	82	88	84	78	93	80	96	76	99	99	98	99
STOCKHOLM	G: Heat. demand	NRMSE	33	34	17	2	5	1	2	22	4	4	2	5	6	8	2	5	1	9	2	1	1	1
		nNRMSE	1	0	50	96	87	100	96	36	92	91	95	87	86	77	96	87	98	76	97	100	99	100
		NMBE	0	-5	7	-1	2	0	-2	-37	2	0	1	1	3	4	-1	-3	0	12	1	0	-1	-1
		NMBE abs	0	5	7	1	2	0	2	37	2	0	1	1	3	4	1	3	0	12	1	0	1	1
		nNMBE	100	88	83	99	95	100	97	0	97	100	97	97	92	90	99	93	100	67	99	100	99	99
		GOF_Heat	71	62	69	98	91	100	96	25	94	95	96	92	89	84	97	90	99	72	98	100	99	100
	G: Cool. demand	NRMSE	34	34	22	3	3	0	3	9	6	5	2	4	4	5	2	4	1	7	0	0	1	0
		nNRMSE	0	0	36	92	90	99	92	75	81	85	95	88	88	86	95	88	98	80	100	99	98	99
		NMBE	3	0	8	-1	1	0	1	10	-5	0	-1	2	1	0	-1	-3	-1	-6	0	0	0	0
		NMBE abs	3	0	8	1	1	0	1	10	5	0	1	2	1	0	1	3	1	6	0	0	0	0
		nNMBE	68	98	22	92	91	100	93	0	51	99	90	85	90	95	87	69	92	39	100	100	100	99
		GOF_Cool	48	69	30	92	90	100	92	53	68	92	93	86	89	91	91	79	95	63	100	100	99	99
		GOF	57	66	46	94	91	100	94	41	79	93	94	89	89	88	94	84	96	67	99	100	99	99

considering the climate of Stockholm. From Fig. A1 it can be noticed that the cases REF and Ref2 present different dynamic behaviour of the operative temperature due to the different control strategy and that case TZ1s is the only one having a good match with the dynamic behaviour of the case Ref2. Considering the cases implementing the one-star model with constant heat transfer coefficient wall model (i.e. TZ1s_UA_), it can be seen that increasing the building capacity has a direct influence on the dynamic behaviour of the temperature and heating and cooling power. The agreement in terms of operative temperature with the reference models (i.e. REF and Ref2) is improved considering the case TZ1s_UA_Ccal2 with respect to the case TZ1s_UA_Ccal. Reducing the capacity (e.g. TZ1s_UA_Cnoncal (EN13786) for the case of Stockholm leads to higher deviations in terms of both temperatures and energy demand.

Table A14
For each climate (Stockholm, Stuttgart and Rome) the results of the following cases are reported: REF, Ref2 (HVAC system is controlled on the operative temperature instead of the convective temperature), TZ1s, TZ1s_UA_Ccal with the $C_{building}$ calibrated on the results of the REF and Ref2 cases, TZ1s_UA_Cnoncal with a predefined $C_{building}$ calculated using the PHPP assumptions and the standard EN13786. The following results are reported: Building Capacity ($C_{building}$), Annual heating demand (HD) and cooling demand (CD), Relative deviation of the annual HD/CD considering as a reference the results of the REF case (ΔHD REF/ΔCD REF) and of the Ref2 case (Δ and of/ΔCD Ref2).

		$C_{building}$ 10^7 [J/K]	HD [kWh/m^2]	ΔHD REF [%]	ΔHD Ref2 [%]	CD [kWh/m^2]	ΔCD REF [%]	ΔCD Ref2 [%]
STOCKHOLM	REF		**17.1**		−3%	**−24.0**		−11%
	Ref2 (ctr Top)		**17.7**	4%		**−26.9**	12%	
	RM		17.0	−1%	−4%	−23.8	−1%	−11%
	RM2 (ctr Top)		17.9	5%	1%	−27.0	13%	1%
	TZ1s		18.2	6%	3%	−25.9	8%	−4%
	TZ1s_UA_Ccal (cal REF)	2.8277	16.3	−5%	−8%	−24.0	0%	−11%
	TZ1s_UA_Ccal2 (cal Ref2)	0.5886	18.7	10%	6%	−26.3	9%	−2%
	TZ1s_UA_Cnoncal (PHPP)	1.3608	17.0	0%	−4%	−24.9	3%	−8%
	TZ1s_UA_Cnoncal (EN13786)	0.3959	21.0	23%	19%	−27.7	15%	3%
STUTTGART	REF		**13.2**		−5%	**−24.4**		−12%
	Ref_2 (ctr Top)		**14.0**	6%		**−27.6**	13%	
	RM		13.1	−1%	−6%	−24.1	−1%	−13%
	RM2 (ctr Top)		14.1	6%	1%	−27.7	13%	0%
	TZ1s		14.6	11%	5%	−26.6	9%	−4%
	TZ1s_UA_Ccal (cal REF)	4.2634	11.3	−15%	−20%	−24.4	0%	−12%
	TZ1s_UA_Ccal2 (cal Ref2)	0.6920	14.4	9%	3%	−27.6	13%	0%
	TZ1s_UA_Cnoncal (PHPP)	1.3608	12.5	−5%	−10%	−26.1	7%	−6%
	TZ1s_UA_Cnoncal (EN13786)	0.3954	18.0	36%	29%	−30.3	24%	10%
ROME	REF		**3.5**		−8%	**−31.3**		−7%
	Ref_2 (ctr Top)		**3.8**	9%		**−33.6**	8%	
	RM		3.4	−4%	−12%	−31.1	−1%	−8%
	RM2 (ctr Top)		3.8	7%	−2%	−33.7	8%	0%
	TZ1s		4.2	18%	9%	−33.3	7%	−1%
	TZ1s_UA_Ccal (cal REF)	1.4808	0.6	−84%	−85%	−31.3	0%	−7%
	TZ1s_UA_Ccal2 (cal Ref2)	0.4117	3.44	−2%	−10%	−33.6	8%	0%
	TZ1s_UA_Cnoncal (PHPP)	1.3608	0.63	−82%	−84%	−31.4	0%	−7%
	TZ1s_UA_Cnoncal (EN13786)	0.3945	3.63	3%	−5%	−33.8	8%	1%

Appendix 5. Cross-comparison of the results of Simulink and TRNSYS 18 implementing the detailed longwave radiation model

In this Section, the results of the Simulink detailed radiation model (RM), proposed in [26], are compared against the TRNSYS 18 model implementing the detailed model for the longwave radiation exchange [27] to verify that Simulink results are in agreement with the results of the well-established tool TRNSYS.

TRNSYS 18 [27] and Simulink [40,26] are both able to model the air in the room as one node while calculating the radiative exchange between the surfaces using view factors for convex and closed volume. These two tools can additionally calculate the view factors between the internal surfaces and a matrix of points in the room, whose location is defined by the user, allowing the calculation of the mean radiant temperature field in the room. A modified version of the TRNSYS model used for the comparison presented in [8], implementing the detailed longwave radiation model (see [27] chapter 5.4.1.6), is used as a reference for the comparison with the results generated by the detailed longwave radiative model implemented in Simulink [26] in order to quantify the deviations between these two models and verify the accuracy of the Simulink model (RM) used in the sensitivity analysis (see Section 3.2). This analysis is carried out for the weather of Stockholm where the temperature gradient within the room is higher because of the cold weather conditions.

The mean radiant temperature (MRT) determined by the sensors located at x: [1 m, 2.25 m, 3.5 m], y: [0.2 m, 3 m, 5.8 m], z: [0.6 m, 1.5 m, 2.4 m] (see red points in Fig. 6) are evaluated in both tools (i.e. Simulink and TRNSYS 18) as well as the internal surface temperatures of the enclosure (i.e. floor, ceiling, external wall, internal walls, frame and glass of the window), the convective temperature (i.e. the temperature of the air node) and the component of the energy balance such as heating demand, cooling demand solar gains and ventilation losses.

Fig. A2 shows the hourly results of Simulink and TRNSYS model implementing the detailed longwave radiation model. In Fig. A2a the convective temperature, infiltration and ventilation losses, solar gains and heating and cooling powers are reported while in Fig. A2b the internal surface temperature of the frame, glass and external wall as well as the mean radiant temperature calculated for the sensor located in × = 2.25 m, y = 0.2 m, z = 2.4 m (see Fig. 6). From Fig. A2 it can be stated that the results of the two models are in good agreement for the represented three days of April. Minor deviations are present for the solar gains during the third reported day and as a consequence also for the cooling demand. In addition, it can be seen that the $\vartheta_{si,frame}$ is slightly shifted, which is probably caused by different considered frame capacities (i.e. the Simulink model applied a finite difference approach while the TRNSYS model is based on transfer functions). The $\vartheta_{si,glass}$ follows the deviations caused by the slightly different solar gains.

The temperature deviations are evaluated on an hourly basis using the Mean Bias Error (MBE), Mean Absolute Error (MAE), maximum and minimum Error. The deviations regarding energies are instead evaluated on a monthly (m) and hourly (h) basis by means of the normalized mean bias error (NMBE) and Root Mean Square Error normalized using the average of the reference absolute value higher than zeros (NRMSE_av > 0) as suggested by [8].

Fig. A3 shows the MBE and MAE on the left axis and the maximum and minimum Error on the right axis for all the evaluated temperatures. Only the deviation of the MRT for the sensors near the window (y = 0.2 m) are reported in Fig. A3 as they are the most critical points. It can be noticed that maximum and minimum error ranges between −1 K and + 1.5 K except for the internal temperature of the glass and frame where it is around ± 2.5 K. The MBE and MAE are both below 0.5 K demonstrating a good match between the hourly temperatures simulated with TRNSYS and Simulink.

Fig. A4 shows the NMBE and NRMSE_av > 0 calculated on an hourly (h) and monthly (m) basis using the energy gain and losses

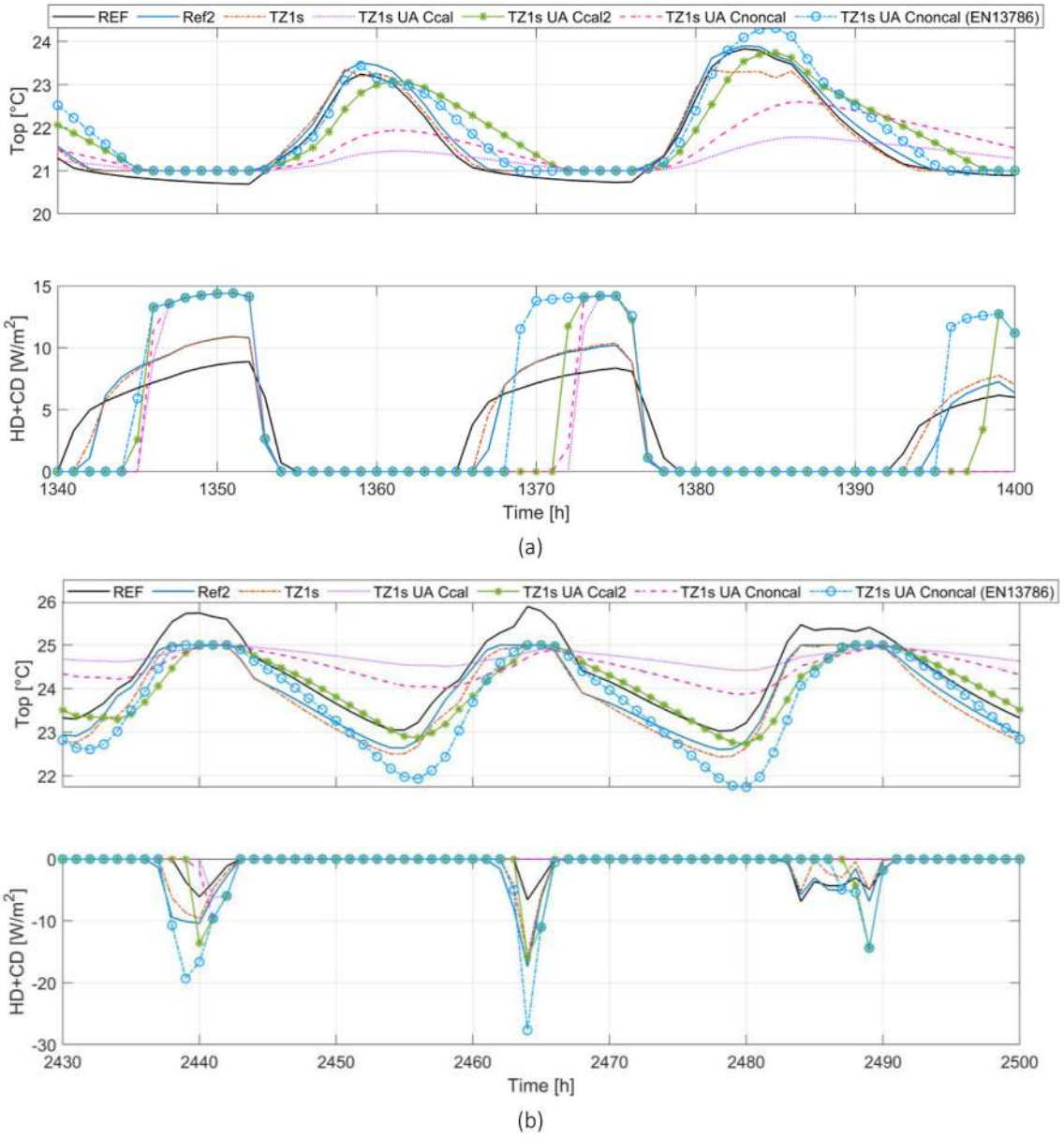

Fig. A1. Average hourly results (i.e. Top: operative temperature and HD + CD: heating and cooling demands) of the cases REF, Ref2 (ctr Top), TZ1s, TZ1s_UA_Ccal (cal REF), TZ1s_UA_Ccal2 (cal Ref_2), TZ1s_UA_Cnoncal (PHPP) and TZ1s_UA_Cnoncal (EN13786), for a winter period 25th-26th Feb. (a) and for a spring period 11th–13th Apr. (b) considering the climate of Stockholm.

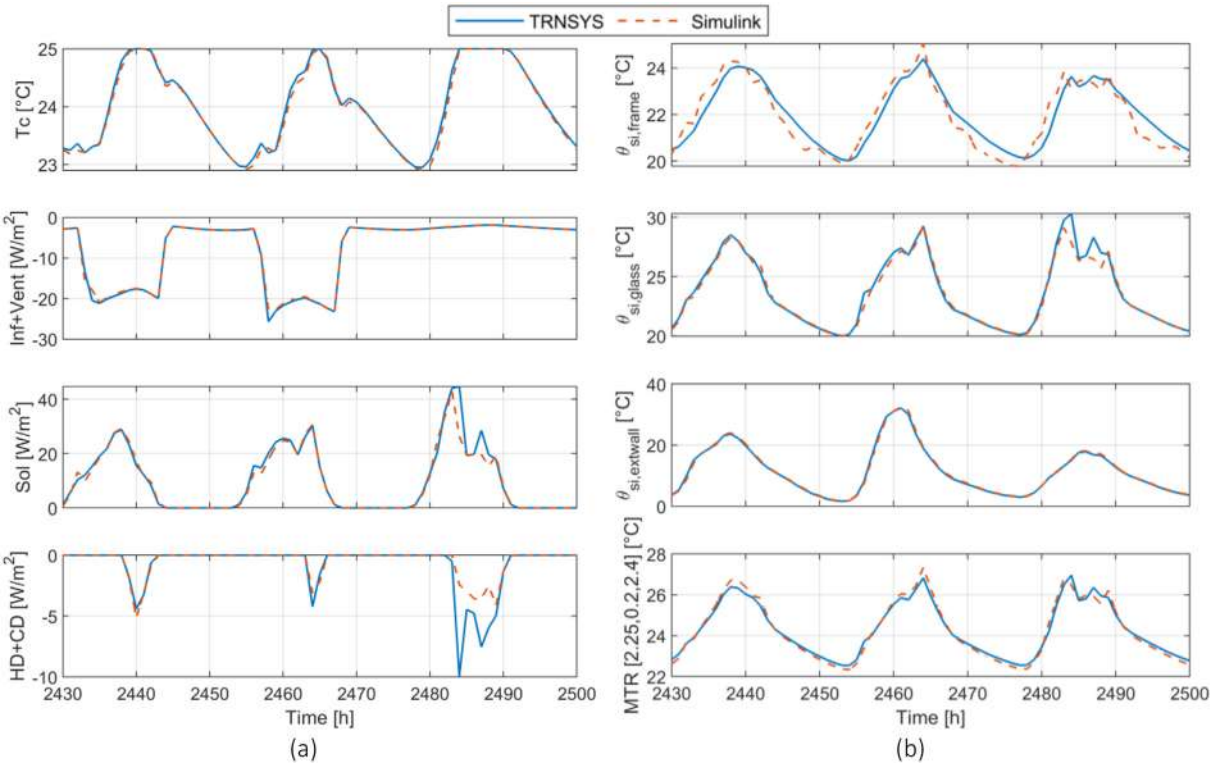

Fig. A2. Dynamic behaviour of the detailed radiation model of Simulink and TRNSYS. (a) reports the convective temperature (Tc), Infiltration and ventilation losses (Inf + Vent), Solar gains (Sol) and heating and cooling demands (HD + CD); (b) reports the internal surface temperature of the frame $\vartheta_{si,frame}$, of the glass $\vartheta_{si,glass}$ of the external wall $\vartheta_{si,extwall}$, the mean radiant temperature simulated in the position [x = 2.25 m, y = 0.2 m, z = 2.4 m] (MTR [2.25, 0.2, 2.4]).

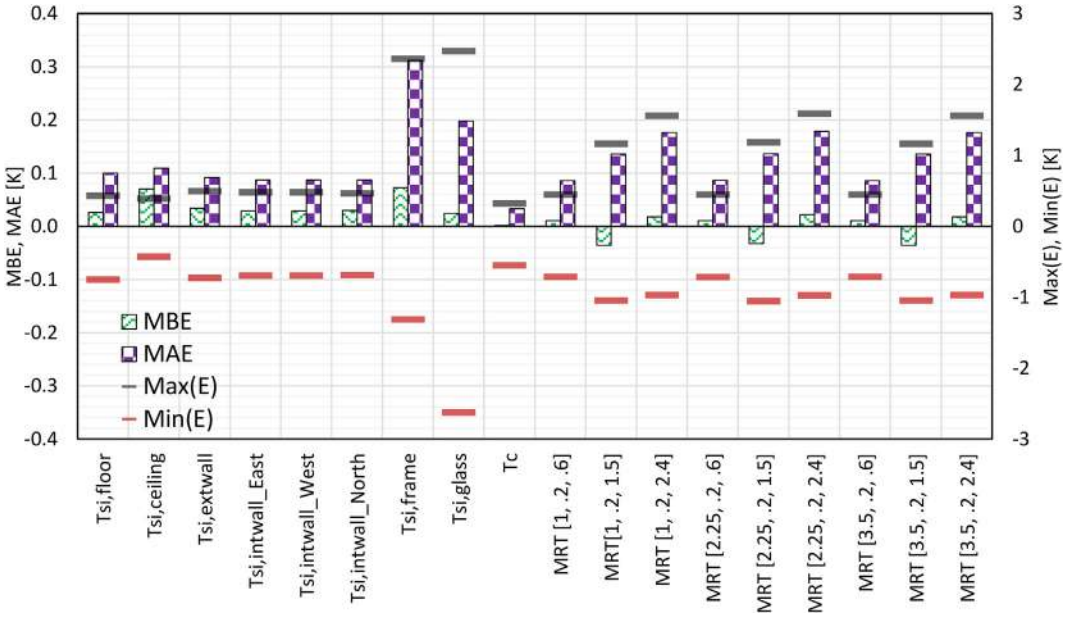

Fig. A3. Mean Bias Error (MBE), Mean Absolute Error (MAE), maximum and minimum Error of the temperatures (i.e. internal surface temperatures, convective temperature and mean radiant temperatures) deviation between the detailed longwave radiation model implemented in Simulink and TRNSYS using the results of TRNSYS as a reference.

associated with heating (HD), cooling (CD), infiltration plus ventilation (Vent) and solar gains (SOL) for the climate of Stockholm. The thresholds suggested by ASHRAE Guideline 14-2014 [41] (i.e. ± 5% for the monthly NMBE, 15% for the monthly NRMSE, ±10% for the hourly NMBE, 30% for the hourly NRMSE [47]) are shown in using dot-dash lines. From Fig. A4 it can be stated that a good agreement in terms of the energy balance is achieved.

Fig. A5 shows the computational cost for Simulink and TRNSYS both implementing the detailed longwave radiation model without output post-processing (in blue) and including it (in red). The rhombs represent the relative additional time required when the output file needs to be prepared. Since the number and format of the analysed outputs are different in both tools, the computational time is shown also without output to make a meaningful compar-

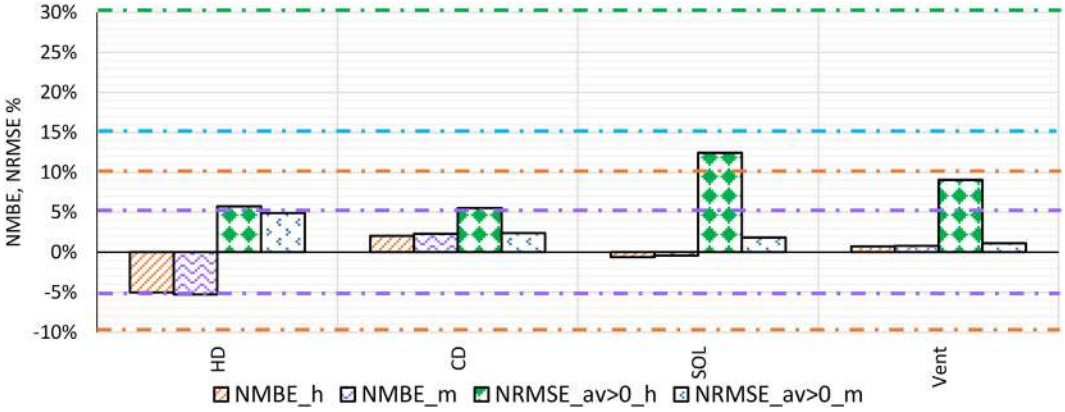

Fig. A4. Hourly (h) and Monthly (m) NMBE and NRMSE_av > 0 calculated for Heating and cooling demand, ventilation and infiltration losses and solar gains using as TRNSYS results as a reference considering the climate of Stockholm. The horizontal dot-dash lines represent the calibration criteria suggested by [41]: ±5% for the monthly NMBE, 15% for the monthly NRMSE, ±10% for the hourly NMBE, 30% for the hourly NRMSE.

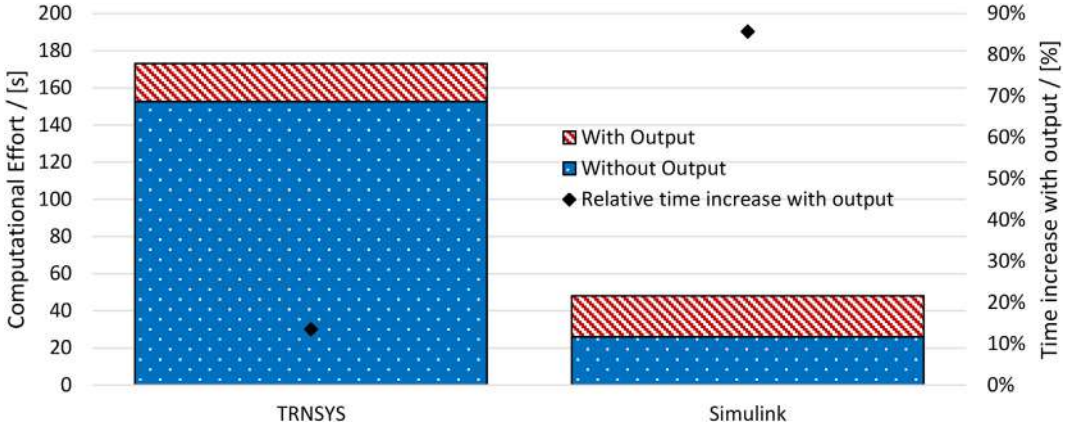

Fig. A5. Computational time of Simulink and TRNSYS both implementing the detailed longwave radiation model without the processing phase of the output (in blue) and the additional time required for the output preparation (in red). The dots represent the relative additional time when the outputs are prepared. (For interpretation of the references to colour in this figure legend, the reader is referred to the web version of this article.)

ison of the effort required by the model itself and at the same time to give an insight on the time required to generate the output file. The computational time of TRNSYS is remarkably higher compared to Simulink.

References

[1] H. Wang, Z. Zhai, Advances in building simulation and computational techniques: A review between 1987 and 2014, Energy Build. 128 (2016) 319–335, https://doi.org/10.1016/j.enbuild.2016.06.080.

[2] U. Ali, M.H. Shamsi, C. Hoare, E. Mangina, J. O'Donnell, Review of urban building energy modeling (UBEM) approaches, methods and tools using qualitative and quantitative analysis, Energy Build. 246 (2021) 111073.

[3] T. Hong, S.K. Chou, T.Y. Bong, Building simulation: an overview of developments and information sources, Build. Environ. 35 (4) (2000) 347–361, https://doi.org/10.1016/S0360-1323(99)00023-2.

[4] D.B. Crawley, J.W. Hand, M. Kummert, B.T. Griffith, Contrasting the capabilities of building energy performance simulation programs, Build. Environ. 43 (4) (2008) 661–673, https://doi.org/10.1016/j.buildenv.2006.10.027.

[5] Building Energy Software Tools, Best Directory | Building Energy Software Tools, (2020). https://www.buildingenergysoftwaretools.com/?__cf_chl_jschl_tk__=333a9062c0deb41f0aedbc09d4de96cab9d74a2d-1595925926-0-Ac80m_md0jCDx9IWiUyqe8WYrQij-imLS12aG2ZaEQAA0YJNQ0m3L4gPuZsqdDSQfZjPvfeemai8ls_wyDsp2znHqB0uwrDsw9iKK61KqCSarbSfBzG2zeBoLKS2ww74sxIaBbi7 (accessed July 28, 2020).

[6] S. Kota, F.J.F. Stipo, W. Jeong, J.B. Kim, J.L.B. Alcocer, M.J. Clayton, W. Yan, J.S. Haberl, Development of a reference building information model for thermal model compliance testing-Part I: guidelines for generating thermal model input files, ASHRAE Trans. 122 (2016) 256–266.

[7] F. Farias, S. Kota, W. Jeong, J.B. Kim, J.L.B. Alcocer, J.S. Haberl, M.J. Clayton, W. Yan, Development of a reference building information model (BIM) for thermal model compliance testing-Part II: test cases and analysis, ASHRAE Trans. 125 (2019) 750–764.

[8] M. Magni, F. Ochs, S. de Vries, A. Maccarini, F. Sigg, Detailed cross comparison of building energy simulation tools results using a reference office building as a case study, Energy Build. 250 (2021) 111260, https://doi.org/10.1016/j.enbuild.2021.111260.

[9] M. Klimczak, J. Bojarski, P. Ziembicki, P. Kęskiewicz, Analysis of the impact of simulation model simplifications on the quality of low-energy buildings simulation results, Energy Build. 169 (2018) 141–147, https://doi.org/10.1016/j.enbuild.2018.03.046.

[10] Z. Pang, Z. O'Neill, Y. Li, F. Niu, The role of sensitivity analysis in the building performance analysis: a critical review, Energy Build. 209 (2020) 109659, https://doi.org/10.1016/j.enbuild.2019.109659.

[11] W. Tian, A review of sensitivity analysis methods in building energy analysis, Renew. Sustain. Energy Rev. 20 (2013) 411–419, https://doi.org/10.1016/j.rser.2012.12.014.

[12] S. Gilani, W. O'Brien, Exploring the impact of office building users' modeling approaches on energy use across Canadian climates, Energy Build. 197 (2019) 68–86, https://doi.org/10.1016/j.enbuild.2019.05.042.

[13] S. Elhadad, C.H. Radha, I. Kistelegdi, B. Baranyai, J. Gyergyák, Model simplification on energy and comfort simulation analysis for residential building design in hot and arid climate, Energies. 13 (8) (2020) 1876, https://doi.org/10.3390/en13081876.

[14] M. Martin, N.H. Wong, D.J.C. Hii, M. Ignatius, Comparison between simplified and detailed EnergyPlus models coupled with an urban canopy model, Energy Build. 157 (2017) 116–125, https://doi.org/10.1016/J.ENBUILD.2017.01.078.

[15] M. Shin, J.S. Haberl, Thermal zoning for building HVAC design and energy simulation: A literature review, Energy Build. 203 (2019) 109429, https://doi.org/10.1016/j.enbuild.2019.109429.

[16] G. Dermentzis, F. Ochs, M. Gustafsson, T. Calabrese, D. Siegele, W. Feist, C. Dipasquale, R. Fedrizzi, C. Bales, A comprehensive evaluation of a monthly-based energy auditing tool through dynamic simulations, and monitoring in a

renovation case study, Energy Build. 183 (2019) 713–726, https://doi.org/10.1016/j.enbuild.2018.11.046.
[17] H. Johra, P.K. Heiselberg, J. Le Dréau, Numerical Analysis of the Impact of Thermal Inertia from the Furniture / Indoor Content and Phase Change Materials on the Building Energy Flexibility, in: Build. Simul., San Francisco, USA, 2017: pp. 35–42. https://doi.org/10.26868/25222708.2017.012.
[18] H. Karlsson, C.-E. Hagentof, Modelling of Long Wave Radiation Exchange in Enclosures with Building Integrated Heating, Proc. 7th Symp. Build. Phys. Nord. Ctries. 2 (2005).
[19] M. Camci, Y. Karakoyun, O. Acikgoz, A.S. Dalkilic, A comparative study on convective heat transfer in indoor applications, Energy Build. 242 (2021) 110985.
[20] M. Mirsadeghi, D. Cóstola, B. Blocken, J.L.M. Hensen, Review of external convective heat transfer coefficient models in building energy simulation programs: implementation and uncertainty, Appl. Therm. Eng. 56 (1-2) (2013) 134–151.
[21] M. Thalfeldt, E. Pikas, J. Kurnitski, H. Voll, Window model and 5 year price data sensitivity to cost-effective façade solutions for office buildings in Estonia, Energy. 135 (2017) 685–697, https://doi.org/10.1016/J.ENERGY.2017.06.160.
[22] M.K. Urbikain, J.M. Sala, Analysis of different models to estimate energy savings related to windows in residential buildings, Energy Build. 41 (6) (2009) 687–695.
[23] T. Zakula, M. Bagaric, N. Ferdelji, B. Milovanovic, S. Mudrinic, K. Ritosa, Comparison of dynamic simulations and the ISO 52016 standard for the assessment of building energy performance, Appl. Energy. 254 (2019) 113553.
[24] T. Zakula, N. Badun, N. Ferdelji, I. Ugrina, Framework for the ISO 52016 standard accuracy prediction based on the in-depth sensitivity analysis, Appl. Energy. 298 (2021) 117089.
[25] G.R. Ruiz, C.F. Bandera, Validation of calibrated energy models: Common errors, Energies. 10 (2017) 1587, https://doi.org/10.3390/en10101587.
[26] M. Magni, J.P. Campana, F. Ochs, G.L. Morini, Numerical investigation of the influence of heat emitters on the local thermal comfort in a room, Build. Simul. 12 (3) (2019) 395–410, https://doi.org/10.1007/s12273-019-0506-8.
[27] Solar Energy Laboratory University of Wisconsin-Madison, TRNSYS 18 documentation, volume 5, multi zone building modeling with type56 and TRN- Build, 2018.
[28] F. Ochs, M. Magni, P. Bonato, M. D'Antoni, D. Geisler-Moroder, M. Hauer, S. de Vries, R. Loonen, IEA SHC TASK 56 | Building Integrated Solar Envelope Systems for HVAC and Lighting: System Simulation Models, Solar Heating & Cooling Programme International Energy Agency, 2020. https://doi.org/10.18777/ieashc-task56-2020-0004.
[29] SIA 2024:2015 Bauwesen: Raumnutzungsdaten für die Energie- und Gebäudetechnik, Schweizerischer Ingenieur- und Architektenverein, Zürich, 2015.
[30] Trnsys, 18 User Manual: Multizone Building modeling with Type56 and TRNBuild, Solar Energy Laboratory, University of Wisconsin-Madison, 2017.
[31] Passivhaus Institut, (2020). https://passiv.de/en/04_phpp/04_phpp.htm (accessed August 25, 2020).
[32] EN ISO 13786:2017, Thermal performance of building components — Dynamic thermal characteristics — Calculation methods, (2017).
[33] J.P. Campana, ALMABEST: a new whole building energy simulation Simulink-based tool for NZEB design, Alma Mater Studiorum –– Università di Bologna DOTTORATO, 2019. https://doi.org/10.6092/unibo/amsdottorato/8993.
[34] B. Glück, Wärmeübergangskoeffizienten an thermisch aktiven Bauteiloberflächen und der Übergang zu Basiskennlinien für die Wärmestromdichte, 2007.
[35] ISO 6946:2017, Building components and building elements — Thermal resistance and thermal transmittance — Calculation methods, 2017.
[36] H.D. Baehr, K. Stephan, Heat and Mass Transfer, Second rev., Springer, 1998, 10.1002/9783527699483.ch14.
[37] CARNOT Toolbox – File Exchange – MATLAB Central, (2020). https://de.mathworks.com/matlabcentral/fileexchange/68890-carnot-toolbox (accessed August 19, 2020).
[38] R. Perez, P. Ineichen, R. Seals, J. Michalsky, R. Stewart, Modeling daylight availability and irradiance components from direct and global irradiance, Sol. Energy. 44 (5) (1990) 271–289, https://doi.org/10.1016/0038-092X(90)90055-H.
[39] I. The MathWorks, Variable Step Solvers in Simulink - MATLAB & Simulink - MathWorks Deutschland, (2021). https://de.mathworks.com/help/simulink/ug/variable-step-solvers-in-simulink-1.html#f11-44943 (accessed September 7, 2021).
[40] J.P. Campana, M. Magni, M. Dongellini, G.L. Morini, The benchmark of a new SIMULINK library for thermal dynamic simulation of buildings, in: Build. Simul. Appl., 2017.
[41] D.R. Landsberg, J.A. Shonder, K.A. Barker, J.S. Haberl, S.A. Judson, D.A. Jump, W. E. Koran, R.L. Hall, D.T. Reindl, J.R. Anderson, C.S. Barnaby, J.A. Clark, J.F. Dunlap, J.W. Earley, S.J. Emmerich, P.T. Graef, Measurement of Energy, Demand, and Water Savings, ASHRAE Guidel. 14-2014. 2014 (2014). www.ashrae.org/technology.
[42] D. K Arasteh, E. U Finlayson, C. Huizenga, WINDOW 4.1: Program Description, (1994) LBNL Report Number: LBL-35298.
[43] C. Curcija, S. Vidanovic, R. Hart, J. Jonsson, R. Mitchell, WINDOW Technical Documentation, Windows and Envelope Materials Group, Lawrence Berkeley National Laboratory; Windows and Envelope Materials Group, Berkeley, 2018.

5.3 Publication C

Title

Hourly simulation results of building energy simulation tools using a reference office building as a case study

Authors

Mara Magni, Fabian Ochs, Samuel de Vries, Alessandro Maccarini, Ferdinand Sigg

Published in

Data in Brief 38 (2021) 107370
https://doi.org/10.1016/j.dib.2021.107370

Own contribution

The first author simulated the reference office cell using ALMABuild, CarnotUIBK, DALEC, PHPP and TRNSYS, made the analysis including the results of all the tools. The third author provided the results of EnergyPlus, the fourth author the results of Modelica building library, the fifth author the results of IDA ICE. The second author contributed by reviewing this work.

Data in Brief 38 (2021) 107370

Contents lists available at ScienceDirect

Data in Brief

journal homepage: www.elsevier.com/locate/dib

Data Article

Hourly simulation results of building energy simulation tools using a reference office building as a case study

Mara Magni[a,*], Fabian Ochs[a], Samuel de Vries[b], Alessandro Maccarini[c], Ferdinand Sigg[d]

[a] Unit for Energy Efficient Buildings, University of Innsbruck, Innsbruck Austria
[b] Eindhoven University of Technology, Eindhoven the Netherland
[c] Aalborg University Copenhagen Denmark
[d] Technische Hochschule Rosenheim Germany

ARTICLE INFO

Article history:
Received 20 July 2021
Revised 1 September 2021
Accepted 13 September 2021
Available online 14 September 2021

Keywords:
Building simulation
Cross comparison
Statistical indices

ABSTRACT

The data presented in this article are the results of widespread building simulation tools (i.e. EnergyPlus, TRNSYS, Simulink/CarnotUIBK, Simulink/ALMABuild, IDA ICE, Modelica/Dymola and DALEC) used to simulate a characteristic office cell, described within IEA SHC Task 56 [1], located in Stockholm, Stuttgart and Rome. Hourly data for each component of the thermal balance (i.e. Heating, cooling, infiltration, ventilation, internal gains, solar gains) and the hourly convective and radiative temperatures are reported for all the tools along with the ambient temperature and solar irradiation on the south façade. The mainly used statistical indices (i.e. Mean Bias Error, Mean Absolute Error, Root Mean Square Error and coefficient of determination) are applied to evaluate the accuracy of the tools. For more insight and interpretation of the results, please see "Detailed Cross Comparison of Building Energy Simulation Tools Results using a reference office building as a case study" [2]. This data set and evaluation methods are made available to ease the cross-validation process for other researchers.

DOI of original article: 10.1016/j.enbuild.2021.111260
* Corresponding author.
E-mail address: Mara.Magni@uibk.ac.at (M. Magni).

https://doi.org/10.1016/j.dib.2021.107370

Specifications Table

Subject	Engineering, Architecture
Specific subject area	Building energy simulation: tools cross-comparison (i.e. EnergyPlus, TRNSYS, Simulink/CarnotUIBK, Simulink/ALMABuild, IDA ICE, Modelica/Dymola and DALEC).
Type of data	Table, Graph, Text
How data were acquired	Output of building energy modeling – Computer simulation using the following software programs: EnergyPlus, TRNSYS, Modelica, IDA ICE, Simulink/CarnotUIBK, Simulink/ALMABuild, DALEC.
Data format	Raw Analysed
Parameters for data collection	The outputs of each building energy simulation tool, included in this comparison are used as a basis for the evaluation.
Description of data collection	Hourly data of each component of the energy balance (i.e. Heating, cooling, infiltration, ventilation, internal gains, solar gains) and convective and radiative temperature along with the ambient temperature and solar irradiation on the south façade as a result of the simulation of the reference office cell located in Rome, Stuttgart and Stockholm.
Data source location	The evaluations are performed considering the following climates: Rome-Fiumicino Country: Italy Latitude and longitude for collected samples/data: 41.80, 12.233 Stuttgart-Echerd Country: Germany Latitude and longitude for collected samples/data: 48.68, 9.22 Stockholm-Bromma Country: Sweden Latitude and longitude for collected samples/data: 59.35, 17.95
Data accessibility	With the article
Related research article	Magni M., Ochs F., de Vries S., Maccarini A., Sigg F., Detailed Cross Comparison of Building Energy Simulation Tools Results using a reference office building as a case study, Energy and Buildings, 250 (2021), https://doi.org/10.1016/j.enbuild.2021.111260.

Value of the Data

- The hourly results of the cross-validated tools (i.e. EnergyPlus v.9.3, TRNSYS 18, Simulink/CarnotUIBK, Simulink/ALMABuild, IDA ICE v.4.8, Modelica Buildings library v.5.0.1 together with Dymola v. 2020x, DALEC) are reported for each component of the energy balance and for the convective and radiative temperature providing a wide dataset that can be used for the validation of other models for the simulation of office buildings.
- All the users of building simulation tools that would like to cross-compare their model and do not have available measurements can benefit from this dataset.
- The hourly results of a building simulation model can be cross-validated using this dataset as a reference, where the main used statistical indices are already calculated and can be used for a detailed evaluation of deviations.
- The proposed method for the evaluation of deviations between time series can be applied to the results of building simulations focusing on different building typologies. In addition, measured data, if available, can replace the median value that is used here as a reference, extending the usability of the proposed excel sheet to different case studies.

1. Data Description

The data set includes an excel file for each considered location (i.e. Rome, Stuttgart and Stockholm). Each spreadsheet includes ten tables (i.e. Heating, cooling, infiltration, ventilation, solar gains, internal gains, convective temperature, radiative temperature, ambient temperature and solar irradiation on the south façade) with the hourly results of each considered tool (i.e. EnergyPlus, TRNSYS, Simulink/CarnotUIBK, Simulink/ALMABuild, IDA ICE, Modelica, DALEC). The names of the tools will be abbreviated as follows and the abbreviations are used in the following sections and in the excel file:

- EP: EnergyPlus;
- TRN: TRNSYS;
- SIM IBK: Simulink/CarnotUIBK;
- SIM BO: Simulink/ALMABuild;
- IDA: IDA ICE;
- MOD: Modelica;
- DAL: DALEC.

In each, excel sheet the median of all the tools is calculated as well as the total annual energy or average temperature. Table 1 reports a section of the table reporting the heating powers for the climate of Stockholm. The first line of Table 1 shows the total energy and the last column reports the median of all the tools for each hour.

Table 1
Hourly heating power for the climate of Stockholm.

TOT [kWh/m^2]	16.7	18.2	16.9	17.1	18.0	16.9	18.0	17.3
				Hourly average power [Wh/m^2]				
Time / [h]	EP	TRN	SIM IBK	SIM BO	IDA	MOD	DAL	MEDIAN
...	...	...	...	...	...	...	...	...
50	5.2	7.6	6.8	7.2	8.1	5.7	0.0	6.8
...	...	...	...	...	...	...	...	...

On the right side of the hourly results, the statistical indices discussed and described in [2] and in Section 2.3 are calculated and reported as shown in Table 2. Here below the used acronyms are listed:

- MBE: Mean Bias Error;
- MAE: Mean Absolute Error;
- RMSE: Root Mean Square Error;
- NMBE: Normalized Mean Bieas Error;
- NMAE: Normalized Mean Absolute Error;
- NRMSE (av): Normalized Root Mean Square Error calculated using the average of the reference values as normalization means;
- NRMSE (|av|>0): Normalized Root Mean Square Error calculated using the average of the absolute reference values higher than zero as normalization means;
- R2: Coefficient of determination.

Table 2
Statistical indices.

	EP	TRN	SIM IBK	SIM BO	IDA	MOD	DAL
MBE [Wh/m^2]	−0.07	0.11	−0.04	−0.03	0.08	−0.04	0.07
MAE [Wh/m^2]	0.41	0.13	0.27	0.09	0.42	0.18	0.60
RMSE [Wh/m^2]	1.59	0.35	0.61	0.26	0.95	0.45	1.37
NMBE [%]	−3.6	5.3	−2.3	−1.3	4.1	−2.3	3.7
NMAE [%]	0.0	6.5	13.8	4.5	21.1	9.3	30.2
NRMSE (av) [%]	80.2	17.5	31.1	13.1	48.3	22.8	69.5
NRMSE (|av|>0) [%]	24.1	5.3	9.3	3.9	14.5	6.8	20.9
R2 [%]	80	99	97	99	93	98	85

To ease the visualization of the hourly results and calculated statistical indices the following graphs are placed in each excel sheet. Fig. 1 where the hourly results of each tool (i.e. in this case, the heating power for the climate of Stockholm is reported) are plotted against the reference results (i.e. median of all the tools). Here the spread of the results can be visualized.

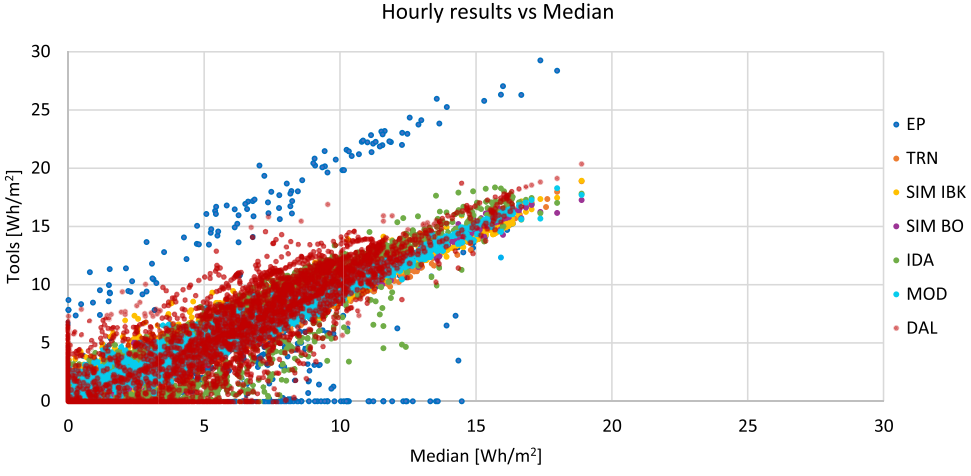

Fig. 1. Hourly results (i.e. heating power for the climate of Stockholm) of each tool plotted against the median value.

In Fig. 2 the hourly results of each tool are reported along with the hourly median value for a time frame that can be selected by the user of the excel file.

In Fig. 3 the results of the absolute statistical indices (i.e. MBE: Mean Bias Error, MAE: Mean Absolute Error, RMSE: Root Mean Square Error) reported in Table 2 are presented.

In Fig. 4 the results of the normalized statistical indices (i.e. NMBE: Normalized Mean Bias Error, NMAE: Normalized Mean Absolute Error, NRMSE (av): Normalized Root Mean Square Error calculated using the average of the reference values as normalization means, NRMSE (|av|>0): Normalized Root Mean Square Error calculated using the average of the absolute reference values higher than zero as normalization means, R2: coefficient of determination) reported in Table 2 are presented.

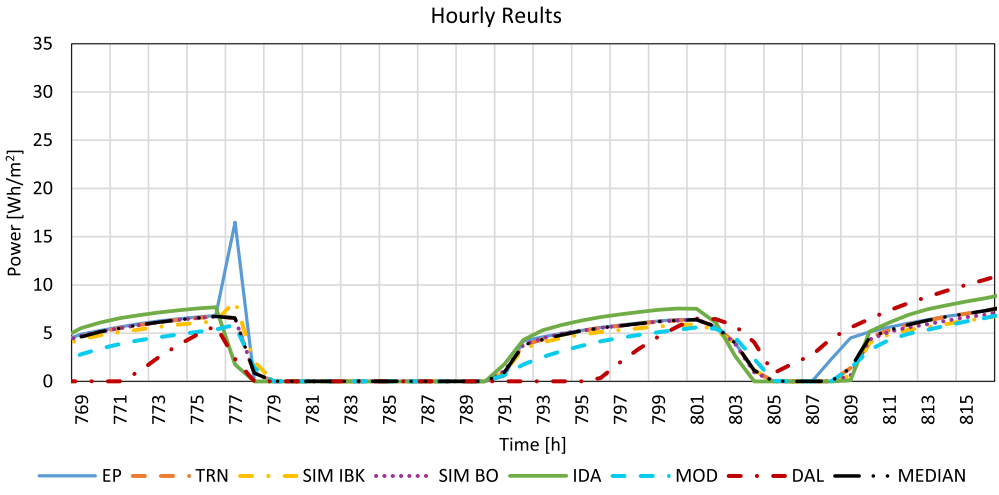

Fig. 2. Hourly results (i.e. heating power for the climate of Stockholm) of each tool and of the median for a user-selected period.

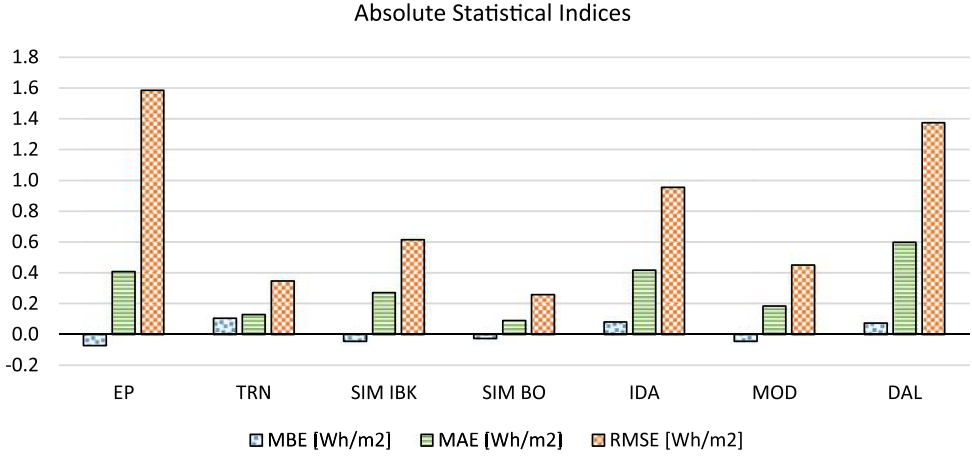

Fig. 3. Absolute statistical indices (i.e. MBE: mean bias error, MAE: mean absolute error, RMSE: root mean square error).

2. Experimental Design, Materials and Methods

Within the following sections, a short description of the office cell is provided, some key information about the applied tools and post-processing of the results are given and finally, the equations used for the analysis of the deviations between the dynamic results are provided. A detailed description of the methodology is also provided in [2].

2.1. Building and boundary conditions description

The reference office buildings described within IEA SHC Task 56 [1], located in Stockholm, Stuttgart and Rome is used within this work as it represents a characteristic office cell located

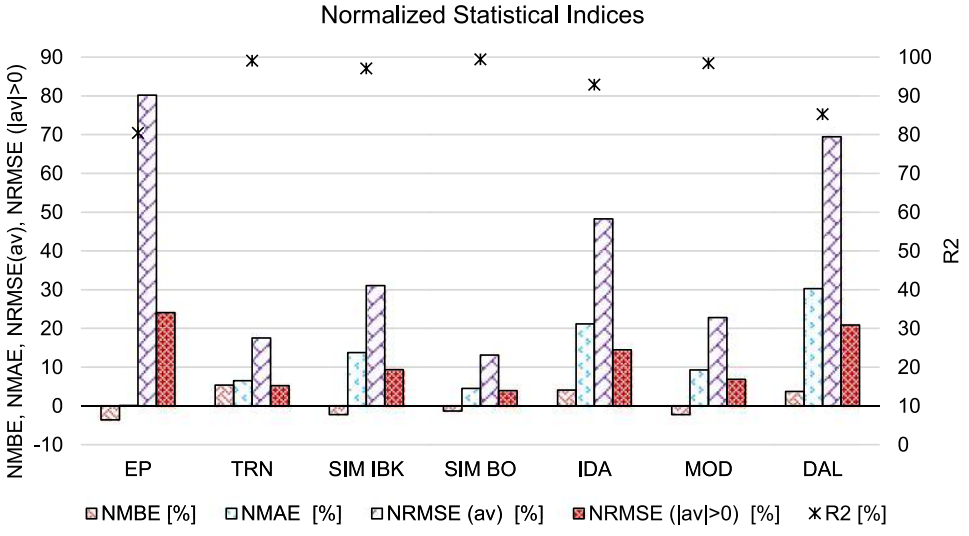

Fig. 4. Normalized statistical indices (i.e. NMBE: Normalized Mean Bias Error, NMAE: Normalized Mean Absolute Error, NRMSE (av): Normalized Root Mean Square Error calculated using the average of the reference values as normalization means, NRMSE (|av|> 0): Normalized Root Mean Square Error calculated using the average of the absolute reference values higher than zero as normalization means, R2: coefficient of determination).

on the middle floor of a high-rise building. The same Typical Meteorological Year (TMY2) for each location is used as input of the dynamic building simulation tools. Table 3 reports the yearly average ambient temperature ($\bar{\vartheta}_{amb,av}$), global irradiation on a horizontal surface ($I_{g,hor}$) and irradiation on a south-oriented vertical surface (I_{south}) characterizing the weather in each considered location.

Table 3
Main boundary conditions: yearly average ambient temperature ($\bar{\vartheta}_{amb,av}$), yearly global irradiation on a horizontal surface ($I_{g,hor}$) and yearly irradiation on a south-oriented vertical surface (I_{south}) [2].

Location	$\bar{\vartheta}_{amb,av}$ [°C]	$I_{g,hor}$ [kWh/m^2]	I_{south} [kWh/m^2]
Rome	15.8	1632	1253
Stuttgart	9.9	1101	889
Stockholm	7.8	952	884

The office has a heated area of 27 m^2 and a volume of 81 m^3 (see Fig. 5). The south-oriented façade disposes of a large window (i.e. window to wall ratio of 60%) and is the only one considered as non-adiabatic. A movable shading system, activated when the direct solar radiation impinging the south façade is higher than 120 W/m^2 and able to block the 70% of the incoming solar radiation is considered within this case study to reduce overheating problems.

The heat transfer coefficient (HTC) of the opaque wall element and the characteristics of the windows such as HTC, Solar Heat Gain Coefficient (SHGC) and the solar transmittance (τ_{sol}) for the three climates are listed in Table 4.

A constant air change rate of 0.15 ACH is assumed to account for natural infiltration while an additional airflow rate of 120 m^3/h is supplied by a mechanical ventilation system with a sensible heat recovery efficiency of 70%. The heat recovery system is bypassed when free cooling is beneficial (i.e. air temperature of the thermal zone higher than 23 °C and higher than the ambient temperature).

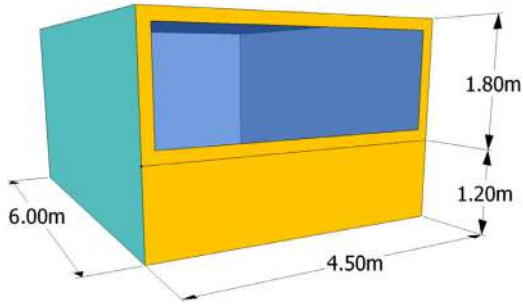

Fig. 5. Representation of the reference office building [2].

Table 4
Main properties of the south-oriented façade [2].

Properties	Rome (Italy)	Stuttgart (Germany)	Stockholm (Sweden)
$HTC_{ext,wall}$ [W/(m^{2}K)]	0.80	0.40	0.30
HTC_{win} [W/(m^{2}K)]	1.26	1.35	0.90
SHGC [%]	0.33	0.59	0.63
τ_{sol} [%]	0.26	0.43	0.46

Hourly schedules different for weekdays and weekends (see Fig. 6) are implemented to model a realistic user behavior (i.e. occupancy, appliances and lighting).

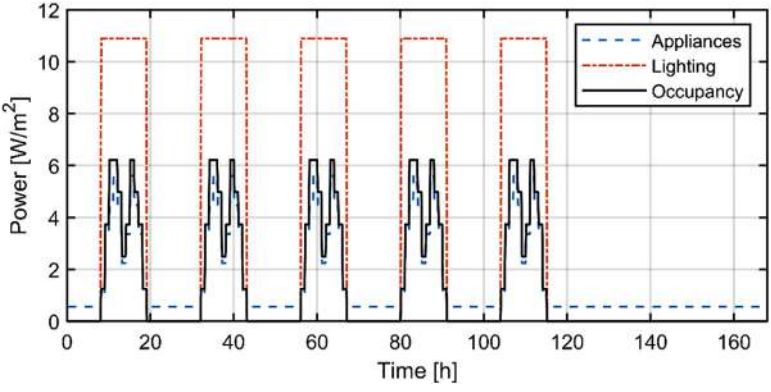

Fig. 6. Internal gains due to appliances, lighting and occupancy [2].

A more detailed description of the office cell is reported in the IEA SHC Task 56 report [1] and in Magni et al. [2].

2.2. Results of the building energy simulation tools

The office building used in this case study is simulated with different building energy simulation tools: EnergyPlus v.9.3, TRNSYS 18, Simulink/CarnotUIBK, Simulink/ALMABuild, IDA ICE v.4.8, Modelica Buildings library v.5.0.1 together with Dymola v. 2020x and DALEC. The different tools have different focuses and implement different models with different levels of detail. An overview of the different approaches is proposed in [2].

The analysed tools solve the numerical equations using different time steps (i.e. EnergyPlus, TRNSYS and DALEC use fixed time step while Simulink, IDA ICE and Modelica are based on variable time step) and solvers. Using a variable time step means that the solver defines the step size during the simulation, which is reduced (to increase the accuracy) when model states are changing rapidly or increased avoiding unnecessary steps when the model states are changing slowly. On the contrary, when a fixed time step is used the step size is kept constant during the whole simulation.

In all the tools the user can define the maximum time step (in case of variable time step) or the time step (in case of fixed time step) and in all the tools, except for DALEC that can only provide hourly calculations, the results are saved every 10 min. To compare the results of all the tools, hourly average powers and temperatures are calculated using the values within each hour. The resulting hourly time series (i.e. Heating power, cooling power, infiltration losses, ventilation losses, solar gains, internal gains, convective temperature, radiative temperature, ambient temperature and solar irradiation on the south façade) for each considered location (i.e. Rome, Stuttgart and Stockholm) are reported in the data file and used for the analysis of the deviations between the different tools.

It is noteworthy to mention that the solar gains can be defined differently within the different tools since they implement different window models. The hourly solar gains presented within this work represent the total solar gains including the direct transmitted solar radiation and the absorbed solar radiation which is subsequently re-emitted inside the thermal zone.

The results of the tools can be used as a reference for the cross-comparison of other office building models. In this case, the user should:

1. Create the building model starting from the description of the office cell provided in Section 2.1;
2. Run the simulation and save the results needed for the comparison with the provided benchmark;
3. If the saved results are sub-hourly, a pre-processing step is required to calculate hourly average results otherwise if the results are already on an hourly basis they can be directly used for the comparison;
4. The hourly data for the whole year can be inserted in a new column before the median column (see Table 1) and the formulas already included in the excel sheet can be used for the analysis of the deviations;
5. If the deviations are too high, the user should try to understand the possible reasons and improve the simulation model and/or inputs and repeat the sequence starting from step 2. For this step, the user could find support reading [2], where the main problems encountered during the comparison process are reported.

2.3. Description of the method applied for the analysis of the deviations

In the current work, not only a detailed data set of results is provided but also an approach for the evaluation of deviations between time series. A deep analysis of the challenges related to the usage of statistical indices is provided in [2] and the equations used are reported also in this section.

Since no measured data are available for this case study, it is necessary to define a set of reference data against which the results of each tool can be compared. For this purpose, the median value of the results of all the tools for each hour is calculated and used as a reference.

Both non-normalized and normalized statistical indices are calculated for the analysis of the deviations and the applied equations are reported in Table 5, where:

- r_i represents the reference value for the i^{th} time step, calculated as the median of the results of all the tools in each considered time step;
- s_i is the simulated value for a particular tool at the i^{th} time step;
- N is the number of considered data (i.e. corresponding to the number of time steps);

Table 5
Non-normalized (Mean bias error, Mean absolute error, Root mean square error) and normalized statistical indices (Normalized Mean bias error, Normalized mean absolute error, Normalized root mean square error, Coefficient of determination) [2].

Non-normalized indices		Normalized Indices	
$MBE = \frac{\sum_{i=1}^{N}(s_i - r_i)}{N}$	(1)	$NMBE = \frac{\sum_{i=1}^{N}(s_i - r_i)}{\sum_{i=1}^{N} r_i}$ [%]	(2)
$MAE = \frac{\sum_{i=1}^{N}\lvert s_i - r_i\rvert}{N}$	(3)	$NMAE = \frac{\sum_{i=1}^{N}\lvert s_i - r_i\rvert}{\lvert\sum_{i=1}^{N} r_i\rvert}$ [%]	(4)
$RMSE = \sqrt{\frac{\sum_{i=1}^{N}(s_i - r_i)^2}{N}}$	(5)	$NRMSE = \frac{1}{\lvert nm\rvert}\sqrt{\frac{\sum_{i=1}^{N}(s_i - r_i)^2}{N}}$	(6)
		$R^2 = 1 - \frac{\sum_{i=1}^{N}(s_i - r_i)^2}{\sum_{i=1}^{N}(r_i - \bar{r})^2}$	(7)

- $\bar{r}$ is the average of the reference values r;
- nm is a normalization means.

Two different normalization means (nm) are considered: the average of the reference values (see Eq. (8)) and the average of the reference values counting only the absolute values of the reference data higher than zero (see Eq. (9)).

$$av = \frac{\sum_{i=1}^{N} r_i}{N} \tag{8}$$

$$av_{>0} = \frac{\sum_{i=1}^{N} r_i}{N_{|r|>0}} \tag{9}$$

As highlighted in [2], normalization issues related to the average value trending to zero can be avoided using the av>0 as normalization means. This problem is particularly relevant when the variant under analysis is often close to zero (e.g. heating and cooling powers).

The normalized indices are needed to compare the calculated deviations against given thresholds (e.g. ASHRAE Guideline 14–2014 [3]) or for the comparison of the deviations between different data sets. ASHRAE Guideline 14–2014 [3] describes a method for the validation of the building model against measurements and suggests that the calculated deviations should remain below the following limits: ±5% for the monthly NMBE, 15% for the monthly NRMSE, ± 10% for the hourly NMBE, 30% for the hourly NRMSE and > 0.75 for the R2.

It is noteworthy to mention that the RMSE is scale-dependent and can be calculated only for data based on a scale with an absolute zero (e.g. Kelvin for temperatures).

The spreadsheet presented in the current work can be used as a reference for the validation of other models of office cell as the one described in this work. In addition, the statistical evaluation included in the spreadsheet can also be used for the comparison of simulation results against measurement data. In this case, the measurement data should replace the median as a reference and the simulated results should overwrite the results of the tools.

Declaration of Competing Interest

The authors declare that they have no known competing financial interests or personal relationships which have or could be perceived to have influenced the work reported in this article.

CRediT Author Statement

Mara Magni: Conceptualization, Methodology, Software, Validation, Formal analysis, Investigation, Data curation, Writing – original draft, Visualization; **Fabian Ochs:** Supervision, Project administration, Funding acquisition, Writing – review & editing; **Samuel de Vries:** Software, Validation; **Alessandro Maccarini:** Software; **Ferdinand Sigg:** Software.

Acknowledgments

This work is performed within the framework of IEA SHC Task 56 international project. We thank, Hauer Martin and Plörer Daniel for supporting the simulations with DALEC, EURAC for the collaboration within the IEA SHC Task 56 project, the University of Bologna for allowing us to use ALMABuild, Nicola Franzoi for the fruitful discussion about the statistical indices, Toni Calabrese and Ellika Taveres-Cachat for contributing in creating the TRNSYS and IDA ICE models.

Supplementary Materials

Supplementary material associated with this article can be found in the online version at doi:10.1016/j.dib.2021.107370.

References

[1] F. Ochs, M. Magni, P. Bonato, M. D'Antoni, D. Geisler-Moroder, M. Hauer, S. de Vries, R. Loonen, IEA SHC TASK 56 | Building Integrated Solar Envelope Systems for HVAC and Lighting: System Simulation Models, Sol. Heat. Cool. Progr. Int. Energy Agency (2020), doi:10.18777/ieashc-task56-2020-0004.

[2] M. Magni, F. Ochs, S. de Vries, A. Maccarini, F. Sigg, Detailed cross comparison of building energy simulation tools results using a reference office building as a case study, Energy Build. 250 (2021) 111260, doi:10.1016/J.ENBUILD.2021.111260.

[3] ASHRAE Guidelines 14-2014, Measurement of energy and demand savings, American society of heating refrigerating and air-conditioning engineers, Atlanta (2014).

5.4 Publication D

Title

Numerical investigation of the influence of heat emitters on the local thermal comfort in a room

Authors

Mara Magni, Jean Pierre Campana, Fabian Ochs, Gian Luca Morini

Published in

Building Simulation (2019) 12: 395–410
https://doi.org/10.1007/s12273-019-0506-8

Own contribution

The first author developed the proposed model and analysed the results for the different cases presented in this paper. The second third and fourth authors supported with fruitful discussions and with writing and reviewing this manuscript.

Build Simul
https://doi.org/10.1007/s12273-019-0506-8

Numerical investigation of the influence of heat emitters on the local thermal comfort in a room

Mara Magni[1], Jean Pierre Campana[1], Fabian Ochs[2], Gian Luca Morini[1] (✉)

1. Deparment of Industrial Engineering (DIN), Alma Mater Studiorum Università di Bologna, Viale del Risorgimento 2, 40136 Bologna, Italy
2. Unit for Energy Efficient Building, University of Innsbruck, Innrain 52, Innsbruck, A-6020, Austria

Abstract

In this paper a numerical analysis of the effect of heat emitter characteristics on the local indoor thermal comfort condition in a room is presented. A dynamic model, able to evaluate the 3D distribution of the mean radiant temperature in the whole volume of a thermal zone is developed. The model allows a fast evaluation, in terms of computational time, of the view factors associated to the inner points of a room thanks to the use of the MATLAB Contour Double Integral Formula (CDIF) routine. The new tool has been used in order to obtain, by means of a series of dynamic yearly simulations, a comparison among different heat emitters (i.e. in-slab radiant floor, in-slab radiant ceiling, lightweight radiant ceiling, radiator, radiant vertical wall and all-air systems) in terms of 3D distribution of the local operative temperature in a room. The knowledge of the 3D distribution of the operative temperature enables the local analysis of the indoor thermal comfort conditions established in the room during the year. The local Predicted Mean Vote (PMV) distribution within the room is calculated for each considered configuration. The results allow to quantify how the reduction of the maximum surface temperature of the emitters, which can be experienced when the envelope thermal insulation is increased, can create more uniform indoor thermal conditions by reducing the differences existing among the heat emitters.

Keywords

indoor thermal comfort,
mean radiant temperature,
operative temperature,
heating emitters,
PMV

Article History

Received: 7 July 2018
Revised: 26 November 2018
Accepted: 14 December 2018

1 Introduction

During the design of a new HVAC system, the designer has to select the best heat emitter system in order to guarantee simultaneously low energy consumptions and optimal indoor thermal conditions in each thermal zone. The position of the heat emitters in a thermal zone (i.e. close to colder walls), their heat transfer features (radiant or convective emitters) and their operative conditions (i.e. heat transfer area, mean surface temperature, control system) have a strong impact on the local thermal conditions as well as on the energy demand of the HVAC system and for this reason a huge effort has been made during the recent years to study and optimize the main features of the heaters available in the market. As an example, due to their increasing diffusion, radiant heating systems are one of the emitters more studied in the last years (Rhee et al. 2017) but the attention on these systems is still high, as demonstrated by the recent analysis made by Ning et al. (2017) focused on the optimal design of radiant emitters based on their thermal response time. As highlighted by Rhee et al. (2017) and Bojic et al. (2015), one of the motivation of the success of the radiant systems concerns their capability to work with lower surface temperature, compared to traditional convective systems, enabling the use of low temperature heat generation systems, like heat pumps. Nowadays, a series of radiant heating systems are available; these systems differ from each other based upon the position assumed by the radiant heating surface (floor, ceiling, vertical walls) and for type of installation (dry or wet). The position and the installation rules of the radiant surface modify the heat emission of the panels in terms of time response to a thermal load variation and the power share of the heat exchanged (radiant and convective). In fact, suspended radiant ceiling systems and dry radiant floor panels are generally very fast to react to a variation of the building thermal loads. On the contrary, in-slab radiant

E-mail: gianluca.morini3@unibo.it

List of symbols

A	area [m^2]
C	thermal capacity [J/K]
F	view factor [—]
G	irradiance [W/m^2]
H	radiosity [W/m^2]
h	convective heat exchange coefficient [W/(m^2·K)]
n	characteristic exponent of the radiator [—]
n_{el}	number of radiator elements [—]
PMV	predicted mean vote [—]
R	thermal resistance [m^2·K/W]
$\dot{Q}$	heat power [W]
T	temperature [K]
z	vertical distance from the floor [m]
α	weight factor of Eq. (1) [—]
$\Delta\tau_{on}$	time interval needed to increase the local operative temperature from 19 °C to 20.5 °C
$\Delta\tau_{off}$	time interval in which the operative temperature decreases from 20.5 °C to 19 °C
ε	emissivity [—]
ρ	reflectivity coefficient [—]
σ_0	Boltzmann constant [W/(m^2·K^4)]
ϑ	temperature [°C]

Subscripts

CV	convective
m	mean
max	maximum
MR	mean radiant
nom	nominal
OP	operative
R	radiative
Rd	radiator
S	surface
tot	total

systems are characterized by long response times (Ning et al. 2017). For radiant ceiling systems in winter, the convection contribution vanishes and the maximum heat flux delivered is lower than the typical heat flux obtainable with radiant floors. For this reason these panels are generally used in thermal zones with a high thermal insulation level of the external walls and/or when dust transportation has to be minimized (i.e. in hospitals), thanks to the reduction of the convective flows in winter (Bojić et al. 2015).

Regarding the performance of different heaters in terms of local indoor thermal comfort, the scientific community has tried for long to come up with an answer to the question if radiant heating systems are or not able to ensure better thermal comfort conditions than convective systems (e.g. Karmann et al. 2017; Lin et al. 2016). Nowadays it is evident that this question must be considered as "ill-posed" because the answer strongly depends upon many boundary conditions, like the level of thermal insulation of the building, the sizing rules adopted for the emitters, the shape of the room, the position of the emitters and of the control sensor and so on. By varying these conditions the radiant systems can become better or worse than the convective systems in terms of resulting indoor conditions.

In particular, the adoption of a specific heat emitter is responsible for the differences in the distribution of the operative temperature in a room. For example, heat emitters based on convection have higher risk of draught, are generally responsible for higher vertical temperature difference and fluctuations. Moreover, in presence of an erroneous direction assumed for the air natural circulation (i.e. due to the position of the emitter in the room) may provide local discomfort conditions close to the floor (Lin et al. 2016). On the other hand, with radiant floors or ceiling heating systems the risk that the occupants feel cooler or hotter respectively the head or feet region is higher (Lin et al. 2016). The impact on the indoor comfort conditions of these systems must be evaluated in detail on a case by case basis in order to select the best one in terms of comfort conditions. As an example, Bojic et al. (2012) investigated the effects of the position of the radiant panels in a room on the primary energy demand and on the indoor thermal comfort by considering their installation on the floor, wall, ceiling and floor-ceiling. For a fixed level of envelope insulation, the results show that the ceiling heating has the highest primary energy consumption, whilst the floor-ceiling heating system has the lowest. However, in this analysis a simplified approach was followed by means of which only one value of mean operative temperature was associated to the rooms during a winter month (January) by ignoring the local distribution of this parameter within the rooms. The approach followed by Bojic et al. (2012) is very diffused nowadays, since the most popular commercial software used for energy dynamic simulations is generally able to associate each room of a building to only one convective as well as one radiant node. In this way, information about the spatial variation of the comfort indoor conditions due to the adoption of a specific heater in a room is lost (Ochs et al. 2017).

On the contrary, for a complete overview of the pros and cons deriving by the choice of a specific heat emitter, it becomes important to be able to reconstruct the local 3D

distribution of the operative temperature in a room. The knowledge of this parameter only at one point (which is considered as representative of the whole room) is not enough if the target is to optimize the position and the features of the heat emitters in order to obtain uniform distribution of the indoor thermal comfort condition in a thermal zone. To calculate the operative temperature distribution in a room it is mandatory to calculate the local value of both the mean radiant temperature and the convective temperature. This can be done by coupling software for dynamic energy simulation with CFD codes, performing steady state simulations, as done recently by Mustakallio et al. (2017) and Zhang et al. (2017), who demonstrated how a complete co-simulation can predict with a high level of detail the distribution of the indoor air velocity and temperature, but this approach requires high computational effort, which limits the application of this methodology to simple cases (Rhee and Kim 2015).

In order to remove this constraint, in this work a nodal model developed in MATLAB/SIMULINK is presented; the model is able to evaluate the 3D distribution of the mean radiant temperature in a room in which a radiant (floor, ceiling or wall) or a convective (radiators or all-air) heating system is installed. Net radiation exchange approach (Baehr and Stephan 2006) is followed for the calculation of the radiant heat power exchanged between the inner surfaces of the room. On the contrary, the rigorous calculation of the local value of the convective temperature in the room is not made in this paper and the convective temperature is considered as uniform in the room (ideal air mixing). This assumption is acceptable in all the cases in which the airflow is low (< 0.15 m/s), as in the case of weak natural convection induced by small temperature gradients, as observed by Lin et al. (2016).

The MATLAB code was implemented in the ALMABuild blockset framework (Campana et al. 2017), a SIMULINK library used for building dynamic energy simulations, with the aim to couple the unique performances of SIMULINK for the dynamic analysis of controlled systems with the detailed evaluation of the local mean radiant temperature obtained by using MATLAB. By following this approach, it is possible to predict the local values of the main parameters linked to the indoor comfort in each point of the room and to optimize the kind, size, position and operative conditions of the heat emitters to obtain the desired indoor comfort conditions.

In this paper the potential of this approach is demonstrated by comparing the effect of the adoption of different heat emitters (i.e. in-slab radiant floor, in-slab radiant ceiling, lightweight radiant ceiling, radiator, radiant vertical wall and all-air systems) on the 3D distribution of the operative temperature in a reference room for the duration of a whole year. The impact of the envelope thermal insulation on the indoor thermal conditions in presence of a specific emitter is also investigated.

2 Mathematical model

ALMABuild blockset (Campana et al. 2017) is a SIMULINK library by means of which a complete building dynamic energy model can be obtained. All the envelope structures are modelled with a set of thermal resistances (R) and capacitance (C) and divided in active (heating surface) or passive surfaces (non-heating surface). More in detail, passive walls, floors and ceilings are modelled with a 3R4C set and the lightweight ceiling with a 6R7C set. The 3R4C set is based on four nodes (see Fig. 1) where two of them are placed on the internal and external surface of the element, whilst the other two nodes are located on the interface between the lighter layer (i.e. insulation) and the massive one and where the first quarter of the total heat capacity is reached starting from the external side. In this way, there is not a complete correspondence between the positions of the four nodes and those of the interfaces between two consecutive wall layers. Once defined the position of the nodes, the thermal resistance of two adjacent nodes is evaluated as the sum of the thermal resistances of the layers contained within the nodes, whilst the thermal capacity of each node is estimated as the sum of half the thermal capacity of the layers adjacent to the node. In addition, it is assumed that each structure has a uniform temperature over the external and internal surfaces. For active surfaces (i.e. radiant floor or ceiling), in order to take into account the heat delivered from the hot water to the structure, an additional value of heat flux is imposed to the internal node in correspondence to the position of the heating elements within the envelope element.

Figure 1 shows the scheme of the 3R4C model of a slab on grade floor. When the floor is an active surface, the power delivered from the heating system is added to the corresponding internal node.

Solar radiation coming from the window is another gain added to the balance of the internal node. The heat exchange between the floor and the other surfaces in the room is represented by the radiative exchange and by the convective exchange between the floor surface and the air node. On the other side, a conductive heat flux is applied to the outside node; two additional capacities are used for the model of the layer of ground in contact with the floor. Roof, internal and external walls are also modelled with a 3R4C network. In presence of an external wall, the following contributions are taken into account on the external node: (i) convective and radiative heat transfer with the surroundings, (ii) incident solar radiation, (iii) longwave radiation to the sky. For internal walls the heat transfer with surrounding is replaced

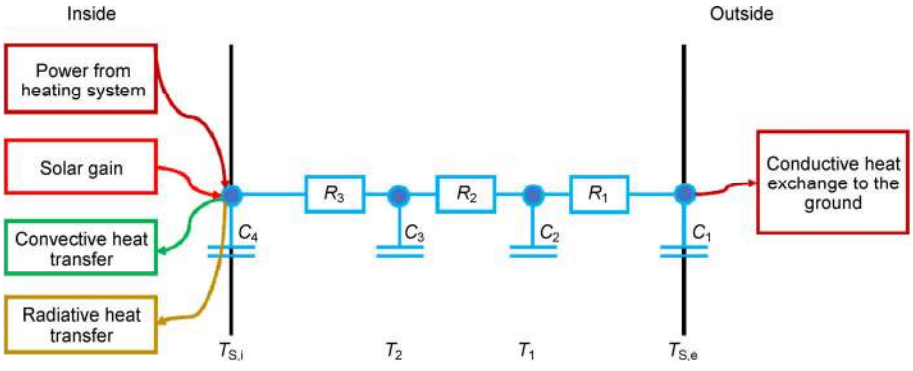

Fig. 1 3R4C model of a slab on grade floor

by the convective and radiative heat transfer with the adjacent zones.

On the contrary, light suspended radiant ceiling is modelled by means of a 6R7C set (see Fig. 2) where R_4 represents the air resistance between the ceiling and the suspended ceiling, R_5 represents the resistance of the insulation and R_6 represents the resistance of the drywall.

The hot water radiator is modelled with the same structure of an adiabatic internal wall having a specific thermal capacity. The radiator is considered as a plane surface for the calculation of the view factors, neglecting its thickness. The total heat power delivered by the hot water radiator can be estimated as follows (EN 2014):

$$\dot{Q}_{\mathrm{Rd,tot}} = \dot{Q}_{\mathrm{nom}} n_{\mathrm{el}} \left(\frac{\vartheta_{\mathrm{m}} - \vartheta_{\mathrm{CV}}}{50} \right)^{n} \tag{1}$$

where $\dot{Q}_{\mathrm{nom}}$ and n are the rating power emitted by the single element of the radiator and the characteristic exponent of the radiator, respectively; n_{el} is the number of elements of the radiator; ϑ_{m} is the average surface temperature of the radiator. The convective heat transfer delivered by the radiator surface is estimated as the difference between the total heat power emitted by the radiator (Eq. (1)) and the radiant heat power exchanged by the radiator surface with the other inner surfaces.

The all-air heating system is modelled in a simplified way by directly imposing a heat flux to the air node.

2.1 Operative, convective and mean radiant temperature

Radiant heat exchange in the room is modelled by using the net radiation exchange approach (Baehr and Stephan 2006). This approach has a higher computational demand with respect to the simplified models adopted by many commercial software for dynamic energy simulations, like TRNSYS (up to version 17), EnergyPlus, IDA ICE among others, as it requires the knowledge of the view factors among the inner surfaces of a thermal zone working at different temperature values. The simplified approach followed by some commercial code allows the calculation of the convective and radiant temperature by using a two-star model where these values are obtained in a single point of the room (i.e. the central point) (Wolfgang 1994). For this reason, only a single value of operative temperature can be linked to each building thermal zone, which then represents the average value of the operative temperature of the zone.

As indicated by ASHRAE (2017), the operative temperature ϑ_{op} can be calculated as weighted mean between the convective ϑ_{CV} and the mean radiant ϑ_{MR} temperature:

$$\vartheta_{\mathrm{OP}} = \alpha \vartheta_{\mathrm{CV}} + (1 - \alpha) \vartheta_{\mathrm{MR}} \tag{2}$$

in which ϑ is the temperature in °C and the value of the weight factor α depends on the ratio between the convective heat transfer coefficient and the total heat transfer coefficient;

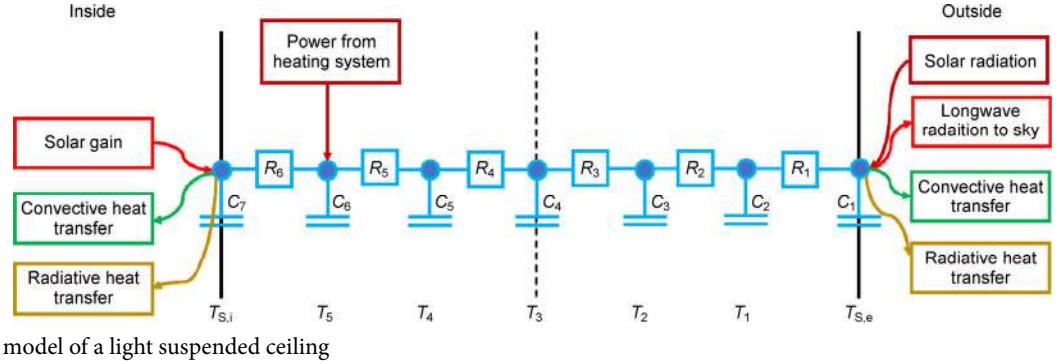

Fig. 2 6R7C model of a light suspended ceiling

this ratio is usually between 0.4 and 0.5. In this work α is assumed equal to 0.5.

When the view factors among the inner surfaces of a thermal zone are not known, the mean radiant temperature linked to the room is obtained by using the following approximated relationship (ASHRAE 2017):

$$T_{MR} = \frac{\sum_{i=1}^{N} A_i T_i}{\sum_{i=1}^{N} A_i} \tag{3}$$

where T_i is the temperature linked to the i-th inner surface of the room and A_i is the area of the i-th inner surface.

If the mean radiant temperature and the convective temperature associated to the room are known, it is possible to calculate all the main parameters which define the indoor comfort characteristics of the room, like Predicted Percentage of Dissatisfied (PPD) and Predicted Mean Vote (PMV), following the definitions given by Fanger (1972). However, according to this approach only an average value of these parameters can be estimated and no information about their spatial variation in a room as a function of the geometry and arrangement of the heaters can be obtained.

In order to calculate the local radiant temperature distribution in a room, the radiant heat transfer between a small surface centred in a point of the room and the inner surfaces must be analysed by using the view factors (Baehr and Stephan 2006). In a room having N inner surfaces with a different temperature, the local value of the mean radiant temperature $T_{MR,j}$ can be estimated, as indicated in (ASHRAE 2017), as follows:

$$T_{MR,j} = \sqrt[4]{\sum_{i=1}^{N} F_{ij} T_i^4} \tag{4}$$

where F_{ij} is the view factor between the room inner surface (i) and the surface (j) placed in the point where the mean radiant temperature is evaluated. In order to calculate the view factors involved in Eq. (4), a small isothermal cubic surface (i.e. a cube with a size of 0.5 cm) is placed in a point of the room. This small cubic surface is used here like a "local sensor". By placing this small cubic surface in different points of the thermal zone, it is possible to evaluate the 3D distribution of the mean radiant temperature, according to Eq. (4).

2.2 View factors calculation

The view factor calculation is time consuming because it depends on the geometry of the surfaces operating at different temperature in a room and on their number. In fact, the number of unknown view factors in a room with N surfaces is equal to $N{\cdot}N$. Anyway, it is possible to demonstrate that, as a consequence of the application of the view factors properties (i.e. summation and reciprocity theorems), the number of unknown view factors can be reduced to $N \cdot (N-1)/2$, if only planar surfaces are present in the room (absence of auto-radiation).

In this paper, the calculation of the view factors linked to the inner surfaces of a room is obtained by following the procedure suggested by Lauzier and Rousse (2017). A MATLAB script was developed, based on the MATLAB Contour Double Integral Formula (CDIF) routine, for the evaluation of the view factors among planar surfaces having any shape and orientation. The use of MATLAB for the evaluation of the view factors allows to couple directly this procedure to the ALMABuild blockset, which works in SIMULINK. This approach is very robust and fast from a numerical point of view and no limitations on shape and number of the involved surfaces there exist. However, in order to process this calculation, it is mandatory to create a reference system by means of which the coordinates of the points which define the perimeter of each surface are assigned univocally to each surface.

When smaller surfaces having a different temperature are embedded in an inner surface (i.e. windows, vertical radiant heaters, radiators), the view factors linked to these smaller surfaces are obtained by using the superimposition rule. In this way, if the geometry of the room is univocally defined, which means that all the dimensions of the surfaces as well as their reciprocal distances are known, the value assumed by each view factor F_{ij} is obtained.

In order to verify the reliability of the numerical procedure followed in this work for the calculation of the view factors, a comparison with the values obtained by using two commercial software, TRISCO version 13.0 (Physibel 2010) and COMSOL version 5.3 (COMSOL 2017), have been made by considering a reference room. A very good agreement among the view factors has been observed with a maximum deviation of 1.17% from the view factors obtained with TRISCO and 2.32% from the values obtained with COMSOL. These results confirm that the numerical procedure for the evaluation of the view factors followed in this work can be considered as validated.

2.3 Radiative and convective heat transfer model

In the SIMULINK models implemented in ALMABuild, the radiative heat transfer among grey inner surfaces is computed on the basis of the following hypothesis (Baehr and Stephan 2006): (i) each inner surface is isothermal; (ii) each surface behaves like a grey Lambert radiator with a uniform

value of emissivity ε_i; (iii) reflected radiation is assumed to be purely diffuse. Under these hypotheses, the total heat flux emitted by the i-th surface is given by its radiosity H_i defined as follows:

$$H_i = \varepsilon_i \sigma_0 T_i^4 + \rho_i G_i \tag{5}$$

where ρ_i is the reflectivity coefficient and G_i is the total radiant heat flux that strikes the i-th surface coming from other surfaces. The net radiant heat power linked to the i-th surface is calculated with the following equation:

$$\dot{Q}_{R,i} = A_i (H_i - G_i) \tag{6}$$

On the other hand, by considering the heat power delivered by the other surfaces (j) which strikes the i-th surface, the radiant heat flux G_i can be written as:

$$G_i = \sum_{j=1}^{N} F_{ij} H_j \tag{7}$$

By combining Eq. (5), Eq. (6) and Eq. (7) it is possible to obtain the radiosity and the heat power linked to each inner surface, if their emissivity and temperature are known:

$$H_i = \varepsilon_i \sigma_0 T_i^4 + (1 - \varepsilon_i) \sum_{j=1}^{N} F_{ij} H_j \tag{8}$$

$$\dot{Q}_{R,i} = \frac{\varepsilon_i A_i (G_i - H_i)}{1 - \varepsilon_i} \tag{9}$$

The incoming solar radiation from the window is distributed among all the surfaces of the thermal zone according to different models for the beam and diffuse fractions. The beam solar radiation transmitted by the window is distributed among all the surfaces of the thermal zone, except those that have the same exposition of the window, whilst the diffuse component is assumed to hit the floor and to be diffusely reflected by it to the other surfaces, according to the model described by Judkoff and Neymark (1995). By introducing Eq. (8) and Eq. (9) in the energy balance of the room, the temperature of all the inner surfaces can be determined (Ochs et al. 2017).

Regarding the convective balance, a simplified approach is followed here in which a single node is associated to the air of the room; this means that the convective temperature is assumed as uniform in the room (i.e. fully mixed air). As mentioned before, this assumption can be considered valid in the presence of (i) fully mixed air; (ii) low air velocity (< 0.15 m/s) which is confirmed from the measurement carried out recently by Lin et al. (2016) in presence of a mean air velocity for the convective heating system equal to 0.127 m/s and for the radiant floor equal 0.098 m/s. Air temperature is obtained by balancing the convective heat fluxes exchanged among air and walls. Convective heat transfer coefficients (h) between air and walls are calculated in agreement with the indications of EN ISO 6946-Annex A.1 (EN 2008) for all the surfaces, except for heated surfaces for which the convective heat transfer coefficient is calculated as described by Awbi and Hatton (1999). The convective heat transfer between the surface i and the convective node is calculated by using the Newton's law:

$$\dot{Q}_{CV} = h_i A_i (\vartheta_{S,i} - \vartheta_{CV}) \tag{10}$$

The temperature linked to each inner surface of the room is obtained by solving the energy balance equation of the thermal zone in which all the convective and radiative contributions are considered.

2.4 Calculation of the thermal indoor comfort indicators

The mean radiant temperature is calculated in 9 × 9 points at three different heights from the floor level (10 cm, 90 cm and 170 cm). The local values assumed by the Predicted Mean Vote (PMV), defined by Fanger (1972), can be calculated from the 3D distribution of the operative temperature in the room. Local PMV is calculated in agreement with EN ISO 7730 (EN 2006); however, the impact of thermal asimmetries on comfort conditions are not taken into account by following the Standard, since they are evaluated in a more precise way in this work by means of the reconstruction of the 3D distribution of the operative temperature.

3 The case study

3.1 The reference thermal zone

In order to show the potential of the numerical approach presented in the previous section, a typical room having a rectangular floor is considered. A complete description of the geometry of the room used as reference zone is reported in Fig. 3(a). The room is part of a one-story detached house located in Bologna (Italy, 44.30′27″ N), a Northern Italian town having a typical climate that the Köppen-Geiger climate classification (Köppen 1936) indicates as Cfa (C: warm temperate, f: fully humid, a: hot summer).

The floor is an insulated slab on grade and the roof is horizontal. The room height is 2.8 m and, as evidenced by Fig. 3(a), there are two external walls (with South and West orientation) and two internal walls. Internal walls separate the room from two heated rooms maintained at 20 °C during the whole heating season. In the simulations, the heat transfer across the internal walls is taken into account. The roof is characterized by five layers (plaster, brick, screed, insulation,

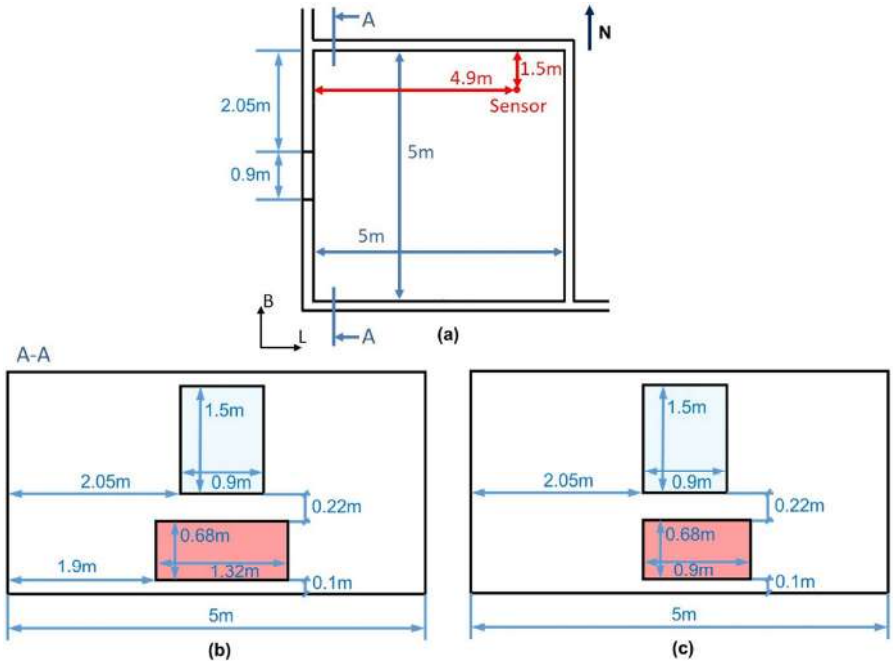

Fig. 3 (a) Plan of the room with indication of the position of the sensor; (b) position and size of window and radiator for Case A; (c) position and size of window and radiator for the Case B

waterproofed); suspended ceiling is characterized by two layers (insulation and drywall) placed 5 cm underneath the roof structure; slab on grade has four layers (tile, screed, insulation, light weight concrete); external walls have four layers (plaster, brick, insulation, plaster).

Two different insulation levels of the envelope are considered in this work (A,B). In Case A, a small insulation thickness of the envelope elements is considered; the *U*-value of external walls and floor is equal to 0.89 and 0.21 W/(m^2·K) respectively, whilst ceiling and suspended ceiling have a *U*-value equal to 0.46 and 0.24 W/(m^2·K). On the contrary, Case B refers to high insulation level of the envelope: the *U*-value of the external walls and ceiling is 0.2 W/(m^2·K), whilst floor and suspended ceiling are characterirsed by a *U*-value of 0.15 W/(m^2·K). In all the cases the internal walls are characterized by a *U*-value of 0.8 W/(m^2·K).

The window, placed on the West external wall, is a double pane window (*U*-value = 1.8 W/(m^2·K), *g*-value = 0.58) for Case A, while a triple pane window (*U*-value = 0.8 W/(m^2·K), *g*-value = 0.65) is considered for Case B.

The emissivity (ε) of the inner surfaces (active and passive) is imposed equal to 0.8. For sake of simplicity, shadings and internal loads are neglected, whilst a costant air infiltration equal to 0.3 Air Changes per Hour (ACH) is considered.

3.2 Heat emitter characteristics

Six different typologies of heat emitters will be compared each to other:

- Emitter #1: classical underfloor heating system in which pipes are immersed in the floor screed (radiant floor);
- Emitter #2: heating system obtained by immersing tubes in the ceiling mass (radiant ceiling);
- Emitter #3: light suspended insulated panels made in drywall in which the tubes are immersed (radiant suspended ceiling);
- Emitter #4: classical hot water radiator;
- Emitter #5: vertical radiant surface installed on the external wall (radiant vertical wall);
- Emitter #6: ideal all-air heating system.

Emitters #1 and #2 are embedded surface systems characterized by a very large thermal inertia; they are able to reduce the peak consumption, which can determine significant energy savings if a proper control system is implemented (Olsthoorn et al. 2017).

Emitter #3 is based on a series of light suspended drywall panels attached to the inner side of the roof with an air cavity having a thickness of 5 cm.

Emitter #4 is a classical hot water radiator placed under the window as indicated in Figs. 3(b),(c). The radiator is made by cast iron elements with low water content (1.2 L/m^3) with a value of $\dot{Q}_{nom}$ = 108 W per element and n = 1.325 (see Eq. (1)).

Emitter #5 covers the whole inner surface of the external wall without windows (see Fig. 3).

Emitter #6 is an ideal all-air heating system based on

the hypothesis of fully mixed air, which leads to a uniform air temperature distribution within the room.

The area of radiant ceiling and floor (Emitters #1 to #3) is 25 m^2 and the area of the radiant wall is 14 m^2, whilst the radiator has a surface of 0.898 m^2 (n_{el} = 12) and 0.782 m^2 (n_{el} =10) in Cases A and B, respectively.

3.3 Heating system control

A room temperature control is adopted for the modulation of the heat delivered by the heaters. The heat flux delivered by the active inner surfaces is controlled by means of two hysteresis cycles based on the active surface temperature and on the operative temperature calculated in the sensor position (Fig. 3(a)). The sensor is placed 1.5 m above the floor.

The control system maintains the operative temperature at the point in which the room sensor temperature is placed within the band 19–20.5 °C. In meantime, the control system avoids that the surface temperature of the heaters becomes larger than: (i) 75 °C for the radiator (Case 4); (ii) 29 °C for the radiant ceiling (Case 2) and suspended ceiling (Case 3); (iii) 28 °C for the radiant floor (Case 1); (iv) 40 °C for the radiant wall (Case 5).

Between these two hysteresis cycles, the control of the active surface temperature has priority on the operative temperature sensed in the room for safety reasons.

3.4 Inputs for the indoor thermal comfort analysis

In order to associate to each point of the room a value of the predicted mean vote (PMV) a series of hypotheses are made on the typical occupant of the room; more in detail, the value of the metabolic rate of the occupant is assumed equal to 70 W/m^2, whilst the mechanical power is neglected. The partial vapour pressure, uniformly distributed in the room, is set to 1160 Pa, whilst the clothing area factor and the clothes surface temperature are fixed to 1.14 (typical of an occupant with trousers and long-sleeve shirt) and 25.5 °C respectively.

4 Discussion of the results

A series of numerical dynamic simulations are made in order to study the effect of: (i) building insulation (Cases A, B) and (ii) typology of emitters (Cases 1, 2, 3, 4, 5, 6) on the local thermal comfort conditions in the room. Each case is individuated by a code; as an example, the Case A1 refers to the room with non-insulated external walls (A) in which a radiant floor (1) is adopted. All the results shown in this section are obtained by means of a yearly dynamic simulation which starts from day 212 (August, 1st) and ends to day 211 of the following year. The weather data of the Typical Meteorological Year (TMY) of Bologna are defined by Comitato Termotecnico Italiano (2018). Only the behaviour of the emitters during the winter season is considered in the analysis.

4.1 Emitters features

In this section, the different emitters are characterized during the winter season in terms of supply power, radiant power share and temperature distribution provided to the room considering the coldest day of the year and the maximum surface temperature.

4.1.1 Radiative power share

In Table 1 the percentage of radiant heat power ($\dot{Q}_R$) delivered by the heaters on the total power exchanged ($\dot{Q}_{tot}$) is shown for all the considered emitters. In the cases of a radiant floor, ceiling, suspended ceiling and radiant vertical wall this percentage is larger than 60% and it assumes its maximum value for radiant ceiling (92%) because natural convection is inhibited during winter. Hot water radiator has a limited percentage of radiant power (21%) due to strong natural convection generated around the radiator surface (in this case $n > 1.3$).

It is interesting to observe that the set point temperature of 20.5 °C is sensed by the room sensor with different combinations of convective and mean radiant temperature depending on the different radiative power share provided by the emitters. Table 2 shows the values of the convective and mean radiant temperature at the point in which the room sensor is placed (see Fig. 3(a)) when the local operative temperature reaches the set point of 20.5 °C for Case A. As expected, emitters characterized by higher radiant power share (see Table 1) are able to maintain the operative set point temperature with a lower value of indoor temperature. As an example, the set point is guaranteed with an indoor air temperature of 20.3 °C adopting the radiant floor (Case A1), 19.2 °C with the suspended ceiling (Case A3) and 21.5 °C when the hot water radiator is used (Case A4). Radiant vertical wall (Case A5) is the heater characterized by a more balanced radiant and convective power (see Table 1); in this case the set-point is reached with the same value of convective and mean radiant temperature.

Table 1 Radiative power share for the different heaters

Emitter #	1	2	3	4	5	6
$\dot{Q}_R / \dot{Q}_{tot}$	61%	92%	89%	21%	62%	0%

Table 2 Convective and mean radiant temperature in correspondence of an operative temperature of 20.5 °C measured by the room sensor during the coldest day of the year as a function of the adopted heat emitters with a low building thermal insulation level (Case A)

Case	A1	A2	A3	A4	A5	A6
ϑ_{CV} [°C]	20.3	19.5	19.2	21.5	20.5	22.2
ϑ_{MR} [°C]	20.7	21.5	21.8	19.5	20.5	18.9

4.1.2 *Inner surface temperature*

Since each emitter is characterized by a different value of the radiative power share, the value assumed by the temperature of the inner surfaces of the room is affected by the choice of the emitter, together with the building thermal insulation. In Table 3 the distribution of the inner surface temperature (ϑ_s) as a function of the emitter and of the building insulation (Cases A and B) is shown by considering the coldest day of the year, when the emitters reach their maximum surface temperature ($\vartheta_{s,max}$). In Table 3 the surface temperature of the heated surface is indicated in bold.

From Table 3 it can be appreciated that the surface temperature of the external, non-heated envelope elements increases with the thermal insulation while the temperature of the heated elements decreases. Moreover, results in Table 3 evidence that the temperature difference among the inner surfaces is reduced in presence of thermally insulated walls and this fact influences the radiative heat transfer; radiation is progressively reduced in presence of a more uniform distribution of the surface temperature among the elements of the room. In addition, Table 3 highlights how the emitters are able to work with a reduced surface temperature in thermally insulated rooms.

4.1.3 *Vertical temperature distribution*

Figure 4 shows the operative temperature profile at the centre of the room as a function of the distance from the floor (z) obtained by adopting the different heaters. The temperature profile shown in Fig. 4 refers to the coldest day of the year when the heaters reach their maximum surface temperature ($\vartheta_{s,max}$). In addition, in Fig. 4 the surface temperature of the floor (z = 0 m) and of the ceiling (z = 2.8 m) are indicated. Two horizontal dashed lines highlight the heights suggested by ASHRAE 55 (ASHRAE 2013) for the evaluation of the comfort in a room for both seated (z = 0.6 m) and standing (z = 1.1 m) occupants. ASHRAE 55 (ASHRAE 2013) recommends temperature differences less than 3 K between 0.1 and 1.7 m levels. Figure 4 shows that, for all the cases analysed in this paper, this condition is fulfilled. In fact, the maximum temperature difference between these levels is 1.1 K (for the worst case A1). For the Cases A2 and A3 the temperature difference is 0.2 K (radiant ceiling) while for the cases in which convection plays a more important role (A4, A5 and A6) this maximum difference is less than 0.1 K. Case B (larger thermal insulation of the room) is not reported in Fig. 4 for sake of simplicity since an increase of the thermal insulation is expected to reduce the vertical temperature difference.

Table 3 Inner surface distribution in the room when the emitters reach their maximum surface temperature ($\vartheta_{s,max}$) during the coldest day of the year as a function of the thermal insulation level (A or B) and of the adopted emitter

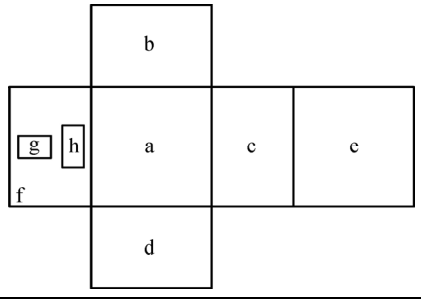

Surf.	A1	B1	A2	B2	A3	B3	A4	B4	A5	B5	A6	B6
a	**27.7**	**25.7**	20.1	20.4	20.0	19.9	19.1	20.0	20.1	19.9	18.5	19.3
b	19.9	19.9	20.2	20.3	20.2	20.1	19.6	20.1	20.1	20.0	19.3	19.8
c	19.9	19.9	20.2	20.3	20.2	20.1	19.6	20.1	20.3	20.0	19.3	19.8
d	16.9	19.2	17.2	19.6	18.2	19.5	16.9	19.5	**32.4**	**30.9**	17.2	19.1
e	18.8	19.4	**29.0**	**26.3**	**29.0**	**28.0**	18.7	19.7	19.0	19.4	18.6	19.4
f	16.9	19.2	17.2	19.6	18.0	19.5	16.7	19.4	17.5	19.3	17.0	19.1
g	14.1	17.9	15.0	18.3	15.3	18.3	13.4	17.5	14.4	18.1	13.9	17.2
h	—	—	—	—	—	—	**75.0**	**55.2**	—	—	—	—

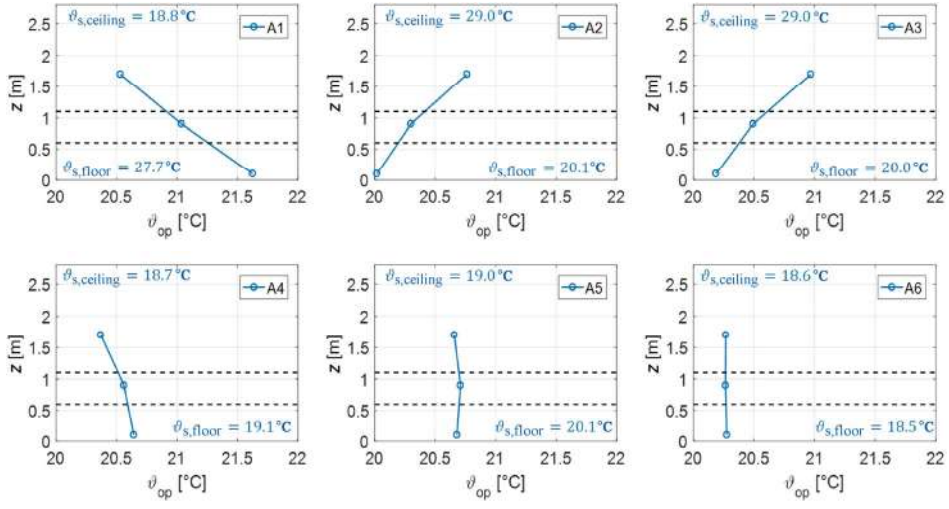

Fig. 4 Vertical profile of the operative temperature at the centre of the room during the coldest day of the year when the heaters reach their maximum surface temperature

4.1.4 Distribution of the operative temperature

Figure 5 shows the operative temperature distribution calculated at a distance of 0.1, 0.9 and 1.7 m above the floor for Cases A1, A2, A3, A4, A5, A6. In order to better highlight the differences existing among the cases presented in Fig. 5, a different scaling is used for the operative temperature plotted for each case.

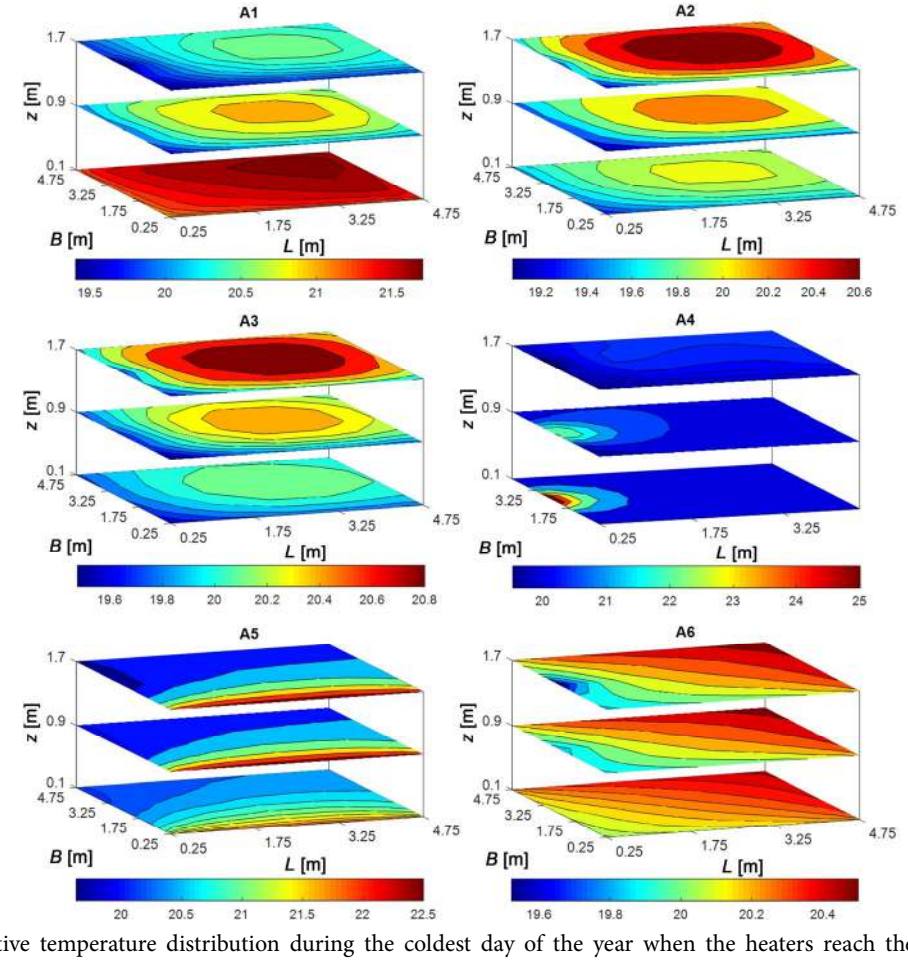

Fig. 5 Room operative temperature distribution during the coldest day of the year when the heaters reach their maximum surface temperature, at three levels above the floor (0.1 m, 0.9 m, 1.7 m) in presence of low thermal insulation (Case A)

The operative temperature distribution is obtained by considering the coldest day of the year when the heaters reach their maximum surface temperature ($\vartheta_{s,max}$). The 3D spatial distribution of the operative temperature clearly demonstrates that radiator (Case A4) and radiant wall (Case A5) generate the larger variation of operative temperature within the room due to the presence of a hot spot close to the heated surface. As underlined by Table 3, Cases A4 and A5 are characterized by the larger surface temperature of the heated surface; this large value is responsible of large operative temperature values close to the emitter. For the all-air system (Case A6), the operative temperature distribution is strongly influenced by the temperature difference existing among the inner surfaces (between the cold external walls and hot internal walls). It is important to highlight that the results obtained for Case A6 have to be considered as approximated because the model presented in this paper is not able to reconstruct the spatial distribution of the convective temperature in a room in presence of significant airflows (air velocity larger than 0.1 m/s). For radiant floor, radiant ceiling and radiant suspended ceiling (A1, A2 and A3), the operative temperature has a more uniform horizontal distribution even if the temperature vertical gradient is maximum with respect to the other emitters.

4.1.5 Emitter dynamic behaviour in presence of variable thermal loads

In presence of variable thermal loads the thermal inertia of the heat emitters becomes important in order to evaluate the capability of the system to follow the thermal building need. In order to highlight the performance of the different emitters in presence of variable thermal loads, the evolution of the operative temperature in the room during a day is analysed.

Figure 6 shows the operative temperature (ϑ_{OP}) at the point close to the inner walls in which the room sensor is placed (see Fig. 3(a)), as a function of time during the coldest winter day from 12:00 to 21:00 where the external temperature goes from −6 °C up to 1 °C. The trend of the operative temperature is shown in Fig. 6 as a function of the thermal insulation of the room by considering low (Case A) and high thermal insulation (Case B). By observing Fig. 6 it is evident how all-air heating system (Cases A6, B6) is the fastest to vary the operative temperature in the room due to the low thermal capacitance of the air node. The radiant floor (Cases A1, B1) is able to react faster than the radiant ceiling (Cases A2, B2), due to higher convective power share guaranteed during winter. On the other hand, the radiant floor (Cases A1, B1) and ceiling (Cases A2, B2) are both significantly slower than suspended ceiling heater (Cases A3, B3), due to the lower active mass of the suspended panel which is based on light elements (i.e. drywall).

In presence of low thermal insulation, the suspended ceiling heater (Case A3), is switched off before the room reaches the set point value of the operative temperature (20.5 °C) because the surface temperature reaches its maximum value (29 °C). This observation is still valid for Case A2. These results put in evidence that for Case A (room with a low level of thermal insulation) suspended ceiling (3) and radiant ceiling (2) are not able to cover completely the maximum winter thermal load of the room due to the reduced contribution of the natural convection. In these cases, the set up value of the operative temperature in the room can be reached only by increasing the surface

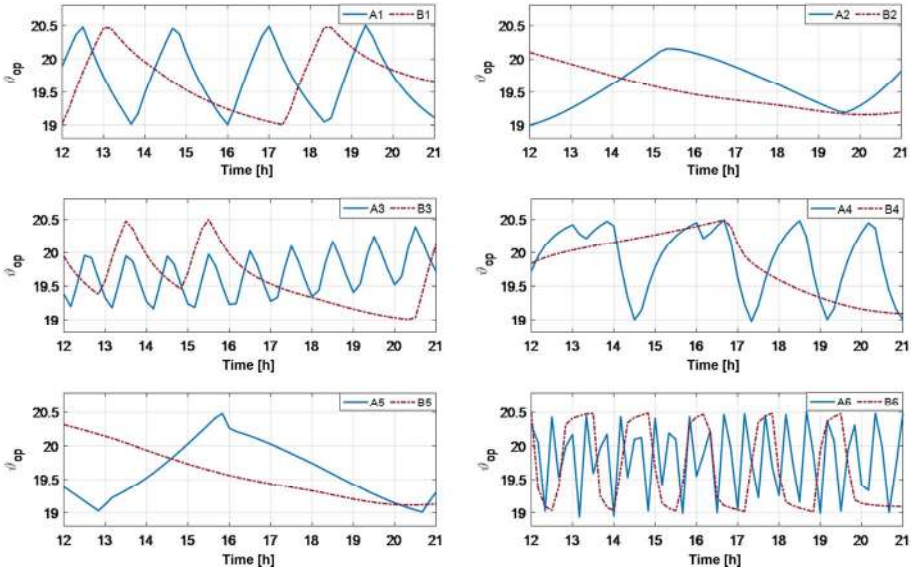

Fig. 6 Room operative temperature sensed during the coldest winter day by the room sensor in presence of different emitters and envelope thermal insulation

temperature of the radiant ceiling over 29 °C.

In addition, Fig. 6 underlines that all the heating systems here considered need more time to reach the set point (20.5 °C) when the building insulation level is increased. In fact, with higher thermal insulation level the thermal power delivered by the emitters is reduced, the temperature of the non-heated room inner surfaces increases and the surface temperature of the radiant emitters decreases (see Table 3).

In Table 4 the maximum thermal power emitted per square meter of the floor and the maximum surface temperature of the emitters in presence of different thermal insulation of the envelope are reported. As previously underlined, the temperature of the inner surfaces (and the convective temperature for the Case 6) decreases as well as the total emitted thermal power when the envelope thermal insulation increases. However, high thermal insulation allows to increase the period in which the operative temperature can be maintained within the band of 19–20.5 °C while the emitter is switched off. It is interesting to calculate the interval of time needed by the emitters to increase the local operative temperature of the point in which the room sensor is placed (see Fig. 3(a)) from 19 °C to 20.5 °C ($\Delta\tau_{on}$) as well as the interval of time in which the operative temperature at the same point decreases from 20.5 °C to 19 °C when the heating system is switched off ($\Delta\tau_{off}$). The sum of $\Delta\tau_{on}$ and $\Delta\tau_{off}$ can be linked to the hourly number of on-off cycles of the heating system.

Figure 7 shows the characteristic time $\Delta\tau_{on}$ and $\Delta\tau_{off}$ obtained for the different emitters by considering a room with a different level of thermal insulation (Cases A and B). The characteristic time is carried out by considering all the on-off cycles done by the different emitters in the coldest month (January). The characteristic time $\Delta\tau_{on}$ depends on many factors associated to the building and emitters characteristics (i.e. the emitter heating capacity, the istantaneous heating demand etc.), while the characteristic time $\Delta\tau_{off}$ depends mainly on the building heat losses and thermal capacity. Figure 7 underlines that the heaters with higher thermal inertia (i.e. radiant floor (1), ceiling (2) and wall (5)) determine higher $\Delta\tau_{on}$ and $\Delta\tau_{off}$ values with respect to the low capacity emitters; by increasing the building thermal insulation (from Case A to Case B) all the emitters increase both $\Delta\tau_{on}$ and $\Delta\tau_{off}$.

Table 4 Maximum specific emitted thermal power as a function of the emitter and of the thermal insulation level (A, B)

		1	2	3	4	5	6
Case A	$\dot{Q}_{tot,max}$ [W/m^2]	67	48	53	57	55	60
Case B	$\dot{Q}_{tot,max}$ [W/m^2]	45	30	43	26	46	31

4.1.6 *Local indoor thermal comfort conditions*

By knowing the yearly local distribution of the operative temperature in the room it is possible to derive detailed information about the indoor thermal comfort conditions provided by the different emitters. The contour plots reported in Fig. 8 give information about the percentage of time during the whole winter in which a local value of PMV between ±0.5 is guaranteed. In Fig. 8 the results obtained with different emitters for a control dead band equal to 19–20.5 °C and different thermal insulation levels (A and B) can be compared each to other. As general observation, when the external walls have a high thermal insulation (Case B) the points of the room close to the external walls remains warmer, therefore the PMV distribution becomes more uniform with respect to Cases A, regardless the emitter. In fact, it can be observed that the minimum value of the percentage of time in which PMV assumes values between ±0.5 increases with the thermal insulation of the external walls for all the emitters considered here; this means that it becomes possible to maintain the room in optimal indoor comfort conditions longer during the year.

With a radiant floor (1) the temperature difference between the feet and the head region rises, leading to a higher risk of local discomfort in the head region, as observed by Lin et al. (2016). However, by comparing Case A1 with Case B1 reported in Fig. 8 it is evident that the region where the occupants may feel the "cold head" effect is strongly reduced by increasing the thermal insulation of the room.

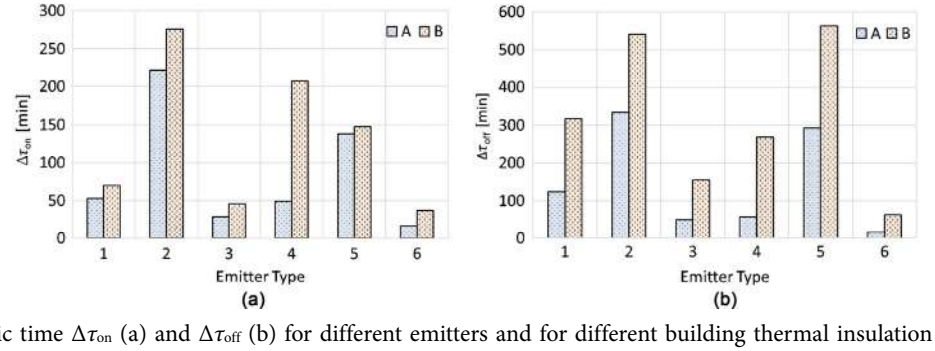

Fig. 7 Characteristic time $\Delta\tau_{on}$ (a) and $\Delta\tau_{off}$ (b) for different emitters and for different building thermal insulation by considering the dead band of the control system equal to 19–20.5 °C

The radiant ceiling (2, 3) generate a lower vertical temperature difference with respect to the radiant floor (see Fig. 4). By comparing the values of the percentage of time in which PMV assumes optimal values close to the floor (z = 0.1 m) for Cases A1, B1, A2, B2, A3, B3 it is evident that lower values are generally obtained in presence of radiant ceiling systems ("cold feet" effect). Between the radiant ceilings (2, 3) lower values are obtained for suspended ceiling (A3, B3). Also in this case, the values become larger and more uniformly distributed in space within the room in presence of higher thermal insulation. Window generates a cold spot close to the external wall which is more evident in presence of high thermal insulation. The installation of a radiator below the window mitigates the effect of the cold transparent envelope element. The radiator (A4, B4) is able to guarantee a uniform distribution of PMV, especially in presence of highly insulated external walls, even if close to the radiator a hot spot is present which determine large local PMV values. However, since the present model uses a single convective node, the spatial distribution of the convective temperature in the room is approximated and, for this reason, the results shown in Fig. 8 have to be considered less accurate for emitters in which the radiative power share is lower (see Table 1). The same conclusion is valid for all-air systems (A6, B6). In these systems the air velocity and the local temperature fluctuations, linked to the fast reaction of these systems to the thermal load variation (see Fig. 6), could play an important role on the distribution of the thermal indoor comfort conditions in the room. Depending on the position of the inner warm air source, there would be a warmer zone and therefore a non-uniform air temperature distribution in the room which is not accounted for in these simulations. For these reasons, in the next future the model will be improved by adding a detailed

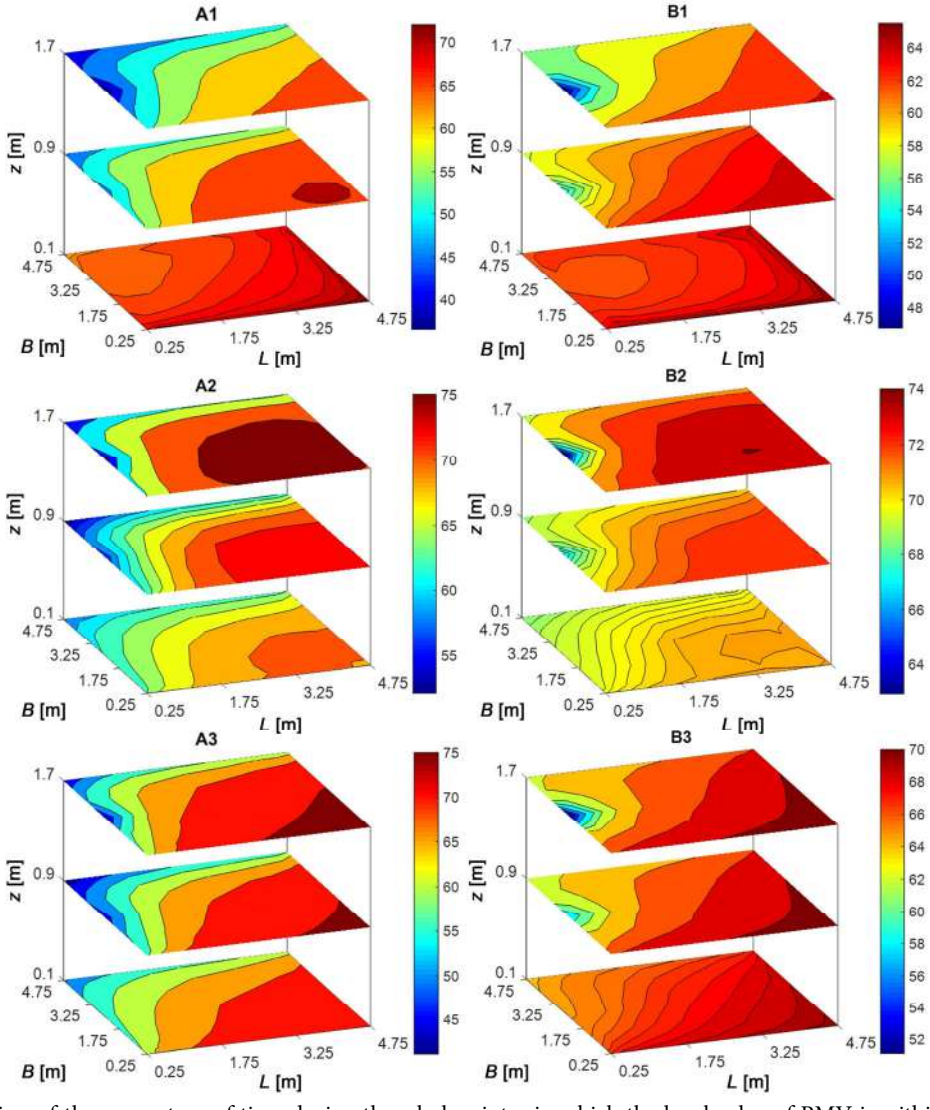

Fig. 8 3D distribution of the percentage of time during the whole winter in which the local value of PMV is within ±0.5, for different emitters and building insulation level

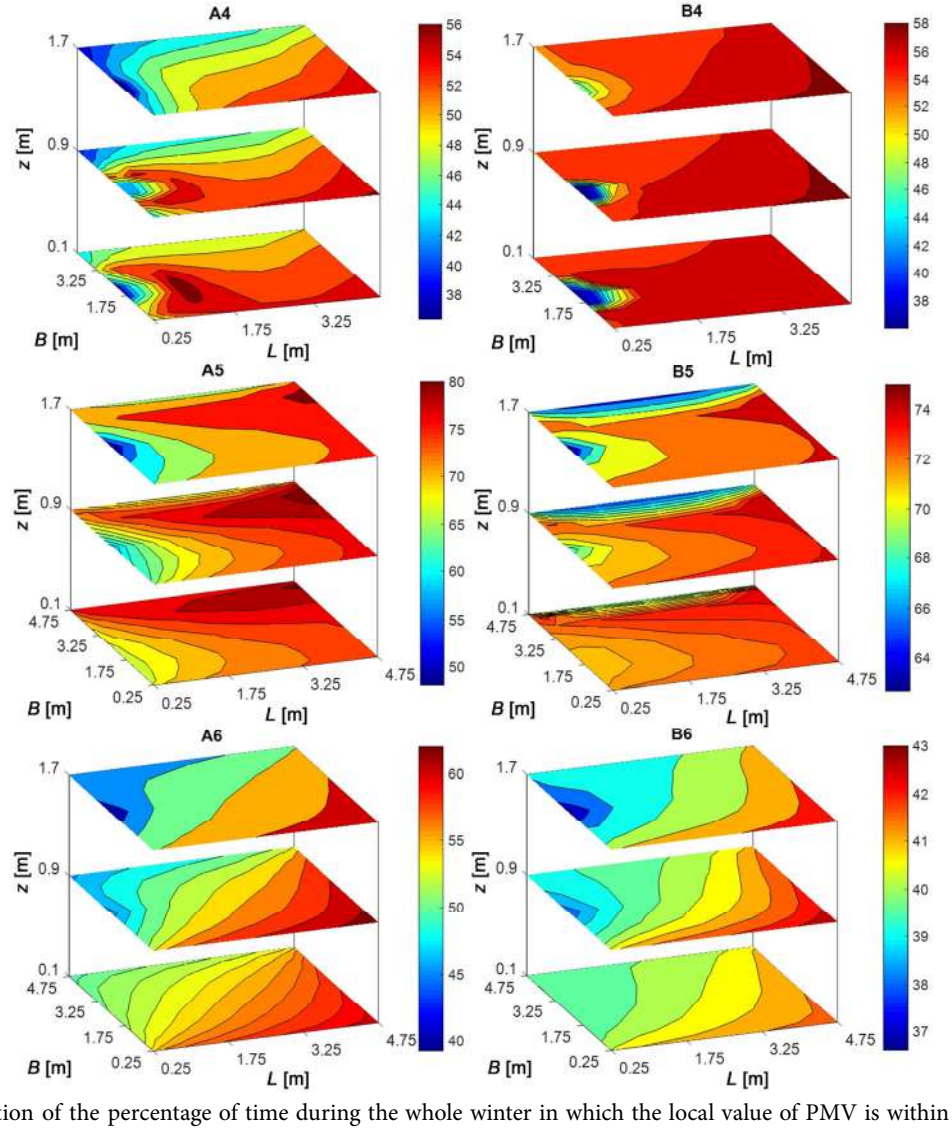

Fig. 8 3D distribution of the percentage of time during the whole winter in which the local value of PMV is within ±0.5, for different emitters and building insulation level (Continued)

convective model based on the "zonal approach" (Megri and Haghighat 2007) in order to enable the evaluation of the air temperature spatial distribution in the room.

5 Conclusions

A dynamic model able to calculate the local distribution of the mean radiant temperature in a room has been presented. The model allows a fast evaluation, in terms of computational time, of the view factors associated to the inner points of a room thanks to the use of the MATLAB Contour Double Integral Formula (CDIF). This calculation method has been validated by comparing the results, in terms of view factors, with those obtained with commercial software (i.e. COMSOL and TRISCO).

The model has been used in order to study the effect of the heat emitters on the local indoor thermal comfort conditions in a reference room by means of a series of yearly dynamic simulations performed by using the ALMABuild blockset, a SIMULINK library for energy dynamic simulations. Six different heating systems (i.e. in-slab radiant floor, in-slab radiant ceiling, radiant suspended ceiling, hot water radiator, radiant wall and all-air system) have been modelled by considering different building thermal insulation levels. The numerical results demonstrate that in-slab ceiling is characterized by the highest radiative power share (92%) and therefore by the highest difference between radiative and convective temperature. The vertical distribution of the operative temperature has been calculated as a function of the emitter. About the behaviour of the emitters in presence of dynamic thermal loads, the numerical results demonstrate that all-air heating systems are faster than

radiant systems. The suspended radiant ceiling is 80% faster with respect to the in-slab radiant ceiling to raise the temperature of the room from 19 to 20.5 °C in presence of low thermal insulation of the walls. However, due to the reduced contribution of the convective heat transfer component in winter, radiant ceiling can have problems to provide enough thermal power to the thermal zone, in particular for rooms having a low thermal insulation. It has been shown that an increase of the envelope thermal insulation is able to reduce the maximum surface temperature of the emitters and it is responsible for a more uniform distribution of the inner surface temperature in the room. In order to study the local indoor thermal condition distribution in the room during the whole winter, by means of a series of dynamic simulations the percentage of time in which the local PMV assumes values between ±0.5 (optimal comfort conditions) has been calculated by varying the emitter and the room thermal insulation. The results show that radiant floor is able to guarantee good performances both in thermally insulated and in non-thermally insulated rooms. On the contrary, radiant ceiling and radiant vertical walls have to be used only in rooms having a good thermal insulation level in order to optimize their performances. As a general conclusion, the detailed numerical results presented in this paper demonstrate that in buildings with very low transmission losses the differences existing among the selected emitters are strongly attenuated. In fact, a more uniform distribution of the temperature of the inner surfaces of the room is able to reduce the differences between convective and radiant emitters in terms of capability to obtain uniform indoor thermal comfort conditions. On the contrary, in presence of low thermal insulation levels, a proper selection of the heat emitter can drastically reduce the local thermal discomfort conditions in a thermal zone. For this reason, the diffusion of this kind of numerical tools to the HVAC designer is highly desiderable. This will enable them to replicate the approach described in this paper with reduced computational costs and programming skills.

Acknowledgements

The research has received funding in the frame of the Emilia-Romagna Regional development fund POR-FESR 2014-2020 Programme under the NANOFANCOIL project.

References

ASHRAE (2013). ASHRAE STANDARD 55. Thermal Environmental Conditions for Human Occupancy. Atlanta: American Society of Heating and Air Conditioning Engineers.

ASHRAE (2017). Handbook Fundamentals. Atlanta: American Society of Heating and Air Conditioning Engineers.

Awbi HB, Hatton A (1999). Natural convection from heated room surfaces. *Energy and Buildings*, 30: 233–244.

Baehr HD, Stephan K (2006). Heat and Mass Transfer, 2nd edn. Berlin: Springer.

Bojić M, Cvetković D, Miletić M, Malešević J, Boyer H (2012). Energy, cost, and CO_2 emission comparison between radiant wall panel systems and radiator systems. *Energy and Buildings*, 54: 496–502.

Bojić M, Cvetković D, Bojić L (2015). Decreasing energy use and influence to environment by radiant panel heating using different energy sources. *Applied Energy*, 138: 404–413.

Campana JP, Magni M, Dongellini M, Morini GL (2017). The benchmark of a new SIMULINK library for thermal dynamic simulation of buildings. In: Proceedings of Building Simulation Applications (BSA 2017), Bolzano, Italy.

Comitato Termotecnico Italiano (2018). Test Reference Year. Available at https://try.cti2000.it. Accessed 8 Jan 2018.

COMSOL (2017). COMSOLMultiphysics Reference Manual, version 5.3", COMSOL, Inc. Available at http://www.comsol.com. Accessed 22 Sept 2017.

EN (2006). EN ISO 7730. Ergonomics of the thermal environment—Analytical determination and interpretation of thermal comfort using calculation of the PMV and PPD indices and local thermal comfort criteria. Brussels: European Committee for Standardization.

EN (2008). EN ISO 6946—Annex A.1. Building components and building elements—Thermal resistance and thermal transmittance—Calculation method. Brussels: European Committee for Standardization.

EN (2014). EN 442–2. Radiators and convectors: Test methods and rating. Brussels: European Committee for Standardization.

Fanger PO (1972). Thermal Comfort: Analysis and Applications in Environmental Engineering. New York: McGraw-Hill.

Judkoff R, Neymark J (1995). International Energy Agency building energy simulation test (BESTEST) and diagnostic method, No. NREL/TP-472-6231. Golden, CO, USA: National Renewable Energy Laboratory.

Karmann C, Schiavon S, Bauman F (2017). Thermal comfort in buildings using radiant vs. all-air systems: A critical literature review. *Building and Environment*, 111: 123–131.

Köppen W (1936). Das geographische System der Klimate.Handbuch der Klimatologie, vol. 1. Berlin: Borntraeger.

Lauzier N, Rousse D (2017). MATLAB function that calculates view factors between two planar surfaces. Available at https://it.mathworks.com/matlabcentral/fileexchange/5664-view-factors. Accessed 22 Sept 2017.

Lin B, Wang Z, Sun H, Zhu Y, Ouyang Q (2016). Evaluation and comparison of thermal comfort of convective and radiant heating terminals in office buildings. *Building and Environment*, 106: 91–102.

Megri AC, Haghighat F (2007). Zonal modeling for simulating indoor environment of buildings: Review, recent developments and applications. *HVAC & Research*, 13: 887–905.

Mustakallio P, Kosonen R, Korinkova A (2017). Full-scale test and CFD-simulation of radiant panel integrated with exposed chilled beam in heating mode. *Building Simulation*, 10: 75–85.

Ning B, Schiavon S, Bauman FS (2017). A novel classification scheme for design and control of radiant system based on thermal response time. *Energy and Buildings*, 137: 38–45.

Ochs F, Magni M, Bianchi M, Siegele D (2017). Steady state and transient simulation of a radiant heating system. In: Proceedings of Building Simulation Applications (BSA 2017), Bolzano, Italy.

Olsthoorn D, Haghighat F, Moreau A, Lacroix G (2017). Abilities and limitations of thermal mass activation for thermal comfort, peak shifting and shaving: A review. *Building and Environment*, 118: 113–127.

Physibel (2010). TRISCO, version 13.0w [Software]. Maldegem, Belgium: Physibel.

Rhee KN, Kim KW (2015). A 50 year review of basic and applied research in radiant heating and cooling systems for the built environment. *Building and Environment*, 91: 166–190.

Rhee KN, Olesen BW, Kim KW (2017). Ten questions about radiant heating and cooling systems. *Building and Environment*, 112: 367–381.

Wolfgang F (1994). Thermische Gebäudesimulation: kritische Prüfung unterschiedlicher Modellansätze. Heidelberg: Verlag C.F. Müller.

Zhang C, Heiselberg PK, Chen Q, Pomianowski M (2017). Numerical analysis of diffuse ceiling ventilation and its integration with a radiant ceiling system. *Building Simulation*, 10: 203–218.

5.5 Publication E

Title

Analysis of the impact of different HVAC configurations and control strategies on primary energy and cost savings for an office building

Authors

Mara Magni, Fabian Ochs

Published in

13th IEA Heat Pump Conference May 11-14, 2020 Jeju, Korea
ISBN 978-91-89385-48-1

Own contribution

The dynamic simulations and the analysis of the results as well as the writing of this paper were carried out by the first author while the second author contributed to this work by reviewing the manuscript.

13th IEA Heat Pump Conference
May 11-14, 2020 Jeju, Korea

Analysis of the impact of different HVAC configurations and control strategies on primary energy and cost savings for an office building

Mara Magni[a], Fabian Ochs[a]

[a]University of Innsbruck, Technikerstraße 13, Innsbruck 6020, Austria

Abstract

In order to mitigate climate change, sustainable and responsible use of resources is required. In the present study, different technologies applicable for the renovation of an office building are evaluated considering, both economic feasibility and environmental impact for the climates of Rome Stuttgart and Stockholm. Decentralized heating and cooling systems represented by different types of heat pumps (i.e. air-to-air On/Off and modulating) are considered in combination with photovoltaic panels (PV), battery and efficient lighting (LED) in order to investigate the achievable energy savings and the additional cost. The environmental impact is evaluated in terms of electricity and total primary energy (PE) savings calculated with constant and monthly conversion factors representing different scenarios with different share of renewables in the electricity mix.
It was observed that the energy savings calculation method influences the ranking of renovation packages. High-energy savings with low additional cost are achievable with HP in combination or not with LED and PV, in Stockholm and Stuttgart, and with LED and PV in combination with electric heating in Rome. Battery brings additional energy savings with high additional cost.

Selection and/or peer-review under responsibility of the organizers of the 13th IEA Heat Pump Conference 2020.

Keywords: Cost optimality; Energy simulations; Office building renovation; HVAC;

1. Introduction

In spite of higher efficiency, the energy consumption of buildings has increased over the past decades and the European Union has set restrictive targets. To reach these goals, buildings have to be transformed from energy consumer to energy provider. In non-residential buildings, the available façade area for the installation of a renewables based system is limited and an optimization of the building system is required in order to reduce the primary energy demand.

The recast of the Energy Performance of Buildings Directive [1] states that member state (MS) must ensure that minimum energy performance requirements for buildings are set "with a view to achieve cost-optimal levels" in terms of global cost and primary energy need. The cost-optimal level must be calculated in accordance with a comparative methodology.

In the literature, some studies dealing with both economic feasibility and environmental impact for office buildings are present but they do not consider different scenarios for the evaluation of the influence of the electricity mix. Pikas E. et al. [2] is focused on the building envelope considering different fenestration design solutions. Gustafsson M. et al. [3] investigated energy renovation packages involving centralized heating and cooling system, windows, envelope insulation and solar photovoltaics (PV), for European office buildings. Sanja Stevanović presented a cost optimality study [4] for an office building located in Serbia where the cooling demands is predominant.

* Corresponding author. Tel.: +43-512-507-63619
E-mail address: Mara.Magni@uibk.ac.at

Ochs F, et al. [5] introduces a PE evaluation method considering different future development of the load (i.e. building stock) and electricity mix (share of REs) with seasonal variations. This works highlight the need of an appropriate evaluation method for comparing and ranking different passive and active technologies on micro- and macro- economic scale. Different EU MS adopts different national conversion factors for PE/CO_2, which are subject to change [5]. Seasonal variations are not considered at all, although the share of renewables within the period of consideration (e.g. 20 years) should be included [5].

In this work different HVAC retrofit solutions (i.e. HP, PV, Batteries, LED etc..) are compared against a reference case involving an electric heating system with an On/Off split unit for cooling and fluorescent lamps combining both economic and environmental analysis. A sensitivity analysis is carried out in order to evaluate the influence of input parameter (i.e. interest rate, investment cost and electricity price) on the results of the economic analysis. The environmental analysis is performed using different share of renewables in the electricity mix showing the impact of the development of increasingly share of RE on the ranking of the different retrofit solutions.

2. Method

2.1. Building model and boundary conditions

The reference building is chosen in order to be representative of a typical European office cell located in middle floor of a high-rise building [6]. Three different European climates are considered in this study: Rome (Mediterranean), Stuttgart (cold moderate) and Stockholm (cold climate). Fig. 1 shows the considered office cell, which has a heated area of 27 m^2 and a volume of 81 m^3. All the surfaces are considered adiabatic, except for the façade oriented toward South (with window-to-wall ratio of 60%) where ambient boundary conditions are applied. Shading from adjacent obstacles is not considered, whereas an external movable shading, able to block 70% of the incoming radiation, is activated when direct solar radiation impinging the south façade is higher than 120 W/m^2.

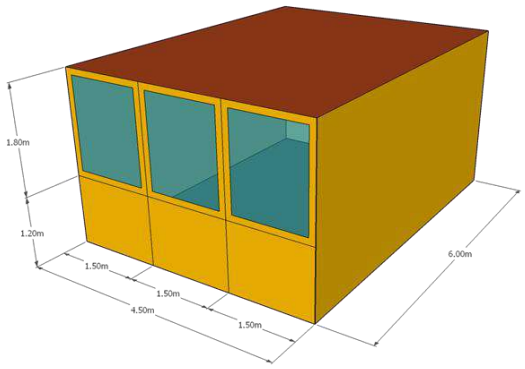

Fig. 1. View of the reference office zone [6]

Table 1 shows the yearly average ambient temperature ($T_{amb,av}$), yearly global irradiation over a horizontal surface ($I_{g,h}$) and yearly irradiation over a south oriented vertical surface (I_{south}) for each climate.

The thermal transmittance of the façade elements ($U_{ext,wall}$) and the characteristics of the windows such as the thermal transmittance (U_{win}), the solar heat gain coefficient (g-value) and the solar transmittance (τ_{sol}) depend on the three climates, as shown in Table 1. The internal walls are typical plasterboard walls, the exterior wall is a three layer structure with different insulation thicknesses depending on the climate.

User behavior (e.g. occupancy, appliances and lighting) is taken into account by means of hourly profiles, different for week and weekend days [7]. A contemporaneity index of 0.8 is used for occupancy and appliances. Three persons are present during the working time and a sensible and latent heat of 70 W/person and 0.08 kg/h/person are considered. The internal gain due to appliances is assumed to be 7 W/m^2 and the electric gain due to lighting is 10.9 W/m^2. The lighting schedule follows occupied hours and is defined considering a non-daylight responsive system

The natural infiltration rate is assumed to be constant and equal to 0.15 1/h. A fresh air supply of 40 m^3/h/person is covered by a mechanical ventilation system with heat recovery (70% sensible efficiency), which is active only during the working time (i.e. from Monday to Friday from 8:00 am until 08:00 pm).

Table 1. Main properties of the south oriented façade and climates [6]

	$T_{amb,av}$ [°C]	$I_{g,h}$ [kWh/m^2]	I_{south} [kWh/m^2]	$U_{ext,wall}$ [W/m^{2}K]	U_{win} [W/m^{2}K]	g-value [-]	τ_{sol} [-]
Rome	15.8	1632	1253	0.80	1.26	0.33	0.462
Stuttgart	9.9	1101	889	0.40	1.35	0.59	0.426
Stockholm	7.8	952	884	0.20	0.90	0.63	0.260

An anti-freezing resistance is heating up the ambient air when the external temperature falls below 0°C while a bypass of the heat recovery is activated when the temperature of the zone is higher than 23 °C and the ambient temperature is lower than the indoor temperature. The set point temperature for the indoor convective temperature during the wintertime and summertime are 21°C and 25°C. A detailed description of the boundary conditions is reported in D'Antoni, et al. [6]. The building model is developed in Matlab/Simulink and it has been validated against other dynamic simulation tools [8].

2.2. Renovation packages

The renovation packages discussed in this paper include the combination of different heating, cooling and lighting technologies optionally combined with PV and battery without modifying to the envelope. In addition, the effect of different control strategies is considered.

Table 2 reports all the technologies involved in this study highlighting in bold the reference system used for the comparison (i.e. electric heating and On/Off HP for cooling with a standby consumption running for the entire year, fluorescent lighting and the reference control system for the ventilation and free-cooling described in section 2.1). The electric heating system can be retrofitted with either a simple On/Off or improved modulating HP that might cover also the cooling load.

In the reference case the free cooling can be activated only during the working time therefore savings in terms of cooling demand can be achieved when the free cooling is activated every time the internal and external conditions makes it effective.

Switching off completely the cooling system during the winter season, enable savings by reducing the standby consumption. Switching off the heating and cooling systems during non-occupied periods (night set-back) might enable further savings. Moreover, using modern LED instead of fluorescent lamps can approximately halve the electricity consumption for lighting purpose.

Table 2. Characterization of the investigated renovation components

	Options	Description
Heating	**Direct electric**	Electric resistance, efficiency equal to 1.
	On/Off (Split type) HP	See Fig. 2. Two different On/Off HP sizes are considered.
	Modulating (Split type) HP	See Fig. 2.
Cooling	**On/Off** (Split type) Air-Con.	See Fig. 2. Two different On/Off HP sizes are considered.
	Modulating (Split type) Air-Con.	See Fig. 2.
PV	Mono-crystalline silicon	PV installed in the available wall area (5.4 m^2) in the south façade with an efficiency of 17.7% and a peak power of 877 Wp.
Battery	Ideal battery	Efficiency of 90% (4kWh capacity).
Control	HP and mechanical ventilation	**On/Off HP** and PI for the modulating HP, for the mechanical ventilation see the building description.
	Free cooling 7/7	Free cooling can be activated every time the internal and external conditions makes it effective.
	Improved standby consumption	Standby consumption of 10W accounted only during the working season of the considered technology (instead of the whole year).
	Night set back	The heating and cooling systems are switched off during non-occupied periods and restarted 4h before the working time.
Lighting	**Fluorescent**	10.9 W/m^2 (500 lux on the working desk, 8 luminaire).
	LED	5.45 W/m^2 (500 lux on the working desk, 8 luminaire).

As specified in Table 2, two On/Off HP with different sizes and one modulating HP are considered in this work. The main characteristics (i.e. COP, EER, heating and cooling power and air volume flows) are reported in Table 3 and the maps of performances in Fig. 2.

Table 3. Main characteristics of the modulating and On/Off heat pumps. The heating power and COP are specified for the external air temperature of 15°C and internal of 22°C while the cooling power and EER are specified for the external air temperature of 35°C and internal of 27°C. For the modulating HP the performances are specified for the maximum f_{max} and minimum f_{min} frequency.

	Internal air volume flow [m³/h]	External air volume flow [m³/h]	Heating power (15°C/22°C) [W]	Cooling power (35°C/27°C) [W]	COP (15°C/22°C) [-]	EER (35°C/27°C) [-]
Modulating HP	648	1872	f_{max}: 4006 f_{min}: 1006	f_{max}: 2510 f_{min}: 1248	f_{max}: 5.44 f_{min}: 5.86	f_{max}: 5.29 f_{min}: 5.05
On/Off HP low power	187	1872	523	1250	4.12	4.28
On/Off HP high power	648	1872	3923	2510	5.38	5.29

Fig. 2 shows the performances of the modulating, On/Off low (lp) and high (hp) power heat pumps in cooling and heating operation used in the simulations. The COP of the On/Off HP (Fig. 2.2b) considers a degradation of the performance due to deicing when the ambient temperature is between 7°C and 2°C. The modulating HP is modelled with a separated deicing model therefore the COP reported in Fig. 2.1b does not consider the losses due to deicing operation.

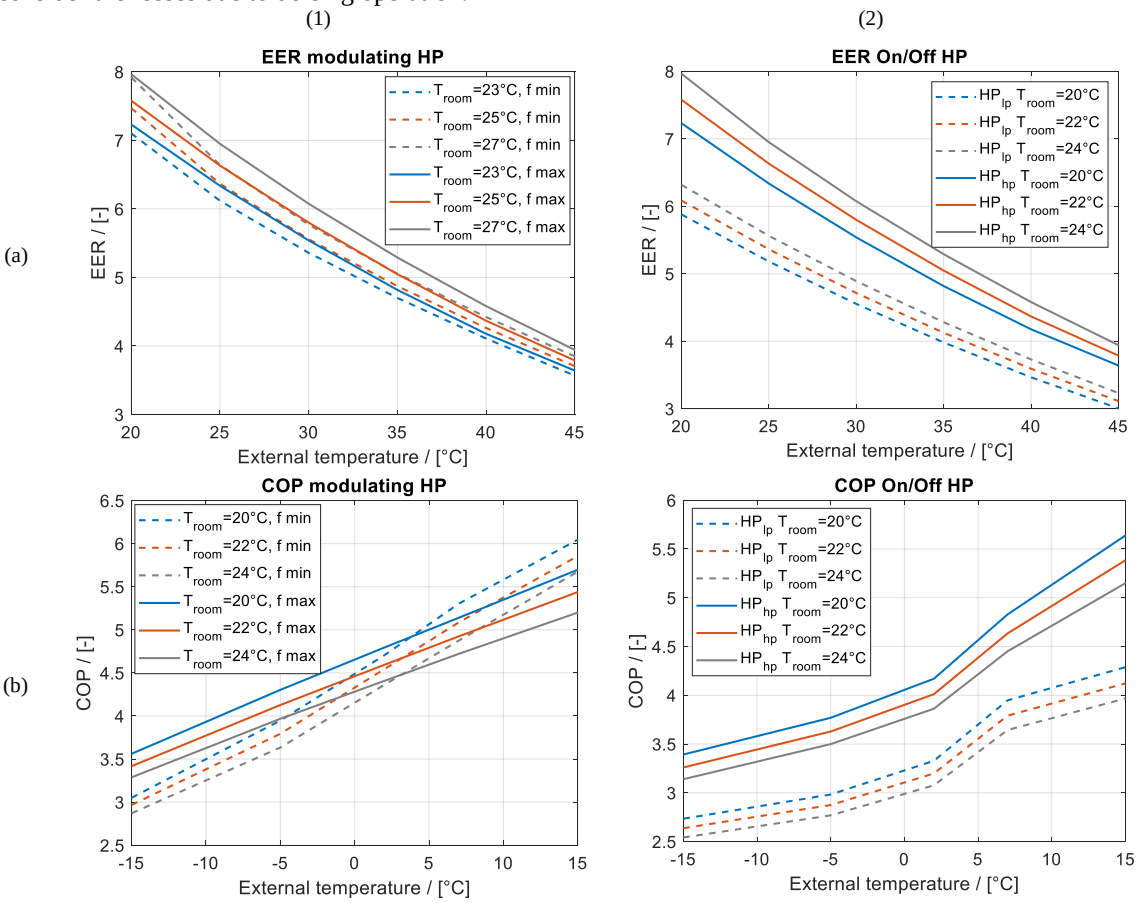

Fig. 2. Maps of performances of the modulating (1) and low power (lp) and high power (hp) On/Off (2) heat pump in cooling (a) and heating (b) mode

The schemes of the control system used for the On/Off and modulating HP are reported respectively in Fig. 3a and Fig. 3b. The On/Off HP is controlled with an hysteresis (±0.5 K) having as input the temperature difference between the heating set point and the air temperature ($T_{set,H}$-T_{air}) during the heating mode and the temperature difference between the air temperature and the cooling set point (T_{air} -$T_{set,C}$) during the cooling mode. The Look-up-Tables (LuT) deliver as output the COP/EER, the absorbed electric power (P_{el}) and the delivered thermal power ($\dot{Q}_{th}$). The transfer function (TF) with a time constant of 130 s is necessary to slow down the

system response and makes the heat pump behaviour more realistic. The LuT have as input the control signal, the air temperature (T_{air}) and the ambient temperature (T_{amb}).
The modulating HP is controlled with a proportional integral (PI) control having as input $T_{set,H}$-T_{air} during the heating mode and T_{air}-$T_{set,C}$ during the cooling mode. The equation (1) shows the PI control rule where the proportional parameter K_p is equal to 1 and the integral time constant T_n is equal to 418.7 s.

$$f(t) = K_p \cdot \left(err(t) + \frac{1}{T_n} \cdot \int err(t)\, dt \right) \tag{1}$$

The control system of the modulating HP includes also a minimum run (t_{ON}) and off (t_{OFF}) time and the deicing (ctr_{deic}). The deicing cycle, which last 600 s, starts only when the time counter reaches the defined waiting time that is a function of the ambient temperature (i.e. 11460 s for an ambient temperature of -7°C and 2406 s for an ambient temperature of 5°C). During the deicing cycle, the HP absorbs electric energy without delivering any thermal energy to the room. When the HP is switched on and is not performing the deicing cycle, it is forced to remain in operation with a frequency between the minimum and the maximum until the minimum run time counter reaches the threshold of 300 s. In the same way, when the HP is switched off, it is forced to remain in this status until when the minimum off time counter reaches the threshold of 600 s.

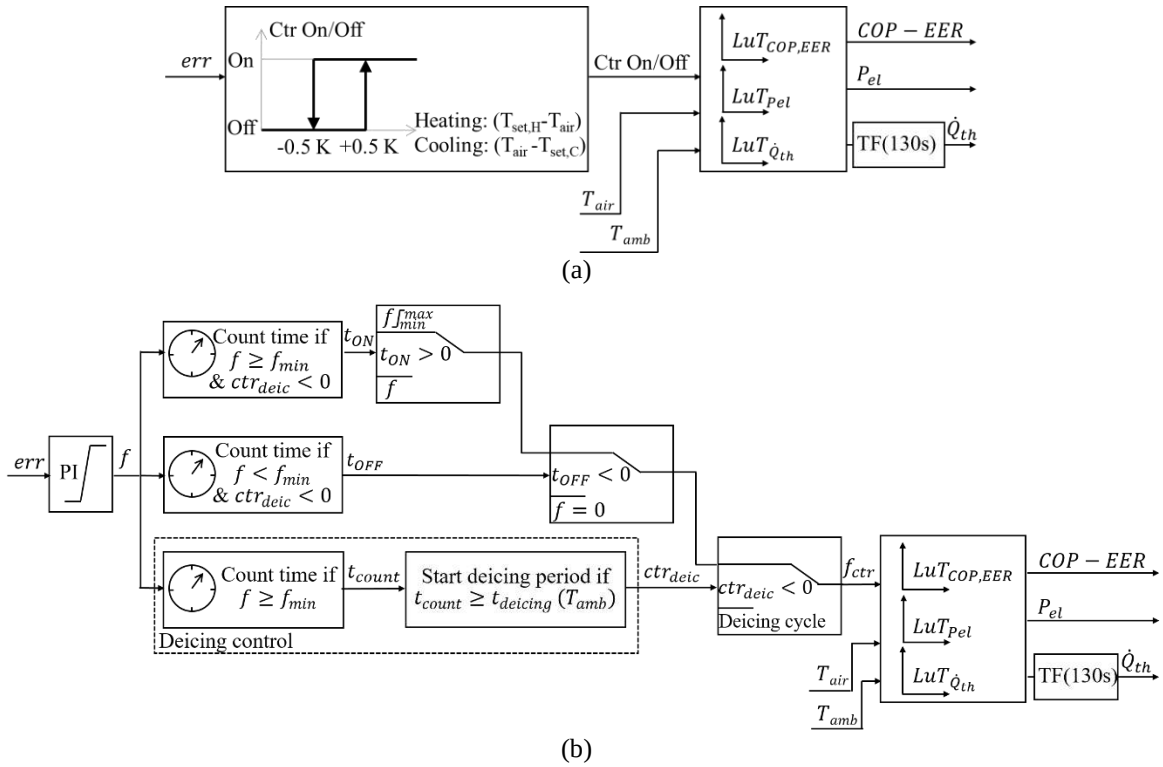

Fig. 3. Control of (a) On/Off and (b) modulating HP

The PV model from the Matlab/Simulink CARNOT library [9] is based on equation (2) and (3).

$$\mathrm{Power_{PV}} = \left((25 - \mathrm{T_{module}}) \cdot \Delta \mathrm{W_{p,T}} + 1 \right) \cdot \mathrm{W_p} \cdot \mathrm{f_{gen}} \cdot \frac{\mathrm{Q_{solar}}}{1000} \tag{2}$$

$$\mathrm{T_{module}} = \frac{\mathrm{Q_{solar}}}{1000 \left(\frac{\mathrm{W}}{\mathrm{m^2}} \right)} \cdot 40 + \mathrm{T_{amb}} \ [°\mathrm{C}] \tag{3}$$

Where:

- $\Delta \mathrm{W_{p,T}} = 0.00375$ is the temperature coefficient [1/K];
- $\mathrm{W_p} = 877\ \mathrm{W}$ is the peak power [W];
- $\mathrm{f_{gen}} = 1 - 0.03$ is the efficiency of the PV considering losses in diodes, power mismatch and dirt;
- $\mathrm{Q_{solar}}$ is the solar irradiation impinging the PV panel corrected with the Incidence Angle Modifier (IAM).

The model of the inverter is provided by the CARNOT library [9]. It considers a standby consumption of 1 W and the efficiency is a function of the output power (i.e. when the output power is between 300 W and 3600 W the efficiency is above 0.95).

2.3. Economic analysis

The economic analysis adopted in this work is based on the Equivalent Annual Cost (EAC), considering investment and running costs over a reference lifetime (N). EAC is the annual cost of owning, operating, and maintaining an asset over its entire life, it allows comparing the cost-effectiveness of various assets that have unequal lifespans. Equation (4) shows the calculation of the EAC:

$$\mathrm{EAC} = \frac{\mathrm{IC} \cdot \mathrm{r}}{1-(1+\mathrm{r})^{-\mathrm{N}}} \tag{4}$$

Where r is the real interest rate (3%). The total annual cost is calculated, for electrically driven systems, as:

$$Total\ \ annual\ \ cost = EAC + MC + FE \cdot el_{price} \tag{5}$$

Where MC is the yearly maintenance cost, FE is the final electric energy and el_{price} is the electricity price that is assumed to be 0.2 €/kWh. An escalation rate of the energy price of 2% is considered. A sensitivity analysis is carried out varying the interest rate, the investment cost and the electricity price in order to assess the sensitivity of the economic results to the input data. The annual interest rate is varied ±1% point from the default value (3%), the electricity price and the investment costs are varied ±20%. In Table 4 the investment, installation, maintenance costs, the technical lifetime and the resulting EAC for each technology are reported. The data for HP and PV are all taken from [3] except the investment cost of PV which is taken from [10] where mono-crystalline silicon PV are considered.

The reference technology for the cooling is the On/Off low power HP therefore when the modulating HP or the On/Off high power HP are considered, as a cooling technology, only the additional costs are accounted for (ΔEAC=143.5€).

The data for battery and LED are assumed considering the current price of different sellers. The battery are usually guaranteed for 10 years while LED for 50000 hours that correspond to a lifetime of 15 years.

The PV self-consumption contributes to the reduction of the electricity demand of the building system. When the battery is considered, the PV surplus energy is stored and later used by the building, otherwise the benefit of selling the surplus to the main grid is disregarded.

Table 4. Investment costs, installation costs, maintenance costs and EAC of the studied renovation measures

Renovation measure	Investment costs [€]	Installation costs [€]	Maintenance costs [€/y]	Technical lifetime [y]	EAC [€]
On/Off HP low power	500 [3]	100 [3]	16 [3]	12 [3]	76.3
On/Off HP high power	1400 [3]	290 [3]	50 [3]	12 [3]	219.8
Modulating HP	1400 [3]	290 [3]	50 [3]	12 [3]	219.8
PV (877 Wp)	2322 [10]	380 [3]	34.2 [3]	20 [3]	215.8
Battery (4.8 kWh) with Inverter	4000	1400	0	10	663.1
LED light (8 luminaire)	640	300	0	15	78.7

2.4. Environmental analysis

In this case study all the analyzed solutions are using electricity as input, therefore they can be compared considering the savings in terms of electricity demand. In order to compare the savings in terms of primary energy there is the need to define the proper conversion factors.

The increasing share of renewables in the electricity mix affects the definition of the PE/CO_2 conversion factors especially because the energy production from renewables is not constant during the year but rather has a seasonal trend. Significantly increased share of RE electricity can be expected in the near future in particular in summer, while in winter only a moderate increase is likely, unless there is a significant further extension of wind power or seasonal storage capacities are strongly build up [5].

For this reasons, different scenarios for the PE conversion factor are taken into account.

Fig. 4 shows the monthly PE conversion factors considering a constant coefficient defined in [11], a simplified

scenario with an energy mix of 10% hydro, 10% wind and 10% PV and an energy mix of 10% hydro, 30% wind and 30% PV. The difference between the EU conversion factor and the 10-10-10 or 10-30-30 scenarios is higher during the summer than during winter. This means that using the EU conversion factor the same value is given to savings obtained in summer and winter while using the monthly conversion factors (i.e. 10-10-10 and 10-30-30) less importance is given to the energy savings occurring in summer.

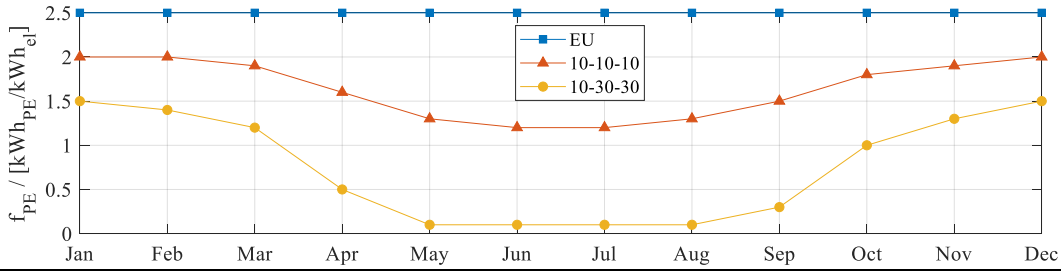

	Jan	Feb	Mar	Apr	May	Jun	Jul	Aug	Sep	Oct	Nov	Dec
EU	2.5	2.5	2.5	2.5	2.5	2.5	2.5	2.5	2.5	2.5	2.5	2.5
10-10-10	2	2	1.9	1.6	1.3	1.2	1.2	1.3	1.5	1.8	1.9	2
10-30-30	1.5	1.4	1.2	0.5	0.1	0.1	0.1	0.1	0.3	1	1.3	1.5

Fig. 4. Monthly total PE conversion factor defined according to (EU) European definition, (10-10-10) scenario where a share of 10 % hydro, 10 % wind, 10 % PV and 70 % fossil is considered in the electricity mix, and (10-30-30) scenario where a share of 10 % hydro, 30 % wind, 30 % PV and 30 % fossil is considered in the electricity mix *[5]*

3. Results

3.1. Reference case and PV yield

The reference case is composed of a direct electric heating system and an On/Off HP_{lp} without PV. Fig. 5a shows, for each climate, the monthly electricity demand per square meter of floor area (27 m^2) for each component of the balance (i.e. heating, cooling, appliances, lighting, anti-freezing resistance of the heat exchanger and fans of the mechanical ventilation). The PV production in each climate is reported by the straight blue line. The cross (EU conversion factor), triangle (10-10-10 scenario) and square (10-30-30 scenario) markers refer to the right vertical axes reporting the primary energy consumption. As highlighted in section 2.4, increasing the renewables share in the grid leads to a reduction of the primary energy demand especially during the summer time.

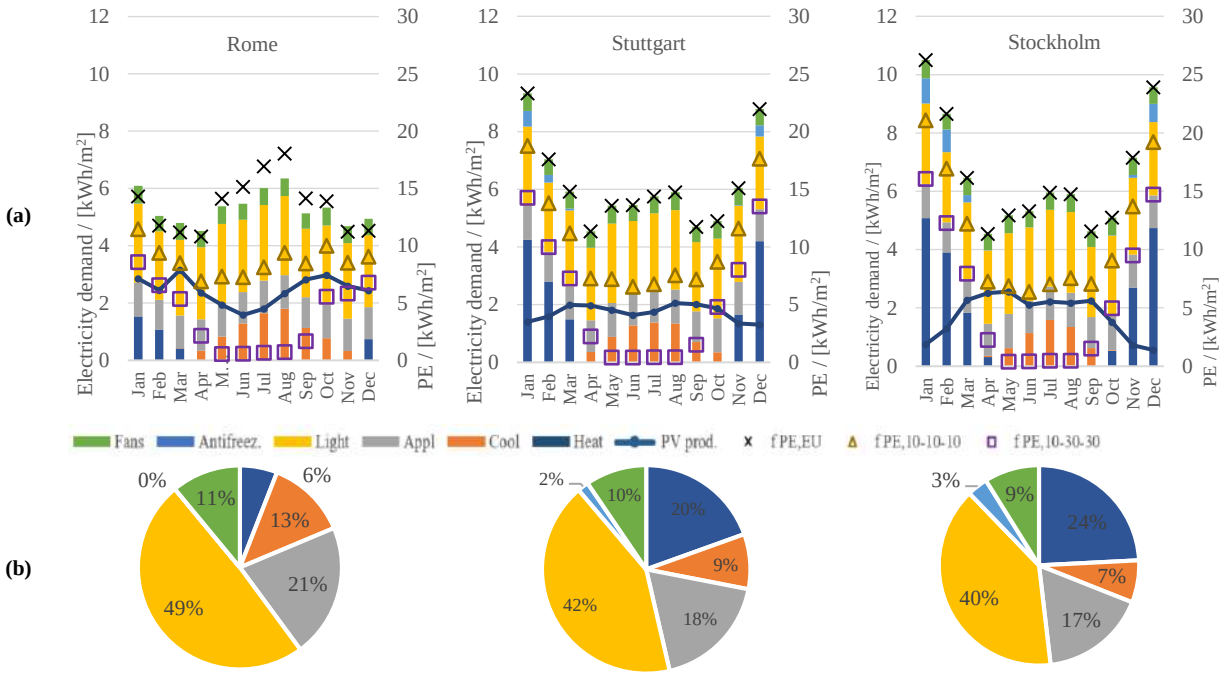

Fig. 5. Results for the reference case (direct electric heating and split HP) for the climates of Rome, Stuttgart and Stockholm. (a) Electricity demand for each end use and PV production; (b) share of electricity required by each end use.

Fig. 5b shows the share of electricity required by each end use, highlighting that the lighting is prevailing in each climate.

Table 5 reports the annual electricity consumption required by each end use and PV production for the climates of Rome, Stuttgart and Stockholm. The total electricity consumption of the reference case is 64 kWh/(m^2y) in Rome, 74 kWh/(m^2y) in Stuttgart, and 79 kWh/(m^2y) in Stockholm. The PV total production would cover the 46%, 28% and 26% of the total consumption in Rome Stuttgart and Stockholm respectively. From this analysis is already clear that the installation of PV in the façade (BIPV) in this case study would bring important energy savings.

Table 5. Annual electricity consumption required by each end use and PV production.

	Heating	Cooling	Appliances	Lighting [kWh/(m^2y)]	Antifreez.	Fans	PV
Rome	4	8	14	31	0	7	29
Stuttgart	14	6	14	31	1	7	21
Stockholm	19	5	14	31	3	7	21

3.2. Pareto solutions

The results of the dynamic simulations investigating different HVAC and lighting solutions (see section 2.2) are compared to the base case considering the additional capitalized cost and energy savings. The latter are expressed in terms of electric energy (E_{EL}) and of total PE calculated with the constant conversion factor (PE_{EU}), with the 10-10-10 scenario ($PE_{10\text{-}10\text{-}10}$) and with the 10-30-30 scenario ($PE_{10\text{-}30\text{-}30}$).

Fig. 6 shows the energy savings in terms of (A) E_{EL}, (B) PE_{EU}, (C) $PE_{10\text{-}10\text{-}10}$ and (D) $PE_{10\text{-}30\text{-}30}$ versus the additional total annual cost (see Equation (5)) of each technology for the climate of Stockholm. Fig. 7 shows the energy savings in terms of (E, F) E_{EL} and (G, H) $PE_{10\text{-}30\text{-}30}$ versus the additional cost for the climate of Rome and Stuttgart, respectively. In both Fig. 6 and Fig. 7, the square markers represent the results of the different technologies together with the PV panels, while the asterisk markers represent the solutions including battery and PV. The error bars shows the results of the economic sensitivity analysis, indicating the impact on the additional total annual cost by varying the investment cost, energy price and interest rate. The investment cost has the highest impact on the economic evaluation.

In this specific case, the analysis of the results does not change considering the PE_{EU} or E_{EL} since all the compared solutions are using electricity as energy source (see Fig. 6 A and B).

The two objects of this optimization are the minimization of the cost and the maximization of the energy savings under the constraint of maintaining thermal comfort. In such a case, typically a feasible solution that minimizes all objective functions simultaneously does not exist. The optimal cases lay on the Pareto front composed by solutions that cannot be improved in any of the objectives without degrading the second object. In Fig. 6 and Fig. 7, the Pareto front, for the set of solutions considered in this work, is highlighted with a light green underlay. The red underlay highlights solutions that are not optimal since enable lower savings and same cost of at least one solution of the Pareto front. The differences in terms of energy savings between the On/Off low or high power and modulating HP are not significant in all the considered climates but the modulating HP and high power On/Off HP are more expansive than the On/Off low power HP.

The night set back slightly reduces the heating demand, therefore it has a small effect in Stockholm and Stuttgart but no effect in Rome where the heating demand is almost zero.

Switching off the air conditioner, when not in operation, i.e. the during the winter season for the case when the electric heating is active), reduces the standby consumption and comes without any additional costs.

The free-cooling active seven days per week on the one hand reduces the cooling demand while on the other hand increases the energy consumption of the fans, increasing also the overall energy consumption. When the $PE_{10\text{-}30\text{-}30}$ instead of E_{EL} is considered, the results of the cases with free cooling (see violet and dark green markers) are overlapped to the respective cases without free cooling (see yellow and light blue markers).

Since in the reference case almost half of the electricity demand is required for lighting, changing the illumination system from fluorescent to LED has a great benefit at low cost. In fact, the solution with electric heating, HP and LED (see light gray circle marker) is close to the Pareto front in all the climates for both E_{EL} and PE savings plots. The same technology with PV (square light gray marker) is close to the Pareto front only for Rome. Since here, the heating demand is almost zero, the HP technology appears between the cost optimal solutions only when it is combined with PV and LED or PV, LED and battery. The reversible On/Off HP (for heating and cooling) either combined or not with LED, is always between the best solutions for the climate of Stockholm and Stuttgart. When the renovation package involving electric heating, On/Off cooling HP and

LED (see light gray circle marker) is compared with On/Off HP H/C (see yellow circle marker), in Stuttgart and Stockholm, it is noteworthy that the scenario for evaluation of the energy savings (i.e. E_{EL} or $PE_{10\text{-}30\text{-}30}$) might change the ranking of the solutions. In Fig. 6.A and Fig. 7.F, it can be seen that the renovation package with electric heating, On/Off cooling HP and LED (light gray marker) gives the same or even more E_{EL} savings than the On/Off HP H/C, but the situation is reversed when the savings are evaluated in terms of $PE_{10\text{-}30\text{-}30}$ (see Fig. 6.D and Fig. 7.H). The monthly conversion factors of the 10-30-30 scenario are almost zero during summer therefore the savings during the wintertime have higher impact on the calculated yearly energy savings. When the PV is considered together with the HP and LED with or without battery (see square and asterisk light blue markers) these solutions are cost optimal in all the climates.

The Pareto front highlights a set of cost optimal solutions from which one renovation package has to be selected based on economic restrictions and other parameters (e.g. thermal and visual comfort, quickness of the retrofitting, personal preferences, etc.). But there are some clear and remarkable trends that can be noted: in Stockholm and Stuttgart the solution with reversible On/Off HP_{lp} H/C + LED have the same cost but guarantee higher energy savings with respect to other solutions such as reversible On/Off HP_{lp} H/C and El. Heating + On/Off HP_{lp} + LED. Adding PV increases the energy savings but also the cost therefore the selection of this solution depend on the economic restriction. Adding battery only slightly increases the energy savings while the cost substantially increases. In Rome El. Heating + On/Off HP_{lp} + LED with or without PV allows to keep the additional cost near to zero enabling high-energy savings.

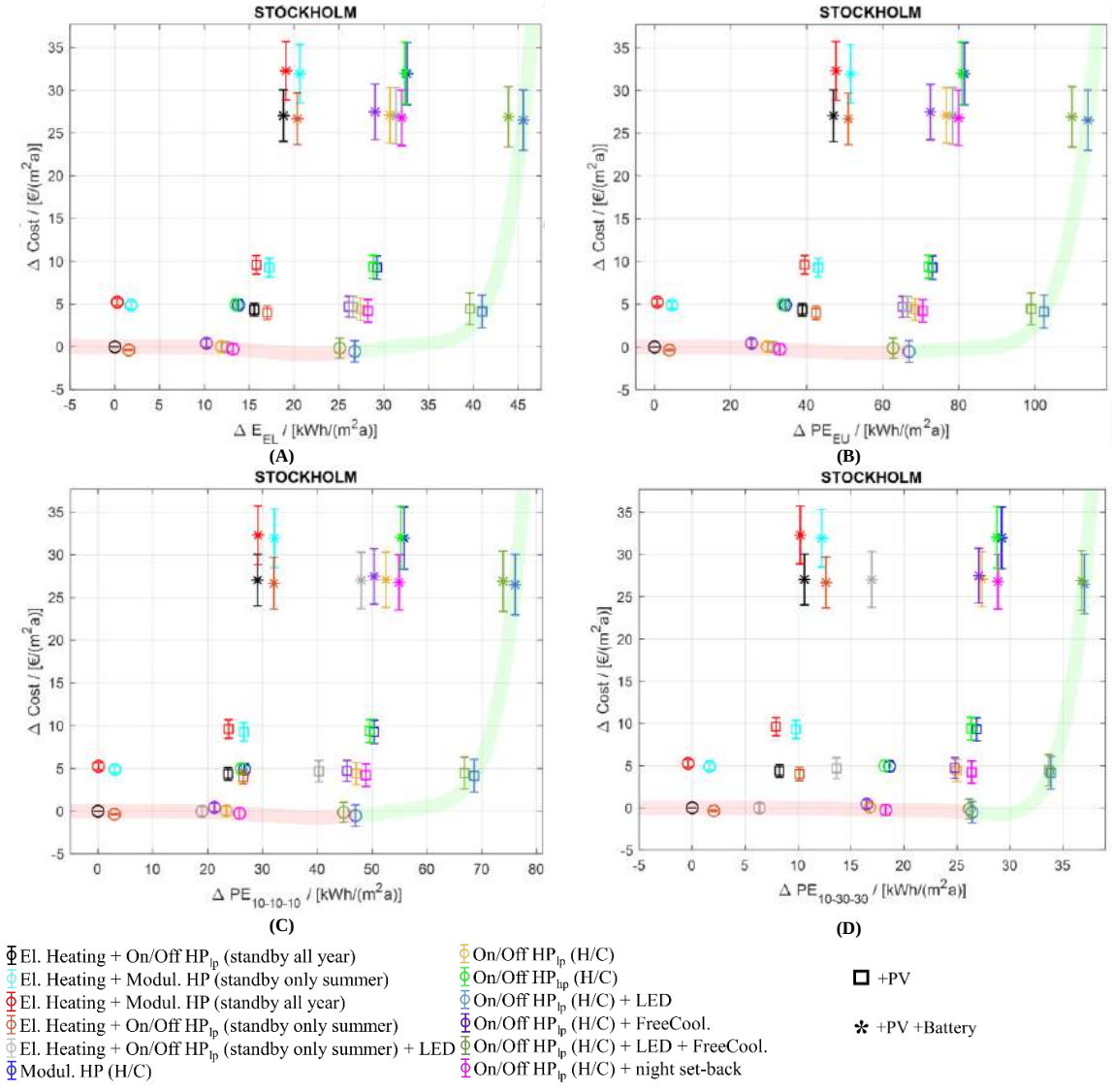

Fig. 6. Savings in terms of (A) Electric energy, (B) Primary energy according to EU conversion factor, (C) Primary energy according to 10-10-10 scenario conversion factors,(D) Primary energy according to 10-30-30 scenario conversion factors vs additional cost of the analysed technologies for the climate of Stockholm

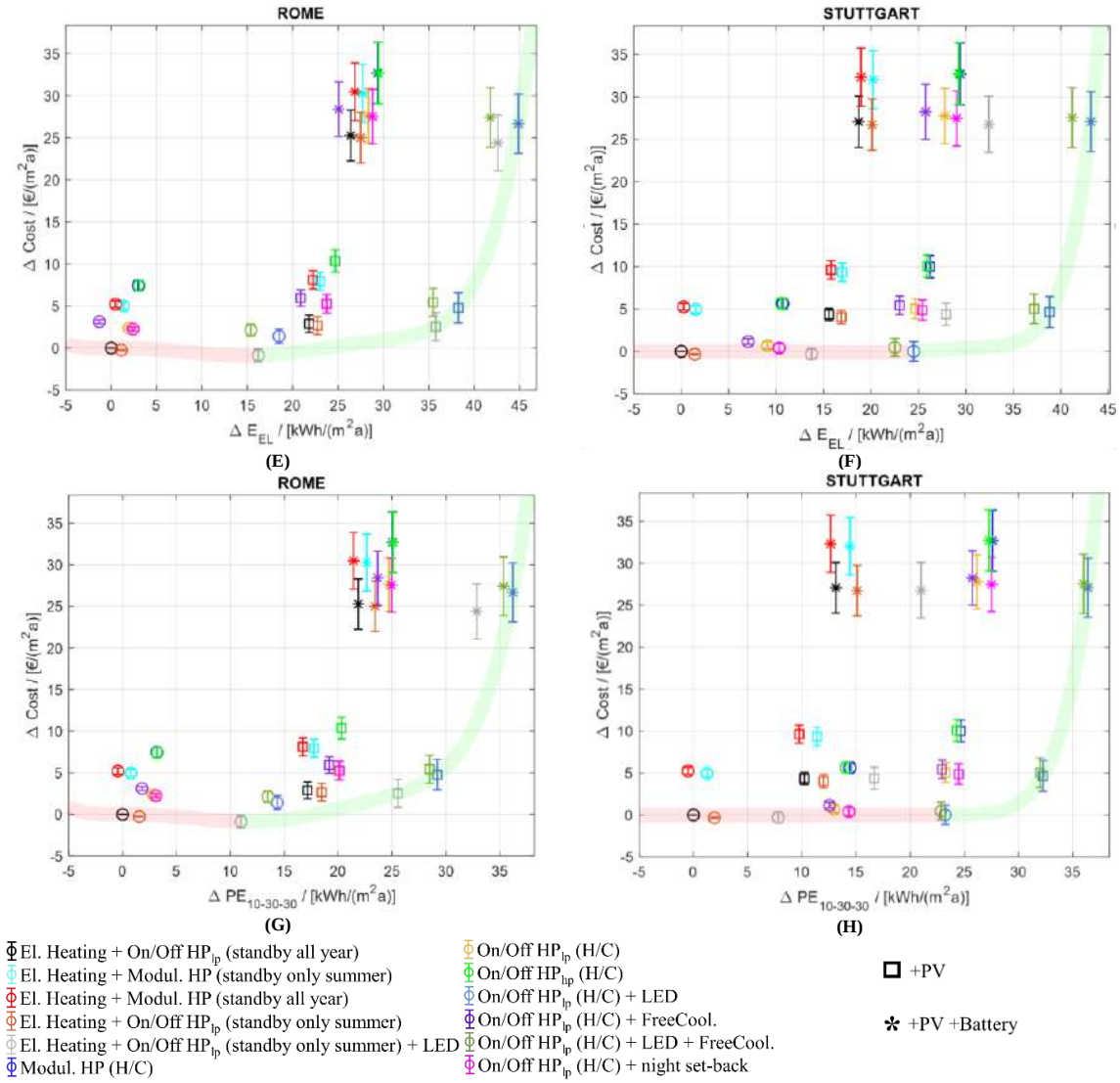

Fig. 7. Savings in terms of (E,F) Electric energy and (G,H) Primary energy according to 10-30-30 scenario conversion factors vs additional cost of the analysed technologies for the climate of Rome and Stuttgart respectively.

Table 6 shows the yearly heating and cooling demands and electricity consumptions for Rome, Stuttgart and Stockholm. Using the HP instead of the electric heating saves around 15% in terms of electricity demand in Stuttgart and Stockholm. The heating demand slightly increases and the cooling demand substantially decreases together with the electricity demand when LED technology is considered. Adding the free cooling to the On/Off HP (H/C) case, reduces the cooling demand while slightly increases the total electricity consumption, this effect is caused by the increased electricity demand of the fans. The night set-back, compared to the case with On/Off HP (H/C), slightly reduces the electricity demand only in Stuttgart and Stockholm.

Table 6. Annual heating, cooling demand and electricity consumption for the climates of Rome, Stuttgart and Stockholm.

	Heating demand [kWh$_{th}$/(m^{2}a)]			Cooling demand [kWh$_{th}$/(m^{2}a)]			Total Electricity demand [kWh$_{el}$/(m^{2}a)]		
	Rome	Stuttg.	Stock.	Rome	Stuttg.	Stock.	Rome	Stuttg.	Stock.
El. Heating+On/Off HP (standby all year)	2.7	13.1	17.2	32.7	26.0	24.5	63.8	73.8	79.0
Modul. HP (H/C)	3.1	13.5	17.6	33.4	26.7	25.0	60.8	63.1	65.2
On/Off HP$_{lp}$ (H/C)	2.7	13.1	17.2	32.7	26.0	24.5	61.8	64.7	67.1
On/Off HP$_{hp}$ (H/C)	2.8	13.1	17.2	32.9	26.2	24.7	60.7	43.3	65.4
On/Off HP$_{lp}$ (H/C) + LED	4.7	17.5	22.8	24.6	19.7	18.7	45.3	49.3	52.2
On/Off HP$_{lp}$ (H/C) + FreeCool	2.8	13.1	17.3	24.9	17.0	14.3	65.1	66.8	68.8
On/Off HP$_{lp}$ (H/C) + LED + FreeCool	4.7	17.5	22.9	17.8	12.0	9.8	48.4	51.3	53.9
On/Off HP$_{lp}$ (H/C) + night set-back	2.2	10.2	14.0	31.3	24.2	23.0	61.4	63.5	65.8

4. Conclusions

Different technologies applicable for the decentral renovation of a typical office building (cell) are evaluated considering, both economic feasibility and environmental impact for the climates of Rome, Stuttgart and Stockholm by means of dynamic building and HVAC simulations. The cost analysis is based on the equivalent annual cost (EAC) and a sensitivity analysis is performed in order to assess the influence of the used inputs on the results. The environmental impact is evaluated in terms of electricity demand and total primary energy (PE) savings calculated with a constant and monthly conversion factors representing different scenarios with different share of renewables in the electricity mix (i.e. 10-10-10: 10 % hydro, 10 % wind, 10 % PV and 70 % fossil and 10-30-30: 10 % hydro, 30 % wind,30 % PV and 30 % fossil). In this specific case study, since all the analyzed technologies require electricity as input, the same conclusion can be derived using the energy savings expressed in terms of electricity or total PE calculated with a constant conversion factor while the results might change if monthly conversion factors for different renewables scenarios are used. In fact, the renovation package with electric heating and LED has the same (in Stockholm) or higher (in Stuttgart) electricity savings than the On/Off HP for heating and cooling without LED but the situation is reversed when the savings are evaluated in terms of PE calculated with the conversion factor of the 10-30-30 scenario. The renovation packages allowing high-energy savings with low additional cost are represented, in Stockholm and Stuttgart, by HP in combination or not with LED and PV and in Rome, by LED and PV in combination with electric heating. Battery in combination with PV, HP and LED brings, in all the climates, additional energy savings with high additional cost. Technologies, which will lead to higher savings in winter with lower availability of renewables and generally higher loads, will be more valuable and this can be quantified by the proposed method.

References

[1] EPBD recast, Directive 2010/31/EU of the European Parliament and Council of May 19, 2010 on the energy performance of buildings (recast), *Journal of the European Union*, 153/13., 2010.

[2] E. Pikas, M. Thalfeldt and J. Kurnitski, Cost optimal and nearly zero energy building solutions for office buildings". *Energy and Buildings*, vol. 74, pp. 30-42, 2014.

[3] M. Gustafsson, C. Dipasquale, S. Poppi, A. Bellini, R. Fedrizzi, C. Bales, F. Ochs, M. Sié and S. Holmberg, "Economic and environmental analysis of energy renovation packages for European office buildings". *Energy and Buildings*, vol. 148, pp. 155-165, 2017.

[4] S. Stevanovic, "Parametric study of a cost-optimal, energy efficient office building in Serbia". *Energy*, vol. 117, pp. 492-505, 2016.

[5] F. Ochs and G. Dermentzis, "Evaluation of Efficiency and Renewable Energy Measures Considering the Future Energy Mix". *7th International Building Physics Conference*, Syracuse, NY,USA, 2018.

[6] M. D'Antoni, P. Bonato, D. Geisler-Moroder, R. Loonen and F. Ochs, "IEA SHC T56 - System simulation Models Part C Office Buildings", 2017.

[7] SIA 2024:2015, Raumnutzungsdaten für di Energie- und Gebäudetechnik, Zurich, Switzerland.

[8] M. Magni, F. Ochs, P. Bonato, M. D'Antoni, D. Geisler-Moroder, S. de Vries, R. Loonen, A. Maccarini, A. Afshari and T. Calabrese, "Comparison of Simulation Results for an Office Building Between Different BES Tools – The Challenge of Getting Rid of Modeller Influence and Identifying Reasons for Deviations". *Bilding Simulation Conference*, Rome, 2019.

[9] S.-I. Juelich, "CARNOT Toolbox," [Online].
Available: https://de.mathworks.com/matlabcentral/fileexchange/68890-carnot-toolbox. [Accessed 12 11 2019].

[10] F. Ascione, N. Bianco, G. Maria Mauro and G. Peter Vanoli, "A new comprehensive framework for the multi-objective optimization of building energy design: Harlequin". *Applied Energy*, vol. 241, pp. 331-361, 2019.

[11] Directive 2006/32/EC of the European Parliament and of the Council of 5 April 2006 on energy end-use efficiency and energy services and repealing Council Directive 93/76/EEC.

5.6 Publication F

Title

Comparison of Simulation Results for an Office Building Between Different BES Tools – The Challenge of Getting Rid of Modeller Influence and Identifying Reasons for Deviations

Authors

Mara Magni, Fabian Ochs, Paolo Bonato, Matteo D'Antoni, David Geisler-Moroder, Samuel de Vries, Roel Loonen, Alessandro Maccarini, Alireza Afshari, Toni Calabrese

Published in

Proceedings of the 16th Conference of IBPSA. 2-4 Sept, Rome.
ISBN 978-1-7750520-1-2, S. 1475 – 1482
http://www.ibpsa.org/proceedings/BS2019/BS2019_210834.pdf

Own contribution

Coordination of the data exchange and analysis of all the data as well as the development of the methodology and the writing of the paper was done by the first author. The second author provided a review, the third, fourth and tenth authors modelled the office cell using TRNSYS, the fifth author using DALEC, the sixth and seventh using EnergyPlus, the eighth and ninth using Modelica building library.

BS 2019 2-4 SEPT ROME 16th IBPSA INTERNATIONAL CONFERENCE AND EXHIBITION

INTERNATIONAL BUILDING PERFORMANCE SIMULATION ASSOCIATION

Comparison of Simulation Results for an Office Building Between Different BES Tools – The Challenge of Getting Rid of Modeller Influence and Identifying Reasons for Deviations

Mara Magni[1], Fabian Ochs[1], Paolo Bonato[2], Matteo D'Antoni[2], David Geisler-Moroder[3], Samuel de Vries[4], Roel Loonen[4], Alessandro Maccarini[5], Alireza Afshari[5], Toni Calabrese[1]
1 University of Innsbruck, Unit for Energy Efficient Buildings, Innsbruck (Austria)
2 Eurac Research, Institute for Renewable Energy, Bolzano (Italy)
3 Bartenbach GmbH, Aldrans (Austria)
4 Eindhoven University of Technology, Eindhoven (The Netherlands)
5 Aalborg University Copenhagen (Denmark)

Abstract

The model of the reference office building, reported in IEA SHC Task 56, is implemented by different experts in building simulations, with different tools (i.e. dynamics simulation tools such as EnergyPlus, TRNSYS, CarnotUIBK, ALMAbuild, DALEC, Modelica and quasi steady state calculation tool such as PHPP). The aim is to set up reference models for (virtually) testing different solar passive and solar active façade systems. Hence, identifying deviations between the resulting energy balance for heating and cooling of the used tools due to different levels of detail of their models is of great importance, while in the same time, trying to get rid of the user influence was experienced as a real challenge.

It can be concluded that even considering a relatively simple case study, it is hard to reach a good agreement between different tools and an additional calibration phase is necessary. In particular, it was found that the resolution of the window model can lead to considerable differences.

As a perspective, it seems to be a challenge if the building modelling is entrusted to non-expert users (e.g. from Building Information Modelling to Building Energy Modelling, where BIM-to-BEM interoperability issues might arise and affect the simulation results).

Introduction

In spite of higher efficiency, the energy consumption of buildings has increased over the past decades and currently accounts for approximately 37% of the total primary energy consumption in European Union (i.e. 26% is taken up by residential and 11% by commercial buildings) (Pérez-Lombard, et al., 2008). The European Union has set three key targets for the year 2030: 40% cuts in greenhouse gas emissions, 27% share for renewable energy, 27% improvement in energy efficiency (Council of the European Union, 2014). To reach this goal, the building system will be required to be an energy producer other than an energy consumer (i.e. prosumers) (Brange, et al., 2016). Nowadays, solar thermal systems for building integration are gaining attention. Advanced materials and technologies are integrated into the building envelope with the aim to reduce the energy needs (energy conservation) or to collect energy from local sources reducing the primary energy consumption (energy collection) (Martinez, et al., 2017). The use of dynamic simulations can play an important role in helping designers and researchers to analyse the integration of renewables, the improvement of the efficiency and the reduction of the demand of the system. However, conclusions from simulation studies can be influenced by the calculation algorithms, numerical errors, non-identical inputs, different processing of climate data and on the choice of physical model (Feist, 1994).

The scientific community contributed to the progress of dynamic simulation by proposing different tools and approaches (Castaldo and Pisello, 2018). Studies regarding the comparison between different tools, are present in the literature. Kim, et al., (2013) presented a stochastic calibration and comparison between a simplified calculation approach (ISO 13790:2008, 2008) and EnergyPlus for an office building. The calibrated ISO 13790:2008 delivers results significantly identical to the dynamic model while the non-calibrated fails. Dermentzis, et al., (2019) evaluated an energy auditing tool (PHPP) against TRNSYS for a set of buildings and climates. The results show that the average deviation between the tools is 8% for the heating demand and 15% for the cooling demand. Strachan, et al., (2016) carried out an empirical analysis involving 21 modelling teams with different simulation programmes. After the building validation phase, in which a significant number of input errors were detected, many of the tested programs showed a good agreement with the measured data. Since new tools (e.g. CarnotUIBK, ALMAbuild, DALEC) and updated software versions are available, it is important to continue carrying out new comparison studies, although some are already present in the literature.

Within this scenario, IEA SHC Task 56 Subtask C, (IEA, 2016) describes the boundary conditions to adopt for the transient simulation of a reference office room, that allows each dynamic simulation tool user to implement the same building system. The office cell is representative for a typical new European office space and is taken as a reference for the study of different solar active façades. To ensure the credibility of this reference, it is important that it can be implemented in different BPS tools, and that there is only modest deviation between the results. In this work, the model of the reference office cell, described in D'Antoni, et al., (2017), is developed by experienced users of building simulation software, with different tools

https://doi.org/10.26868/25222708.2019.210834

(i.e. the dynamic simulation tools EnergyPlus, TRNSYS, CarnotUIBK, ALMAbuild, DALEC, Modelica and the quasi steady state calculation tool PHPP). The tools analysed in this work have different focus and depending on it, component models (window, wall, HVAC, control, etc.) vary from simplified to detailed. The results of the different tools are compared considering all the components of the building energy balance. Particular attention is given to the window model because, in this case study, it strongly influences the results.

Methods

Boundary Conditions

The reference building is chosen in order to be representative of a typical European office cell located in middle floor of a high-rise building. Three different European climates are considered in this study: Rome (hot temperate), Stuttgart (cold temperate) and Stockholm (cold climate). Figure 1 shows the considered office cell, which has a heated area of 27 m^2 and a volume of 81 m^3. All the surfaces are considered adiabatic, except for the façade oriented toward South (with window-to-wall ratio of 60%) where ambient boundary conditions are applied and solar active technologies such as daylighting systems can be installed (not applied in the present comparison). Shading from adjacent obstacles is not considered, whereas an external movable shading, able to block 70% of the incoming radiation, is activated when direct solar radiation impinging the south façade is higher than 120 W/m^2.

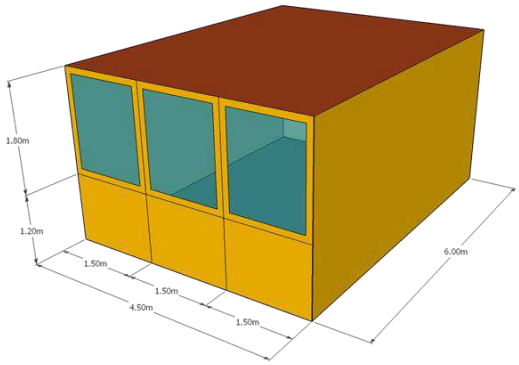

Figure 1: View of the reference office zone.

The thermal properties of the wall infill element and the characteristics of the windows depend on the three climates, as shown in Table 1. The internal walls are typical plasterboard walls, the exterior wall is a three layer structure with different insulation thicknesses depending on the climate.

Table 1: Main properties of the south oriented façade.

Properties	Rome (Italy)	Stuttgart (Germany)	Stockholm (Sweden)
$U_{ext,wall}$ [W/m^2K]	0.80	0.40	0.20
U_{win} [W/m^2K]	1.26	1.35	0.90
g-value [-]	0.33	0.59	0.63
T_{sol} [-]	0.462	0.426	0.260
Rf_{sol} [-]	0.237	0.266	0.218
T_{vis} [-]	0.749	0.706	0.659

Table 2 shows the yearly average ambient temperature ($T_{amb,av}$), yearly global irradiation over a horizontal surface ($I_{g,h}$) and yearly irradiation over a south oriented vertical surface (I_{south}) for each climate.

Table 2: Main boundary conditions: yearly average ambient temperature ($T_{amb,av}$), yearly global irradiation over a horizontal surface ($I_{g,h}$) and yearly irradiation over a south oriented vertical surface (I_{south}).

Location	$T_{amb,av}$ [°C]	$I_{g,h}$ [kWh/m^2]	I_{south} [kWh/m^2]
Rome	15.8	1632	1253
Stuttgart	9.9	1101	889
Stockholm	7.8	952	884

User behaviour (e.g. occupancy, appliances and lighting) is taken into account by means of hourly profiles, different for week and weekend days (SIA, 2015). Figure 2 reports the schedule profiles for occupancy, appliances and lighting. A contemporaneity index of 0.8 is used for occupancy and appliances. Three persons are present during the working time and a sensible and latent heat of 70 W/person and 0.08 kg/h/person are considered. The internal gain due to appliances is assumed to be 7 W/m^2 and the electric gain due to lighting is 10.9 W/m^2.

The lighting schedule follows occupied hours and is defined considering a non daylight responsive system

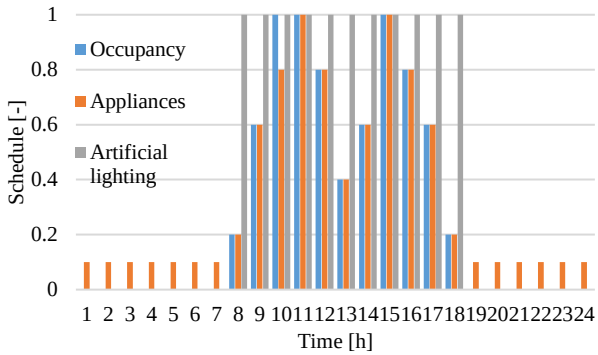

Figure 2: Schedule profile for occupancy, appliances and lighting.

The natural infiltration rate is assumed to be constant and equal to 0.15 1/h. A fresh air supply of 40 m^3/h/person is covered by a mechanical ventilation system with heat recovery (70% sensible efficiency). A bypass of the heat recovery is activated when the temperature of the zone is higher than 23 °C and the ambient temperature is lower than the indoor temperature.

Simplified all-air heating and cooling systems are included within the models. The set point temperature for the indoor convective temperature during the wintertime and summertime are 21 °C and 25 °C. When the convective temperature is between 21 °C and 25 °C neither the cooling system nor the heating system are activated. A detailed description of the boundary conditions is reported in D'Antoni, et al., (2017).

General modelling features

The tools analysed in this work have different focus:

- EnergyPlus™ (EP) is a whole building energy simulation program that engineers, architects, and researchers use to model both energy consumption for heating, cooling, ventilation, lighting and plug and process loads and water use in buildings (Crawley, et al., 2000) ;
- TRNSYS (TRN) is a transient system simulation program based on a component approach with modular structure. The TRNSYS library includes a detailed multizone building model and components for HVAC systems, renewable energy systems, etc. (Klein, et al, 1979);
- Simulink UIBK (SIM_IBK) is a Matlab/Simulink library, compatible with CARNOT Toolbox, developed by the University of Innsbruck, based on object-oriented programming of a parameterized building model (Siegele, et al., 2019);
- ALMAbuild (SIM_BO) is a Matlab/Simulink library, compatible with CARNOT Toolbox, developed by the University of Bologna where a user develops a building model by means of a series of Graphical User Interfaces (Campana, et al., 2017);
- DALEC (DAL) is a free web tool developed by Bartenbach, University of Innsbruck and Zumtobel. The main focus is on combined thermal and lighting building simulations in early design phases (Werner, et al., 2017);
- MODELICA (MOD) is a non-proprietary, object-oriented, equation based language to conveniently model complex physical systems, with a wide open source library (in this case the LBNL Buildings library is used) (Wetter, et al., 2014);
- PHPP Passive House Planning Package is a quasi steady state calculation tool, developed as spread sheet, for the use of architects and planning experts (Feist, 2019).

The different tools implement models with different level of detail and approach the numerical solution of the building system with different equations.

Table 3 reports the physical models used by the different tools for the calculation of the room balance and the time step used in the numerical simulations. The two star node model includes a convective node (representing the thermal capacity of the air) and a radiative node (the long-wave radiative exchange between the surfaces is modelled using the star network). In the simplified calculation mode, TRN implements a star network where an artificial temperature node (Tstar) is used to consider the parallel energy flow from the inside wall surface to the zone air by convection and the long-wave radiation exchange between the surfaces. EP uses a grey interchange model (ScriptF) involving an approximation of direct view factors for the radiative exchange between surfaces.

MOD implements a more detailed model for the radiative exchange based on net radiation exchange approach (Wetter, et al., 2011). DAL model is based on the Standard ISO 13790:2008 where the room heat balance is solved considering three nodes and both the air temperature and mean radiant temperature are calculated. The nodes are connected between each other by means of specific coupling conductance defined by the standard. The whole thermal capacity of walls and air volume is connected to the node representing the mean radiant temperature. PHPP is a quasi steady state tool that calculates losses and gains considering a fixed set point temperature. It performs two different balances by using the two set point temperatures for winter and summer.

Each tool performs the simulation using different time steps and, in particular: SIM_IBK and SIM_BO use variable-step solvers, which vary the step size during the simulation depending on the required numerical accuracy and the solver. All the other tools perform the calculation with a constant time step as reported in Table 3. The definition of the time step influences the run time and the accuracy of the results.

Table 3: Model of the room heat balance and simulation time step.

Tools	Surface to zone heat transfer	Time step
EP	Radiative and conv. node	Const.: 15 m
TRN	Star node model	Const.: 60 m
SIM_IBK	Two star node model	Var.: max 10 m
SIM_BO	Two star node model	Var.: max 10 m
DAL	Standard ISO 13790	Const.: 60 m
MOD	Radiosity and conv. node	Const.: 15 m
PHPP	Steady state balance	Monthly

Table 4 reports the model used for the wall structure in each tool. EP and TRN model the opaque structure with the transfer function method, whereas both Simulink libraries and MOD are based resistance-capacity (R-C) method. DAL and PHPP implement a simplified model of the walls, based on the overall heat transfer coefficient (H) of the external structures.

Table 4: Model of the walls.

Tools	Wall model
EP	Transfer function
TRN	Transfer function
SIM_IBK	R-C
SIM_BO	R-C
DAL	Unique H value
MOD	R-C
PHPP	Unique H value

Different window models are implemented in the analysed tools, (Table 5). In particular, EP, TRN, SIM_BO and MOD perform an energy balance over each pane of the window while DAL, SIM_IBK and PHPP are based on a simplified window thermal model where the transmission losses of the window are calculated by using a constant heat transfer coefficient. An additional layer representing the shading system is involved in the thermal balance of the window only in EP and MOD.

Gains from solar radiation are computed differently in each tool. EP, TRN, SIM_BO and MOD consider how

solar radiation is absorbed by each pane of the window, which increases the pane temperature, and influences convective and radiative exchange.

In the presented heat balances for EP, SIM_BO and MOD solar gains are defined as directly transmitted radiation (convective and radiative gains from the inner pane do contribute to the room heat balance but they are not reported as 'solar gains' in the presented balances). The calculation of the solar gain in DAL is based on an angular dependent g-value of the façade dependent on the sun position, SIM_IBK calculation is based on an angular dependent g-value of the glazing system, dependent on the sun position. Depending on the definition of the solar gain (total or only transmitted part), also the definition of the transmission losses is different. When only the directly transmitted part of the solar radiation is reported as solar gain, the transmission loss is represented by the exchange between the internal side of the window and the thermal zone ($\dot{Q}_{int,p2}$ in Figure 3). Contrariwise, when the total solar gain is reported (including absorbed solar radiation reemitted to the inside), the transmission losses are calculated as ($\dot{Q}_{tr,p1-p2}$ in Figure 3).

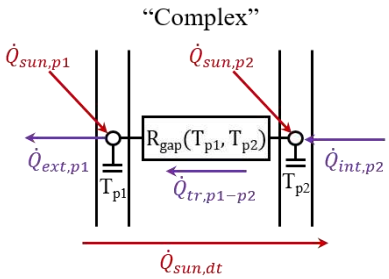

Figure 3: Sketch of the Complex window model.

The models used to predict the diffuse radiation on a tilted surface can be based on either isotropic or anisotropic sky models. All the tools except for DAL calculate the diffuse radiation on a tilted surface with anisotropic sky models while DAL uses an isotropic sky model.

Table 5: Window model.

Tools	Window model	Solar Gain
EP	'Complex'	Directly transmitted (τ-sol)
TRN	'Complex'	Total
SIM_IBK	'Simplified'	Total (g-value)
SIM_BO	'Complex'	Directly transmitted (τ-sol)
DAL	'Simplified'	Total (g-value)
MOD	'Complex'	Directly transmitted (τ-sol)
PHPP	'Simplified'	Total (g-value)

The profiles for the occupancy, appliances and lighting could not be implemented in DAL and PHPP. In DAL a constant internal gain of 8.79 W/m^2 from 8 a.m. to 19 p.m. is considered while in PHPP a constant internal gain of 6.5 W/m^2 is considered.

With regard to the ventilation system, EP, TRN, SIM_IBK, SIM_BO and MOD calculate the ventilation rate, bypass control and infiltration losses as described in the report (D'Antoni, et al., 2017) while DAL uses a constant energy equivalent air exchange rate that takes into account the infiltration and energy effective air exchange rate. The additional ventilation losses due to activation of the bypass are modelled as window/night ventilation. PHPP considers ventilation losses using a constant equivalent air exchange rate. A different rate is used, for summertime and wintertime, which account for the frequency with which the bypass is activated in that period. These equivalent air exchange are calibrated in order to match the ventilation losses calculated by SIM_IBK.

The shading control system is modelled based on a 120 W/m^2 beam direct solar radiation threshold as described in the report (D'Antoni, et al., 2017) for all the tools except for the PHPP where it is only possible to set a constant value for the summer and winter time. The shading values are calibrated in order to match the solar gain calculated by SIM_UIBK.

Table 6: Internal gain profile and ventilation rate.

Tools	Internal Gain	Ventilation rate/control	Shading control
EP	Profile	Profile/Dynamic ctr.	Dynamic
TRN	Profile	Profile/Dynamic ctr.	Dynamic
SIM_IBK	Profile	Profile/Dynamic ctr.	Dynamic
SIM_BO	Profile	Profile/Dynamic ctr.	Dynamic
DAL	Constant	Constant	Dynamic
MOD	Profile	Profile/Dynamic ctr.	Dynamic
PHPP	Constant	Constant	Constant

Simulation Results

Comparison between simulation results

The reference office building is simulated with the different tools considering three different locations (i.e. Rome, Stuttgart and Stockholm, see Table 2. The properties of the wall and windows are varied with the climate (see Table 1). Table 7 shows the yearly simulation results, for each scenario, reporting heating demand Q_h, cooling demand Q_c, sum of ventilation and infiltration losses Q_{vv}, transmission losses Q_{tr} and solar gains Q_{sol}. Internal gains Q_{gi} are not shown because the annual sum is the same for each tool in each instance (i.e. 56.5 kWh/(m^{2}a)).

PHPP outputs only the heating and cooling demand, the other components are estimated starting from the summer and winter balance calculated by the PHPP. The transmission losses and solar gains have to be analysed bearing in mind, the different definitions used by the different tools (see previous section).

The heating demand increases with the colder climates in spite of the higher insulation level of the envelope. The solar gain is higher in Stuttgart and Stockholm compared to Rome because the glazing system has lower g-value (see Table 1) and because of lower solar altitude angles. The presence of a high efficiency heat recovery unit ensures lower ventilation losses.

Table 8 shows the relative deviation of the results reported in Table 7 with respect to the median value. The high relative deviation for the heating demand in Rome is caused by the low absolute values of heating demand. For the cooling demand, which contributes most to the energy demand in all the climates, the deviation between the

different tools reaches the maximum value of 21% in Stockholm.

Table 7: Yearly simulation results for all the cases.

Loc.	Tools	Q_h	Q_c	Q_{vv}	Q_{tr}	Q_{sol}
		[kWh/(m^{2}a)]				
ROME	EP	3.6	-36.4	-27.1	-19.8	25.4
	TRN	3.5	-33.3	-30.6	-29.1	32.9
	SIM_IBK	5.8	-38.2	-30.4	-30.3	36.8
	SIM_BO	3.1	-33.4	-29.5	-23.1	25.9
	DAL	5.9	-35.9	-31.7	-37.7	42.7
	MOD	7.1	-34.0	-31.0	-30.0	31.4
	PHPP	5.7	-37.9	-28.6	-34.1	36.6
	MEDIAN	5.7	-35.9	-30.4	-30.0	32.9
STUTTGART	EP	15.8	-28.1	-42.4	-47.3	48.4
	TRN	18.7	-23.2	-45.8	-66.2	59.9
	SIM_IBK	16.0	-31.7	-47.4	-49.7	56.4
	SIM_BO	13.2	-23.9	-45.1	-37.7	37.1
	DAL	18.2	-28.4	-45.9	-56.2	56.8
	MOD	17.1	-27.9	-49.3	-42.2	45.8
	PHPP	14.5	-27.6	-47.7	-56.5	56.7
	MEDIAN	16.0	-27.9	-45.9	-49.7	56.4
STOCKHOLM	EP	17.0	-32.2	-50.2	-34.2	46.0
	TRN	21.3	-23.8	-50.5	-61.6	58.0
	SIM_IBK	14.5	-31.0	-54.3	-41.9	56.2
	SIM_BO	17.4	-23.6	-49.3	-38.6	37.7
	DAL	16.9	-28.2	-52.7	-44.6	52.8
	MOD	14.5	-30.0	-54.4	-39.3	52.7
	PHPP	14.6	-31.0	-55.1	-44.8	56.2
	MEDIAN	16.9	-30.0	-52.7	-41.9	52.8

Table 8: Relative deviation with respect to the median value.

Loc.	Tools	Q_h	Q_c	Q_{vv}	Q_{tr}	Q_{sol}
ROME	EP	-36%	1%	-11%	-34%	-23%
	TRN	-38%	-7%	1%	-3%	0%
	SIM_IBK	2%	6%	0%	1%	12%
	SIM_BO	-46%	-7%	-3%	-23%	-21%
	DAL	4%	0%	4%	26%	30%
	MOD	25%	-5%	2%	0%	-5%
	PHPP	0%	6%	-6%	14%	11%
STUTTGART	EP	-1%	0%	-8%	-5%	-14%
	TRN	17%	-17%	0%	33%	6%
	SIM_IBK	0%	13%	3%	0%	0%
	SIM_BO	-17%	-15%	-2%	-24%	-34%
	DAL	14%	2%	0%	13%	1%
	MOD	7%	0%	7%	-15%	-19%
	PHPP	-9%	-1%	4%	14%	1%
STOCKHOLM	EP	1%	7%	-5%	-18%	-13%
	TRN	26%	-21%	-4%	47%	10%
	SIM_IBK	-14%	3%	3%	0%	6%
	SIM_BO	3%	-21%	-6%	-8%	-29%
	DAL	0%	-6%	0%	6%	0%
	MOD	-14%	0%	3%	-6%	0%
	PHPP	-13%	3%	5%	7%	6%

A good agreement is reached for the ventilation and infiltration losses, where the relative deviation is lower than 11%. Transmission losses and solar gain have to be analysed considering the different definition of these components used by the different tools (see previous section). Solar gain and transmission losses are expected to be lower or equal to the average for EP, SIM_BO and MOD. SIM_IBK and PHPP have similar ventilation-infiltration losses and solar gain because the average air exchange rate and the effective shading value used in the PHPP were "calibrated" taking as a reference SIM_IBK.

Figure 4 reports the monthly heating and cooling demand for each tool for the climates of Rome, Stuttgart and Stockholm. From March to November in Rome, and from April to October in Stuttgart and Stockholm, the cooling demand is higher than the heating demand. TRN and SIM_BO have the lowest cooling demand in each climate, with deviations with respect to the median values of each month, ranging for the climates of Stockholm from -93% to -1%, for Stuttgart from -85% to +0% and for Rome from -49% to 0%. The results present higher deviation, especially for the cooling demand, during the transition months, when longer periods in which the temperature is free to float are present, while during the central summer month deviations are contained between +15% and -10%. TRN features the highest heating demand during the winter months, with deviations from the monthly median values, ranging from +24% to +36% and +9% to +21%, for the climates of Stockholm and Stuttgart respectively. SIM_BO has the lowest heating demand every month for the climates of Rome and Stuttgart.

Figure 5 shows the monthly average convective temperature. The internal and solar gains cannot be easily dissipated through the well-insulated envelope and therefore, high indoor temperatures also occur during mid-seasons. This can be clearly seen in Figure 5, where all the tools have an average temperature higher than the heating set point also during the coldest month of the coldest climates. In Rome, the heating demand is nearly zero and the convective temperature is higher than the heating set point. Longer periods in which the convective and mean radiant temperatures are not controlled by either the heating system or the cooling system occur during the transition months.

The dynamic behaviour of the free floating temperature is influenced by the way in which the tools model the thermal capacity of the building and the convective and radiative exchange occurring within the studied office cell. DAL models the office zone with only one thermal capacity and this assumption has an influence on the convective average temperature, which is the highest during the winter months. Deviations in convective and mean radiant temperature influence heating and cooling demands. The deviation with respect to the median value for each month (excluding the temperature from PHPP) are within -2% and +3%. The maximum deviation is reached during the transition months. Figure 6 shows the monthly solar irradiation impinging the south façade for every tool in each climate. It can be seen that all tools are in good agreement except for DAL, which presents lower irradiation (in average -15% with respect to the median value). This is due to the different methods used for the calculation of the solar radiation on a tilted surface, all the tools are based on anisotropic model of the sky while DAL models the diffuse part of the sky radiation as isotropic.

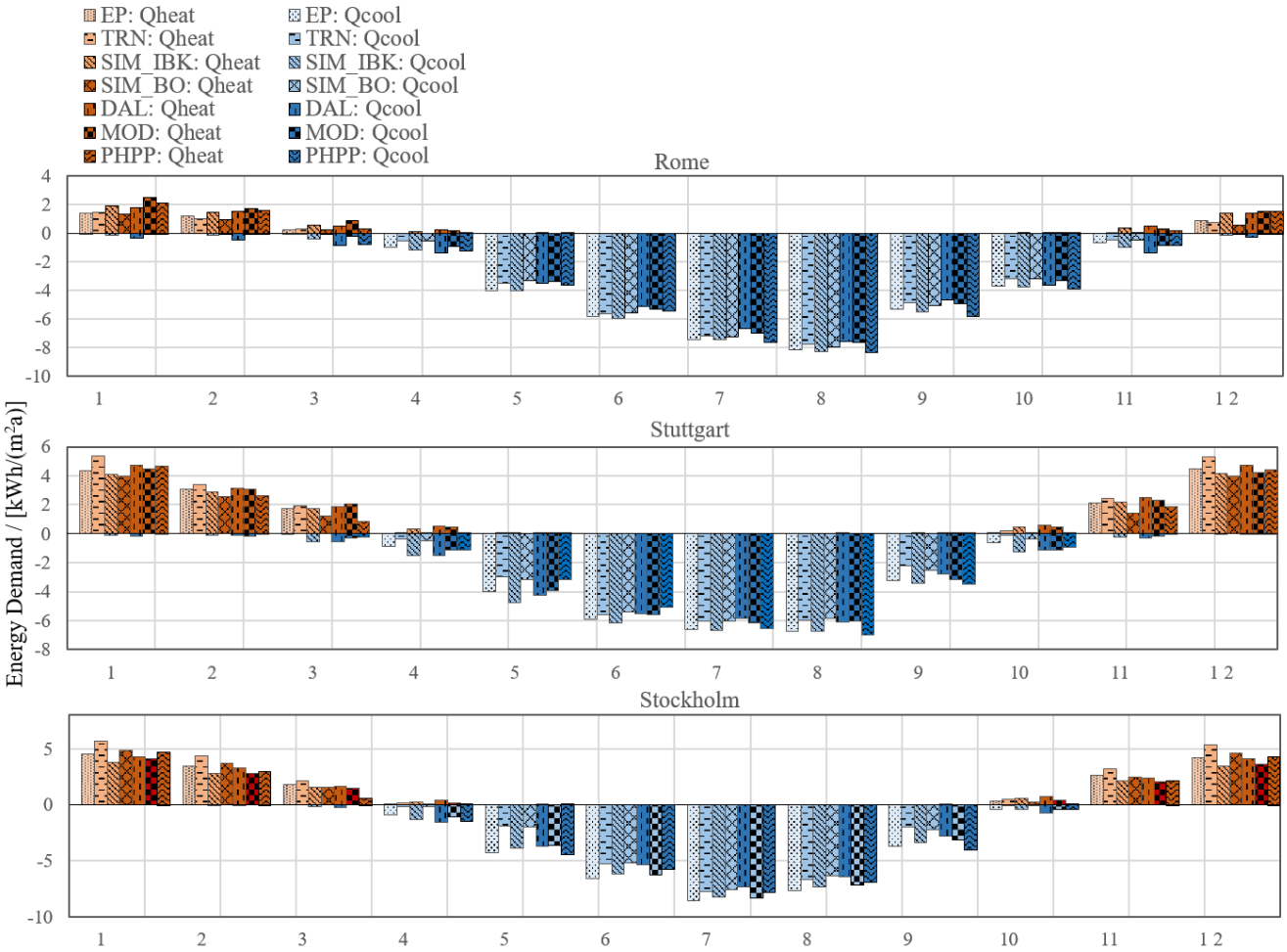

Figure 4: Comparison of monthly heating and cooling demands simulated with all the considered tools and climates.

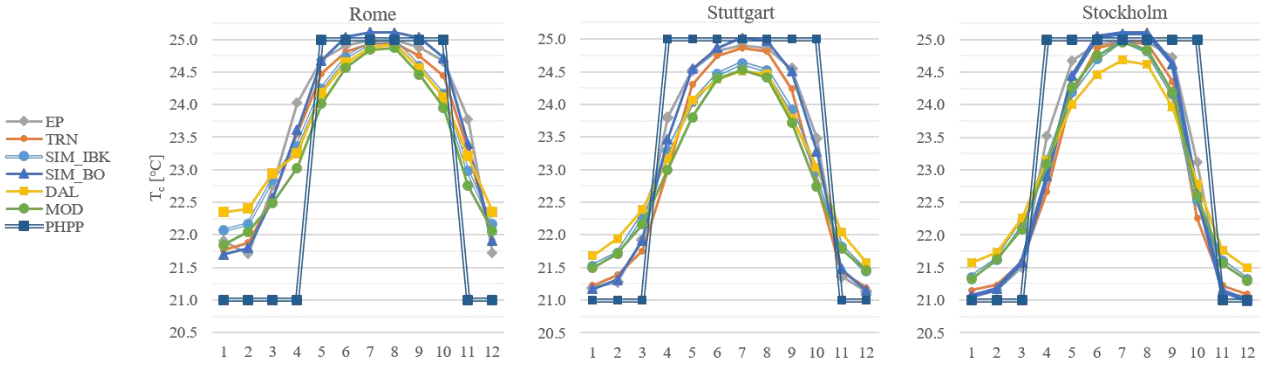

Figure 5: Monthly average of the convective temperature for all the considered tools and climates.

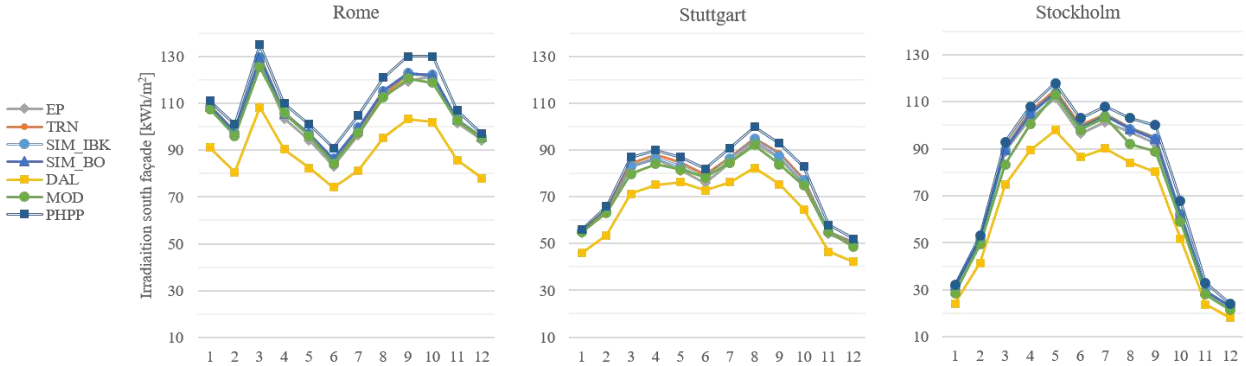

Figure 6: Monthly values of the solar radiation impinging the south façade for all the considered tools and climates.

Figure 7 shows the yearly transmission losses through the wall and windows for each tool in each climate. The wall transmission losses are in the same range in every climate. The median value ranges from -8.2 kWh/(m²a) in Rome to -7.1 kWh/(m²a) in Stuttgart.

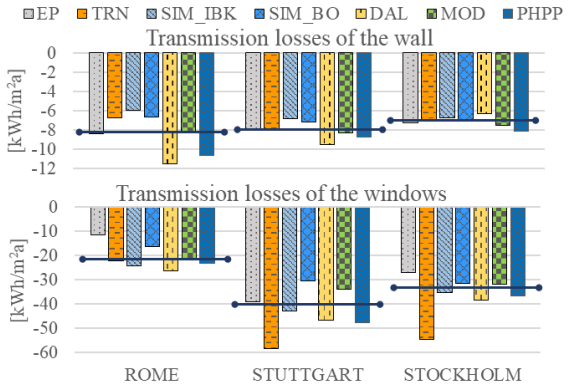

Figure 7: Yearly values of the transmission losses of the walls (top) and windows (bottom).

The deviation of the yearly transmission losses through the wall with respect to the median value (considering the results from EP, TRN, SIM_IBK, SIM_BO and MOD) ranges in Rome from +41% (DAL) to -27% (SIM_IBK), in Stuttgart ranges from +19% (DAL) to -15% (SIM_IBK) and in Stockholm ranges from +15% (PHPP) to -11% (DAL). The transmission losses through the windows are significantly higher than those through the wall and are in the range of 80% of the total transmission losses. The deviation of the windows transmission losses are due to different definitions of the transmission losses, different models of the window and thus different assumptions for the input data.

Influence of the window model

Detailed inputs are required for those tools that use a complex window model (i.e. reflectivity and absorption coefficients for each layer of each pane). The Task56 report (D'Antoni, et al., 2017) describes only the overall glazing system properties defined using a specific set of boundary conditions (i.e. U, g-value, T_{sol}, R_{sol} and T_{vis}, see Table 1). The translation of these overall properties into detailed pane level properties was identified as a source of deviations. In this reference office, the window model plays an important role in the building energy balance of the thermal zone since its properties define the admission of solar gains and 80% of the transmission losses.

To illustrate the influence that user interpretation of overall glazing properties can have on the overall results, four different window system alternatives are tested for the Rome case with EP. The alternatives have similar overall glazing properties but differ in the position and characteristics of the solar control coating, (see Table 9 and Table 10). The window system alternatives are based on measured glass properties from the IGDB.

EP case 1 has the coating placed outside of the inner pane (pos. 3), EP case 2 has the same type of coating placed inside the outer pane (pos. 2) and EP case 3 has an alternative coating in the same position as case 2 which was selected to better match the overall glazing properties, EP case 4 assumes an equivalent layer single pane glazing system with the same overall glazing system properties, under NFRC boundary conditions, as case 3.

Table 10 reports the overall glazing properties and the properties of the coated pane used by EP, TRN, SIM_BO and MOD. TRN, SIM_BO and MOD placed the coating inside the external pane (pos. 2). SIM_BO does not use T_{vis} and T_{sol} because the directly transmitted irradiation is calculated with the overall transmission value of the window.

Table 9: Overall glazing system properties.

Cases	U [W/m²K]	SHGC [-]	T_{vis} [-]	Coating Position
Reference	1.290	0.333	0.659	?
EP: Case 1	1.223	0.359	0.594	Pos. 3
EP: Case 2	1.202	0.326	0.607	Pos. 2
EP: Case 3	1.260	0.350	0.593	Pos. 2
EP: Case 4	1.260	0.350	0.593	Pos. 2
TRN	1.290	0.333	0.659	Pos. 2
SIM_BO	1.290	0.333	0.659	Pos. 2
MOD	1.322	0.334	0.614	Pos. 2

Table 10: Properties of the coated pane.

Cases	Emissivity (coated side) [-]	T_{vis} [-]	T_{sol} [-]
Reference	?	?	?
EP: Case 1	0.021	0.656	0.250
EP: Case 2	0.014	0.673	0.305
EP: Case 3	0.034	0.658	0.269
EP: Case 4	-	-	-
TRN	0.110	-	-
SIM_BO	0.110	-	-
MOD	0.016	0.671	0.310

Table 11 shows the heating and cooling demand of the four variants of the window analysed in EP. Different user interpretations of the overall glazing properties lead to relative deviations, taking as a reference the case 4, in the heating and cooling demand up to 55% and 27%, respectively. The largest deviations can be explained by the position of the solar control coating. With the coating positioned on the inside pane (pos. 3), a smaller fraction of the solar radiation which is reflected and absorbed by the coating, will exit the glazing system on the front side. The overall glazing properties, however, do not represent the angularly dependent nature of the interreflections between the panes well, as can be seen from the deviations of results between cases 3 and 4.

Table 11: Heating and cooling demand for the climate of Rome, with different windows system alternatives.

Cases	Q_h	Q_c	Q_{tr}	Q_{sol}
	[kWh/(m²a)]			
EP case 1	1.6	-46.3	-9.4	28.2
EP case 2	2.5	-39.7	-21.6	32.3
EP case 3	3.6	-36.4	-19.8	25.4
EP case 4	3.4	-40.0	-24.4	33.5
TRN	3.5	-33.3	-29.1	32.9
SIM_BO	3.1	-33.4	-23.1	25.9
MOD	7.1	-34.0	-30.0	31.4

Conclusion

The model of the office cell, reported in IEA SHC Task 56, is implemented by experts in building simulations with different simulation tools (i.e. dynamic tools EnergyPlus, TRNSYS, CarnotUIBK, ALMAbuild, DALEC, Modelica and calculation tool PHPP). The heating and cooling demands, heat losses and gains are investigated considering three different climates (i.e. Rome, Stuttgart and Stockholm). Even when high caution is taken in defining the boundary conditions of a geometrically simple space, user interpretation and implementation in the software remains one of the main reasons for deviations. After several feedback loops, agreement between the experts was achieved to have comparable simulation models implemented. The results, proved to be particularly sensitive to user interpretation of overall glazing system properties. Such deviations amongst tools can be reduced by describing glazing systems using a combination of detailed pane properties as well as overall system properties under varying boundary conditions. A future work will be carried out in order to calibrate the models considering more weather conditions so that they can be used for testing solar passive and solar active façade systems.

Reference

Brange, L., Englund, J., and Lauenburg, P. (2016). Prosumers in district heating networks – A Swedish case study. *Applied Energy 164*, 492-500.

Campana , J., Morini , G., and Magni, M. (2017). The benchmark of the SIMULINK open library ALMABuild for dynamic modelling of buildings. *Proceedings from SET 2017: 16th International Conference on Sustainable Energy Technologies.* Bologna (IT), 17-20 July 2017.

Castaldo, V., and Pisello, A. (2018). Uses of dynamic simulation to predict thermal-energy performance of buildings and districts: a review. *Energy and Environment 7*, 269.

Council of the European Union. (2014). *A policy framework for climate and energy in the period from 2020 to 2030*. Brussels.

Crawley, D. B., Pedersen C. O., Lawrie L. K. and Winkelmann F. C. (2000). EnergyPlus: Energy Simulation Program. *ASHRAE Journal 42*, 49-56.

D'Antoni, M., Bonato, P., Geisler-Moroder, D., Loonen, R., and Ochs, F. (2017). *IEA SHC T56 - System simulation Models Part C Office Buildings*.

Dermentzis, G., Ochs, F., Gustafsson, M., Calabrese, T., Siegele, D., Feist, W., Dipasquale, C., Fedrizzi, R., and Bales, C. (2019). A comprehensive evaluation of a monthly-based energy auditing tool through dynamic simulations, and monitoring in a renovation case study. *Energy & Buildings 183*, 713-726.

Feist, W. (C.F. Müller). (1994). *Thermische Gebäudesimulation: kritische Prüfung unterschiedlicher Modellansätze*. Heidelberg (D).

Feist, W. (2019) *PHPP - Passive House Planning* Package, 1998. Accessed Jan 16, 2019. https://passivehouse.com/04_phpp/04_phpp.htm.

IEA, 2016. International Energy Agency, Solar Heating and Cooling Programme. *IEA SHC Task 56 "Building Integrated Solar Envelope System for HVAC and Lighting".*

ISO 13790 (2008), *Energy Performance of Buildings – Calculation of Energy Use for Space Heating and Cooling* (ISO 13790:2008).

Kim, Y.-J., Yoon, S.-H., and Park, C.-S. (2013). Stochastic comparison between simplified energy calculation anddynamic simulation. *Energy and Buildings 64*, 332-342.

Klein S.A., Beckman W.A., Mitchell J.W., Duffie J.A., Duffie N.A., Freeman T.L., et al., 1979. *TRNSYS 17, TRaNsient SYstem Simulation program*. University of Wisconsin, Madison, WI, USA.

Martinez, R., Goikolea, B., Paya, I., Bonnamy, P., Raji, S., and Lopez, J. (2017). Performance assessment of an unglazed solar thermal collector for envelope retrofitting. *Proceedings from AREQ 2017 International Conference – Alternative and Renewable Energy Quest*. Barcellona (SP), 1-3 Feb 2017.

Pérez-Lombard, L., Ortiz, J., and Pout, C. (2008). A review on buildings energy consumption information. *Energy and Buildings 40*(3), 394-398.

SIA (2015). *Raumnutzungsdaten für die Energie- und Gebäudetechnik* (SIA 2024:2015).

Siegele, D. and Leonardi, E., Ochs, F. (2019) A new MATLAB Simulink Toolbox for Dynamic Building Simulation with B.I.M. and Hardware in the Loop compatibility. *Proceedings from BS 2019: Building Performance Simulation conference*. Rome (IT), 2-4 Sept 2019. Submitted.

Strachan, P., Svehla, K., Heusler, I., ans Kersken, M. (2016). Whole model empirical validation on a full-scale building. *Journal of Building Performance Simulation 9*(4), 331-350.

Werner M., Geisler-Moroder D., Junghans B., Ebert O. and Feist W., 2017. DALEC – A Novel Web-Tool for Integrated Day- and Artificial Light & Energy Calculation. *Journal of Building Performance Simulation 10*(3), 344-363.

Wetter, M., Zuo, W., and Nouidui, S.T. (2011). Modeling of Heat Transfer in Rooms in the Modelica "Buildings" Library. Proceedings of Proceedings from BS 2011: *Building Performance Simulation conference*. Sydney (AUS), 14-16 Nov 2011.

Wetter, M., Zuo, W., Nouidui, S.T., and Pang X. (2014). Modelica Buildings library. *Journal of Building Performance Simulation*, 7:4, 253-270.

6 Bibliography

[1] United Nations Environment Programme, Global Status Report for Buildings and Construction: Towards a Zero-emission, Efficient and Resilient Buildings and Construction, Nairobi, Kenya, 2021.

[2] F. Ochs, M. Magni, G. Dermentzis, Integration of Heat Pumps in Buildings and District Heating Systems - Evaluation on a Building and Energy System Level, Energies 2022, Vol. 15, Page 3889. 15 (2022) 3889. https://doi.org/10.3390/EN15113889.

[3] M. Ploß, T. Hatt, T. Roßkopf-Nachbaur, A. Peter, M. Reis, F. Ochs, M. Magni, G. Dermentzis, F. Sigg, M. Wirnsberger, M. Großklos, R. Vallentin, C. Drexel, G. Rohregger, Low-Cost nZEB, Paris-kompatible Mehrfamilienhäuser, 2022.

[4] C. Wemhoener, L. Rominger, S. Buesser, M. Magni, F. Ochs, T. Dippel, Simulation-based Methodology For Comparison Of nZEB Requirements In Different Countries Including Results Of Model Calibration Tests, in: 16th IBPSA Int. Conf., 2019: pp. 5060–5067. https://doi.org/https://doi.org/10.26868/25222708.2019.210996.

[5] European Commission, In focus: Energy efficiency in buildings, (2020). https://ec.europa.eu/info/news/focus-energy-efficiency-buildings-2020-lut-17_en (accessed May 30, 2022).

[6] Y. Wang, K. Qu, X. Chen, G. Gan, S. Riffat, An innovative retrofit Motivation-Objective-Criteria (MOC) approach integrating homeowners' engagement to unlocking low-energy retrofit in residential buildings, Energy Build. (2022) 111834. https://doi.org/10.1016/J.ENBUILD.2022.111834.

[7] G. Liu, K. Ye, Y. Tan, Z. Huang, X. Li, Factors influencing homeowners' housing renovation decision-making: Towards a holistic understanding, Energy Build. 254 (2022) 111568. https://doi.org/10.1016/J.ENBUILD.2021.111568.

[8] M. Magni, F. Ochs, A. Knotzer, T. Roßkopf-nachbaur, G. Dermentzis, E. Venturi, Supporting the decision-making process related to the renvation of multi-family houses, in: 2nd Int. Sustain. Energy Conf., 2022.

[9] T. Hong, J. Langevin, K. Sun, Building simulation: Ten challenges, Build. Simul. 11 (2018) 871–898. https://doi.org/10.1007/S12273-018-0444-X.

[10] H. Wang, Z. Zhai, Advances in building simulation and computational techniques: A review between 1987 and 2014, Energy Build. 128 (2016) 319–335. https://doi.org/10.1016/J.ENBUILD.2016.06.080.

[11] I. Beausoleil-Morrison, Fundamentals of Building Performance Simulation, Taylor & Francis Group, New York, 2021.

[12] T. Hong, S.K. Chou, T.Y. Bong, Building simulation: an overview of developments and information sources, Build. Environ. 35 (2000) 347–361. https://doi.org/10.1016/S0360-1323(99)00023-2.

[13] D.B. Crawley, J.W. Hand, M. Kummert, B.T. Griffith, Contrasting the capabilities of building energy performance simulation programs, Build. Environ. 43 (2008) 661–673. https://doi.org/10.1016/j.buildenv.2006.10.027.

[14] Building Energy Software Tools, Best Directory | Building Energy Software Tools, (2020). https://www.buildingenergysoftwaretools.com/?__cf_chl_jschl_tk__=333a9062c0deb41f0aedbc09d4de96cab9d74a2d-1595925926-0-Ac80m_md0jCDx9IWiUyqe8WYrQij-imLS12aG2ZaEQAA0YJNQ0m3L4gPuZsqdDSQfZjPvfeemai8ls_wyDsp2znHqB0uwrDsw9iKK61KqCSarbSfBzG2zeBoLKS2ww74sxIaBbi7 (accessed May 30, 2022).

[15] L. Zhang, L. Zhou, B.K.P. Horn, Building a right digital twin with model engineering, J. Manuf. Syst. 59 (2021) 151–164. https://doi.org/10.1016/J.JMSY.2021.02.009.
[16] E. Kamel, A.M. Memari, Review of BIM's application in energy simulation: Tools, issues, and solutions, Autom. Constr. 97 (2019) 164–180. https://doi.org/10.1016/J.AUTCON.2018.11.008.
[17] S.-J. Arora, C. Ceccolini, M. Rabe, Approach to Reference Models for Building Performance Simulation, in: Proc. 10th Int. Conf. Model. Eng. Softw. Dev. - Model., 2022: pp. 271–278. https://doi.org/10.5220/0010888800003119.
[18] R. Fujimoto, C. Bock, W. Chen, E. Page, H.J. Panchal, Research Challenges in Modelling and Simulation for Engineering Complex Systems, Springer, 2017. https://doi.org/10.1007/978-3-319-58544-4.
[19] L. Zhang, L. Zhang, Y. Liu, Y. Laili, W. Zhang, Model maturity towards modeling and simulation: Concepts, index system framework and evaluation method, Int. J. Model. Simulation, Sci. Comput. 11 (2020). https://doi.org/10.1142/S1793962320400012.
[20] T. Østergård, R.L. Jensen, S.E. Maagaard, Building simulations supporting decision making in early design - A review, Renew. Sustain. Energy Rev. 61 (2016) 187–201. https://doi.org/10.1016/J.RSER.2016.03.045.
[21] G. Augenbroe, Trends in building simulation, Build. Environ. 37 (2002) 891–902. https://doi.org/10.1016/S0360-1323(02)00041-0.
[22] A.M. Malkawi, G. Augenbroe, Advanced Building Simulation, Spon Press Taylor and Francis Group, 2016.
[23] S. Robinson, Conceptual modelling for simulation Part I: definition and requirements, J. Oper. Res. Soc. 2007 593. 59 (2007) 278–290. https://doi.org/10.1057/PALGRAVE.JORS.2602368.
[24] S. Robinson, Conceptual modelling for simulation: Progress and grand challenges, J. Simul. 14 (2019) 1–20. https://doi.org/10.1080/17477778.2019.1604466.
[25] J. L.M. Hensen, R. Lamberts, Building Performance Simulation for Design and Operation, Routledge Taylor and Francis Group, 2019.
[26] Y. Li, Z. O'Neill, L. Zhang, J. Chen, P. Im, J. DeGraw, Grey-box modeling and application for building energy simulations - A critical review, Renew. Sustain. Energy Rev. 146 (2021). https://doi.org/10.1016/J.RSER.2021.111174.
[27] B.P. Zeigler, A. Muzy, E. Kofman, Theory of Modeling and Simulation, Discrete Event and Iterative System Computational Foundations, ELSEVIER Academic Press, London, United Kingdom, 2019.
[28] K.E.A. Ohlsson, T. Olofsson, Benchmarking the practice of validation and uncertainty analysis of building energy models, Renew. Sustain. Energy Rev. 142 (2021) 110842. https://doi.org/10.1016/J.RSER.2021.110842.
[29] Q. Wang, G. Augenbroe, Verification of Probabilistic Building Energy Models, in: 16th IBPSA Int. Conf., 2019. https://doi.org/10.26868/25222708.2019.210879.
[30] G.R. Ruiz, C.F. Bandera, Validation of calibrated energy models: Common errors, Energies. 10 (2017) 1587. https://doi.org/10.3390/en10101587.
[31] N. Jain, E. Burman, S. Stamp, D. Mumovic, M. Davies, Cross-sectoral assessment of the performance gap using calibrated building energy performance simulation, Energy Build. 224 (2020) 110271. https://doi.org/10.1016/J.ENBUILD.2020.110271.
[32] P. De Wilde, The gap between predicted and measured energy performance of buildings: A framework for investigation, Autom. Constr. 41 (2014) 40–49. https://doi.org/10.1016/J.AUTCON.2014.02.009.
[33] S. Homaei, M. Hamdy, A robustness-based decision making approach for multi-target high performance buildings under uncertain scenarios, Appl. Energy. 267 (2020) 114868. https://doi.org/10.1016/J.APENERGY.2020.114868.
[34] A. Ashouri, F. Petrini, R. Bornatico, M.J. Benz, Sensitivity analysis for robust design of building energy systems, Energy. 76 (2014) 264–275. https://doi.org/10.1016/J.ENERGY.2014.07.095.
[35] G. Calleja Rodríguez, A. Carrillo Andrés, F. Domínguez Muñoz, J.M. Cejudo López, Y. Zhang, Uncertainties and sensitivity analysis in building energy simulation using macroparameters, Energy Build. 67 (2013) 79–87. https://doi.org/10.1016/j.enbuild.2013.08.009.
[36] R. Judkoff, D. Wortman, J. Burch, Empirical Validation of Building Analysis Simulation Programs: A Status Report, Solar Energy Research Institute, Golden, Colorado, 1982.

[37] R. Judkoff, J. Neymark, Building Energy Simulation Test (BESTTEST) and diagnostic Method, Colorado, 1995.

[38] ANSI/ASHRAE 140-2017, Standard method of test for the evaluation of building energy analysis computer programs, American Society of Heating, Refrigerating and Air-Conditioning Engineers, Atlanta, 2017.

[39] J. Neymark, R. Judkoff, M. Kummert, R. Muehleisen, A. Johannsen, N. Kruis, J. Glazer, R. Henninger, M. Witte, E. Ono, H. Yoshida, Y. Jiang, X. Zhou, T. McDowell, M. Hiller, J. An, D. Yan, J. Allison, P. Strachan, Update of ASHRAE Standard 140 Section 5.2 and Related Sections (BESTEST Building Thermal Fabric Test Cases), Argonne National Laboratory, ANL-20/26 158451, Argonne, 2020. https://doi.org/https://doi.org/10.2172/1643690.

[40] O. Balci, Validation, verification, and testing techniques throughout the life cycle of a simulation study, Ann. Oper. Res. 53 (1994) 121–173.

[41] M. D'Antoni, D. Geisler-Moroder, P. Bonato, F. Ochs, M. Magni, S. de Vries, R.C.G.M. Loonen, R. Fedrizzi, Definition of a Reference Office Building for Simulation Based Evaluation of Solar Envelope Systems, (2019) 1–10. https://doi.org/10.18086/eurosun2018.06.13.

[42] F. Ochs, M. Magni, P. Bonato, M. D'Antoni, D. Geisler-Moroder, M. Hauer, S. de Vries, R. Loonen, IEA SHC TASK 56 | Building Integrated Solar Envelope Systems for HVAC and Lighting: System Simulation Models, Solar Heating & Cooling Programme International Energy Agency, 2020. https://doi.org/10.18777/ieashc-task56-2020-0004.

[43] F. Ochs, G. Dermentzis, Evaluation of Efficiency and Renewable Energy Measures Considering the Future Energy Mix, in: 7th Int. Build. Phys. Conf., Syracuse, NY, USA, 2018: pp. 1271–1276.

[44] IEA, World Energy Outlook 2021 - revised version October 2021, Int. Energy Agency. (2021) 43–44. www.iea.org/weo.

Verpflichtungs- und Einverständniserklärung

Ich erkläre, dass ich meine Dissertation selbständig verfasst und alle in ihr verwendeten Unterlagen, Hilfsmittel und die zugrunde gelegte Literatur genannt habe.

Ich nehme zur Kenntnis, dass auch bei auszugsweiser Veröffentlichung meiner Dissertation die Universität, das/die Institut/e und der/die Arbeitsbereich/e, an dem/denen die Dissertation ausgearbeitet wurde, und die Betreuerin/nen bzw. der/die Betreuer zu nennen sind.

Ich nehme zur Kenntnis, dass meine Dissertation zur internen Dokumentation und Archivierung sowie zur Abgleichung mit der Plagiatssoftware elektronisch im Dateiformat pdf ohne Kennwortschutz bei der/dem Betreuer/in einzureichen ist, wobei auf die elektronisch archivierte Dissertation nur die/der Betreuerin/Betreuer der Dissertation und das studienrechtliche Organ Zugriff haben.

Innsbruck am . . . .

Dipl.-Ing Mara Magni